Composite Materials Impact Damage Detection Using Neural Networks

Ning Liu

Submitted for the Degree

of

Doctor of Philosophy

THE UNIVERSITY OF ASTON IN BIRMINGHAM

June 2002

The University of Aston in Birmingham

Composite Materials Impact Damage Detection Using Neural Networks

Ning Liu

A Thesis Submitted for the Degree of Doctor of Philosophy

June 2002

Summary

This thesis considers two basic aspects of impact damage in composite materials, namely damage severity discrimination and impact damage location by using Acoustic Emissions (AE) and Artificial Neural Networks (ANNs). The experimental work embodies a study of such factors as the application of AE as Non-destructive Damage Testing (NDT), and the evaluation of ANNs modelling. ANNs, however, played an important role in modelling implementation.

In the first aspect of the study, different impact energies were used to produce different level of damage in two composite materials (T300/914 and T800/5245). The impacts were detected by their acoustic emissions (AE). The AE waveform signals were analysed and modelled using a Back Propagation (BP) neural network model. The Mean Square Error (MSE) from the output was then used as a damage indicator in the damage severity discrimination study. To evaluate the ANN model, a comparison was made of the correlation coefficients of different parameters, such as MSE, AE energy, AE counts, etc. MSE produced an outstanding result based on the best performance of correlation.

In the second aspect, a new artificial neural network model was developed to provide impact damage location on a quasi-isotropic composite panel. It was successfully trained to locate impact sites by correlating the relationship between arriving time differences of AE signals at transducers located on the panel and the impact site coordinates. The performance of the ANN model, which was evaluated by calculating the distance deviation between model output and real location coordinates, supports the application of ANN as an impact damage location identifier. In the study, the accuracy of location prediction decreased when approaching the central area of the panel. Further investigation indicated that this is due to the small arrival time differences, which defect the performance of ANN prediction. This research suggested increasing the number of processing neurons in the ANNs as a practical solution.

Key Words: Damage level discrimination; Damage location; NDT; Acoustic Emissions

To my family and friends

Acknowledgement

I would like to take this opportunity to extend my appreciation and thanks to Dr J.E.T. Penny, my supervisor, for his invaluable guidance and constant encouragement throughout the duration of this research. Credits also have to be attributed to Dr Q.M. Zhu, who gave substantial guidance in writer's first year research.

I am grateful to Professor P.E. Irving and Dr. C.Y. Wei, at Cranfield University, for their cooperation and advice in the study. The experimental work was basically conducted under their guidance at Cranfield University. It therefore plays an irrefutable vital role in this research project.

I also wish to acknowledge the University of Aston and Overseas Research Student Awards Scheme (ORS), who provide the financial assistance.

Last but not least, my acknowledgement would not be completed without expressing my indebtedness to my family for their continuous encouragement in my pursuits.

List of Contents

List of Figures and Tables

Chapter I

Chapter II

Chapter III

Chapter IV

Chapter V

Chapter VI

Chapter VII

Nomenclature

Symbols	Description
$y = (y_1, y_2 \cdots, y_n)$	neuron output vector
f_h	hard-limiting function
$x = (x_1, x_2, \cdots, x_n)$	input vector
$\omega = (\omega_1, \omega_2, \cdots, \omega_n)$	weight vector
E	error surface or error function
$\Delta\omega_i$	weight update
η	learning rate
$\partial E / \partial \omega_i$	gradient of the error with respect to each weight
$f(.)$	transfer function
y^p	neuron output with p patterns
t^p	target with p patterns
I	input layer
J	hidden layer
K	output layer
$g(.)$	transfer function
ω_{ij}	weights to connect layer I and J
ω_{jk}	weights to connect layer J and K
y_j	output of layer J
y_k	output of layer K
$e^{(.)}$	Exponent function
$\Phi_j(x)$	basis function
μ_j	the j_{th} prototype vector

δ_j	width of the Gaussian for that prototype
ω_{0k}	bias weight to output unit k
$\Re^n$	n-dimensional real-valued input space
$\Re^k$	K-dimension real-valued output space
C_j	training patterns set
m_1	mass of the impactor
V_1	velocity of the impactor
m_2	mass of the target
V_2	velocity of the target
R_1	radius of a spherical impactor
ν	Poisson's ratio
E (Chapter-III)	Young's modulus
P	impact force
x(Chapter-III)	distance
n	equation term
a	radius of contact area
q_0	surface pressure at centre of contact area
t (Chapter-III)	time
C_r	curvature parameter
δ_r	radial stress
δ_z	normal stress
δ_θ	circumferential stress
δ_t	maximum tensile stress
δ_c	compressive stress
δ_s	shear stress
σ_x, σ_y	X axial and Y axial normal stress,
τ_{xy}	the shear stress

$\sigma_1, \sigma_2, \sigma_3,$	principle stresses
σ_e	von Mises stress
$\{+45°, -45°, 0°, -45°, +45°\}_s$	lay-up sequence, each figure included in the {.} represents a layer, value represents the lay-up angle, s is for stacking
$\Delta t_{..}$	time difference
X	x coordinate of a location
Y	y coordinate of a location
V	speed
t (Chapter-IV)	arrival moment
$[y(t\text{-}1) \ldots]$	time series as neural network input
N	data length
$a_2(t)$	ANN predicted output
tansig	tangent sigmoidal transfer function
purelin	Linear transfer function
P1	Input vectors
IW1	weights of the first layer
IW2	weights of the second layer
b1	biases of the first layer
b2	biases of the second layer
a1	output of the first layer
a2	output of the second layer

Abbreviation	**Description**
2D	two dimensions
3D	three dimensions
AE	acoustic emission
BP	backpropagation
ANN	artificial neural networks

FEA	finite element algorithm
NDT	non-destructive damage test
CFRP	carbon fibre reinforced plastics
PA	peak amplitude
RDC	ringdown counts
ED	event duration
SST	standard surface treatment
ASTM	American Society for Testing and Materials
FA	frequency analysis
FFT	fast fourier transform
RBF	Radial Basis Function
MLPs`	Multilayer Perceptrons
SLP	Single Layer Perceptron
Prepregs	Preimpregnated materials
LE	Location error
PZT	Piezo-electronic transducers
ARX	Auto-Regression with eXtra inputs model
ALE	average location error
L-M	Levenberg-Marquardt algorithm
BFGS	Broyden, Fletcher, Goldfarb, and Shanno algorithm
Rprop	Resilient propagation
LMS	Least Mean Square Error

Chapter 1 Introduction

"A research degree is the academic equivalent of scaling an unclimbed peak."

(James Irvine, Chair, National Postgraduate Committee, 1993-1995)

This thesis describes the development of a method for detecting impact damage in composite materials using acoustic emission (AE) linked to artificial neural networks (ANN). There are two fundamental subjects within the study, namely impact damage severity discrimination and impact damage location. In the first aspect of the study, a numerical indicator has been generated to associate with impact damage energy by using a back propagation (BP) neural network model. The results correlated well with the applied impact damage events. In the second aspect, a new BP neural network model has been designed and applied to predict impact site location. The results were validated using the distance deviation between neural network prediction and real location coordinates. Both numerical models yielded reasonable good results.

1.1 Background

New materials continually emerge as modern technology advances. Composite materials, known for their outstanding mechanical performance and designable properties, have been widely used as structural material in various fields, particularly in aero-structure. Composite materials are superior to many other materials, having lower density, higher strength, and higher stiffness. But, advantages usually don't come alone without disadvantages. The poor impact

tolerance of the composite materials has impeded their further use in a good number of industries. Therefore impact damage study is vital for composite materials (Kubo and Nelson 1975). For years, efforts have been made to find a better understanding and render solutions. In aerospace industry, common practice has first been tested on coupon-sized samples and then tested on two typical full-scale components (Davies *etc*, 1994). Because of its difficulty, impact damage study on composite materials is rich in diversity and is multidisciplinary. Literature revealed the studies covering many subjects such as damage mechanism, damage detection approaches, and diagnosis procedures *etc*. However, the clarification of an engineering problem is always based on the fact that the problem can be detected and evaluated. Under this circumstance, the question of impact damage detection is too significant to be neglected.

This project, however, generally accepted that the procedures of impact damage detection can be equivalently interpreted into those of answering the following questions:

1) Has a failure event ever occurred?

2) Should a failure have been occurred, how severe is the damage?

3) And, where is the damage location?

This thesis considered all these questions and developed a relevant damage detection scheme according to each of the problems. In the succeeding chapters,

the mechanism of impact damage detection will be explained progressively. Numerical solutions for the problems are then presented and practised by applying AE and ANNs technologies.

1.2 Project objectives

The basic objective of this research was to investigate what neural networks can achieve in terms of determining the impact damage level and locating impact site of composite materials. In the first part of the study, a new approach was expected to associate certain variables with the damage severity using ANNs. The method was designed to discriminate the damage level when an impact damage event took place on the composites. As to the second part of the study, the approach taken was to adopt system perspectives and implement artificial neural networks for the impact damage location detection.

The holistic idea of this study, therefore, was to carry out impact damage detection in a quantitative and qualitative fashion. In addition and probably of more significance was the understanding of the physical model of impact damage and its embodiment in ANN models.

The circumstances of this project were such that the goals were well defined at early stage. However, some alternations and changes in application were experienced and finalised eventually. These included deciding between time domain and frequency domain methods and consideration as to which modelling

tool to deploy, ANN or Finite Element Algorithm (FEA). After systematically comparison and discussion, the research objectives were fixed and summarised as follows:

1) To identify and correlate the factors for impact damage level discrimination;
2) To identify and correlate the factors for impact damage location;
3) To understand the mechanism and develop the method of impact damage level study on composite materials;
4) To understand the mechanism and develop the method of impact damage location on composite materials;
5) To validate the methodologies and propose optimised solutions.

Most of the results presented in this thesis have been or will soon be published. A list of published papers and their abstracts are included in Appendix D.

1.3 Research environment

This project involved two advance research institutes namely Aston University and Cranfield University. It was an example of transferring knowledge and technology into practice. Some novel knowledge has been put in both damage level detection and impact site locating. The methodology adopted in the project was "action research" using an interdisciplinary approach. This is inevitably due to the complexity of the problem and the fact that, at the outset, these problems are rarely

formulated into research questions. In the writer's opinion, the research environment of this project was different from a conventional project. Firstly, this was a subjective project with high requirement using latest technology to work out the mechanism of a physical model. Secondly, the researcher was both an apprentice and a proficient, sometimes simultaneously during the project. As the problem becomes more clearly defined, the researcher is seen increasingly in the role of a proficient. Finally, the "esprit de corps" was essentially vital due to the fact this was a cooperative project between two research teams.

In the project, most computation work was conducted at Aston, such as data mining, modelling, neural computation, *etc*. The computational environment was based on Pentium II 600 MHz PC with Windows 98, MATLAB5.0 (Neural network toolbox 2.0) installed. Meanwhile, the majority experimental work was based at Cranfield University. Sophisticated experimental equipments were used for data acquisition such as C-Scanner, Impact tester and AE acquisition system. A task distribution diagram is shown in Figure 1-1. The writer of this thesis undertook all the modelling tasks at Aston and actively participated in the experimental work at Cranfield University. The following summarises the distribution of work.

1) Tasks undertaken at Aston University

a. Data processing

b. Modelling and signal processing for damage level discrimination

c. Modelling and signal processing for damage site locating

d. Impact damage theory studying

e. Result analysis and evaluation

f. Summarisation

2) Tasks undertaken at Cranfield University

a. Experiment organisation and samples preparation

b. Data collection (participated)

c. Experimental record archiving (participated)

d. Result analysis and evaluation (participated)

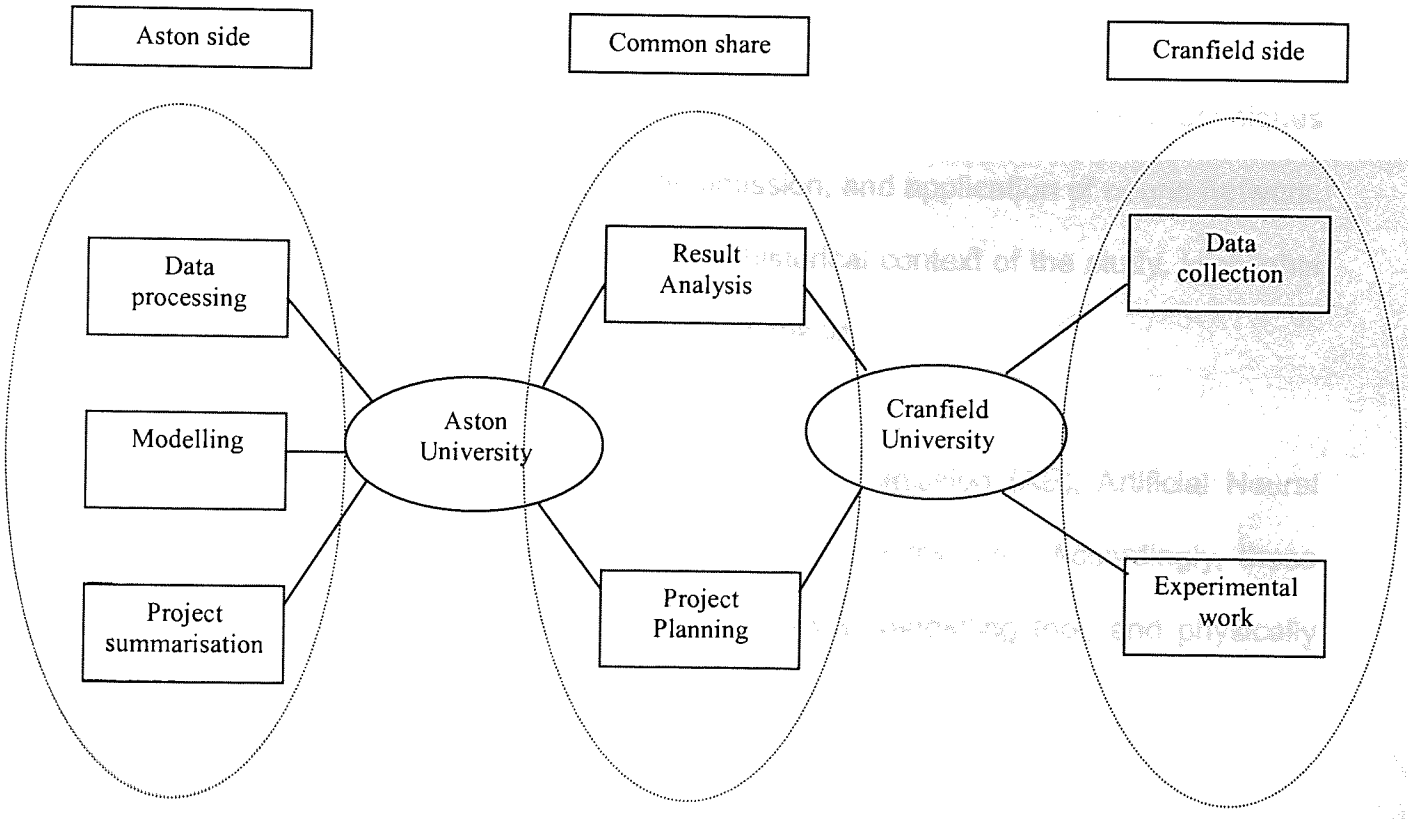

Figure 1-1 Task sharing of Aston University and Cranfield University

1.4 Structure of thesis

This thesis is organised in a logical order but not necessarily in a chronological order. This is to give a much clearer and concise outline and could provide a more logic picture for the reader.

Chapter 1 is the introduction to the thesis, in which the objectives and environment of this project are described. A brief description of task-share is also given in this chapter. It generally provides an overview of the main content, layout and background about the thesis.

Chapter 2 is a literature review. It reviews the literature on the current techniques for impact damage modelling, acoustic emission, and application of neural network. The chapter also includes a survey of the historical context of the study. Highlights are cast on parallel studies that inspired this thesis.

Chapter 3 studies the fundamentals of Acoustic Emission (AE), Artificial Neural Networks (ANN), Impact dynamics and System identification. Accordingly, these methodologies served as data acquisition means, modelling tool, and physically theoretical basis, modelling principle in this study.

The experimental work and data collection are presented in Chapter 4. It also discusses instrumentation and experiments employed in this research project. The

experimental programmes are introduced on damage level detection and damage locating separately.

Chapter 5 and Chapter 6 describe the mechanism and the procedures of neural modelling of the study of impact damage level discrimination and impact damage location. Two independent neural network models were successfully constructed to accomplish the tasks accordingly. Furthermore, the analysis and validation of ANN computation are key issues addressed in these two chapters.

Chapter 7 addresses other important matters of the project, such as the criterion of input selection, computational speed and neural structure optimisation *etc.*

Finally, in Chapter 8, conclusions are drawn from the study of impact damage detection using neural networks. Recommendations for future work are also given in this chapter.

1.5 Plan of this research project

Figure 1-2 illustrates the main events of this project and their interaction.

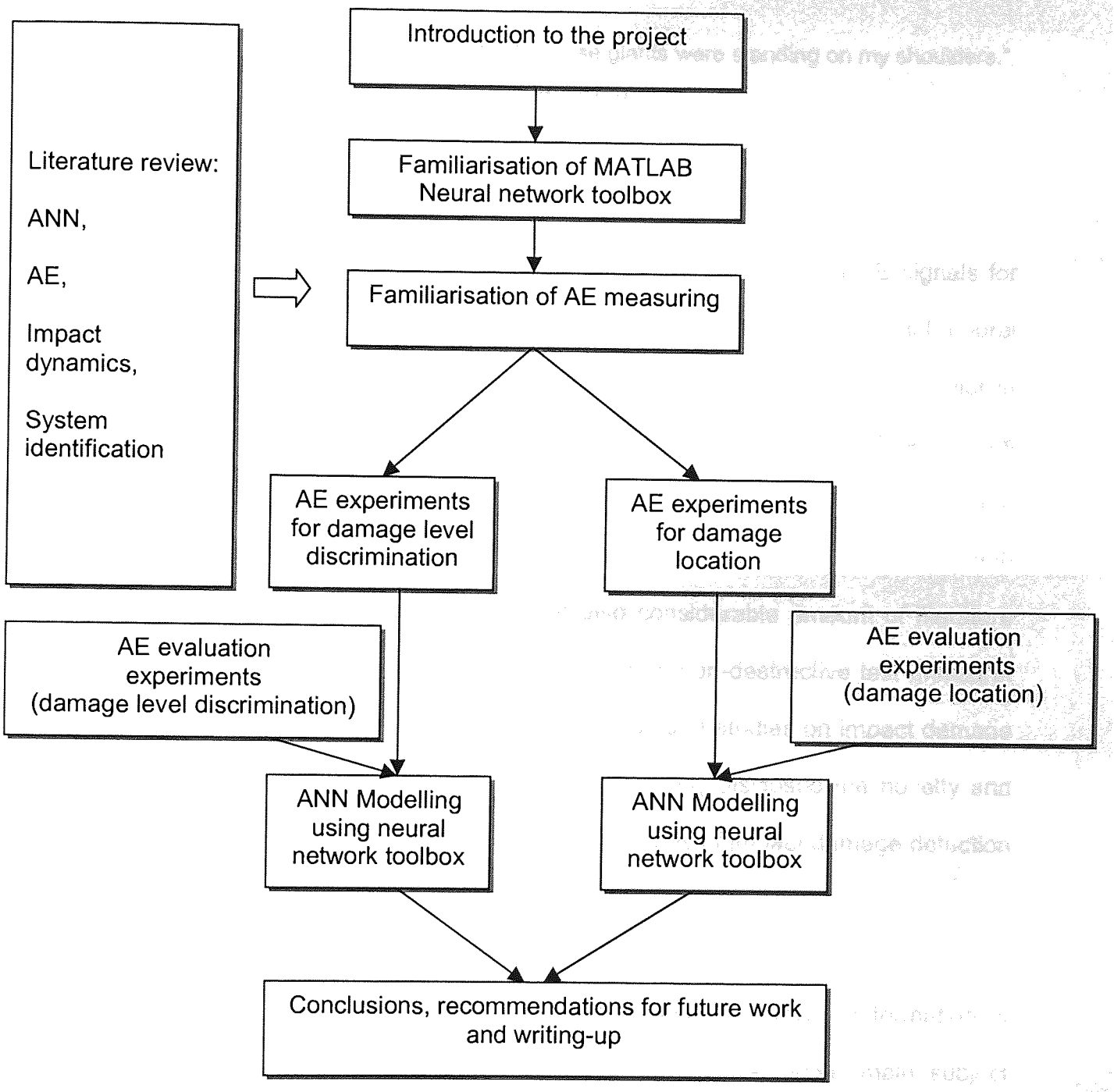

Figure 1-2 Major phases of this project

Chapter 2 Methodology (A literature review)

"If I have not seen as far as others, it is because giants were standing on my shoulders."
(Hal Abelson)

2.1 Introduction

As the project title suggests, this study focuses on the analysis of AE signals for impact damage assessment of composite materials by using artificial neural network. According to statistics, the ANN studies remained being very popular in research in recent years. As a result, documentation and publication of papers has mushroomed, which is evidenced by Figure 2-1. Through the online search (Sciencedirect.com), the key word "neural network" yielded 319 results in 1998 (The initial year of the project). There are also considerable amount of literature discussing and investigating acoustic emission as a non-destructive test measure. However, as a contrast, there were modest numbers of studies on impact damage detection in the last five years. This fact quantitatively disclosed the novelty and potential to implement the ANNs and AE into the study of impact damage detection of composite materials.

This chapter presents an overview of AE, ANN, and the relevant information of impact damage detection. The areas covered here come under main subject outlines, which are:

1) application of acoustic emission

2) application of neural network

3) literatures on impact damage detection

4) a brief discussion of the modelling algorithm

Due to the length of the thesis, the writer listed only part of the leading studies here. A more complete survey of the literature can be found in NDT abstracts (1992-2001), Proceedings of DAMAS (1997-2001), Journal of Neural networks (1995-2001) and other leading papers.

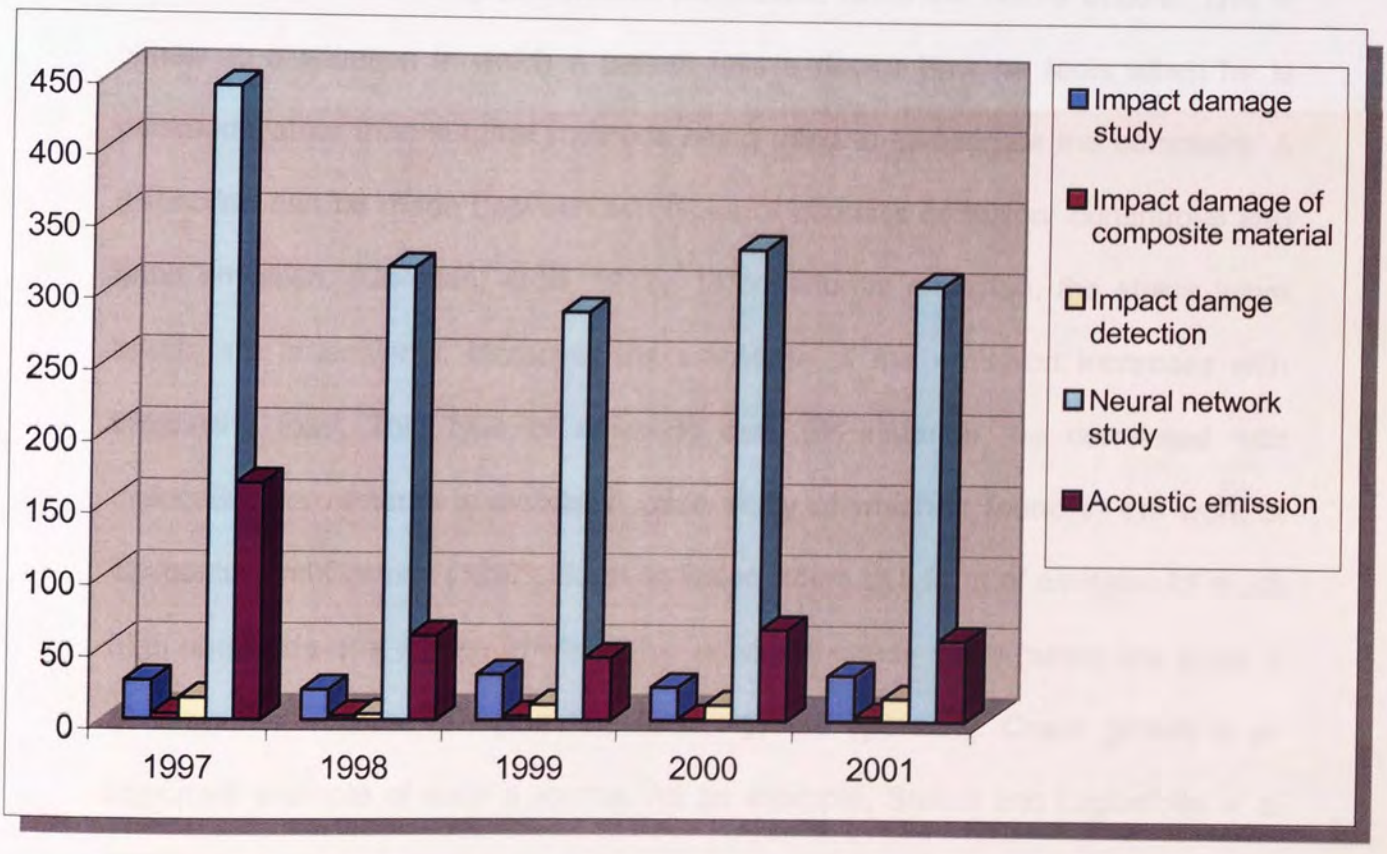

Figure 2-1 Survey chart for research background

2.2 Application of AE – Listening to the sound of materials

Acoustic emission techniques allow us to detect sounds of high frequencies and lower intensities. Crack propagation, phase transformation, and dislocation movements are all examples of processes that create acoustic emission. The basic mode of operation for stress wave detection is simple. When the stress waves reach the specimen surface, they produce the small displacements that are detected by a piezoelectric transducer. The amplified signal is then conditioned, record and finally analysed. AE distinguishes from other methods to investigate failure/deformation processes, e.g. optical microscopy, in that it utilises information supplied by the fracturing/deformation processes, while the failure occurs. This is similar to a situation in which a patient tells a doctor how he feels when he is punched, rather than surgical methods being used to investigate the complaint. A distinction can be made between two types of acoustic emission: continuous and burst emission. (Chretien, *et al*, 1972) In continuous emission, the stress wave bursts are irresolvable. Moreover the amplitude of the emission increases with increasing load. This type of emission can, for instance, be correlated with dislocation movements in metals. A case study of which is found in the work of Carpenter and Gorman (1997). Burst emission refers to a form of emission of much high amplitude and energy in which the individual stress wave bursts are seen. It occurs when sources of higher impact energy are operating. Crack growth is an important example of such a source. As an example, Stebut and Lapostolle *et al* (1999) investigated single cracking events on metal coatings to associate AE

variations with crack growth. Their study is based upon the analysis of amplitude and resonant frequency of the AE signals. The experiments have been performed on a commercial, semi-automatic LSRH-Revetest scratch tester equipped with a standard off-line Zeiss metallographic microscope (magnification: ×200). This instrument has been complemented by a special specimen mounting table (allowing friction force monitoring) as well as two displacement transducers. One is for vertical indenter-shaft displacement; the other is for horizontal distance. However, in this study, Stebut and Lapostolle applied vertical load only to generate cracks. Figure 2-2 shows the experimental principle.

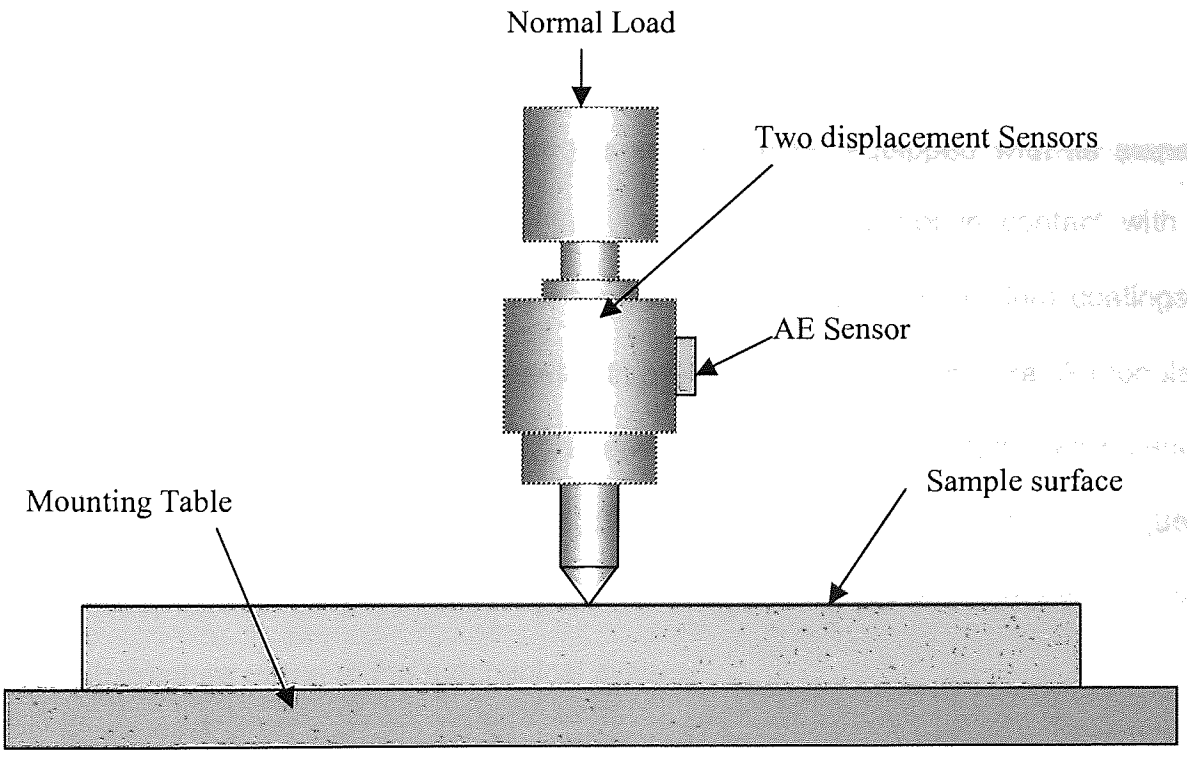

Figure 2-2 Principle of the testing of scratch tester

Four sets of tests have been performed to investigate the relationship between AE signals and crack damage information. In test1, the cracking events were mimicked by breaking a 0.5 mm diameter graphite refill of a pencil. For a freestanding, unmounted sensor, Figure 2-3 (a) shows the response waveform plotted versus time. As anticipated, the sensor response consists of an extremely short-lived wave package with a sensor-specific centre frequency. The very steep rise from the system noise to the maximum amplitude is followed by a rapid exponential attenuation, characteristic of a damped oscillator. The FFT spectrum assessed for the time window on the initial pulse is rather structureless.

In test2, the cracking event is mimicked on the system comprising the sensor mounted on the indenter shaft of the scratch tester equipped with its standard Rockwell-C diamond. This time, the diamond holder is not in contact with the coated specimen, which is 10 μm thick stainless steel or aluminium coatings on AFNOR 35 CD 4 construction steel with a bulk modulus of 205 GPa. A modulated waveform can be observed with gradually decreasing peak amplitudes extending over roughly 100 μs. In Figure 2-3(b), FFT analysis reveals a similar frequency envelope as for the pure sensor spectrum of Figure 2-3 (a), but with a considerable substructure owing to the mechanical system.

In test3, the indenter is in contact with the specimen under a 5 N contact load yielding essentially the same result as in Figure 2-3(b).

In test4 (Figure 2-3(d)), it finally indicated the signal corresponding to standard indentation when the indenter slowly drove into the coated specimen until real cracking takes place. It showed that the steep initial signal rose with only minor residues of wave modulation. The AE signature of a cracking event is seen to contain essentially the features developed above:

1)steep initial signal onset (short rise-time);

2)exponential decay extending over less than 1000 μs;

3)some modulation of the decay suggesting minor mechanical system instabilities or echo effects.

Stebut and Lapostolle believed that the frequency spectrum of the acoustic waveform arriving at the sensor is essentially test instrument-specific (rockwell diamond identer + indenter shaft + load frame) but not specimen-specific. The information that remains characteristic of the cracking event thus is the maximum amplitude of an AE impulse which related to the crack energy release. The corresponding instantaneous AE impulse time is another important indicator. This precise impulse time, when correlated with the logged instantaneous tribo-system parameters like friction as well as vertical and horizontal position, is clearly strategic for crack damage mechanism diagnosis. It can be used to trigger micrographs of the corresponding damaged surface area on the specimen.

y (kHz)

y (kHz)

Aston University

Content has been removed due to copyright restrictions

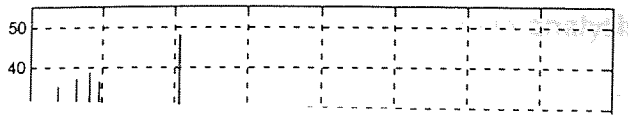

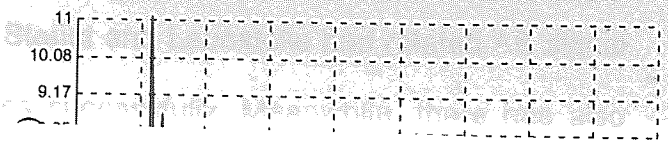

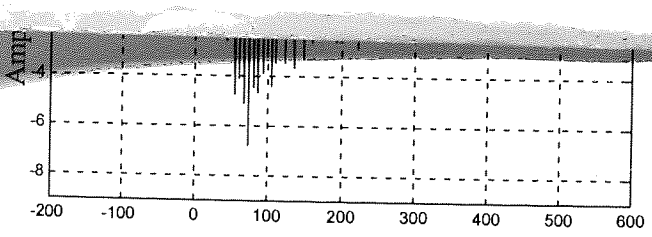

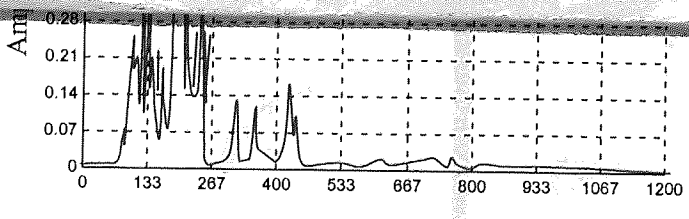

Time (μs)

Frequency (kHz)

(d) test4

Figure 2-3 Waveform and FFT for different cases simulating crack events.

(a) Unmounted sensor. (b) Sensor mounted. (c) Sensor mounted on the indenter, which is in contact with the surface of an Inox-N coating. (d) Real crack in a stainless steel doped with a nitrogen coating.

(Stebut, 1999)

Using the frequency domain analysis, Stebut and Lapostolle had related AE signal to the crack growth in coating samples successfully. Meanwhile, there has also been outstanding AE research conducted in time domain. (Anderson and Delacy, 1972, Owston, 1972, Clark, G, 1992, and Wevers, M., 1997). Wevers studied the tensile fatigue loading of CFRE cross-plies with different epoxies/matrix interface properties. Filters for AE peak amplitude (PA), Ringdown counts (RDC), event durations (ED) were applied in this study. Fatigue tests were performed on $(0^0_2,90^0_2)_s$ specimens having AS-4 carbon fibres, which are two layers structure with the lay-up sequence at 0 and 90 degree. They were characterised by four different levels of surface treatment: untreated 0% SST (commercial standard surface treatment), and treated 10%, 50%, and 100% SST. Toughened epoxy HG 9106 was used as matrix. The distribution graphs of the peak amplitude of different specimens are given in Figure 2-4.

Figure 2-4 Distribution graphs of the PA of AE signals during the fatigue tests a: untreated fibre, b: 50% treated fibre, c: 100% treated fibre; d: 10% treated fibre (Wevers, 1997)

The number of AE signals is the highest for the intermediate treatment level of 50%, apart from untreated fibre. A correlation with the result was obtained by microscopic studies of the edges of the fatigue specimens. Wevers indicated that the AE signals with a high PA are caused by unstable matrix cracks: a transverse crack immediately spans the entire 900 ply. This phenomenon is different from many other carbon/epoxies. (Dvorak and Laws, 1987, and Lafarie-Frenot, 1991).

The above studies show that AE has been used not only to determine the onset of damage growth and to observe the number of AE signals for the different materials and loading conditions, but also to obtain additional information on different damage types. It is evident that AE, independently or jointly with other techniques (C-scan, Microscopy, Deply, Penetrant radiography *etc*), is a valuable detection measure for collecting material damage information.

2.3 Application of Neural networks – Thinking with an artificial brain.

Advances in neuroscience and in computer science have given insight in neural network models for complex problem solving. It has been proved that neural networks can adjust dynamically to environmental variations, infer general rules from specific examples and recognise invariance from complex high-dimensional data (Rumelhart *et al*, 1986, Lippman, 1987, and Flood, 1994). Therefore the paradigms of ANN application can be found in pattern recognition, system identification, and many other empirical and theoretical studies and in many

different industries. A list of some of the applications mentioned in the literature is as follows:

1) Aerospace. There are applications of neural networks in real-time prediction of the unsteady aerodynamics to enhance the aircraft control (Faller and Schreck, 1995), in 3D dynamic reattachment modelling over a broad parameter range (Faller, *et al.*, 1995) and in predicting rotor system component loads during high-speed manoeuvring flight (Hass, *et al.*, 1995). General speaking, the applications of ANN in aerospace practices are for providing reference to pilots during the flight rather than directly controlling the manoeuvre. However, ANNs technically can be and have been applied to unmanned pilot outfits.

2) Robotics control. ANN approach has the potential for adding the robotic ability to learn, adapt and integrate information from multi-inputs. Therefore it can be implemented in most robotic tasks, such as task planning (Guo and Cherkassky, 1989, Arteaga-Bravo, 1990), control (Eckmiller, 1989), system integration (Miller, 1987, Josin, 1988), obstacle detection and avoidance (Kuperstein, 1988) and grasping and hand control (Bullock, 1990), *etc.*

3) Business. Business is a diversified field with several general areas of specialisation such as accounting or financial analysis. Almost any neural network application could be used to advantage in one business area or another. Hutchison and Stephens (1987) had applied ANN into Airline

Marketing Tactician (AMT) system for monitoring and recommending booking advice for each departure. In planning and scheduling, Hopfield *et al* (1984, 1990) also described an ANN algorithm, which has been based on Travelling Salesman Problem. In Financial analysis, NeuralWare was able to develop a neural system, which performed 5 percent better than professional analysts. (Ghosh *et al*, 1988)

4) Control. There are many applications of ANN in process control. Underneath the apparent complexity, there are really only five generic designs now used in neurocontrol (Warbos, 1990). They are applications of supervised control (Widrow, 1963), direct inverse control (Miller, 1990), neural adaptive control (Narendra and Boskovic, 1990, Thapa, 2001), back propagation of utility (Jordan, 1989), and adaptive critic methods (Barto, Sutton, and Anderson, 1983).

5) Structure engineering and monitoring. There are quite a few reports concerning the utilisation of ANN in structure engineering and structure monitoring. (Barai, 1996, Pandey and Barai, 1995, Szewczyk, *et al*, 1994, Wu, *et al*, 1992). The writer found the ANN applications within this area are especially inspiring to this study due to the similarities in research nature. In Barai's study, he presented an application of multi-layer perceptron in the damage detection of steel bridge structures. There was an extensive neural networks investigation carried out on the problem of 21-bar truss bridge as shown in Figure 2-5.

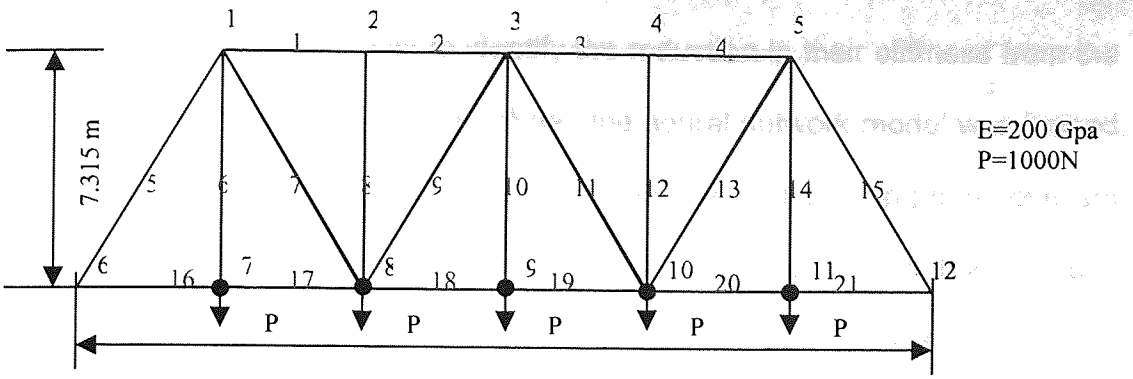

Figure 2-5 Bridge-truss configuration

A multi-layer neural network was constructed using 5 vertical displacements at the nodes (from node7 to node11) as inputs and the stiffness (represented by cross-sectional areas a1 to a21) of 21 truss-bars as output. A topological diagram of the neural network model is given in Figure 2-6.

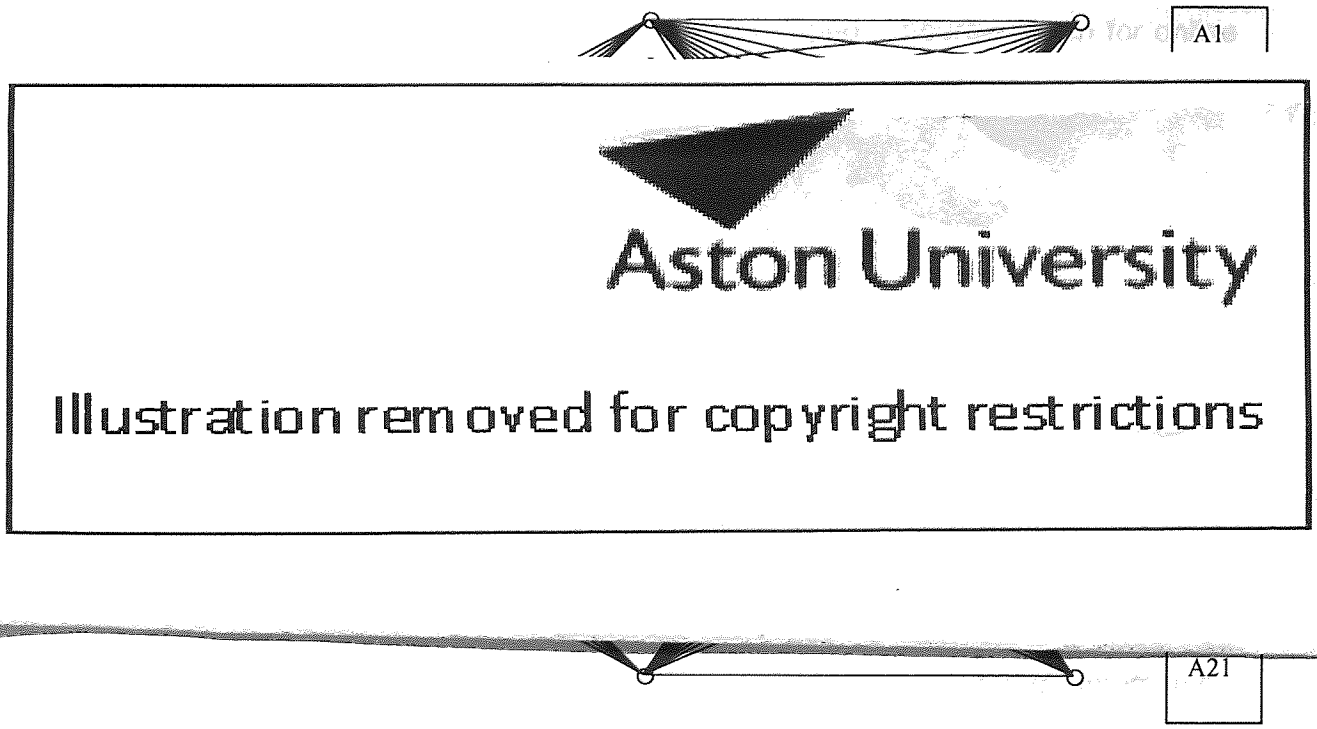

Figure 2-6 ANN model for damage detection of bridge structure (Barai, 1996)

The purpose of the exercise was to identify the reduction in their stiffness from the response data (vertical displacement). When the neural network model was trained, it then can calculate the cross sectional area of each truss according to a novel set of displacement at loading nodes. The outputs of the ANN model were quite promising. Compared with FEM results, trained networks had provided reasonable calculation (4% average error) of cross sectional areas of all the members for the testing patterns (Pandey and Barai, 1993). The engineering significance of the investigation is that measured data at only a few locations in the structure was needed to train the network for the identification exercise.

6) Other applications. There are also successful stories of ANN implementation in other industries. Susic and Grabec (1994) developed a neuro-system for online estimation of the roughness and hardness parameters of surfaces involved in sliding friction process. The recognition reliability for placing given cases in correct classes was found to be greater than 94% for the majority of the experiments. Patrick (1990) discussed issues of sonar signal processing with neural networks. ANN has been exploited to process Sonar signals in beam-forming and bearing estimation based on its information extracting capability. There are also applications in medical diagnosis (Blumenfeld, 1990), data communication (Alston and Chau, 1990), and data flow compression and fusion (Anthony, 1990) *etc*, using neural networks. Jones and Sirkis (1995) have developed a method of determining the location and extent of impact induced damage in isotropic plates.

Statistically, the mining of ANN application literature yields a rich harvest. The results are high in quantity as well as diversity. Those successful industrial applications embody the versatility and competence of ANN. Based on its high performance and capacity, ANN is an attractive approach to handle problems of composite material impact damage detection and render reasonable and effective solutions in this particular study.

2.4 Other studies on impact damage detection – Bringing grist for the mill

The studies on impact damage detection can be catalogued as damage characterising study (Philippidis, 1998 and Greenhalgh, 1996, *etc*), new NDT approaches (Claus, 1985, Irving, 1997, Seo and Lee, 1999), damage source locating (Jones and Sirkis 1995), smart materials and damage *on-line* diagnosis (Bleay, 2001), signal processing (Staszewski, 2001) *etc*. Inspiring ideas and practical exercise were suggested by these literatures. In Seo and Lee's study, damage detection of CFRP laminates was conducted using electrical resistance measurements and neural networks. The researchers investigated the electrical resistance change as a damage parameter for fatigue damage to be associated with the degradation of residual strength and stiffness. Neural networks correlated electrical resistance with fatigue damage by learning the electrical resistance, stiffness and fatigue cycle data. ANN results showed good agreement with the experimental results. On the other hand, Irving has also undertaken a similar study. In Irving's research, in-plane and out of plane electrical conduction processes in CFRP composites were studied to associate damage detection with electrical

potential. There are also fundamental issues, which have arisen in sensor studies. Staszewski (1996, 1997) worked on fail-safe sensor distributions for damage detection. Genetic Algorithms (GAs) has been used in the study to render an optimised or near-optimal sensor distributions for fail-safe damage detection. Previous studies also covered areas of theoretical issues such as the dynamics of impact events (Abrate, 1998) and numerical modelling of impact damage (Davis, 1994). As to the location studies, Worden *et al* (2001) examined and validated a damage location method on a stiffened panel. In order to detect and locate damage, natural frequencies and mode shapes were extracted for each level of damage and model strained-energy damage indicators were computed along the stringer at each level of damage. A 15 mm saw cut was detected and located over a 725 mm stringer. Shaw *et al* (1995) demonstrated location of impacts on a polymer matrix composite panel by using a neural network to process the outputs of embedded fibre optical strain sensors. It was a successful example of neural network determining an impact's location.

An interesting phenomenon is that there are, more or less, increased numbers of ANN applications in the damage detection study. (Sung, *et al* 2000, Lansing, *et al* 1999, Doyle, *et al*, 1998). In the meantime, the writer noticed that considerable literatures have investigated the impact behaviours. Li, *et al* (1999) has studied the impact behaviour of elastoplastic sphere against a rigid wall. Li's work is illustrated in the Figure 2-7. Finite Element Method (FEM) is a major weapon in this sort of

researches. Similar research has also been undertaken by Hardy (1971), Thornton (1997), and Vu-Quoc, (2001).

The aforementioned goals of the project are to analyse the impact damage severity and develop a method to locate the damage source. It may be the first intuition to know that methods like FEM are incapable of pinpointing damage location due to their nature. However, question can still be asked as "should the FEM or ANN approach be used in damage severity analysis?" A decision was required at early stage in the research to determine a suitable modelling algorithm.

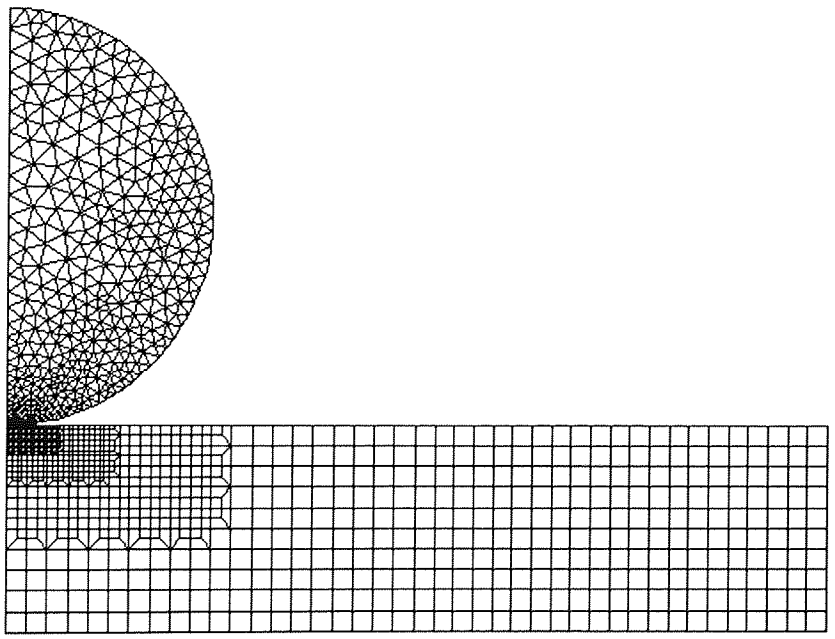

Figure 2-7 Physical model and finite element mesh

2.5 A brief discussion of modelling algorithm

In the sense of system identification, a system can be simulated and represented through a mathematical model, which imitates the performance of its physical counterpart. The model will then be able to manipulate data and send out the desirable outcome after the identification. There are several potential candidates that fit the task. According to the previous research, there are two major methodologies in the impact damage study, namely Finite element analysis (FEA) and Artificial Neural Networks (ANNs). They each have their own strength and limitations in a certain application. The mechanism of FEA is to discretise the structure into an assembly of subdivisions called elements, which are considered to be interconnected at joints, know as nodes (Kwon and Bang, 1996). After the problem has been subdivided, the governing equations for each element are calculated and then assembled to give the system equations. The element equations may be found in a variety of ways, but it turns out that the equations of a particular type of element for a specific problem area have a constant format. This property helps to simplify the procedures. Thus, once the general format of the equations of an element type is derived, the calculation of the equations for each occurrence of that element in the body is straightforward. It then is simply a question of substituting the nodal coordinates, material properties and loading conditions of the element into the general format (Fagan, 1992).

FEA is good at conducting detailed modelling, which describes details using specified values. It provides a solution to the problems in a quantitative manner (e.g. the detailed stress calculation on every single element). ANNs, however, is an information generalisation algorithm. It extracts the feature message out of the data flow through the training. Being different from FEA, ANNs provides solution of the problems in a qualitative manner. Rather than calculating every single point of the sample panel, it derives the information from measured data. It gives out prediction based on generalisation. Using ANNs algorithm, it is possible to set up a mathematical criteria to distinguish different properties or a numerical response to reflect physical events of impact damage. Therefore, it is clear that FEA would be the first choice if the study aimed to reveal the mechanism and behaviours of the impact damage or to discuss the dynamics between impacting parties. Otherwise, if the study was based on probing the impact damage detection in a qualitative way, the ANNs algorithm will prevail. Of course, the difference between these two methods may not necessarily lead to the contradiction or conflicts. Rather, ANNs and FEA can supplement each other from case to case. In this study, however, ANNs became the dominant approach to conduct the research according to the objectives of this project. Apart from the previous reasons, the potentiality to use ANNs in hardware for online implement is also a vital factor helping to justify the decision. Nominated in this study, ANNs and AE technique has been proved a good combination for modelling the process of the impact damage detection.

2.6 Conclusions

Chapter III reviewed the methodologies cited in this study. An introduction to previous study was given to describe the current and earlier research within the area. It inspired the researcher of this project to focus and develop the right approaches and methodologies to complete the task. Systematically, the literature review has been given on AE application, ANN application. Current studies of impact damage detection have been also reviewed.

From the literature survey, the versatility of ANNs and advances of AE technique were clear. Finally, this chapter ended in the comparison between FEA and ANNs, which justified and consolidated the writer's methodology decision.

Chapter 3 Fundamental knowledge

"If I have seen further, it is by standing on the shoulders of giants"
(Isaac Newton, Letter to Robert Hooke, 1676)

3.1 Introduction

There is an old Chinese saying "Lofty towers are all built up from solid ground." Likewise, although an engineering application appears in a kaleidoscopic fashion, there are always rudimentary laws behind it. This chapter therefore introduces the fundamental knowledge involved in impact damage detection study. It starts from basic acoustic emission. The theorem of ANNs and impact dynamics are introduced next. Knowledge of system identification is also studied as complementary.

3.2 Fundamental of AE

Acoustics Emission (AE) is the term used to describe the resulting stress waves when strain energy is released rapidly due to the occurrence of microstructural rearrangement in a material (Pollock, 1989). In the case of an impact damage event, the material structure subjected to the impact load. From the impact site, the impact stress yields a structure transformation, such as deformation and cracking *etc*, and acoustic emission waveforms are also generated. They propagate in every direction within the material until the whole component is full of such "sound". The frequencies of AE signals are usually in the range 150-300 kHz, which is well above the frequency of audible sound. The AE is a form of energy and it is also a

form of sound wave. Unlike that of electromagnetic radiation, the spreading of AE or sound in general sense requires medium (solid, liquid, or gas) in which to travel. The speed of AE propagation is a variable influenced by its Young's modulus and the density of the medium as in the form of $V = \sqrt{E/D}$, where E is Young's modulus and D is density . The production, propagation and detection of AE waves are generally related to the setting up of the oscillations. Detected AE have practical application in the non-destructive testing of structures and components. It is possible, in principle, to obtain information about the nature and the severity of changes occurring at defects, which may be "audible" but "invisible" since the scenario occurred underneath the surface.

The idea of utilising sound or AE is not new (Sagoo, 1987). Early observations of acoustic emission in metals were made by tinsmiths, who noted "Tin Cry", or twining, during the deformation of tin. In the 1950s, Joseph Kaiser and his co-workers in Germany are generally credited with initiating the present effort in acoustic emission. Since then considerable time and effort has been expended by researchers in producing a comprehensive and solid foundation. Many studies such as of Schofield (1958), Tatro (1959), and Liptai (1972) are available for a detailed background to the theory of acoustics emission.

3.2.1 Terminology

There are some technical terms to be addressed beforehand. They are:

1) AE signal start: the beginning of an AE signal as recognised by the system processor, usually defined by an amplitude excursion exceeding threshold.

2) AE signal end: the recognised termination of an AE signal, usually defined as the last crossing of a threshold level.

3) AE signal duration: the time between AE signal start and AE signal end.

4) AE signal rise time: the time between AE signal start and peak amplitude of that AE signal.

5) Dead time: any interval during data acquisition when the instrument could not accept new data for any reason.

6) Floating threshold: any threshold with an amplitude established by a time average measure of the input signal.

7) Hit: any signal that exceeds a threshold and causes the data logger to accumulate data.

8) Processing capacity: the number of hits that can be processed at the processing speed before the system must interrupt data collection to clear buffers or otherwise prepare for accepting additional data.

9) Processing speed: the sustained rate (hits/s), as a function of the parameter set and number of active channels, at which AE signals can be continuously processed without interruption for data transport.

10) Voltage threshold: a voltage level on an electronic comparator such that signals with amplitudes larger than this level will be recognised. The voltage threshold may be user adjustable, fixed, or automatic floating.

Only the terminology that is appropriate to the project is given here. They are the important parameters and coefficients in the project experimental tests. The ASTM Standard: E610 Terminology Relating to Acoustic Emission gives more details. (See Appendix E)

3.2.2 Physical features of AE signal

The original AE waveform located at a source is usually a relatively simple, broadband pulse. But after the transmission through the internal material structure, the detected signal is much more complex, being largely shaped after the waveform propagates from the source to a sensor. Important aspects of wave propagation are wave modes, wave velocity, attenuation, reflections, multiple paths, and reverberation. These play an important role in setting up a valid and optimum test, and they are also important in the interpretation of the signal waveform detected by an AE device.

1) Wave mode and Wave velocity

Wave velocity is particularly important for source location because source location algorithms use the wave velocity in the computation. When stress waveforms are emitted, there are different wave modes that travel at different velocities. These velocities depend on the material structure and properties, such as the thickness of a structure, and the elasticity of a material. The velocity of a group waveform can be measured by putting a wave pulse into the structure and measuring the time it takes for the wave to arrive at a distant sensor. Because of the complexity of wave velocities, careful attention needs to be paid when measuring the velocity. Otherwise an erroneous result could be produced in source location.

2) Attenuation

As a wave travels, its peak amplitude diminishes. This means that it will be harder to detect sources at greater distances from the sensor. The attenuation of AE waveforms is a function of three important factors: 1) geometric spreading of the wave front, 2) absorption or damping in the propagating medium, and 3) "leaking" of the wave energy into adjacent media, such as containing fluids.

Attenuation measurements are routinely made as a preliminary to AE testing, in order to assist in planning or validating sensor placement and operating frequency. It may cause little problem in small structures such as laboratory specimen. But, as the structure becomes larger, it then becomes a sensitive issue as attenuation may affect the fidelity of AE signals. Attenuation applies not only to the AE signals that

one is trying to detect but also to the background noise that is always present. This fact can be turned to an advantage to deduce noise from real damage signals.

3) Reflection and Multiple Paths

Waves are reflected at structural discontinuities and boundaries. The amount of energy reflected depends on the geometric and material mismatch at the reflecting boundary. Typically, AE waveform will propagate within the structure through different paths as shown in the Figure 3-1 below. Due to the varied length of paths, AE waveform can be break into a quicker arrival section and a slower delayed section.

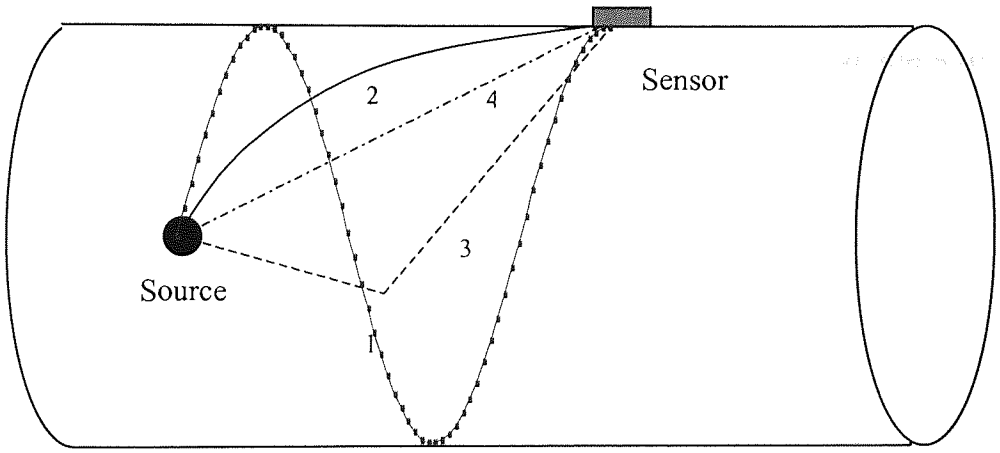

Figure 3-1 Possible paths from source to sensor of cylinder

1 ---Long path on surface of the cylinder
2 ---Short path on surface cylinder
3 ---Long path inside cylinder (with a reflection)
4 ---Short path inside cylinder

For source location, analysis utilises only the first part of AE waveform. In contrast, mainstream AE technology accepts the waveform in its entirety, for example it was applied in damage level discrimination of this project.

One way of understanding the complex nature of the AE signal received at the sensor is to think of the wave as made up from successive arrivals via these multiple paths. Thus the final shape of the signal is interwoven with ringing of the sensor along with multiple paths and reflections within the structure.

5) Reverberation

The test piece, subjected to AE, acts rather like bell: the wave spreads out, reflects off the surfaces and bounces around within the specimen until the whole structure is reverberating with acoustic energy. Then, the energy slowly leaks out through the specimen grips or is absorbed in the test piece and the reverberation decays away. This is the reason for the fast rise and slow decay appearance of the typical AE burst-type signal on an oscilloscope. The measured AE parameters are strongly affected by the reverberating nature of the process and damping in the material. In metals, signals often have durations of several milliseconds. While in composites, they usually only have durations of only a fraction of a millisecond as the materials quickly absorb and "digest" the AE energy.

6) Background Noise

Successful AE testing relies on being able to detect the relevant signals above the background noise. Background noise problem range from negligible to severe, depending on the test conditions.

The sources of noise fall in to two main categories: electrical and mechanical. The electrical noise source generally is generated from the laboratory facilities such as "White Noise", which is natural and unavoidable noise and sets the ultimate limit to achievable sensitivity, "Ground Loop Noise" which is caused by improper electrical grounding of system and structure, and "Other Noise" which is the noise from electromagnetic radiation sources inside the equipment as well as environmental electromagnetic radiation outside. The mechanical noise sources include "Test Machine Noise" which occurs in laboratory testing and "Plant Operating Noise" when the testing is undertaken on site. A lot of "Other Noise" such as all types of frictional processes, mechanical impact and human activity are also in the category of mechanical noises.

Techniques are used for overcoming noise problems that can occur in AE testing. Sometimes the problem is eliminated at the source. Sometimes it is addressed by simple or refined techniques of instrumentation selection, setup or data analysis. These techniques have allowed the employment of AE in a series of increasingly difficult test environments.

3.2.3 AE parameters and conventional methods for signals analysing

AE signals detected by transducers are a series of waveforms. Practical solutions are to use some parameters to define each AE event. The following parameters are mostly used to characterise AE signals:

(a) rate of AE counts;

(b) number of AE emissions;

(c) amplitudes of AE hits;

(d) frequency of AE signals;

(e) energy of AE event.

Figure 3-2 and Figure 3-3 give the brief illustration of the parameters mentioned above. The simplest way of characterising a pulse or series of pulses produced in an acoustic emission experiment is called 'ring-down' counting, which counts the number of times per second that the amplitude exceeds a preset voltage and results in a simple number to characterise the signal. It should be noted that this simple approach relies on pulse counting, or in some cases, the measurement of averaged signal amplitudes. Other parameters, such as amplitude, count rate, total count, can also be associated with damage mechanism. Since AE is attribute to the release of energy in the material due to changes in the state of stresses, measurement of the energy content of the AE signal is believed to be an indication of this energy release (Williams, 1980). A basic circuit for determination of the energy is shown in Figure 3-3. It consists in measuring the area under the envelope of the square of the signal using a digital integrator.

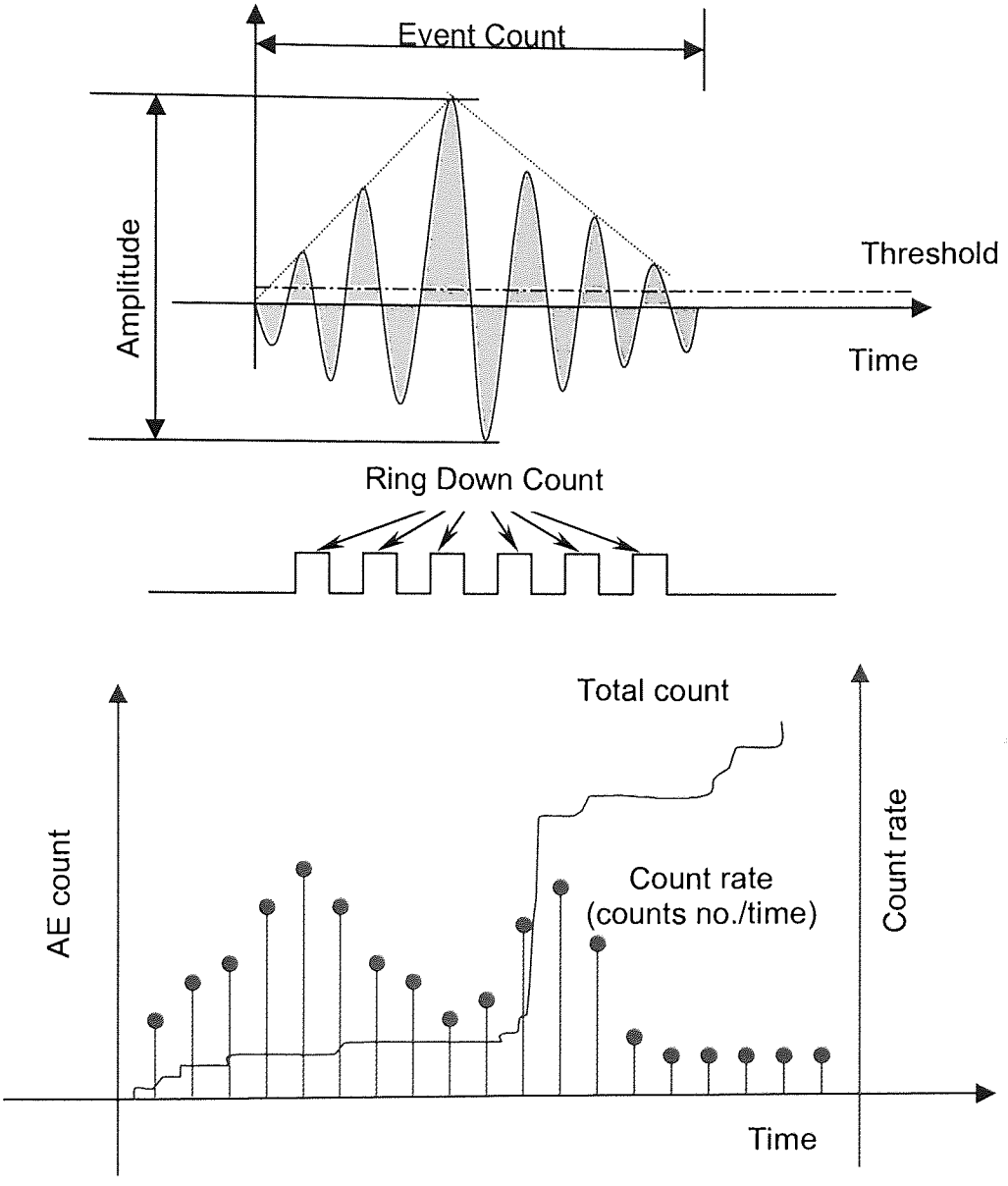

Figure 3-2 Ring down counting and other parameters of AE event

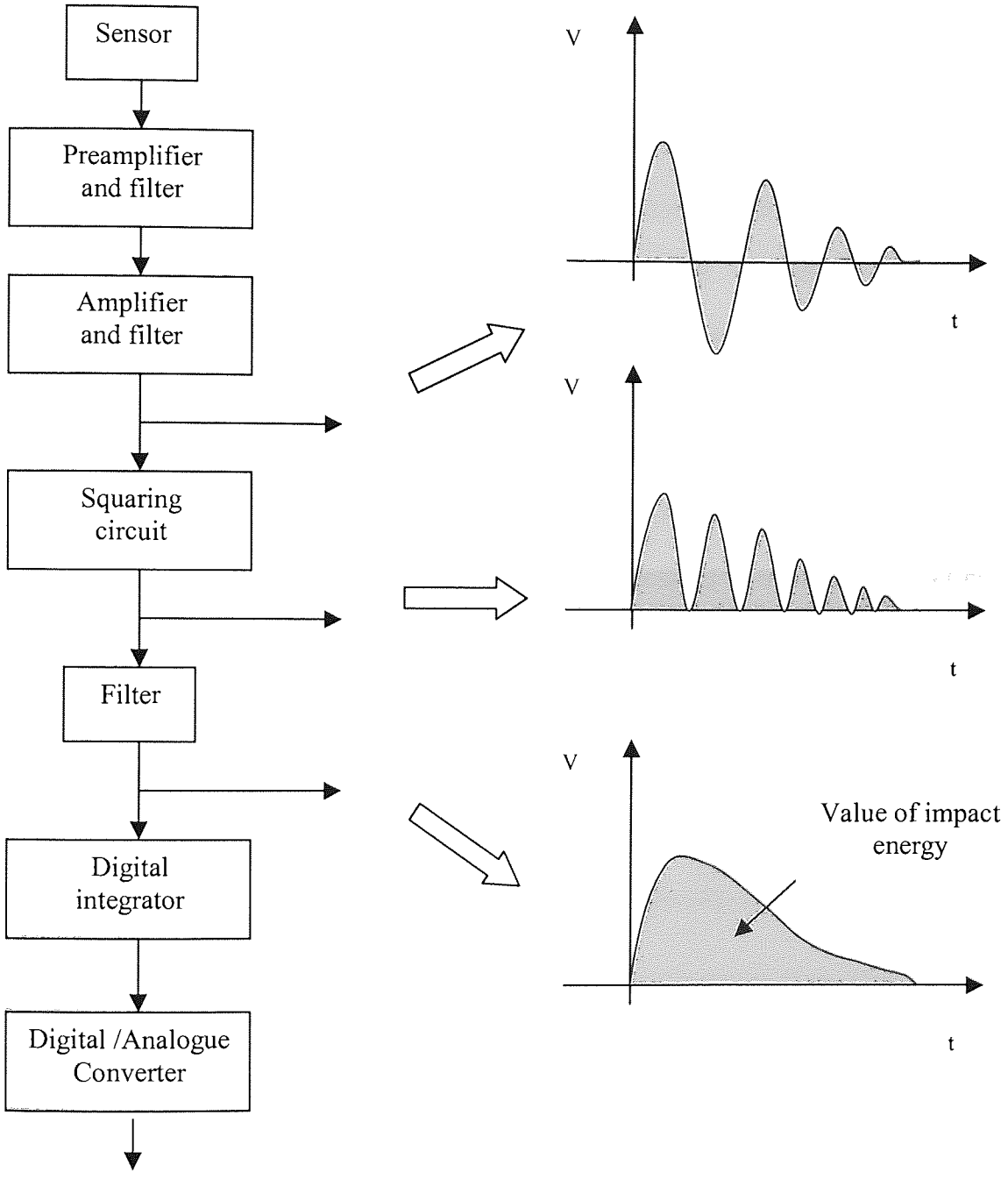

Figure 3-3 Block diagram for measuring the energy of AE signals

At this stage, it must be noted that when a stress wave propagates through a testing sample or a structure it is subject to modification due to discontinuities: the place of damage for example, or from reflections at free surface (particularly where there are physical changes in the specimen geometry). As a result, the form of the acoustic emission as recorded in the experimental equipment (which has to be placed on a surface) may well differ from the form of emission generated by deformation or a cracking process within the sample. Therefore, AE signals in return can reflect the geometry of the structure of the testing sample.

Time and frequency domain analyses have both been reported on investigating AE signals. In time analysis, perhaps the most commonly used technique is ringdown counts and count rate (Bassim, 1981). These are related to the cumulative damage and the rate of occurrence of the damage respectively. Figure 3-2 illustrates the procedure and shows the methods of evaluation of the total count and count rate of an AE signal. AE has also been used to study plastic deformation, fracture and crack propagation, where Dunegan *et al* (1968) and o thers have proposed a relationship between the total count N_t and stress intensity factor K_I, given by

$$N_t = AK_I^m \tag{3-1}$$

where m and A are constants that depend on the material.

Despite its wide utilisation, ring down counting is only directly related to the physical characteristics of the event at the transducer. It is in fact an indirect

relationship to the nature of emission source. Another approach in time domain analysis is the measurement of the energy of the acoustic emission signal. The whole procedure is shown in Figure 3-3, which consists of measuring the area under the envelope of the square of the signal using a digital integrator. In this project, impact energy has been associated with damage severity to indicate the damage level of an impact event. The mechanism of which is to be introduced in the succeeding chapters.

Another important approach for AE analysis is frequency analysis (FA). It has been widely applied to identify physical mechanism in materials qualitatively (Simmon and Clough, 1980). The basic principles of FA are to transform the signal using FFT, low or high filters so as to reveal the characteristic frequencies of the sources. Presently, however, the use of such an analysis is limited to comparative studies due to attenuation, reflections and mode conversion as well as the restricts from the transducer and electronic system. This project however wasn't a study of impact damage behaviour and mechanism using FA. However, FFT was implemented during the impact force data collection in damage level discrimination transformed.

3.2.4 Advantages of acoustic emission

To create a better understanding in the initiation, growth, and interaction of the different damage types, damage monitoring during mechanical testing can be very

helpful. Different non-destructive test techniques can be used to measure the amount of damage. The techniques often used are: edge microscopy, replica technique, penetrant enhanced radiography, ultrasonic C-scan and acoustic emission. In Table 3-1, the possibilities of these techniques to assess damage in composite materials are summarised. This table clearly indicates that acoustic emission is the only possible technique to detect all the mentioned damage types. However, the distinction between the AE signals coming from different damage type is not straightforward (Wevers, 1997). This is the main reason why acoustic emission techniques are often only used in detecting onset of damage or the severity of damage in a composite material.

Table 3-1 Overview of the different techniques used in composites damage

	Acoustic emission	Ultrasonic C-scan	Penetrant radiography	Microscopy
Fibre fracture	Possible	No	No	No
Delamination	Possible	Yes	Yes	At the edge
Matrix cracking	Possible	No	Yes	At the edge
Debonding	Possible	No	No	No

Generally speaking, there are three mayor advantages of AE technique over other NDT. 1) The principle of the AE damage detection technique is that the defect makes its own signal as it grows and a remote sensor can detect the defect-derived signal. In other words, it is non-localised (Nichols, 1976). This is fundamentally different from most Non-damage Technology (NDT) methods. 2) It is

physically easy to scan a large structure using AE probes. This ability is in direct contrast to alternative methods, such as ultrasonic or radiography. 3) Another reason why AE is particular attractive is that it offers major cost savings and added effectiveness to NDT. These advantages also sum up the reasons why AE was the final choice in this study. Two case studies in subsequent chapters will illustrate its application.

3.3 Fundamental of artificial neural networks (ANNs)

Artificial Neural Networks (ANNs) have been described as 'computers that think'. This description is based on the phenomenon that ANNs can remember, generalise and extract feature information out of a problem, like its biological counterpart __ human brain. The name of neural network thus derives from these similarities. However, describing the technology this way has no intention in leading to unrealistic expectations and discrediting an important and valuable engineering tool. For years, ANNs have been applied in a vast range of industries and have earned a reputation for solving problems in a highly qualified and efficient fashion. The neural networks model typically consists of a number of nodes in an input layer and any number of 'hidden' node layers to an output node layer (Thomas and Flockton, 1994). The behaviour of a neural network is therefore defined by the way that individual computing elements are connected and by the strength of those connections or weights. For a given neural network, the optimum set of weights is established by training the network. The training is carried out by

passing a set of examples of input-output pairs through the model and adjusting the weights in order to minimise the error between the answer that the network gives and the desired output (Swingler, 1996). Once the weights have been set, the model internal variables are fixed and can produce output responses to input stimulation, which were not included in the training data. However, a neural network does not work simply like a black box solution into which data can be poured in and an answer will emerge automatically. The performance of ANNs will, to a large degree, depend on how much knowledge of the problem domain can be incorporated into the design and training of the neural network.

There are different types of neural network models, which are based on the definition of transfer functions, classification of network architectures, and training mechanism, *etc.* In this section, a brief review will introduce what ANNs are, how ANNs function and which ANN is which. However, the amount of the theory is deliberately kept to a minimum due to the length of the thesis. The reader should refer to the textbooks and technical papers (Bishop, 1995 and Haykin, 1994 and 1999) for further information.

3.3.1 Brief historical background

The easiest way to describe the concepts of ANNs is from a historical point of view. Artificial neurons as information processing devices were first proposed more than fifty years ago (McClloch and Pitts, 1943). Follow this early work, the pattern

recognition capabilities of preceptrons, in which the neurons are arranged in layers, were investigated both theoretically and experimentally throughout the 1950s by Rosenlatt and his co-workers, mainly in the US. As shown in Figure 3-4, a neuron computes a weighted summation of its n inputs, the result of which is then thresholded to give a binary output y, which is either +1 or –1. The neuron assigns input patterns, represented by the vectors of numbers $x=(x_1, x_2, \ldots, x_n)$, either to class A (in the case y is 1) or class B (in the case y is -1). Thus

$$y = f_h(\sum_{i=1}^{n} \omega_i x_i) \qquad \textbf{(3-2)}$$

where y is the neuron output (±1) and f_h is a hard-limiting function, also known as transfer function or activation function, which gives an output of +1 whenever $\sum \omega_i x_i$ is positive or an output of –1 if negative.

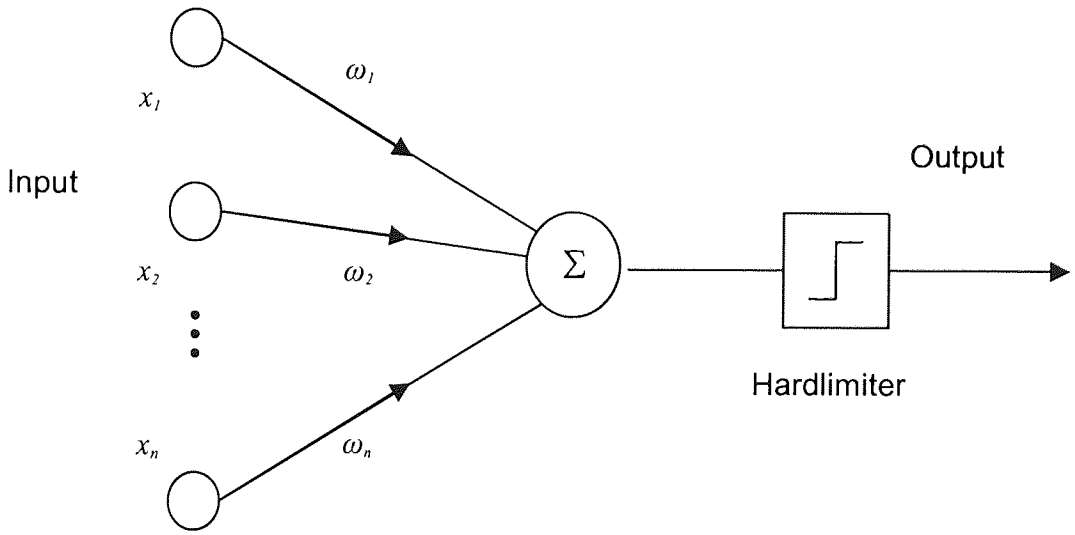

Figure 3-4 Schematic diagram of an artificial neuron

In the sense of neural networks, learning consists of adjusting the weights ω_i (parameters of neural network) so that the neuron performs the classification tasks correctly. Using a number of neurons operating in parallel, multi-class problems can also be solved. By analogy with neurobiology, the weights ω_i here are known as synaptic weights. This model, however, represents a gross over-simplification of biological neural networks. The model of Figure 3-4 is a basic perceptron model.

In the late 60s, the single-layer perceptrons were replaced by more complicated multi-layer perceptrons, which are more capable of pattern recognition. A multi-layer network is basically two or more layers patched together. There is a necessity for a learning rule to connect different layers. The lack of a linking algorithm had stalled the development of neural networks for more than a decade before a learning algorithm was developed. As a result, neural networks have only become firmly established over the last twenty years. Applications of ANNs were promoted in 1980s and 1990s due to the contribution of sharply increased computation power.

3.3.2 The strength and advantages of neural networks.

In computing terms, ANNs have a unique set of characteristics. They are not "programmed", instead they are trained by being repeatedly shown large numbers of examples for the problem under consideration. As a result, they can provide

good results in relatively short time scales, which usually needs a great attention on data collecting, the pre-processing, and the network design.

The key features of ANNs can be summarised as follows:

1) Learning from experience. ANNs are particularly suited to problems whose solution is complex and difficult to specify, but which provide abundance of data from which a response can be learnt

2) Generalising from examples. A vital attribute of any practical self-learning system is the capacity to interpolate from a previous learning experience. With careful design, a neural network can be trained to give the correct response to data that it has not previously encountered.

3) Developing solution faster and with less reliance on domain expertise. ANNs learn by examples, and as long as examples are available and an appropriate design is adopted, effective solutions can be constructed far more quickly than tradition approaches, which are entirely reliant on experience in a particular field.

4) Computation efficiency. Training a neural network is computational intensive, but the computation requirements of a fully trained neural network for validation can be modest. In another sense, speed can be gained through parallel processing. The ANNs are intrinsically parallel structures.

5) Non-linearity. Many other processing techniques are based on the theory of linear systems. In contrast, neural networks can be trained to generate non-linearity mappings and this often gives them an advantage for dealing with complex, real world problems.

Comparing with traditional methods, ANNs can show the outstanding vantages as shown in the table as follows

Table 3-2 Comparison between traditional method and neural network

Traditional programming approach	**Neural computing approach**
• follows rules	• learns from data
• solution formally specifiable	• fuzzy rules
• not generalisable	• generalisable
• poor error tolerance	• copes with noise

Of course, it should never be assumed that ANNs is a panacea for all problems. It also has shortcomings. During the training, over training may occur in an ANN application. As shown in Figure 3-5, a curve fitted with too many parameters follows all the small details or noise but gives very poor interpolation on the test set. Similarly, an MLP with too many hidden units will generalise very poorly. Hence, the problem of defining the network architecture, in other word choosing hidden units, is very important. This is an issue of model order selection and depends on the complexity of the underlying function which the ANN is approximating.

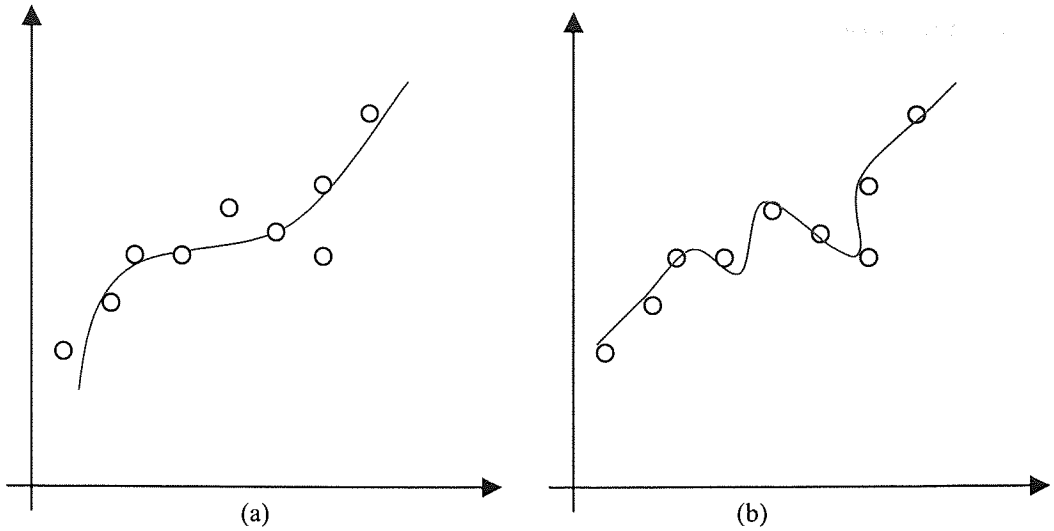

Figure 3-5 (a) A good fit to noisy data (b) Over-fitting. (O= training data set)

Nevertheless, the occurrence of over-fitting or over-training didn't necessarily prevent ANNs from being an outstanding engineering tool to solve real-world problems. It is evident from numerous successful neural network applications that, with careful design and sufficient training, ANNs can learn from the problems and render optimising results. In this research project, the ANNs and its attributes are exploited and successfully deployed for impact damage detection.

Different types of ANNs have been developed to suit different circumstances. The next subdivision reveals the mechanism and characteristics of several major ANNs used in modern neural computation.

3.3.3 Varieties of Neural Networks

1) Single layer perceptron

The perceptron was originally designed as a pattern classifier from a geometrical perspective. In a two-class pattern recognition problem, a separating line is expected so that pattern A can lie in one side of the line and pattern B can lie in the other side. As mention previously, preceptron can produce +1 to indicate pattern A, while –1 to indicate pattern B. The mechanism is revealed here. As shown in the equation below, the output of the perceptron y is given by

$$y = f_h(\sum_{i=0}^{n} \omega_i x_i) = f_h(\sum_{i=1}^{n} \omega_i x_i + \omega_0 x_0) \qquad x_0 = +1 \tag{3-3}$$

The goal is to find a set of ω_i such that y responds as +1 and –1 according to pattern A and B. In order to arrive at a weight set which solves the problem, the perceptrons use error feedback to adjust weights. It measures an error E at the output of the network and then to minimise the error E based on the gradient descent method. Figure 3-6 below illustrates how the gradient descent algorithm applying on error surface. It starts from an arbitrarily chosen weight vector ω_0 and computes the gradient of the error with respect to each weight i.e. $\partial E / \partial \omega_i$ for all ω_i. Next vector ω_1 then can be obtained by moving a small distance in the direction of steepest decent i.e. along the negative of the gradient. For an individual weight ω_i in the weight vector ω, the weight update $\Delta\omega_i$ is given by

$$\Delta\omega_i = -\eta \frac{\partial E}{\partial \omega_i} \tag{3-4}$$

η , known as the learning rate, is a small parameter, which sets the step size.

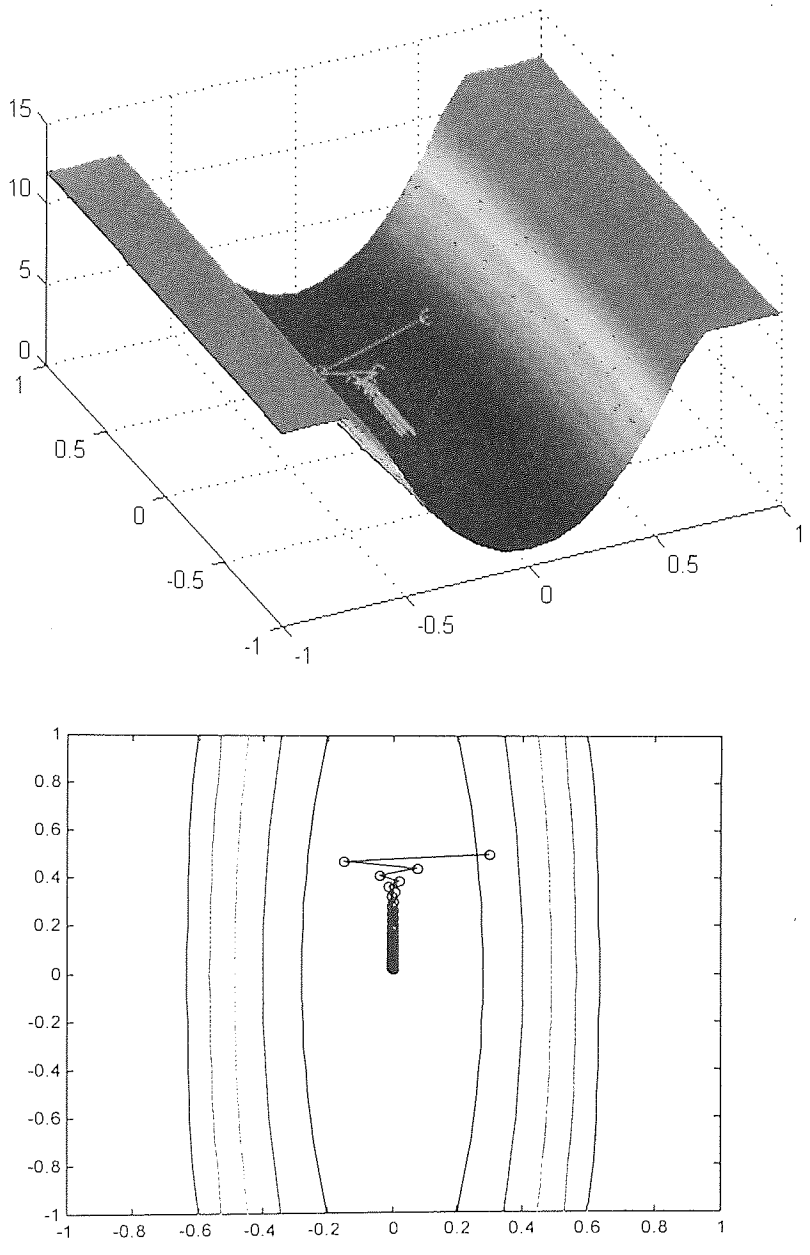

Figure 3-6 Approaching the minimum of Error surface using gradient descent algorithm

Learning is an iterative process whereby all the patterns in the training set are presented in turn several times. This procedure has to be reiterated until a set of weights is obtained which is able to minimise the error function E. On the other hand, the choice of learning rate η is vital as it can influent the speed of convergence, but overshooting and oscillation may occur if it is set too high. A typical example is given schematically in the Figure 3-7. In this example, two learning coefficients were preset before the calculation. The value of η_1 is a bit less than the critical point while η_2 is just above the critical point. The result is rather obvious. Case one gave a steady convergence that finally arrives at the local minimum on the error surface. However in the case two, the learning rate is deliberately set too high and eventually leads the trajectory running all over the error surface. Conventionally, reasonable value for η is set between 0.01 and 0.1.

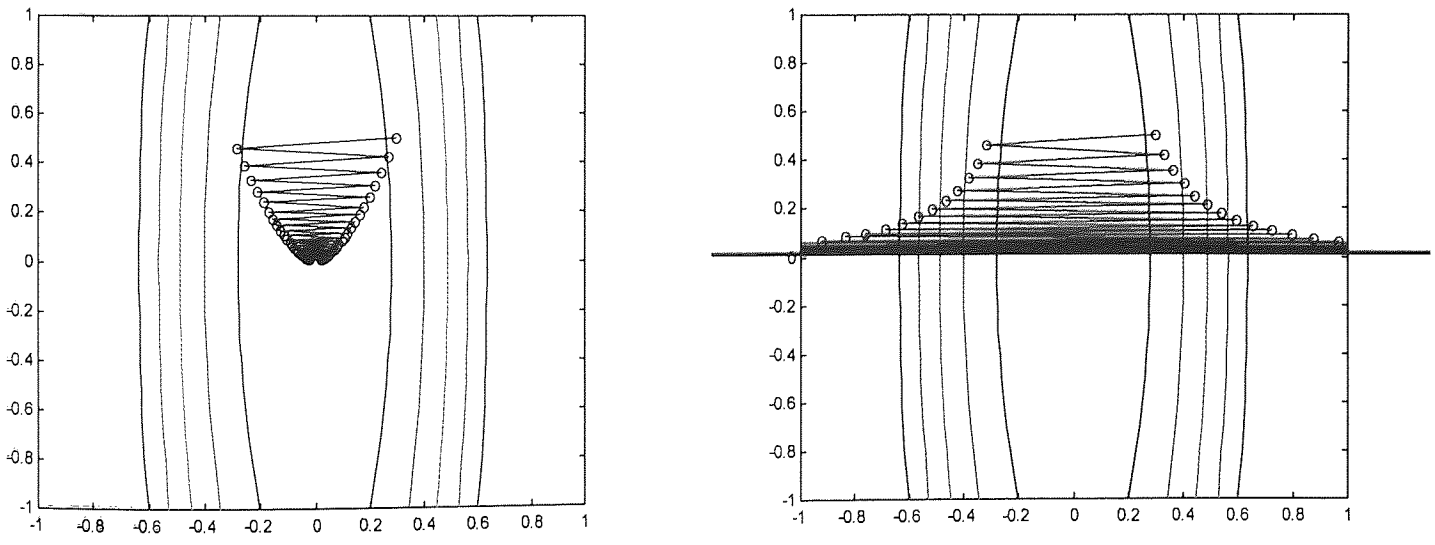

$\eta_1 = 2.31$ $\eta_2 = 3.60$

Figure 3-7 Impact of learning rate on the convergence.

The perceptrons is generally based on gradient descent to approach the minimum of the error function. Therefore it can successfully separate pattern A from pattern B in a linear case. However, if the class is not linearly separable, the perceptron model alone will not converge and the decision boundary oscillates between a number of positions. The inability of a single layer network to solve non-linear separation motivated the study of multi-layer networks. The concept of multi-layer perceptrons derived from the possible solution to the Exclusive-OR (XOR) problem. As shown in Figure 3-8, the outputs of the OR gate and NAND gate(both of which can be implemented by a perceptron), in the first layer, act as inputs to an AND gate(another perceptron) in the second layer. Thus the XOR function can be computed with a multi-layer architecture and this was recognised as a way round the shortcomings of single-layer perceptron.

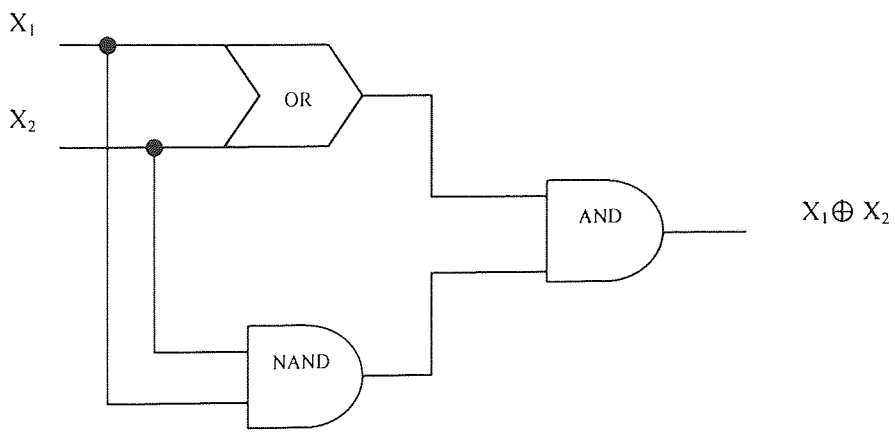

Figure 3-8 A possible solution to the Exclusive-OR problem

However, there was initially limited progress in the early days due to lack of a learning rule, which links different layers. Eventually, the new Back Propagation (BP) algorithm emerged and completed the missing piece of the jigsaw puzzle.

2) Multi-layer network with back propagation algorithm

Based on the work of previous researchers in this field, it is now generally accepted that the strength of neural networks lies in their ability to analyse and recognise complex patterns in real-world data. There is one characteristic of real-world data, which dominates all others: it is intrinsically noisy. With real-world data sets, it is not possible to classify all of the data correctly; there will always be regions of overlap in input space such that some of the pattern will end up on the wrong side of the decision boundary. In such context, the perceptron criterion shown in (3-5)

$$E = y^p - t^p \tag{3-5}$$

no longer makes sense and instead a sum-of-squares error function is used as follows:

$$E = \frac{1}{2}\sum_{p=1}^{n}(y^p - t^p)^2 \tag{3-6}$$

where y^p is the output of the network and t^p is the corresponding target value. In order to minimise E using gradient descent, it needs to be differentiatable with respect to every weight in the network. It is not possible to do this by using the neural structure that retain the hard-limiting and non-linearities as of the function

single-layer preceptron. They have to be replaced by new structure with continuous differentiable functions, which can respond linearly to small inputs and saturate to large inputs.

Figure 3-9 is a schematic diagram for an *I-J-K* (two layers) perceptron, for which input layer I has 3 input parameters, hidden layer J has 2 units while output layer K has 3 units. Bias weights are not shown on this diagram. As before, the bias weights represent an extra weight for each unit whose input is fixed at 1.0 but whose value is otherwise adjusted in exactly the same as the other weights in the network.

For a K-class problem, K output units are needed instead of just a single unit, which is for a 2-class problem only. The error function therefore becomes:

$$E = \frac{1}{2}\sum_{p=1}^{p}\sum_{k=1}^{K}(y_k^p - t_k^p)^2 = \frac{1}{2}\sum_{p}\sum_{k}(g\sum_{j}\varpi_{jk}y_j^p - t_k^p)^2 \qquad \textbf{(3-7)}$$

g here is the transfer function or activation function. In the (3-7), y_k is defined by

$y_k = g(a_k) = g(\sum \omega_{jk}y_j) = \frac{1}{1+e^{-\sum \omega_{jk}y_j}}$, where $a_k = \sum_{i=0}^{n}\omega_{jk}y_j$. Similarly, since $y_j = g(a_j) =$

$= g(\sum \omega_{ij}x_i) = \frac{1}{1+e^{-\sum \omega_{ij}x_{ij}}}$, where $a_j = \sum_{i=0}^{n}\omega_{ij}x_i$, (3-7) therefore becomes

$$E = \frac{1}{2}\sum_{p}\sum_{k}(g\sum_{j}\omega_{jk}g(\sum_{i}\omega_{ij}x_i^p) - t_k^p)^2 \qquad (3\text{-}8)$$

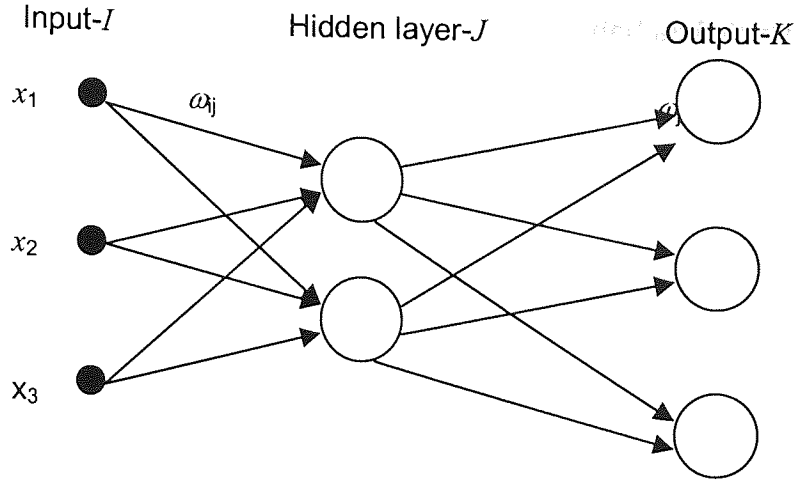

Figure 3-9 Layout of a 3-2-3 multi-layer perceptron

From the equation above, it is concisely demonstrated that E is now a continuous differentiable function of every weight since the transfer function g, the sigmoid function, can be differentiated. The calculation of the gradient of the error function with respect to each weight in the network (i.e. the $\partial E / \partial \omega_{ij}$ or $\partial E / \partial \omega_{jk}$ terms) only requires the application of the chain rule and some knowledge of mathematics. This gives rise to the error back propagation algorithm for updating the weights in a multi-layer perceptron. For a ω_{jk} weight, the minimisation of E by gradient descent can be expressed as

$$\Delta \varpi_{jk} = -\eta \frac{\partial E}{\partial \omega_{jk}} \tag{3-9}$$

While $\frac{\partial E}{\partial \omega_{jk}}$ can be expanded using chain rule:

$$\frac{\partial E}{\partial \omega_{jk}} = \frac{\partial E}{\partial a_k} \frac{\partial a_k}{\partial \omega_{jk}} \qquad \text{where } a_k = \sum_j \omega_{jk} y_j \tag{3-10}$$

The first of the two terms on the right-hand side is expanded as follows

$$\frac{\partial E}{\partial a_k} = \frac{\partial E}{\partial y_k}\frac{dy_k}{da_k} \tag{3-11}$$

now the terms can be worked out in turn. From (3-7), $\frac{\partial E}{\partial y_k} = y_k - t_k$ .As the transfer function here is the sigmoidal transfer function, that is $y_j = \frac{1}{1+e^{-a_j}}$ (where $a_j = \sum_{i=0}^{n} \omega_{ij} x_i$). Then

$$\frac{dy_k}{da_k} = \frac{d}{da_k}\left(\frac{1}{1+e^{-a_k}}\right) = \frac{e^{-a_k}}{(1+e^{-a_k})^2} = y_k(1-y_k) \tag{3-12}$$

Now combine these results with the fact that $\frac{\partial a_k}{\partial \omega_{jk}} = y_j$, (3-10) becomes:

$$\Delta\omega_{jk} = -\eta\frac{\partial E}{\partial \omega_{jk}} = -\eta\delta_k y_j \tag{3-13}$$

$$\text{where } \delta_k = \frac{\partial E}{\partial a_k} = (y_k - t_k)y_k(1-y_k) \tag{3-14}$$

With the same algorithm, the input -to-hidden layer weights:

$$\Delta\omega_{ij} = -\eta\frac{\partial E}{\partial \omega_{ij}} = -\eta\delta_j y_i \tag{3-15}$$

$$\text{where } \delta_j = \frac{\partial E}{\partial a_j} = \sum_k \delta_k \omega_{jk} y_j(1-y_j) \tag{3-16}$$

The forms of (3-13) and (3-15) are identical, the only difference between the two equations being in the definition of the δs in (3-14) and (3-16). The δ_j for a hidden

unit depends on the δ_ks of all the output units to which it is connected via its ω_{jk} weights. Thus the minimisation of E using gradient descent requires the propagation of errors (δs) backwards and this gives rise to the name of the algorithm. The details of the algorithm's mechanism are quoted in Appendix C.

3) Radial basis function network

Radial basis function (RBF) methods have their origins in techniques for performing exact interpolation of a set of data points in a multi-dimensional space (Powell, 1987). The units of RBF network are activated by the distance between the input vector and a prototype vector. A RBF network is a two-layer network, the output of which forms a linear combination of the basis functions computed by the hidden units. Whereas the neurons in a multi-layer perceptron compute a non-linear function of the scalar product $\omega \cdot x$, the activation of the hidden units in a RBF network is determined by the Euclidean distance between x and a set of prototype vectors. A typical RBF network is shown in Figure 3-10 (Note that the bias weights to the output units are again not shown as they were in Figure 3-9). The first layer's non-linear mapping is constructed using a set of basis functions whose centres correspond to the prototype vectors in input space. The basis functions are usually chosen to be unnormalised Gaussians and the output activity of the j_{th} hidden unit is then given by

$$\Phi_j(x) = \exp(-\frac{\|x - \mu_i\|^2}{2\sigma_j^2}) \qquad \textbf{(3-17)}$$

where x is an n-dimensional input vector, μ_j is the j_{th} prototype vector known as prototype/cluster centre. Using Cluster criterion, the cluster centre μ_j is characterised by taking the mean of all the patterns within that cluster. μ_j can be viewed as the most representative pattern within the whole clusters. σ_j is the width of the Gaussian for that prototype. This parameter of is chosen so as to ensure that the basis functions give rise to a localised response for any input pattern (algorithm is given later), i.e. they only produce a significant non-zero response when the input pattern belongs to a small localised region of input space close to μ_j. The name 'radial basis function ' comes from the fact that the Gaussian functions are radially symmetric and each hidden unit j produces an identical output for input patterns that are found at a fixed radial distance from μ_j.

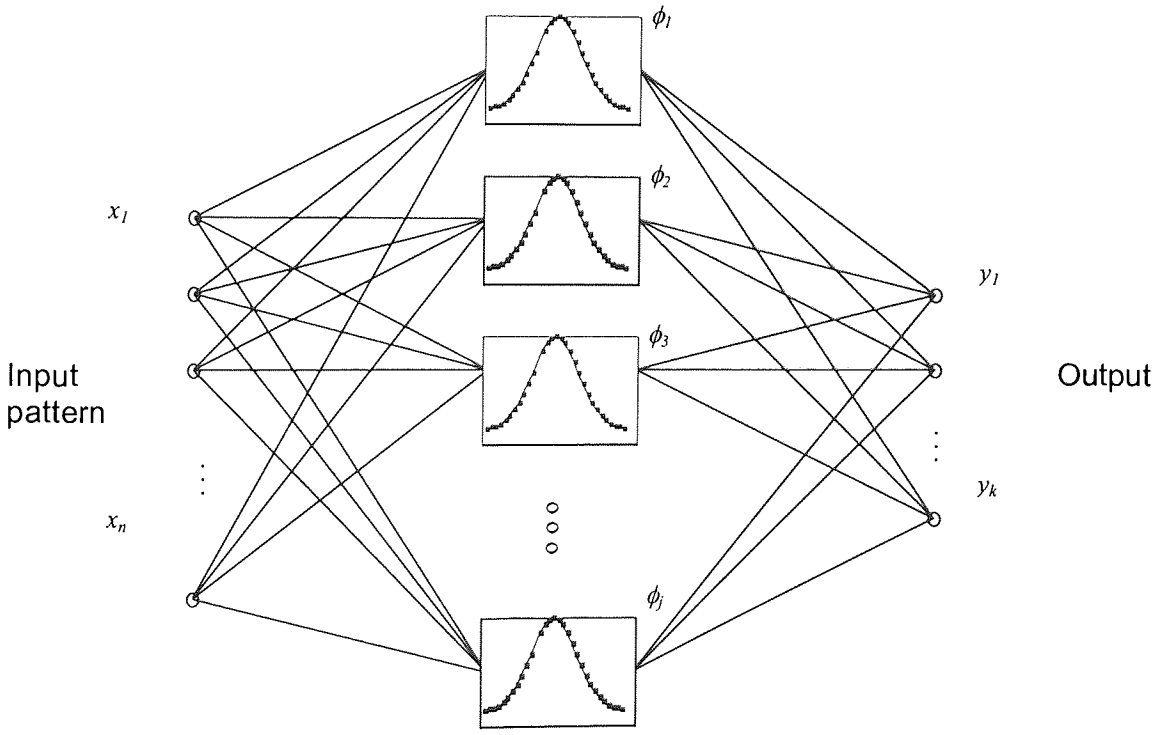

Figure 3-10 Architecture of RBF network

The Gaussian basis functions are not normalised since their amplitude is effectively set by the weights ω_{jk} of the second layer:

$$y_k = \sum_{j=1}^{J} \omega_{jk} \phi_j + \omega_{0k} \tag{3-18}$$

where ω_{0k} is the bias weight to output unit k. Thus the output layer forms a weighted linear combination of the hidden unit activations. Hence an RBF network performs a non-linear transformation from $\Re^n$, the n-dimensional real-valued input space, to $\Re^k$ K-dimension real-valued output space using a linear combination of non-linear basis functions. Previous study from Lowe (1995) also revealed the possibility to replace Gaussians basis functions by using thin plate splines and other non-local basis functions.

The training of RBF networks is a bit different from that of Multilayer Perceptrons (MLPs). It sets the free parameters of the hidden units without having to perform a full non-linear optimisation of the network (as with the back-propagation algorithm). In other words, the training of a RBF can be broken down into two independent phases: the selection of the basis functions μ_j and their σ_j, then the learning in the output layer (ω_{jk} weights). The former task is typically carried out using an unsupervised method, say the K-mean algorithm. The basis function widths σ_j are set once the clustering procedure has been completed. These widths should represent a measure of the spread of the data associated with each μ_j. They will

therefore vary according to the date density in different regions of input space, but the over-riding factor is that the basis functions should overlap to some degree in order to give a relatively smooth representation for all training data. This can be achieved, for example, by setting the σ_j s to be the average distance between the centres μ_j and the training patterns, which belong to that cluster (Hush and Horne, 1993), thus:

$$\sigma_j^2 = \frac{1}{p_j} \sum_{x \in C_j} (x - \mu_j)^T (x - \mu_j) \qquad \textbf{(3-19)}$$

where C_j is the set of training patterns grouped with centre μ_j and p_j is the number of patterns in C_j.

Learning in the output layer takes place after the selection has been completed. The basis functions are kept fixed while the output layer weights ω_{jk} are obtained by making use of the available labelled data. It is a linear optimisation task and can either be done using matrix inversion techniques (Singular Value Decomposition) or iteratively using the Least Mean Square (LMS) algorithm (See Appendix A). The use of latter is very similar to the training of MLP with only the transfer function altered. Thus (3-13) simply becomes:

$$\Delta\omega_{jk} = -\eta \frac{\partial E}{\partial \omega_{jk}} = -\eta \delta_k y_j \qquad \textbf{(3-20)}$$

where

$$\delta_k = \frac{\partial E}{\partial a_k} = \frac{\partial E \partial y_k}{\partial y_k \partial a_k} = (y_k - t_k) \qquad \textbf{(3-21)}$$

The training set consists of input and output pairs (x, t) as before (t is the target output vector). But the input pattern x are processed by the first layer to generate $\phi(x)$ values, which are then presented to the second layer for the iterative optimisation of the weights using LMS algorithm. There is no need to use a validation set of data as with an MLP. The first-layer parameters are determined using unsupervised learning, which gives a global optimum. Thus training continues until the mean squared error stops decreasing on the training set at which point the generalisation performance is assessed on the test set.

4) Selection of the ANNs.

Historically, from studies of biological networks, many novel concepts in neural computing have been generated. As the result, different types of neural networks were developed with different characteristics, such as Regression Neural Networks, Elman Neural Networks, Hopfield Recurrent Neural Networks, Probabilistic Neural Networks, *etc.* But, in main, those alternative network architectures are simply variations on the existing MLP and RBF architectures. (Tarassenko, 1998). Thus, in the context of this thesis, three major neural networks were addressed in this section. Table 3-3 gives a brief summary of the different ANNs discussed here. They are single layer perceptrons (SLP), multi-layer perceptrons (MLP) and radial basis function networks (RBF).

Single-layer perceptron is the prototype and starting point of neural computation. It provides a modest solution to real problems. Therefore, the selection of ANN for

this project will principally be between RBFs and MLPs. A comparison of the features and application ranges between two neural networks has been provided by Bishop (1995). It is also the basis on which the writer chose the appropriate neural network to fit in this project. Basically, there are five points that summarise the difference and similarity of these two neural networks.

1) RBF networks and MLPs play very similar roles in that they approximate non-linear functional mapping between input and output

2) Mechanism of MLPs is based on linear summation of inputs and transformed by sigmoidal transfer function, while RBFs use the distance to a prototype vector followed by transformation with a localisation function.

6) The MLP forms a *distributed representation* in the space of activation values for the hidden layer. The RBFs forms a representation in the space of the hidden units, which is *local*.

4) All the parameters in an MLP are usually determined at the same time as part of a single global training strategy using supervised learning. The training of RBF however is divided into two stages

5) The final difference is generalised by the thesis writer. Practice test has shown that the RBF may require more neurons than standard BP networks (MLP) and the performance improvement will mainly base on the fact that many training

vectors are available. From economical and practical point of view, the writer proposed BP instead of RBF as the modelling tool for neural computation.

Table 3-3 Comparison between different neural networks

Architecture	Description	Map
SINGLE LAYER Neurons	Only one layer is applied in the network and each element of the input vector p is connected to each neuron input through the weight matrix ω.	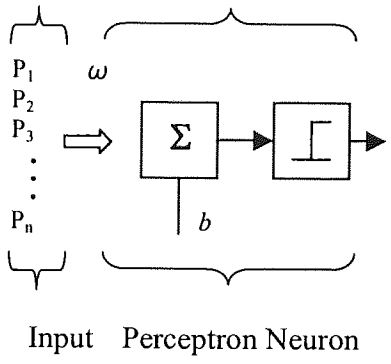
MULTIPLE LAYERS (BP)	More than two layers are used in this network. Each preceding layer's output became the following layer's input, and so on.	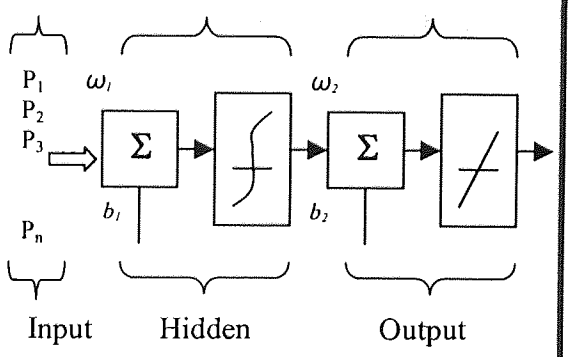
Redial Basis Function (RBF)	Redial Basis Function Network is different from other networks. It maps the input and output using a set of basis transfer function. The main feature of which is that the variables of the transfer function are the distances between input vector and weights.	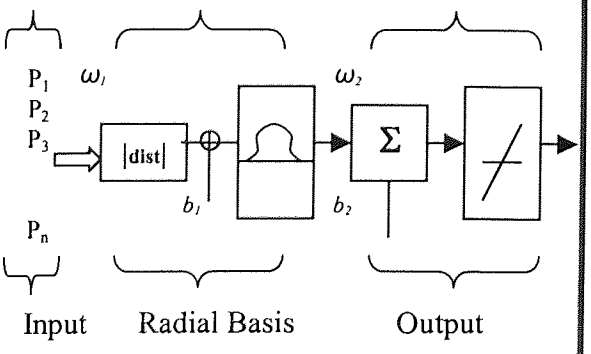

3.4 Impact dynamics theory

As impact damage detection is the main objective of this study, an understanding of the impact damage mechanism is essential. Impact dynamics provides the fundamental knowledge to reveal the impact damage principle. Because of the nature of the project, the theory reviewed here concentrates only on composite materials with a low velocity load applied.

Studies of low velocity impact on composite materials began in the 1970s. A systematic understanding of impact response of composites was described in ASTM (1975) publication. Using empirical and experimental approaches, responses due to foreign-body impact on composites were carefully examined, covering the various combinations of constituent materials, layups, stacking sequences, and constructions.

3.4.1 Impact study on isotropic materials

The study on the low velocity impact response from isotropic and composite materials can be divided into three steps according to Greszczuk (1982): 1) determination of impactor-induced surface pressure and its distribution, 2) determination of internal stress in the composite target caused by the surface pressure, 3) determination of failure modes in the target caused by the internal stresses. The procedure is illustrated in Figure 3-11.

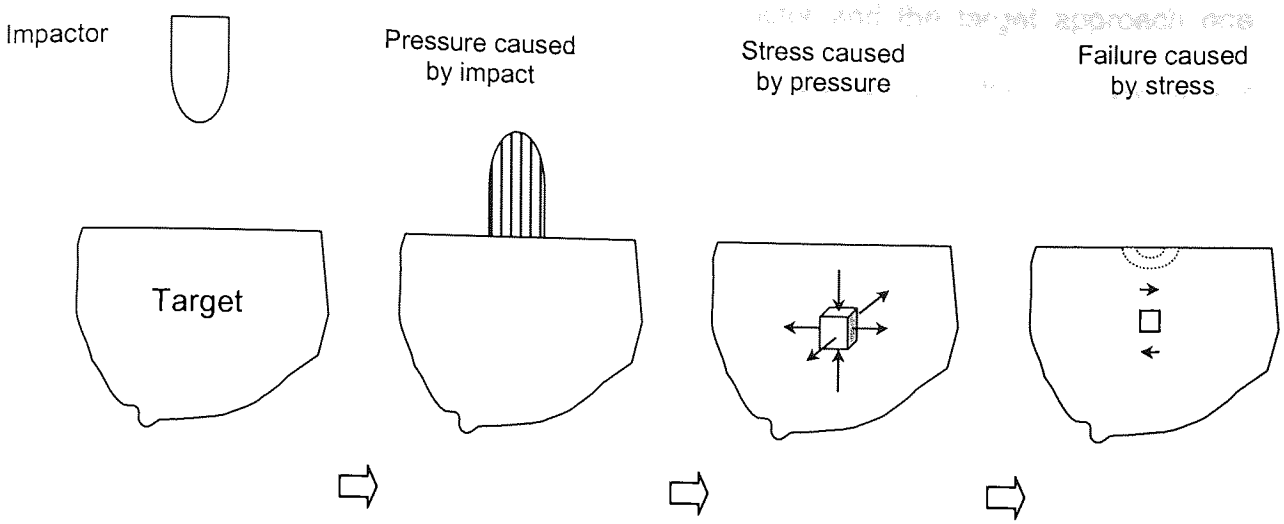

Figure 3-11 Essential features of the approach

1) Pressure and its distribution caused by impact

Analytically combining the dynamic solution to the problem of impacting solids with the static solution for the pressure between two contact bodies, magnitude and distribution of surface pressure can be provided. This approach is similar to the method described by Timoshenko (1934) for impact of spheres.

Denoting the mass and the velocity of the impactor as m_1 and V_1 while m_2 and V_2 are the mass and the velocity of the target. The rates of velocity change (acceleration) are:

$$m_1 \frac{dV_1}{dt} = -P \qquad m_2 \frac{dV_2}{dt} = -P \tag{3-22}$$

where P is the impact force.

If we denote by x the distance that the impactor and the target approach one another because of local compression at the point contact, the velocity of this approach is

$$\frac{dx}{dt} = V_1 + V_2 \tag{3-23}$$

Results obtained by Rayleigh (1906) show that if the contact duration between the impactor and target is very long in the comparison with their natural periods, vibrations of the system can be neglected. It can therefore be assumed that the Hertz Law

$$P = nx^{3/2} \tag{3-24}$$

that was established for special conditions, applies also during impact. The term n is defined as

$$n = \frac{4\sqrt{R_1}}{3\left(\frac{1-\nu_1^2}{E_1} + \frac{1-\nu_2^2}{E_2}\right)} \tag{3-25}$$

where R_1 is the radius of a spherical impactor, ν and E are the Poisson's ratio and Young's modulus respectively, subscripts 1 and 2 refer to the impactor and the target. Differentiating (3-23), combining it with (3-22), and substituting (3-24) into resultant equation yields

$$\frac{d^2x}{dt^2} = n\left(\frac{1}{m_1} + \frac{1}{m_2}\right)x^{3/2} \tag{3-26}$$

Timoshenko (1934) transformed the equation by multiplying it by $\frac{dx}{dt}$ on both sides and integrating with respect to the resultant equation to yield

$$\left(\left(\frac{dx}{dt}\right)^2 - V^2\right) = -\frac{4}{5}Mnx^{5/2} \qquad \textbf{(3-27)}$$

where V is the approach velocity of the two bodies at t=0, that is, at the beginning of impact. M here is $\left(\frac{1}{m_1}+\frac{1}{m_2}\right)$. Maximum deformation, x_1, occurs when $\frac{dx}{dt}$=0 and is given by (3-28) as follows

$$x_1 = \left(\frac{5V}{4Mn}\right)^{2/5} \qquad \textbf{(3-28)}$$

An alternative way to draw the conclusion given by (3-28) is to start with the energy balance of the system. Assuming that the target is semi-infinite and stationary and the impactor is moving at velocity V_1, the energy balance becomes

$$\frac{1}{2}m_1V_1^2 = \int_0^{x_1} P dx \qquad \textbf{(3-29)}$$

Substituting (3-24) into the equation above, followed by evaluation of the resulting integral gives

$$\frac{1}{2}m_1V_1^2 = \frac{1}{2}nx_1^{5/2} \qquad \textbf{(3-30)}$$

which when solved for x_1 is identical to the result from (3-28). It is noted that in this case, the velocity of the mass can be ignored and only the mass of impactor will be

taken into account. (That is $V_1 \equiv V$ and $M \equiv 1/m_1$). Then the final relationship can be obtained as follows:

$$P = n^{2/5}\left(\frac{5V^2}{4M}\right)^{3/5} \tag{3-31}$$

In Hertzian contact problems, the relationship between the force P and the radius a of that area of contact is revealed as (Hertz, 1881)

$$a = \left[\frac{3\pi P}{4}(k_1 + k_2)R_1\right]^{1/3} \tag{3-32}$$

where $k_1 = \frac{1-\nu_1^2}{\pi E_1}$ and $k_2 = \frac{1-\nu_2^2}{\pi E_2}$.

Combining (3-31) and (3-32) the maximum radius of the area of contact between a flat target and a spherical impactor then becomes

$$a = (R_1)^{1/2}\left(\frac{5V^2}{4Mn}\right)^{1/5} \tag{3-33}$$

It has been shown (Hertz, 1881, Timoshenko, 1934, Belajef, 1924) that the pressure distribution over the area of contact is

$$q_{X,Y} = q_0\left[1 - \frac{X^2}{a^2} - \frac{Y^2}{a^2}\right]^{1/2} \tag{3-34}$$

where q_0 is the surface pressure at centre of contact area, mathematically at X=Y=0. At the boundary of the surface $\frac{X^2}{a^2} + \frac{Y^2}{a^2} = 1$ and therefore $q_{X,Y} = 0$. Summing up the pressures acting on the area of contact and equating the result to P, yields

$$q_0 = \frac{3P}{2\pi a^2} \tag{3-35}$$

After combining (3-31), (3-33), (3-34), and (3-35) and introducing polar co-ordinates, the following equation is obtained for the magnitude and distribution of the surface pressure:

$$q_r = \left(\frac{3P}{2\pi R_1}\right)\left(\frac{5V^2}{4nM}\right)^{1/5}\left[1-\frac{r^2}{a^2}\right]^{1/2} \tag{3-36}$$

and

$$q_0 = \left(\frac{3P}{2\pi R_1}\right)\left(\frac{5V^2}{4nM}\right)^{1/5} \tag{3-37}$$

Equations (3-31), (3-33) and (3-36) are the final equations that give the impact force, radius of the area of the contact, and magnitude and distribution of the surface pressure in terms of velocity, geometry and masses of the impactor and target, as well as their elastic properties. These are critical formulae to determine the impact mechanism in a quantitative way.

2) Internal stress caused by impact pressure

The maximum pressure q_0 occurs at a time of 0.5 t_0 where t is the impact duration. An equation is given by Greszczuk (1980), which yields the following expression for q_0 as a function of time, t

$$q_0(t) = \frac{3ns}{8\pi C_r w\gamma}\left(x_1 \sin\frac{\pi t V}{2.94x_1}\right)^{1/2} \tag{3-38}$$

where C_r is the curvature parameter, w, γ and s are the parameters proposed by Whittemore and Petrenko (1921). Knowing the surface pressure, its distribution, as well as the area of contact, all as a function of impact velocity and time, the internal triaxial stresses in isotropic, multilayered orthotropic, or anisotropic targets can be determined. (Greszczuk, 1982).

a)Semi-infinite isotropic solid

In the case of a semi-infinite isotropic solid subject to a surface load q_r distributed according to (3-34), the internal stresses can be determined from the equation given by Love (1929), Huber (1956), Belajef (1954), Sneddon (1951), or from the curves given in a paper by Morton and Close (1922). Figure 3-11 shows internal triaxial stress contours for δ_r, δ_z, and δ_θ. The stresses have been normalised with respect to maximum surface pressure while the dimensions have been normalised with respect to the radius of the area of contact, a. In addition to showing the results from a closed form solution, Figure 3-12 also shows the stresses determined from SAAS III finite element code developed by Crose and Jones (1968). The maximum tensile, compressive and shear stresses (δ_t, δ_c, and δ_s respectively) that occur in targets made of isotropic materials are related to the surface pressure by the following simple equations (Timoshenko, 1934):

$$\delta_t = \left(\frac{1-\nu_2}{3}\right) q_0(t) \qquad \textbf{(3-38)}$$

$$\delta_c = q_0(t) \qquad \textbf{(3-39)}$$

$$\delta_s = \left[(1+\nu)(s\cos^{-1} s - 1) + \frac{3}{2(1+s^2)} \right] q_0(t) \qquad \textbf{(3-40)}$$

with the maximum δ_s occurring at $s \approx 2/(1+\nu)\pi$ where s is the quotient of displacement Z and contact area radius a and where $q_0(t)$ is the maximum surface pressure at a given time, t. The locations of maximum stresses are noted in Figure 3-13. Thus for brittle materials the failure due to impact would be expected to be governed by tensile strength and would initiate at the periphery of the area of contact. Materials with low shear resistance would produce surface shear failure. For the case of flexible isotropic targets subjected to impact, calculation of the three dimensional internal stress state caused by impact–induced surface pressure can best be carried out by finite element analysis.

b) Semi-infinite and Flexible Composite Targets

The computation of internal triaxial stresses in semi-infinite or flexible composite targets is not the main subjects of this study. However, an example is introduced to determine the surface pressure by using finite-element analysis package such as SAASIII (Crose and Jones, 1968). In the case of transverse isotropic materials, SAASIII is applicable, whereas the modified version ASAAS (Greszczuk and Chao, 1975) is applicable to multi-layer, generally orthotropic solids having orthogonal symmetry. Other available codes that can be used for determining the internal triaxial stresses in generally orthotropic solid include NASTRAN, ANSYS, MARC, SAP IV, NISA, *etc*. These codes can also be used for determining the internal triaxial stresses in generally orthotropic plates.

Figure 3-12 Comparisons of closed form and computer solutions for internal triaxial stresses in a solid subjected to surface pressure caused by impact.

(Crose and Jones, 1968)

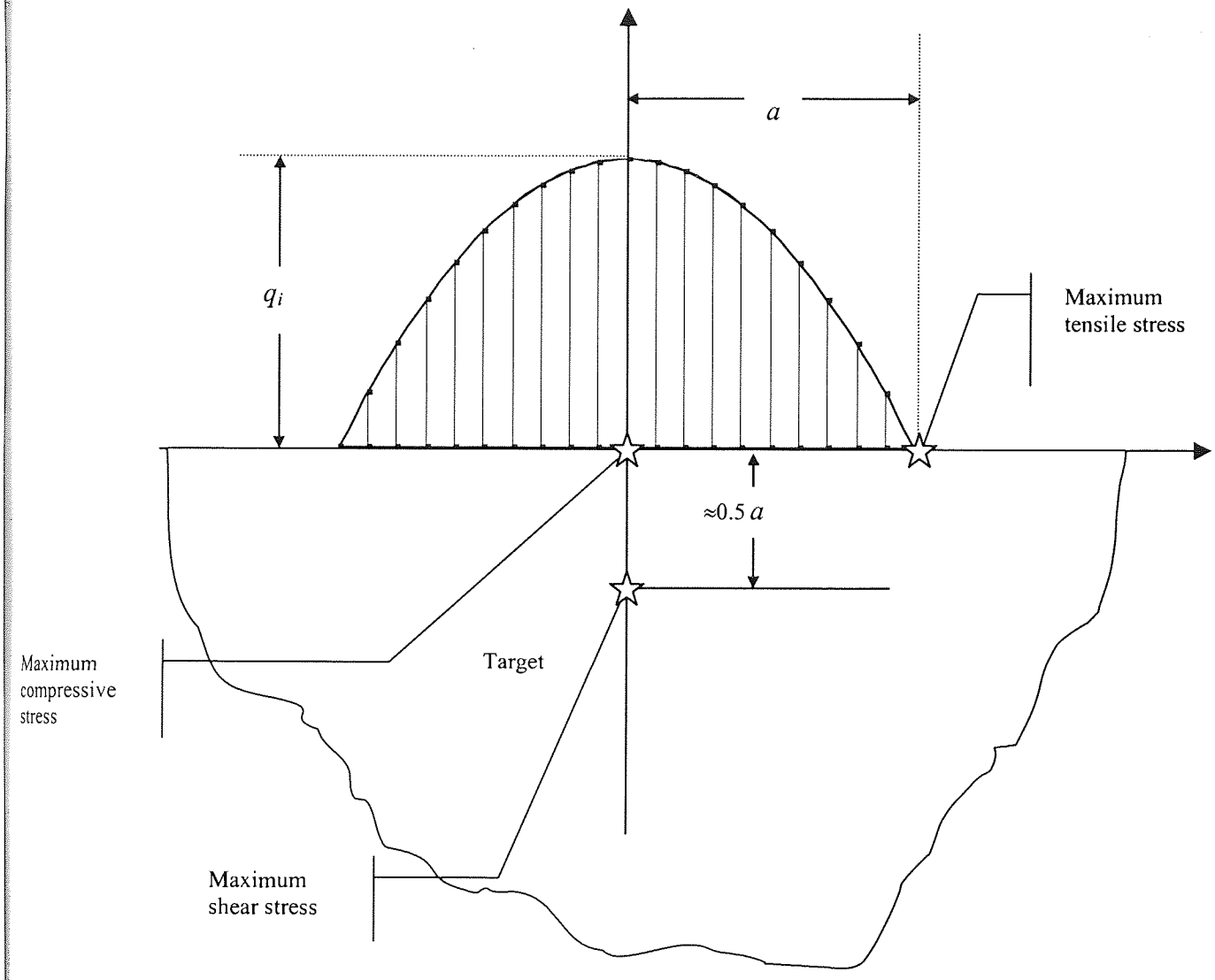

Figure 3-13 Locations of maximum tensile, compressive, and shear stresses under surface loading.

3) Failure caused by internal stress

The final step in the theoretical development is to establish failure modes from internal triaxial stresses caused by impact-induced surface pressure, as well as the time sequence for the occurrence of the various failure modes. In Greszczuk's study (1982), there is a brief description on applying appropriate failure criteria to the impact-induced triaxial stress state at each point in the target. As no experimentally verified dynamic failure criteria exist for composites, to get some insight into the type and extent of impact damage, static failure criteria will be assumed. In conjunction with the latter, one has a choice of using: (1) failure criteria based on maximum stress or strain (maximum-normal-stress theory/ maximum-shear-stress) or 2) failure criteria that accounts for stress interaction such for example, as one based on distortion energy theory (also known as Mises-Hencky theory). The advantage of using a failure criterion based on maximum stress is that it allows determination of the mode of failure as well as sequence of failures, that is whether impact causes tensile failure transverse to the direction of fibres, tensile failure in the fibre direction, interlaminar shear failure, or compression failure in the fibre or transverse direction. Thus it applies to high velocity impact damage of composites. The stress interaction criteria, however, allows only for determination of a failure envelope within which failure has taken place due to interaction of multiaxial stresses. Therefore, such damage criteria are suitable in low velocity impact damage of composites. The mathematical definitions of above three criteria are shown in equation below

Max normal stress criteria:
$$\sigma_{1,2} = \frac{\sigma_x + \sigma_y}{2} \pm \sqrt{\left(\frac{\sigma_x - \sigma_y}{2}\right)^2 + \tau_{xy}^2} \quad \textbf{(3-41)}$$

Max shear stress criteria:
$$\tau_{\max} = \sqrt{\left(\frac{\sigma_x - \sigma_y}{2}\right)^2 + \tau_{xy}^2} \quad \textbf{(3-42)}$$

Stress interaction criteria:
$$\sigma_e = \sqrt{\frac{(\sigma_1 - \sigma_2)^2 + (\sigma_2 - \sigma_3)^2 + (\sigma_3 - \sigma_1)^2}{2}} \quad \textbf{(3-43)}$$

where σ_x, σ_y are X axial and Y axial normal stress, τ_{xy} is the shear stress $\sigma_1, \sigma_2, \sigma_3$ are principle stresses, σ_e is von Mises stress.

The theory of failure is a statement that predicts whether failure should occur at a given level of stress. (3-41), (3-42) and (3-43) separately calculate the maximum stress according to different criterion at the specific stressed point. It can then be compared with allowable stress to determine whether there is a failure or not. In this study, a novel criterion has been proposed to indicate the impact damage level by implementing artificial neural network.

3.5 Fundamental of system identification

System identification deals with the problem of building mathematical models of dynamical systems, based on observed system data. Studies in this area have matured into an established collection of basic techniques that are well understood and known to perform successfully in practical applications. As the nature of this project includes system identification, it is necessary to review the methodology.

The identification of models from data involves decision making as well as fairly demanding computation to furnish bases for these decisions. A user typically goes through several iterations in the processing of arriving at a final model, where earlier decisions are revised at each step. This golden rule also applied in the neural modelling as shown in the later chapters.

3.5.1 Approaches to model building

Physical models are either reduced-size copies of the original system following the laws of model similarity, or analogies. The idea of an analogy implies that there exists "something" at every instant of time that is to be analogous to the dependent variables of the original physical system. Mathematical models map the relationships between the physical variables in the system to be modelled onto mathematical structures like simple algebraic equations, differential equations or systems of differential equations. Design of mathematical models is necessary in order to understand and predict the dynamic behaviour of systems, and modelling enables a mathematical treatment of the systems. Mathematical models can be developed in different ways: either purely theoretically based on the physical relationships about the system which are deducible, or purely empirically by experiments on the already existing system, or by a sensible combination of the two. Models obtained by the first method are often called *a priori* or first principle or theoretical models, while models obtained in the second way are called *a posterior* or experimental (black-box) models.

3.5.2 Classification of models

Mathematical models can be represented in time domain, in operator domain (e.g. s, Z, *etc.* transforms) or in frequency domain. Regarding time domain, the continuous time models are closer to physical considerations, whereas the discrete-time system behaviour is considered to be defined at a sequence of time instants related to measurements. The discrete-time models are closely related to implementation problems of digital processing. Many models have been defined in a given form but are dependent on a finite number of real parameters. Such models are said to be parameterised or parametric models, although there is no clear cut distinction from other models such as spectra or impulse responses, which are referred to as non-parametric models. Examples of parametric models are algebraic and differential equations, systems of these equations, transfer functions, *etc.* In these cases, the model building consists of determination of parameters in fixed structures. Theoretical model building always yields a parametric model. A non-parametric model is the response obtained directly from an experimental analysis of a physical system. The recorded step response of a system, for example, is a non-parametric model. By various identification methods a parametric model can be produced from a non-parametric model. By experimental identification a parametric model can be obtained directly if the structure of the system can be defined a priori.

A system can also be represented by non-linear and linear models. Very often, especially in control theory, systems exhibit non-linear behaviour and therefore the

use of non-linear models would be appropriate. Often, the system dynamics are described by linear models, which allow simpler mathematical treatment. In this section, only methods for identifying linear models will be discussed. For methods of non-linear identification refer to Johansson (1993).

3.5.3 Classification of identification methods

A natural method to classify identification methods is by the type of the resulting mathematical model. Again, practical implementation and the applied identification techniques are considered. The practical aspects of classification:

a) Errors between process and model

Judging the error between model and process one can use output-signal error or equation errors. For mathematical reasons, errors are preferred which depend linearly on the model parameters. Therefore, the output-signal error is utilised if the weighting function is used as a model, and equation errors if difference or differential equations and transfer functions are used.

b) Algorithms used

Concerning the parameter identification methods, one can distinguish between algorithms for direct estimation and algorithms for iterative estimation. With algorithms for direct estimation, the parameters are evaluated in a straightforward manner. On the other hand, algorithms for an iterative estimation evaluate the parameters stepwise.

Furthermore, algorithms can be recursive or non-recursive. With recursive algorithms, the parameters are evaluated after each new set of data. The latest set of data is used to improve the parameter estimation from the proceeding step. With non-recursive algorithms, the entire set of data is stored, and only one computation is used to find the parameters.

c) Sequence of measurements and evaluation

If a digital computer is used for the identification, two kind of coupling between the process and the computer have to be distinguished; the off-line (indirect coupling) and the on-line (direct coupling). In off-line operation, first the data are stored in a data storage device. Later on the data are transferred to the computer and evaluated. For this type of identification, mostly batch processing of data is applied, and the whole data set is evaluated at once. This thesis used off-line analysing in both damage level discrimination and damage location detection study. When running an on-line operation, the computer is directly coupled to the process, and directly fed with data. Then, two ways of processing can be distinguished: *real-time processing* when data is evaluated immediately after each sample or *batch processing* when the data set is evaluated at once after the all measurements have been made. The various ways of processing the measured data are depicted on Figure 3-14.

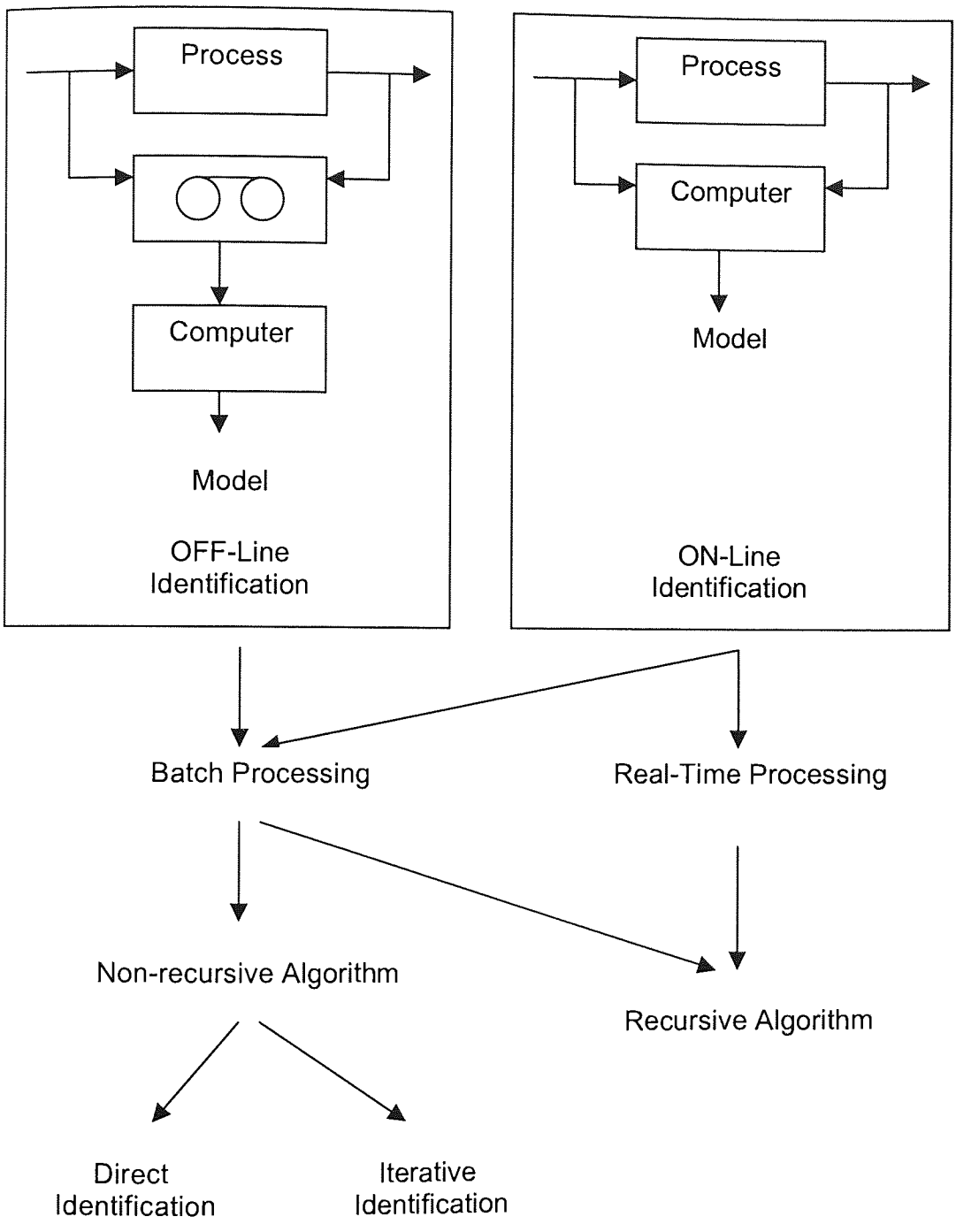

Figure 3-14 Methods of data processing for system identification (Isermann, 1980).

As to the applied identification techniques, there are two major types, non-parametric and parametric identification accordingly. The most important classes of non-parametric identification techniques suitable for digital computer implementation are summarised in the following:

- a) Transient response analysis

This is mainly used for obtaining step and impulse responses. The test signals are usually step or impulse signals, and the recorded output constitutes the corresponding model.

- b) Correlation analysis

This is a time-domain method, and is suitable for linear processes with continuous as well as discrete signals. Admissible input signals can be stochastic or periodic signals. As a result, correlation functions (and, a special case, the weighting function) are obtained.

-c) Frequency analysis

They are used to directly estimate the frequency response. Fourier analysis is mainly used for the determination of the frequency response characteristics of linear processes using continuous signals. Spectral analysis is used under the same conditions as the correlation analysis. The results are values of the frequency response characteristics.

Non-parametric methods assume that the processes are linearisable. A particular model structure does not have to be assumed. Therefore, those methods are suited for processes with an arbitrarily complicated structure. If a parametric identification method is to be applied, a certain model structure, generally linear, has to be assumed. The model parameters are evaluated by minimising an error between model and process. The two main classes of parametric identification techniques are as follows:

- a) The model-fitting methods

These methods are developed for models with continuous signals. They yield the parameters of differential equations. These methods will not be covered here.

- b) The parameter estimation methods

These methods can be used with discrete as well as continuous signals. In most cases, the prediction error, and in some cases the output error are used as the error signal between model and process. If the error signal depends linearly on the parameters, simple estimation algorithms are obtained. For parametric identification methods, assuming the correct model structure is known in advance, an iterative search for the model order and dead time follows. The most important classes of parameter estimation methods are the methods based on the following principles: least square parameter estimation; maximum likelihood method. The choice of identification method highly depends on the purpose of model building. A

summary of the relationship between the methods and the goals is given below in Table 3-4 (Isermann, 1980).

Table 3-4 Classification of the applications and their identification methods (Isermann, 1980)

Final goal of model application	**Type of process model**	**Required accuracy of model**	**Identification method**
Verification of theoretical models	Linear, continuous-time, nonparametric / parametric	Medium / high	off-line, transient response, frequency response, parameter-estimation
Controller parameter tuning	Linear, nonparametric, continuous-time	Low for input / output behaviour	off-line, transient response
Computer aided design of digital control algorithms	Linear, parametric , (nonparametric) discrete-time	Medium for input / output behaviour	on-line / off-line parameter- estimation
self-adaptive digital control	Linear, parametric , discrete-time	Medium for input/output behaviour	on-line parameter-estimation
Process parameter monitoring and failure detection	linear / nonlinear, parametric, continuous-time	High for process parameters	on-line parameter-estimation

3.6 Conclusions

This chapter summarised the fundamental knowledge involved in the impact damage studies, namely Acoustics Emission, ANNs, and impact dynamics. They are the stepstones this study is generally based upon. Terminology, history and brief technique specification, which are appropriate to the scope of the project, have been given in this section to produce a better understanding of the techniques. Moreover, a good portion of this chapter also has been devoted to the theory of system identification in light of modelling. It addressed issues such as the classification of system identification approaches and how to conduct systematic analysis over physical models *etc*. These basic concepts and ideas benefited this study to a great extent.

So far, this thesis generally introduced methodologies involved in this project which ranges from data collection to modelling algorithms. The comparison of data acquisition measures reviewed in this section justified the reason of applying acoustic emission as a comprehensive NDT method. So did the comparison in modelling approaches that yielded artificial neural networks (especially, BP neural networks). The proceeding studies, however, illustrates how to make the full use of these two techniques to determine impact damage severity and to pinpoint the impact damage site.

Chapter 4 Experimental work and measuring procedure

"In God we believe, else bring the data"

(Anonymous)

4.1 Introduction

The instrumentation and measurement procedures adopted to investigate the impact damage are described in this chapter. In this research, the experimental work and procedures are essential to both the impact level discrimination and damage location detection. Due to the different nature of these two subjects, separate experiments were designed and conducted and different equipment was adopted. The experimental equipment in this study can be catalogued into two major classes; those to stimulate or generate signals and those to detect, measure and record generated signals. The topology of the test rigs is illustrated in Figure 4-1. The experiments generally followed the instruction of EN13554 (Non-destructive testing - Acoustic emission - General principles), which specifies the general principles required for the acoustic emission (AE) testing of industrial structures, components, and different materials under stress and for harsh environment, in order to provide a defined and repeatable performance. Relevant information can also be obtained from other British standards, such as EN 1330, EN 473, and EN 13477 *etc*. As mentioned early, all the experiments were conducted at Cranfield. A datasheet of the experiments is enclosed in Appendix F.

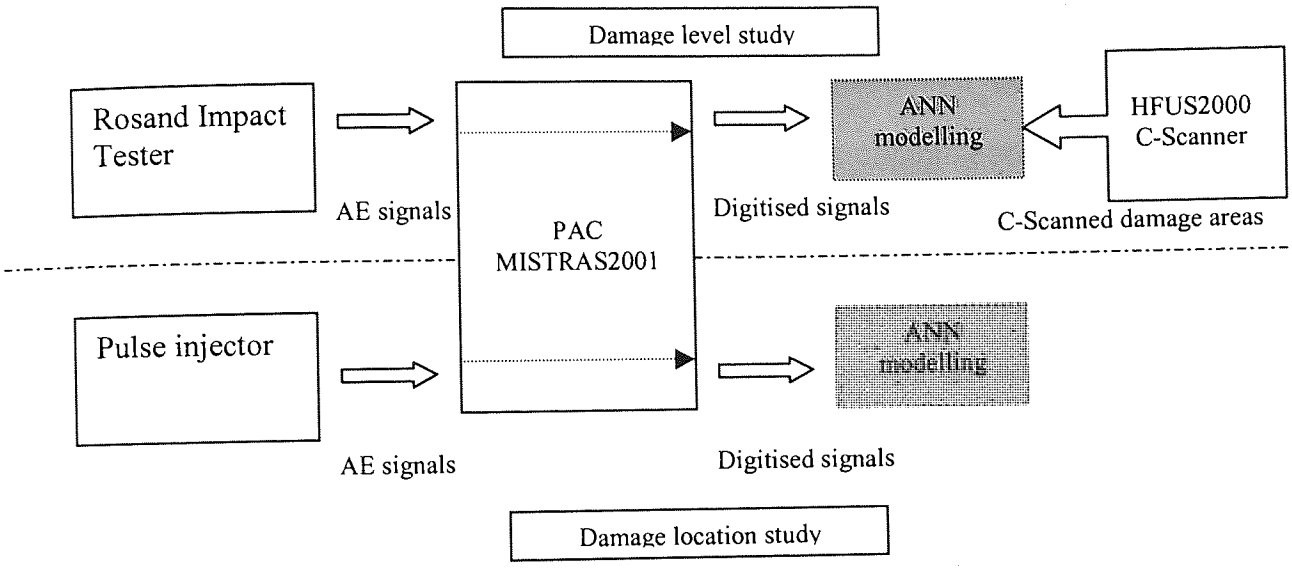

Figure 4-1Topology of test rigs of both damage level study and location study.

4.2 Instruments description

As illustrated in Figure 4-1, there are several pieces of equipment used in the damage level discrimination study. They are:

a. *Rosand Instrumented Falling Weight Impact Tester, type 5* was used to conduct impact testing. It is designed for testing a wide range of materials, or structures, that can fail due to impact, i.e. at high rates of strain. Tests can be carried out in an environmental chamber, allowing a temperature range of -100 to +200 °C to be studied. The maximum drop height is 1.6 m. Variable drop weight ranges from 2 kg to 20 kg. The system is also equipped with Merlin firmware/software for machine control and data analysis. Figure 4-2 shows the measuring scheme of the impact

testing. The outlook of the equipment is shown in Figure 4-3. In the tests, the impactor is raised upwards and released from certain height. It free-falls and strikes the sample panel, which is fastened to the instrument platform. The potential energy of the impactor will then transfer into the sample panel in the form of acoustic emission. Consequently, AE signals will be generated from impact site and will spread out within the geometric boundary of the sample panel. The data acquisition apparatus will then be able to detect and convert the AE signals into manageable data flow for further analysis or storage. The Rosand impact tester is accompanied by a pressure sensor for measuring the transient impact force between the impactor and the sample panel. Test results may vary according to different situations, such as different impactors, material structure and releasing height *etc.* The analysis is based on the study of the AE parameters as well as the transient impact forces.

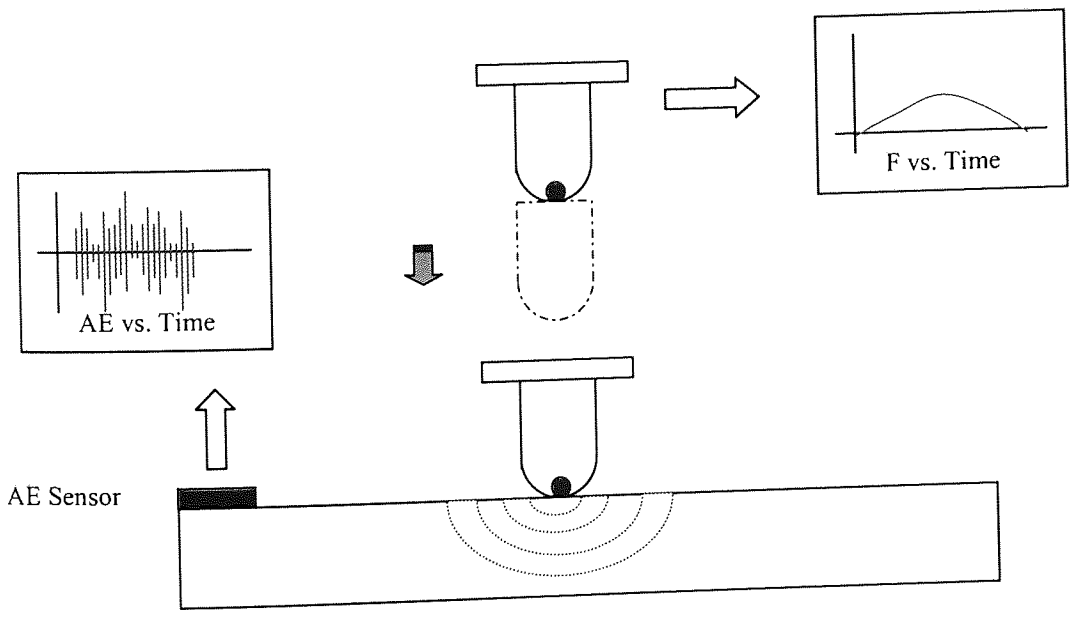

Figure 4-2 Measuring scheme of falling weight impact tester

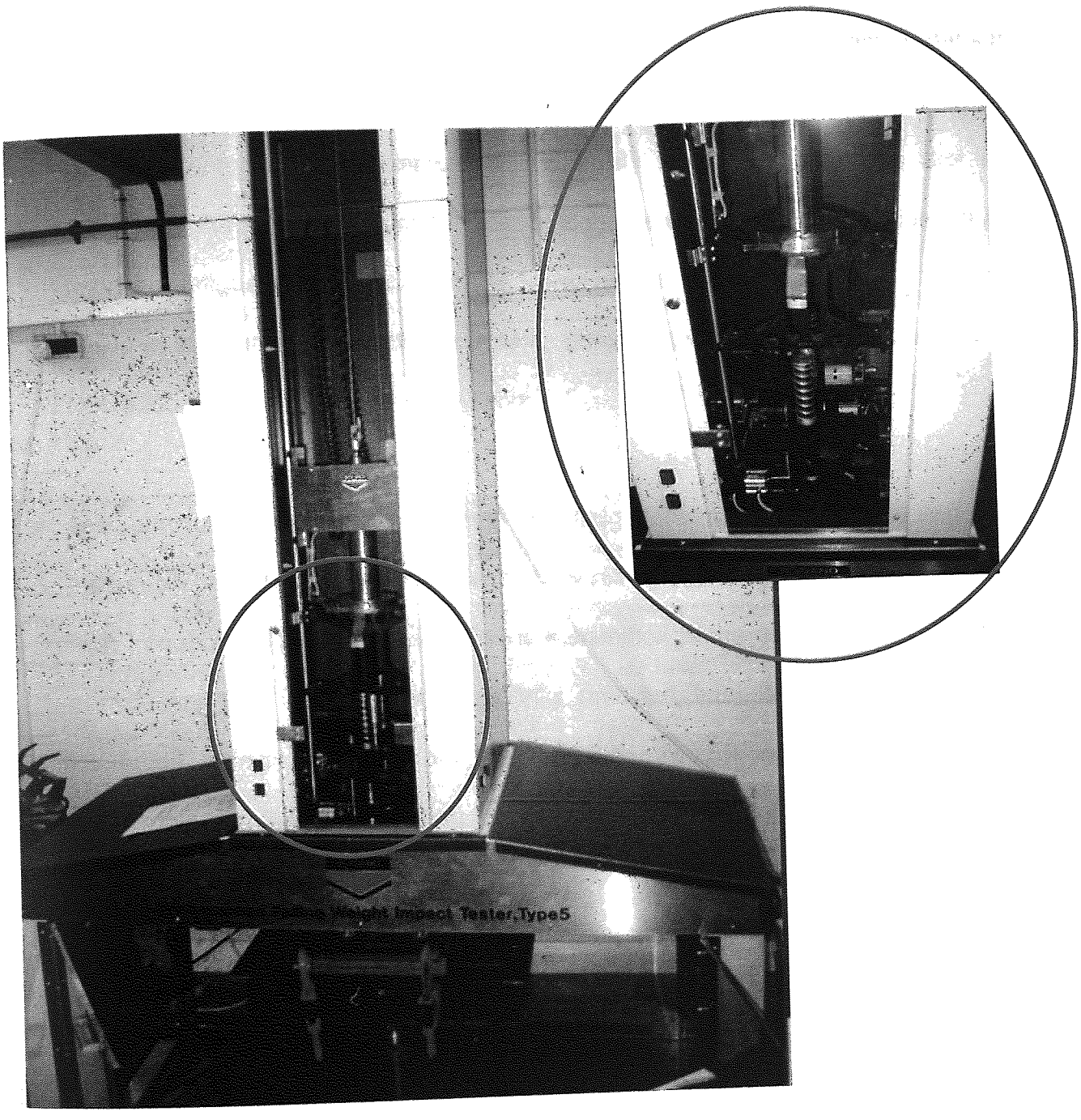

Figure 4-3 Layout of falling weight impact tester from Rosand

b. *HFUS 2000 (Ingenieurbüro dr Hillger)* is the high frequency ultrasonic C-scan equipment, which can be used as a non-destructive technique to examine defects inside a material. This apparatus allows the researcher to identify the depth of the observed defect in the sample. This capability makes it a valuable tool for monitoring the precise location of delaminations between certain plies, caused by impact or fatigue loading. In this study, it was used to verify the prediction from the ANNs in the damage level discrimination. Some of the technical specifications of HFUS2000 C-scanner are given in Table 4-1.

The principle of C-scan equipment is straightforward. The sample and the transducer are submerged in water that serves as the coupling medium. A very high frequency signal (up to 50 MHz) is transmitted to the sample by a (focused) transducer. The initial signal is partially reflected back to the transducer at interfaces, defects, porosities and at strong differences in acoustic impedance in the sample and the rest of the signal; if not fully reflected, it continues through the sample. The peak amplitudes, as well as the time-of-flight of each returning signal, is then converted and stored in a computer data-file and processed off-line to produce maps of the scanned area at a particular depth, showing the virgin and the damaged regions. The detecting mechanism is illustrated in Figure 4-4.

Table 4-1Technical specification of HFUS2000 C-scanner

Technical details:		
Scan system		
	Dimensions (BxWxH)	1300 x 1300 x 380 mm, 630 x 630 x 200 mm
	Scan area	1250 x 1250 mm^2, 600 x 600 mm^2
	x-resolution y-resolution	0,0375 mm 0,0375 mm
Ultrasonic system		
	Type Modules Available sensors	HFUS 2000 (Ingenieurbüro dr Hillger) type 2011: pulse generator/amplifier type 2023: amplifier/filter type 2024: main amplifier type 2060, 2061: ports IAP-FS 50.2.1 (50 MHz, KrautKrer) H2K (20 MHz) IM.15.10.F15 (15 MHz, Rhosonics) IM.2,25.25.F54 (2,25 MHz, Rhosonics) IM.1.25.F54 (1 MHz, Rhosonics)
Oscilloscope		LeCroy 9400A dual 175mhz digital oscilloscope
Computer (recommended)		
	Type RAM System	Pentium II 350 MHz 128 Mb Windows NT

The output of the ultrasonic C-scan equipment is usually in the form of a two dimensional graphical presentation, in which the discontinuity echoes are displayed in a plan view on the test surface. In this presentation, reflected pulses are known as events. A mono-colour or multi-colour marks can then be obtained to represent the events by different evaluations. Using zero-one method*, a black/white mark can be generated if an echo exceeds a preset threshold. Alternatively, a multi-colour palette or (greyscale) mark, which is proportional to the amplitude of the signal, can be obtained if an echo exceeds a preset threshold. The later evaluation is applied to pulse echo and transmission techniques. Usually no indication of depth is given unless the complete scan represents the time of flight evaluation, such as D-scan**. In computerised and more sophisticated systems, due to digitalisation and storing, post processing is available for displaying various kinds of presentations.

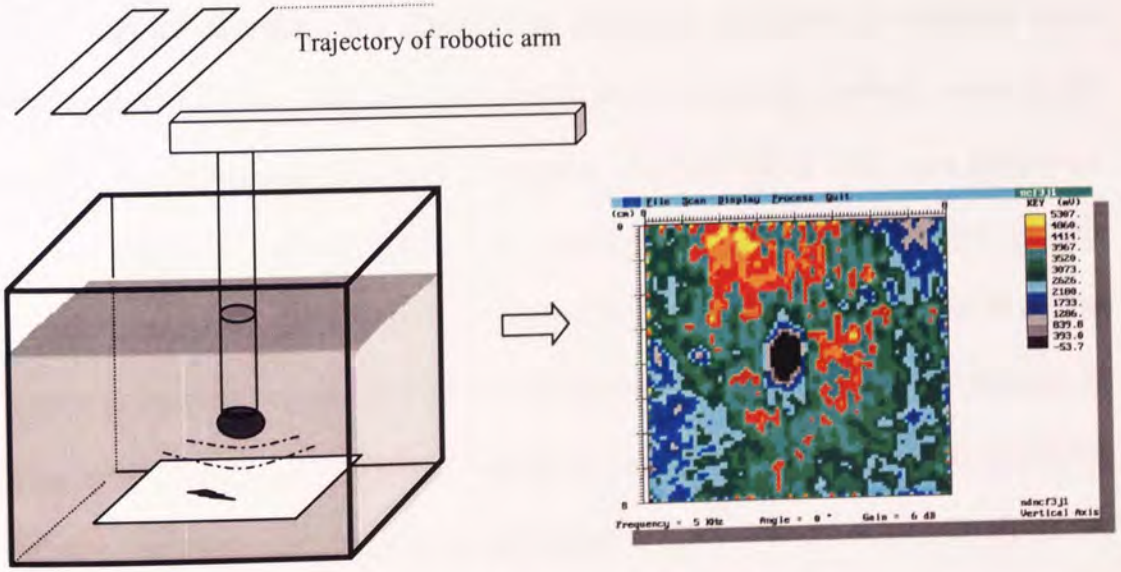

Figure 4-4 Principle of ultrasonic testing C scan

* zero-one method: threshold which produces 1 if it is over or 0 if it is below
** D-scan: a modified C-scan in which depth or amplitude is displayed

The diagram on the right hand side of figure is the c-scan result of a test. As shown in Figure 4-4, the sample panel has a damage within/on its structure. Ultrasonic signals therefore behave differently at damage area apart from the rest area. A black hole-like zone then can be produced in the diagram to indicate such area. Nevertheless, geometric topographies, such as non-flatness, may also be reflected in the form of different colour (orange/blue) zones in the picture.

c. Physical acoustics corporation (PAC) MISTRAS 2001 is used to detect AE waveforms in both the impact damage level study and the impact damage location. The MISTRAS 2001 is a fully digital, multi-channel, computerised, acoustic emission system that performs AE waveform and signal measurement and stores, displays and analyses the resulting data. The main components that make up the MISTRAS system consist of hardware and software, the specifications of which are shown in Table 4-2 below. The MISTRAS has been designed to conduct non-destructive testing and monitoring in a flexible way. And it can perform most of AE applications currently used. Generally speaking, the MISTRAS 2001 is a hit-driven AE system. The principle of this equipment involves the measurement of key parameters of each hit, that is, each AE signal that crosses the threshold. A digital description of each hit is generated by the front-end hardware and is passed in sequence with other hit description through a computer system, which provides data storage, a variety of graphic displays, and replay for post-test analysis. A system block diagram is shown in Figure 4-5.

Table 4-2 System composition of MISTRAS 2001.

Technical details:		
Hardware:		
AEDSP-32/16 Boards		Data acquisition board16-bit A/D(>85dB), 8MHz sampling
AE sensors		R6I, R15I, R50I , R6-AST, R6, U30 WDI-AST and WDI
Preamplifier		1220A-AST preamplifier
Software:		
Type: MISTRAS MI-TRA Windows 95 Grafplus PAC-PARS (Optional)		32 bit software containing GUI software for AE data acquisition and replay Transient recorder analyser software for detailed waveform data acquisition, storage, *etc* System platform Screen printing program Pattern analysis and recognition software for use with both AE features and waveform data.
Computer		
	Type RAM System	Pentium 80586 90 MHz 16 Mb Windows 95

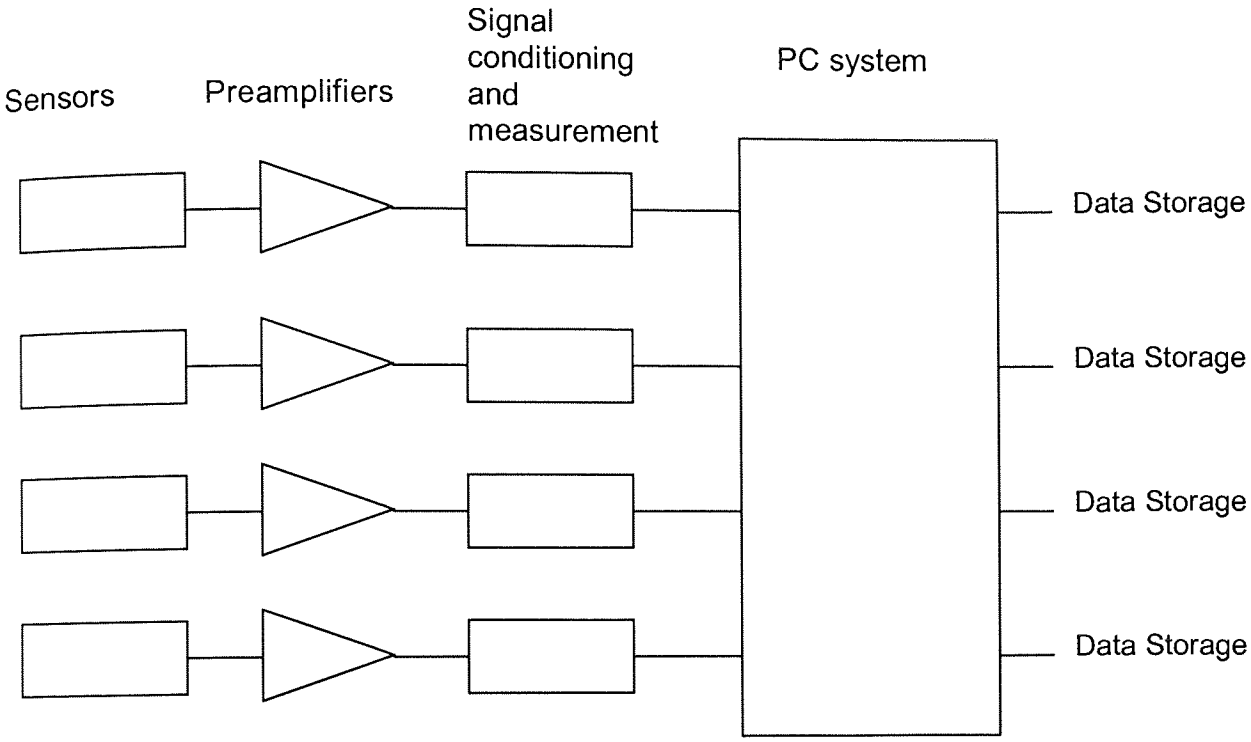

Figure 4-5 Generic block diagram of a four-channel acoustic emission system.

After the AE signal is acquired, the software part of MISTRAS 2001 can then convert signals into data and store data into bite files. Usually, in the first instance, the system is able to briefly give some basic analysis and prediction with its own built-in computational features. Pictures have been captured from system to display the features, as shown in Figure 4-6 to Figure 4-8. The MISTRAS 2001 gives a prediction of impact location using its own internal software. However, this function is generally limited to isotropic cases. In later chapters, a comparison will be given between MISTRAS prediction and ANNs prediction to demonstrate the superiority of the ANN approach.

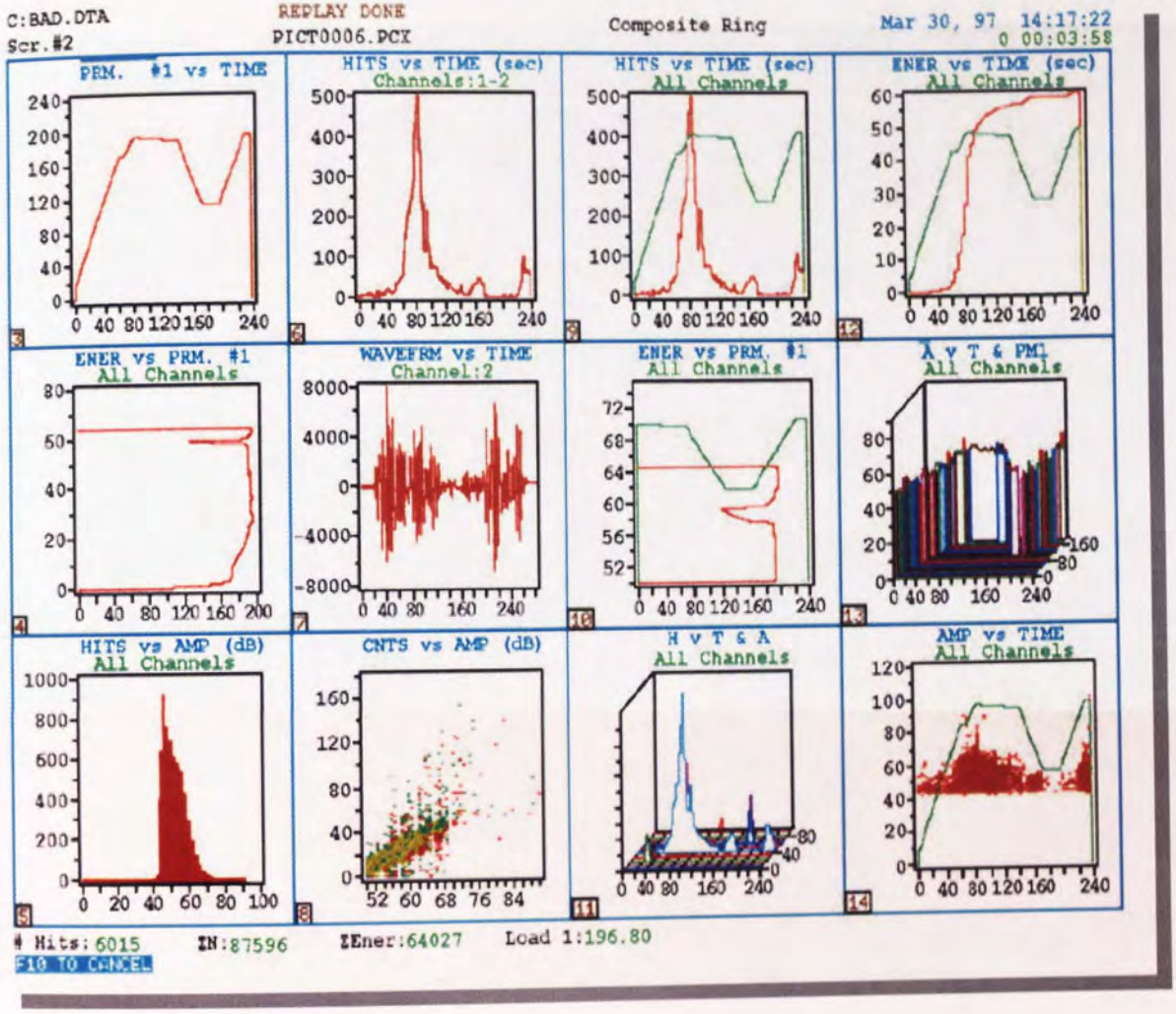

Figure 4-6 Multi-channel feature of MISTRAS 2001.

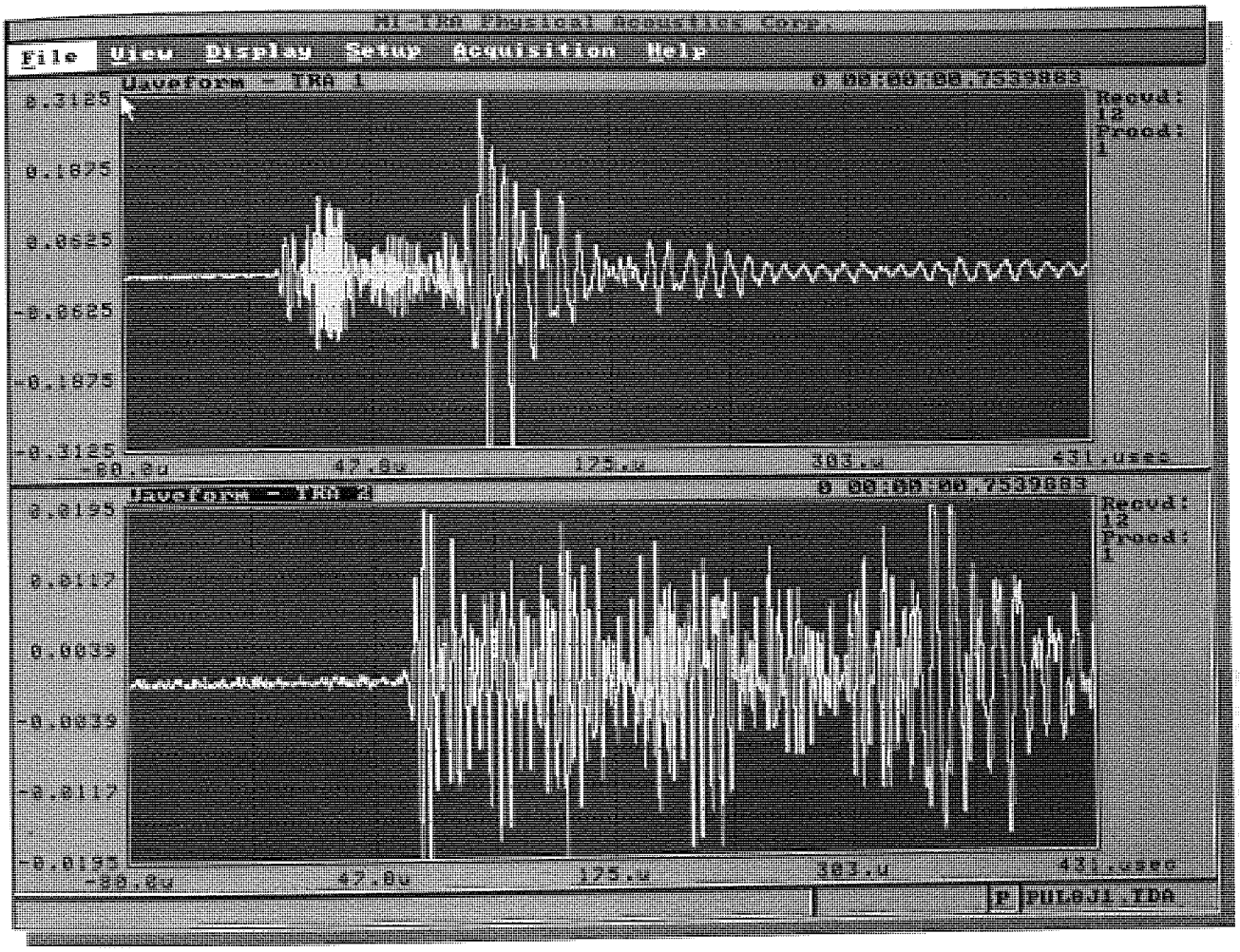

Figure 4-7 AE waveform capturing feature of MISTRAS 2001.

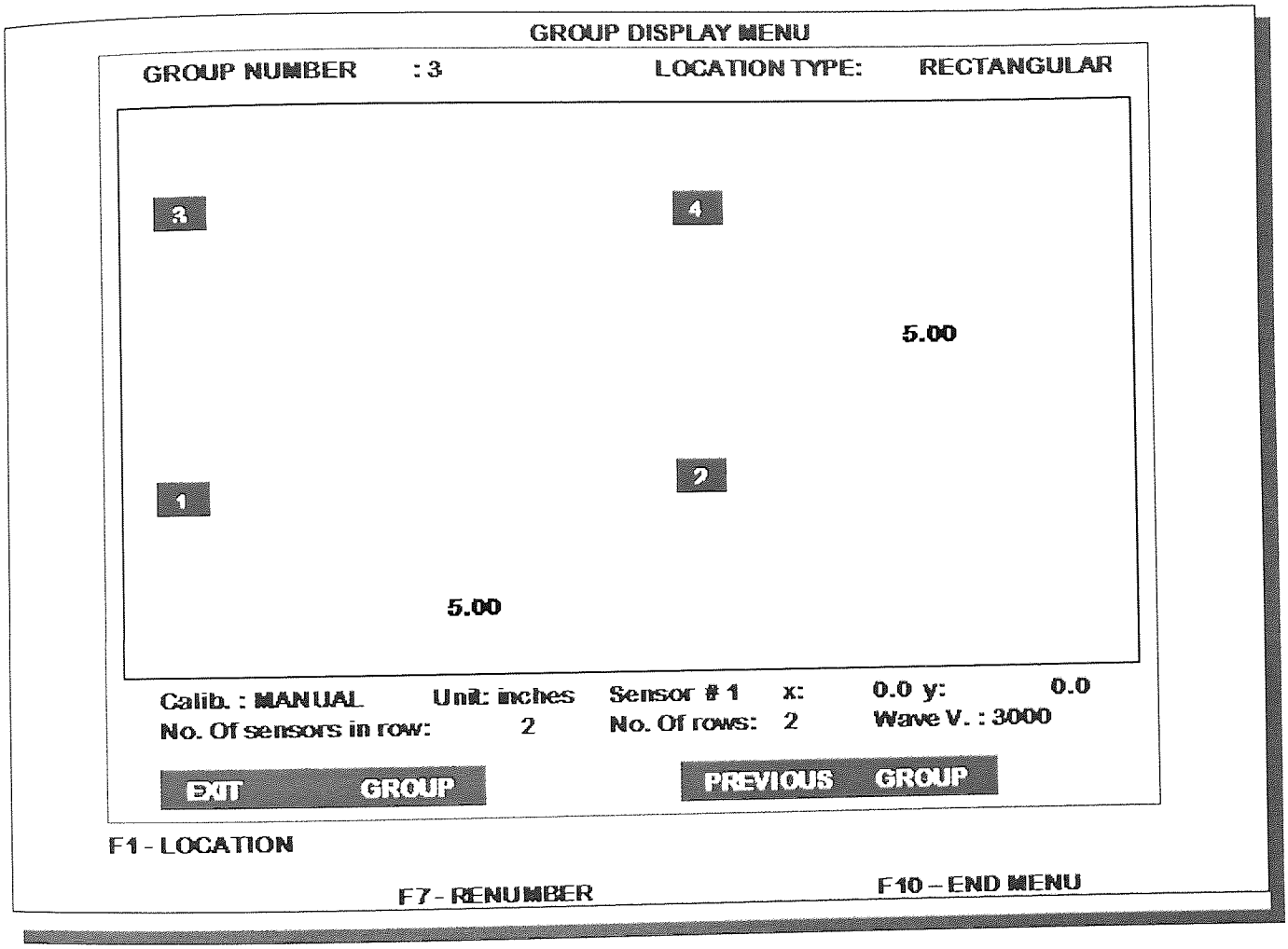

Figure 4-8 Site location feature of MISTRAS 2001.

4.3 Experimental programme for damage level discrimination

In damage level discrimination, the objective was to discriminate and indicate impact damage severity level by extracting information from acoustic emission signals. Thus a series of experiments were based on measuring and acquisition following variables:

1) AE waveform.
2) Impact event energy.
3) Damage area.
4) Impact force history.

Variable 1) and 2) are the raw data for ANN modelling, which can be catalogued as AE measurement. Variable 3) is for the evaluation of modelling outcomes, which can be catalogued as C-scan measurement. 4) is for analysing the impact force data to verify the occurrence of impact damages. Force history monitoring is a feature provided by Rosand impact testor.

4.3.1 Samples description and the AE measurement

Two types of carbon fibre composite were investigated in this study. The first one was fabricated from non-crimp fibre fabrics (T300 carbon fibres and Hexcel 914 resin) supplied by BTI Europe Ltd. It is first fabricated in the form of laminate, which consisted of 4 layers of triaxial {0°±45°} non-crimp fabric, manufactured from 12k T300 carbon fibre tows stitched together with polyester thread. The lay-up sequence was $\{+45°, -45°, 0°, -45°, +45°\}_s$. The fabrics were impregnated with

Hexcel 914 resin using a resin film infusion process to produce, after cure in an autoclave, a laminate 3.8 mm thick with 53% volume fraction fibre (Backhouse, 1998). The second material was BASF 5245 C with T800 carbon fibre (T800/5245) in the form of Preimpregnated materials (Prepregs). The Prepregs layers were assembled in a quasi-isotropic sequence $\{0°,+45°,-45°,90°\}_s$. After autoclave cure, the laminates were 2mm thick, with a volume fraction of 60%. They are typical quasi-isotropic and non-isotropic composite materials widely used in engineering.

The samples for impact testing, 100 mm × 150 mm in size, were cut from the laminate. In the tests of T300/914 composites, a 7.2 kg drop-weight impactor with 20mm tup (head of impactor) diameter was released to strike the specimens once only. Impact energies of the tests ranged from 2J to 15J. Four T300/914 samples were impacted under energy of 7 J to compare the impact damage at the same energy level. Similarly, the T800/5245 samples were treated in the same fashion. The T800/5245 composites were subject to impact striking in energies of 5.4 J, 9.3 J and 13.8 J. Three T800/5245 samples were tested at each energy level. One test was conducted under energy of 20 J. The impactor weighted 2.2 kg with a tup diameter of 20 mm. The training of the BP model was based on the lowest impact event for both materials.

In the tests, two broadband piezo-electronic transducers (PZT) were used for AE signal acquisition and measuring (one for detecting, one for reference). They had a bandwidth of 100 kHz-1.2 GHz and were firmly attached on the surface of the

specimens 80mm away from the impact site (along the diagonal of the panel). Impact events were created by using the Rosand falling weight impact tester. Samples were fixed on the platform of the instrument. The impactor was released to strike the centre of the coupon sample panels from different heights, which in turn gave different impact energy levels. The impact site was designed to locate in the geometric centre of the sample panels, whereas the sensors were placed along the diagonal line at the corners. The layout of the impact site and AE sensors is given in Figure 4-9, which illustrates the position of the sensors and impact sites.

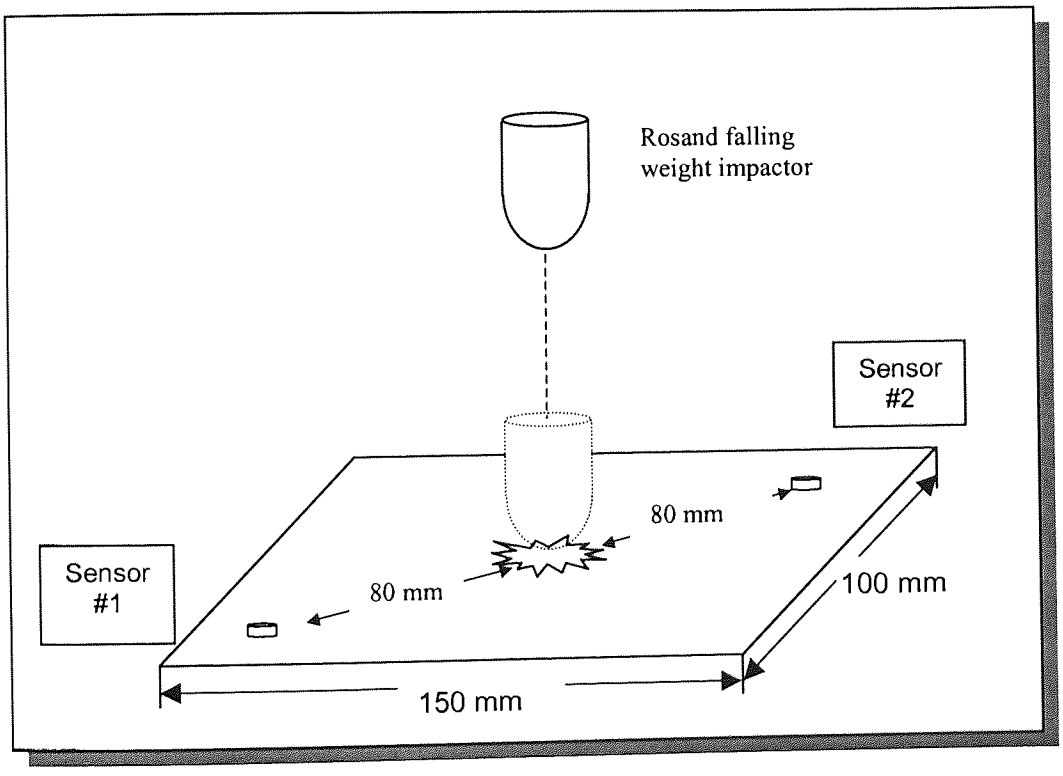

Figure 4-9 Test layout for impact damage level discrimination.

During each impact test, acoustic emissions were recorded using a PAC MISTRAS 2001 system. The signal from a single, discrete deformation event is known as a

burst-type signal. Impact events produce burst-type waveforms. In the tests of the T300/914 composites, the sampling rate used in the AE acquisition was 2 MHz, while a sampling rate of 4 MHz was used on the AE measurements of the T800/5245. This was maintained over the 10 ms duration of the impacts. Typical waveforms from the tests of the T300/914 are shown in Figure 4-10. As illustrated, the intensity and density of the acoustic emission waveform is generally proportional to the impact energy. This inspired the development of a criterion, which can indicate the damage severity associated with impact energy. Based on this idea, an artificial neural network has been implemented to render a solution.

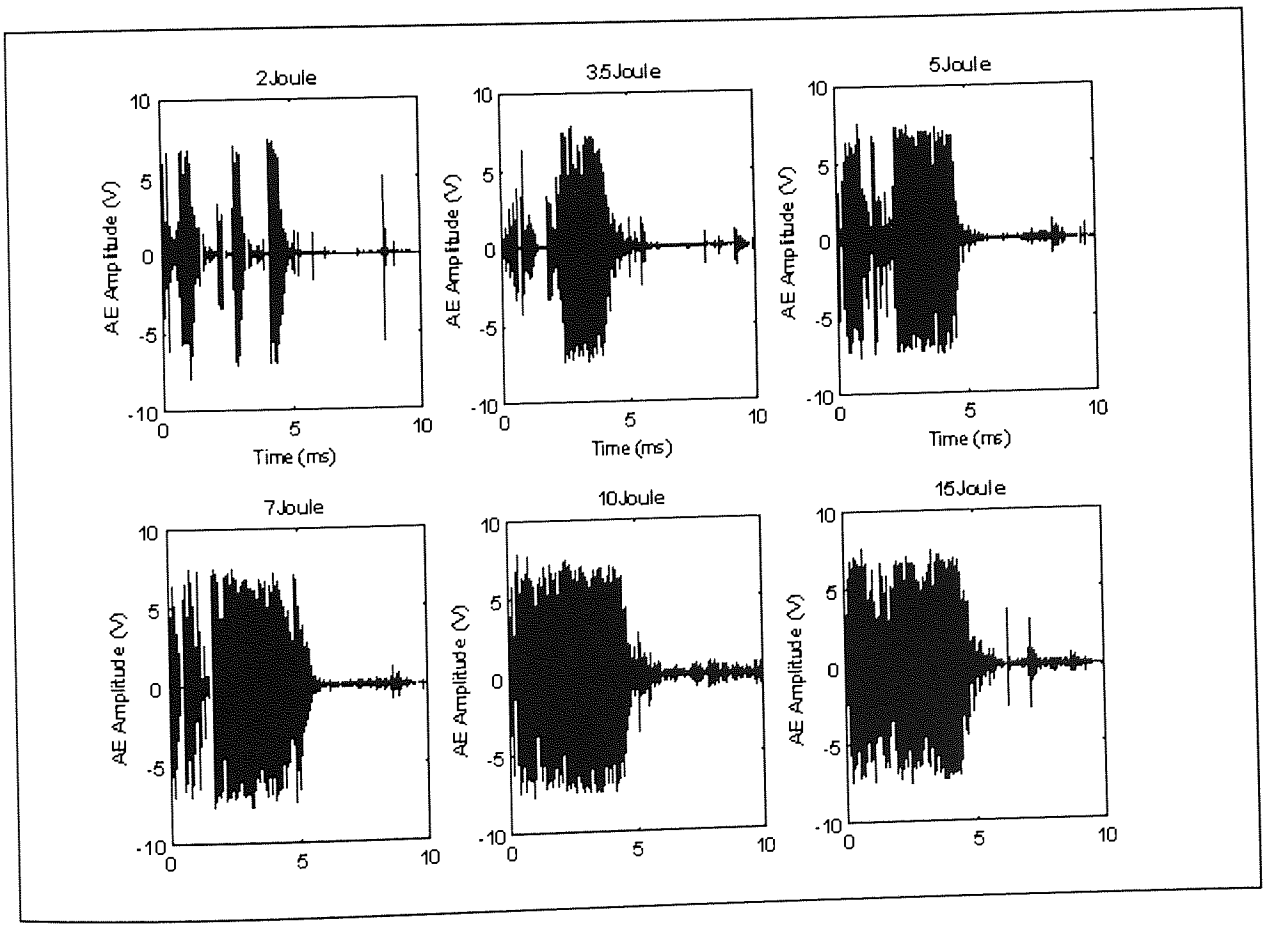

Figure 4-10 Signals detected from AE sensors.

4.3.2 Damage area and impact dynamic measurement

To verify the prediction of ANN model, damage areas firstly were scanned using the HFUS2000 ultrasonic C-scan system. Then an image processor was used to visualise and calculate such areas. The plates were supported vertically inside a tank of water using brackets. Due to high attenuation in composites, a pulsing frequency of 500 kHz was used, with a scan speed of 0.019 m/s. The sampling rate was set to 64 MHz. The transducer sweeps backwards and forwards across the component, receiving and analysing the signal reflected from different surfaces of the damaged specimen and glass plate. The data is analysed and the signal amplitude is converted into a voltage. Finally the data is displayed on a monitor for post analysis, calculation and interpretation. C-scan images of amplitude measurements were recorded for each sample. The analysis and investigation were given in the proceeding chapters.

Meanwhile, as aforementioned, *Rosand Instrumented Falling Weight Impact Tester* also processes a feature of dynamic tracing. In this study, force - time histories were recorded during the AE waveform measuring. The force - time histories were to be used to study the occurrence of impact damages. Some of the results are illustrated in the figures as follows.

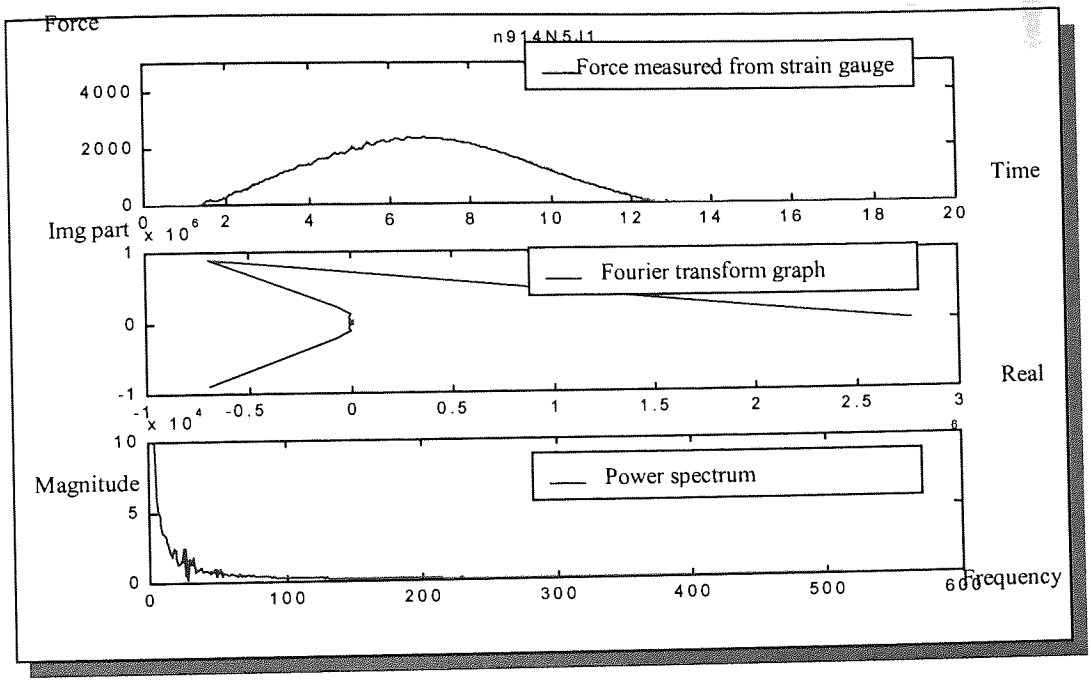

Figure 4-11 Force history of 5J impact and its frequency spectrum

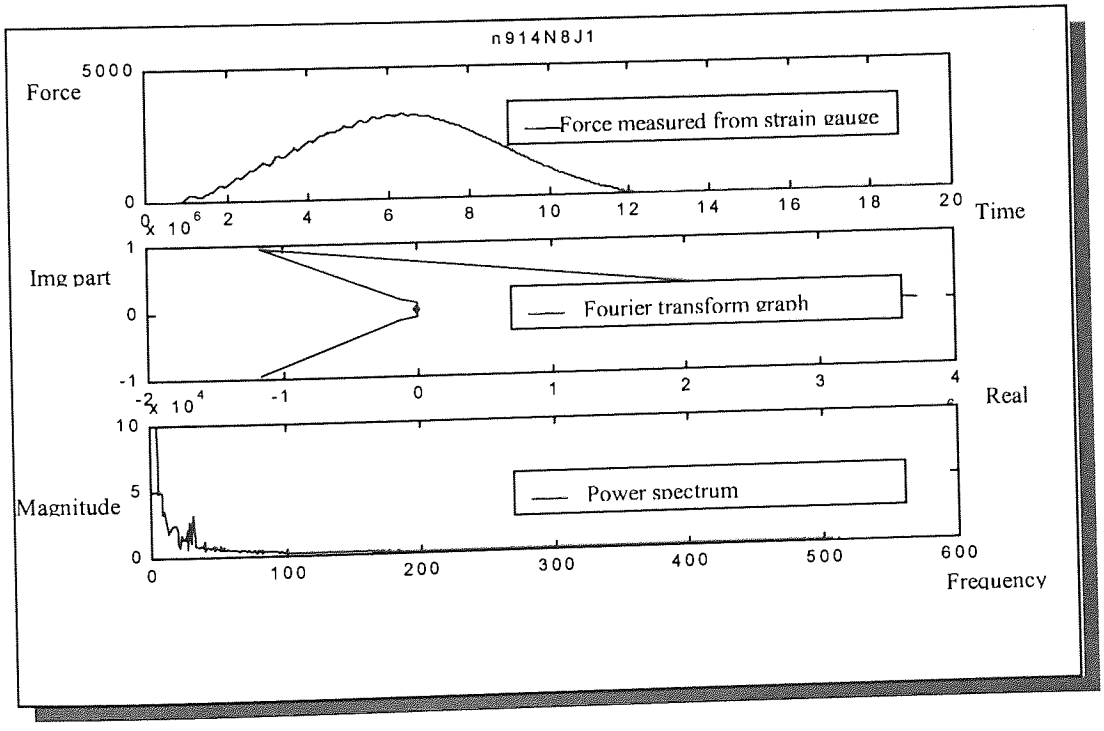

Figure 4-12 Force history of 8J impact and its frequency spectrum

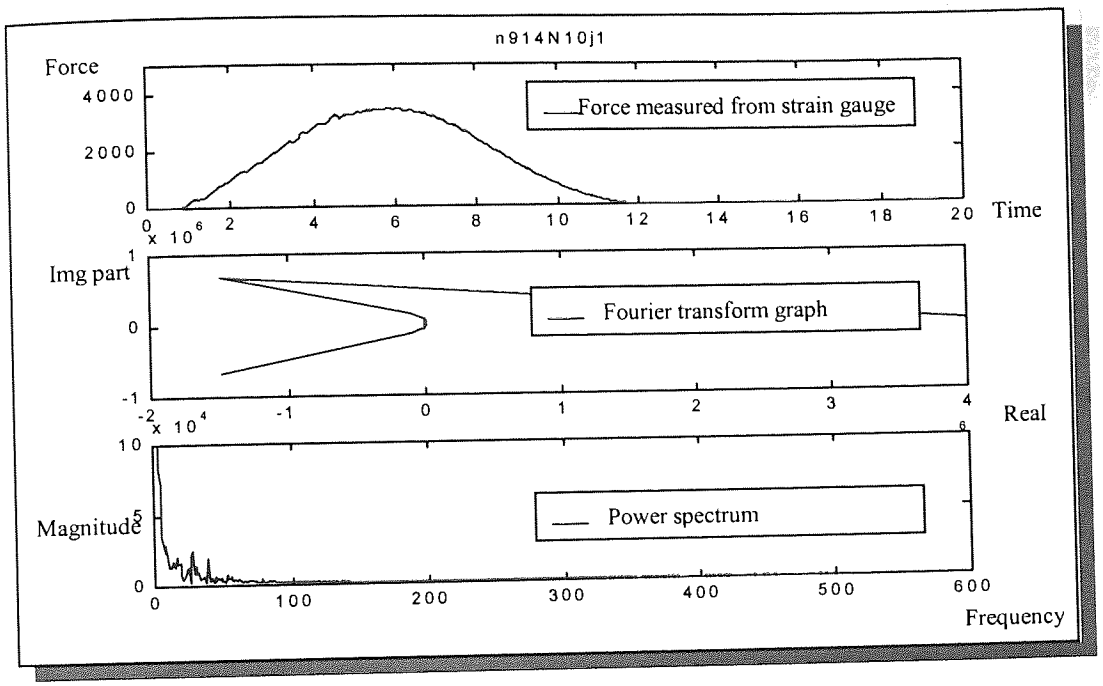

Figure 4-13 Force history of 10J impact and its frequency spectrum

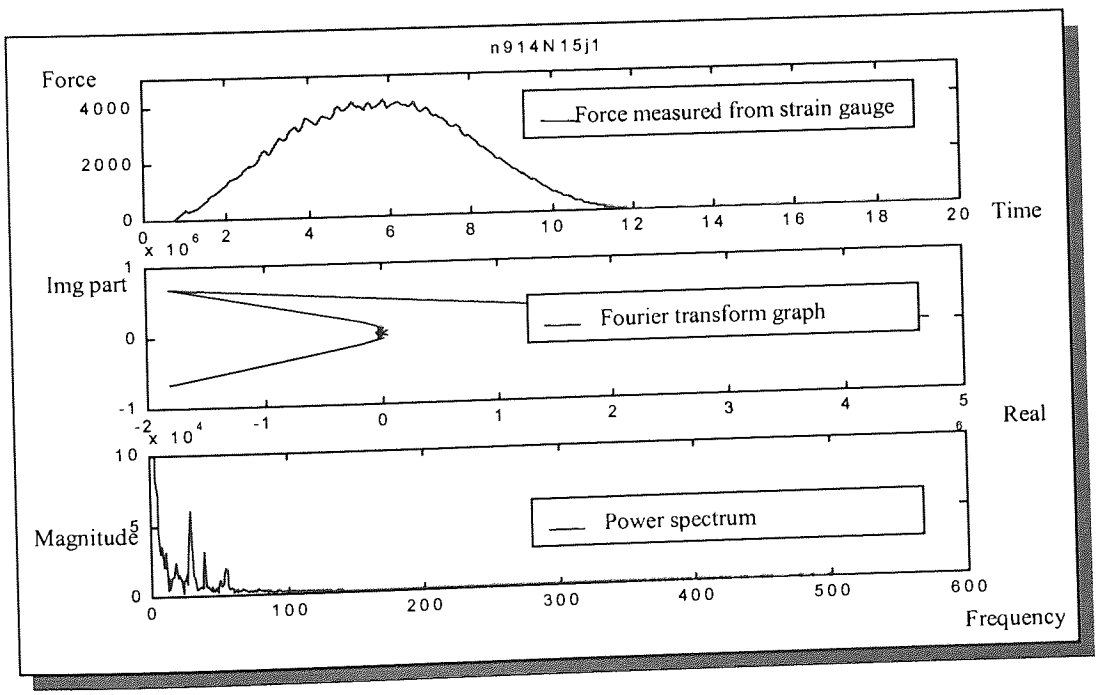

Figure 4-14 Force history of 15J impact and its frequency spectrum

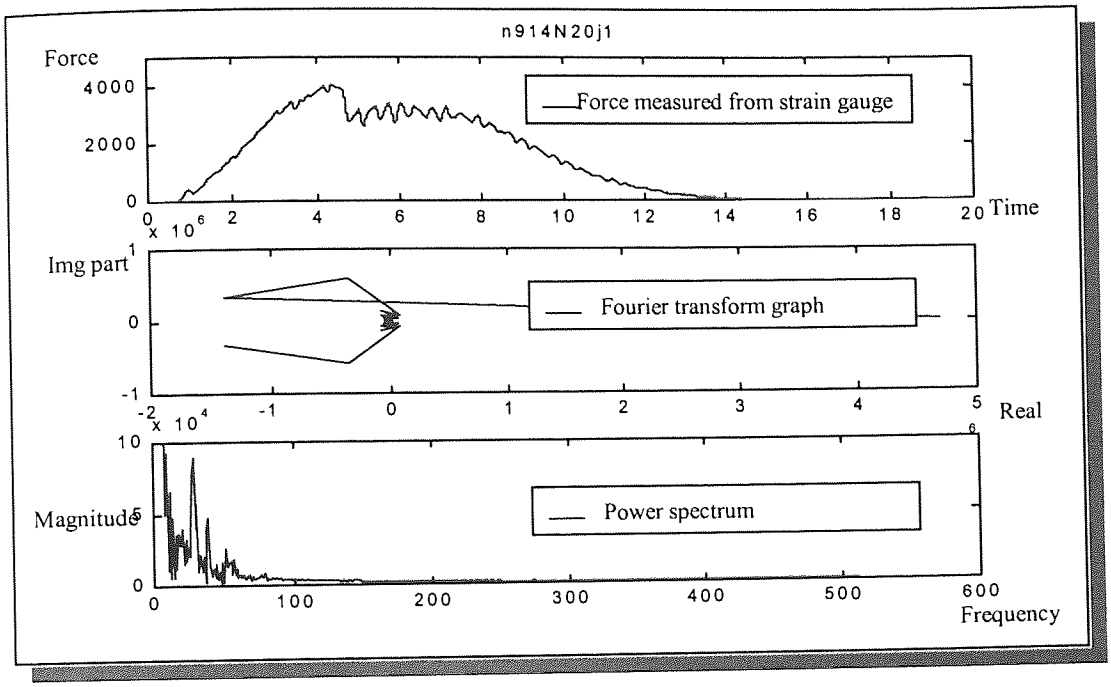

Figure 4-15 Force history of 20J impact and its frequency spectrum

The top diagrams are the force history traces read from the instrument. The middle and bottom diagrams are from FFT, which were performed to show the frequentcy spectrum (The application of FFT is shown in Appendix B). From the Force vs. Time diagrams, vibrations can be observed from the peak areas of the force history curves. The modulations can also be found from the counterpart diagrams in the frequency domain. As the impact energy is increased, there is increasing density of the vibration in terms of amplitude. A further study is given in the succeeding section to verify the occurrence of the impact damage. Although the impact analysis in this project is basically conducted within time domain, the frequency domain outputs are still valuable here as a good general reference.

4.4 Experimental programme for damage location

In the study of damage location detection, the required measurements are as follows:

1) Arrival moments.
2) Time difference (converted from Arrival moment).
3) Coordinates of the impact sites.
4) AE wave propagation velocity.

4.4.1 Experiments description and the measurement

A sample panel used for the damage location experiments was constructed with 3 attached ribs to simulate aircraft structures. It was made of Hexcel T300/914 unidirectional Prepregs with a quasi-isotropic lay-up sequence: $\{-45°_3, 90°_3, +45°_3, 0°_3\}_S$. The surface fibres of the skin were aligned at 45°. The rib and spar caps were fabricated from non-crimp fibre fabrics (T300/914) supplied by BTI Europe Ltd. The laminate consisted of 4 layers of triaxial {0°, ±45°} non-crimp fabric manufactured from 12k T300 carbon fibre tows stitched together with polyester thread. The rib and spar caps contained 60% of 0° carbon fibres, and 40% of ±45° carbon fibres. All the components: skin, ribs and spar caps were co-cured together by applying an epoxy adhesive in an autoclave. The back-face of the panel is shown in Figure 4-16. The cross-section is schematically illustrated in Figure 4-17, labelled with dimensions. The panel size is 900mm by 700mm, with a

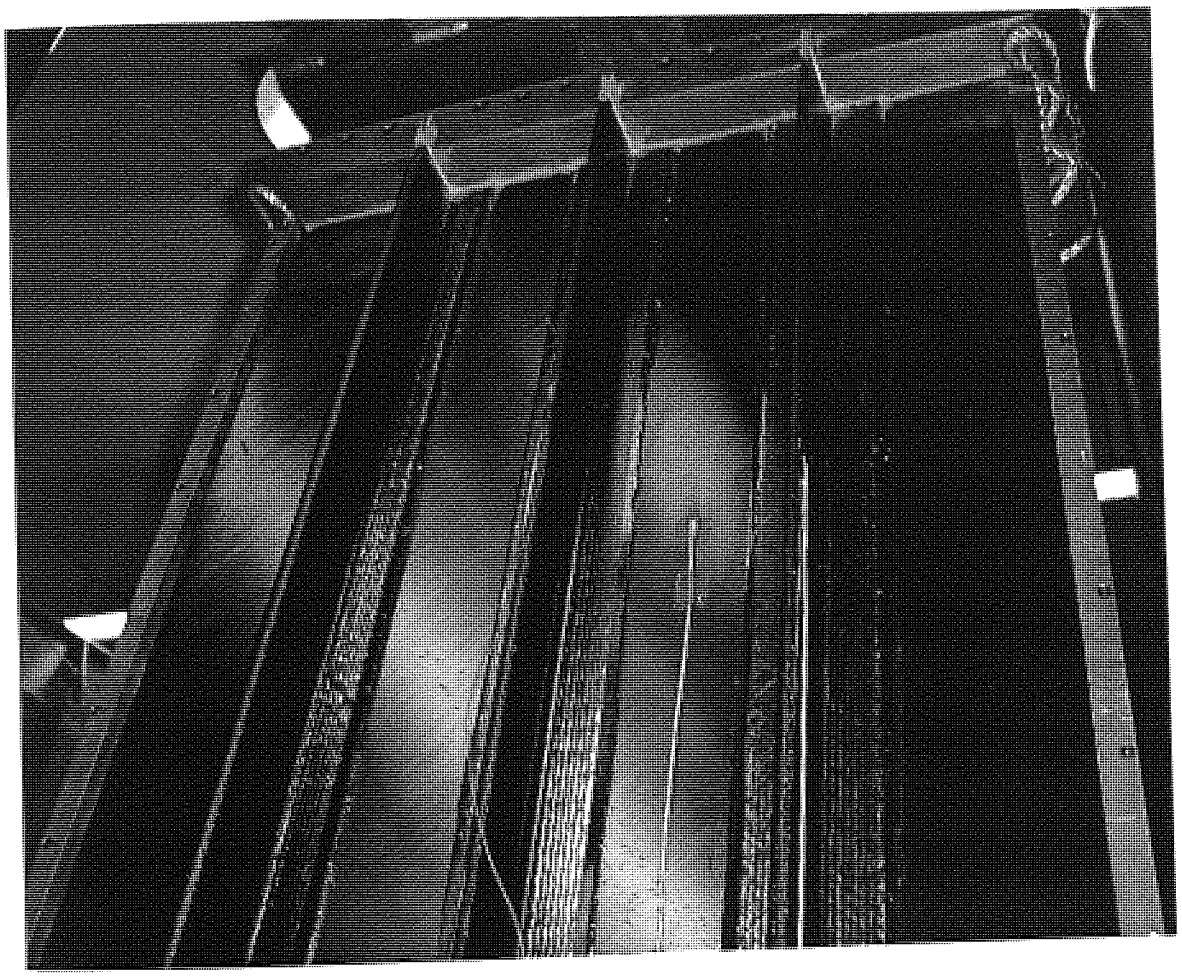

Figure 4-16 Composite panel back face, showing three joint ribs

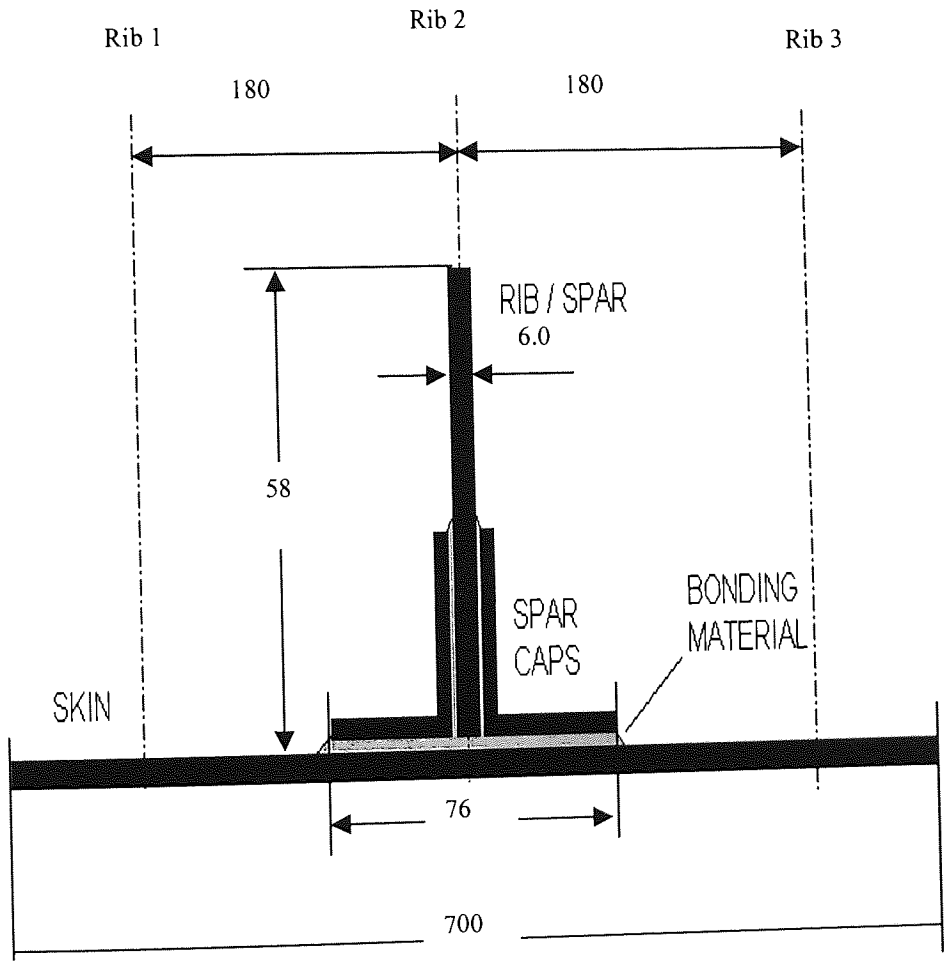

Figure 4-17 Cross-section of the composite panel structure

thickness of 3.3 mm, within which the sampling zone is a 760 x 580 mm rectangle defined to study the damage location.

To locate a source on a flat surface, usually a rectangular, triangular, or star shaped sensor configuration is employed. These sensors are placed about a structure and are independent of one another, as they each have their own co-ordinates and monitoring area. When a data capture is triggered at the nearest sensor to the fault, that moment will be regarded as the first arrival moment, the rest of the sensors will be activated accordingly. Simultaneously, the arrival moments were to be recorded by the data acquisition instrument. In this study, a four-sensor array in a rectangular arrangement was used as shown in Figure 4-18.

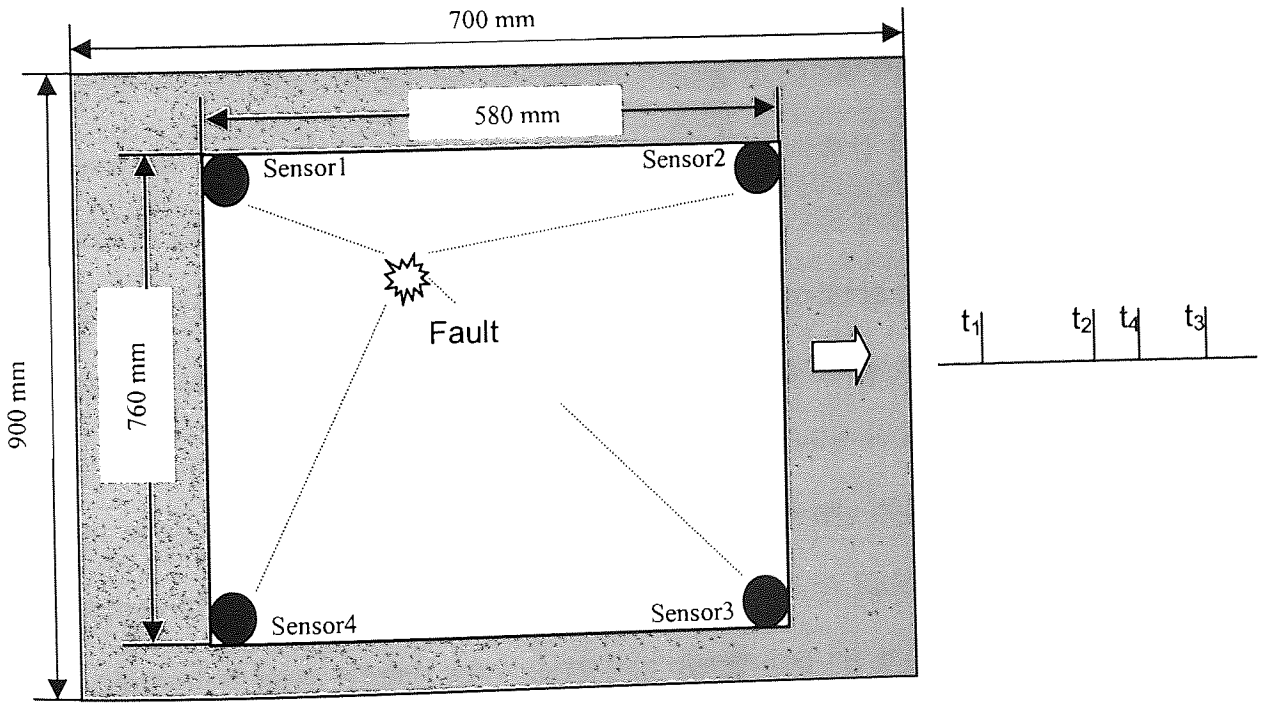

Figure 4-18 Sensor array for receiving acoustic waves in sequence

The experiments for impact location require flexibility and high precision. The falling weight impactor could not produce sufficiently high position precision and could introduce unwanted noise into the experiments. Thus, a conventional test rig could not be used. To generate an acoustic emission pulse similar to an impact event, a pulse piezo ceramic transmitter was built. This pulse injector produced a reproducible burst-waveform, similar to an impact event at a 1s interval. The duration of each burst was about 0.5 ms. The injector was coupled to the surface of the skin by silicone grease. Thus it could be re-positioned to different sites on the panel to simulate impacts at different locations.

As mentioned, a sensor array of rectangle configuration was used in this study. Four broadband piezo sensors (S1-S4) were attached at each corner of a 760 x 580 mm rectangular panel, as shown in Figure 4-19. A PAC MISTRAS 2001 system was used to record the acoustic waves travelling from the site of the injector to each sensor. The sampling rate used in the AE acquisition was 2 MHz. The arrival time of the pulse was defined when the amplitude of the acoustic wave exceeded 40 dB. To train the neural network, arrival time measurements were made on a set of 42 simulated impact events, which were evenly located over the planar surface, also shown in Figure 4-19. It geometrically divided the anisotropic properties of the panel into distributed studying zones. A further set of 24 events was generated later. These were randomly distributed on the flat surface of the panel and were used for validation of the predictions of the trained network. As aforementioned, the PAC system also provides a function to locate an impact

event by applying an arrival time analysis using a single wave speed. This method performs well in the case of an isotropic material panel. However, when applying PAC system to non-isotropic or quasi-isotropic materials, the equipment often fails to produce accurate locations. The prediction from artificial neural network, however, should give a much better location performance. The results from both PAC and ANN models have been listed and compared in Chapter 6. The outcome of ANN prediction is encouraging after the model training. Detailed analysis was given in the proceeding chapters.

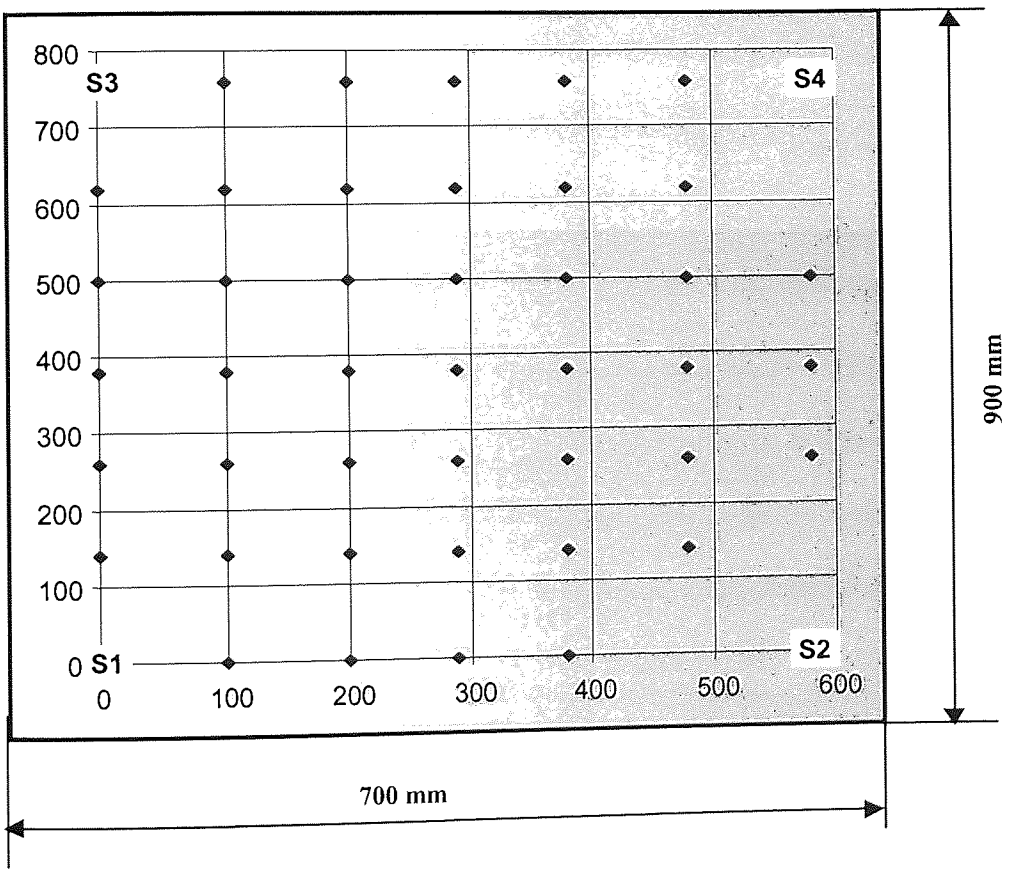

Figure 4-19 Sensor arrangement on the skin surface and the location of simulated impacts for neural network training.

(S1, S2, S3 and S4 are locations of AE sensor)
(♦--Location of hits generated by a piezo-transmitter)

4.4.2 Acoustic Wave velocity measurement

Acoustic emission propagating velocity is an important parameter in the study of impact damage location. Unlike isotropic materials, composite structures usually have a far more complicated speed-distribution due to variances of fibre and matrix properties. In order to gain better understanding of acoustic wave behaviour within the composite, a velocity test was designed to produce a contour plot of the T800/914 panel. The results of the test are also very helpful in terms of analysing and evaluating the ANNs impact damage location prediction. The principle of the test is based on the relationship between time, speed and distance.

To detect AE signals, two piezo-electronic transducers (PZT) were used. One of them was bonded in the geometric centre on the panel surface using Glycerin (the couplant). The other PZT was placed onto the surface 110 mm away from the central sensor using the same couplant, then 190mm, and finally in the distance of 270mm. Impact inciting point is 80mm away on the contrary direction along the project which links up two sensors sites. The whole panel was then divided into 24 evenly spaced zones. Sampling took place in every 15 degree as shown in a topo-map for the speed test is given in Figure 4-20 and Figure 4-21.

As the PZT sensor was moved outwards the centre of the panel, different arriving times are detected from the sensor 2. Provided its position is known and the time difference can be measured, V, the velocity, then can be calculated using the (4-4).

$$V = \frac{\left|\sqrt{(X_1 - X_0)^2 + (Y_1 - Y_0)^2} - \sqrt{(X_2 - X_0)^2 + (Y_2 - Y_0)^2}\right|}{\Delta t_{12}} \quad \textbf{(4-4)}$$

where Δt_{12}, the time difference between sensor #2 and sensor #1

V: the velocity of acoustic emission wave

(X_1, Y_1) is the co-ordinates of the pulse injector

(X_0, Y_0), (X_2, Y_2), are the coordinates of sensor #1 and sensor #2.

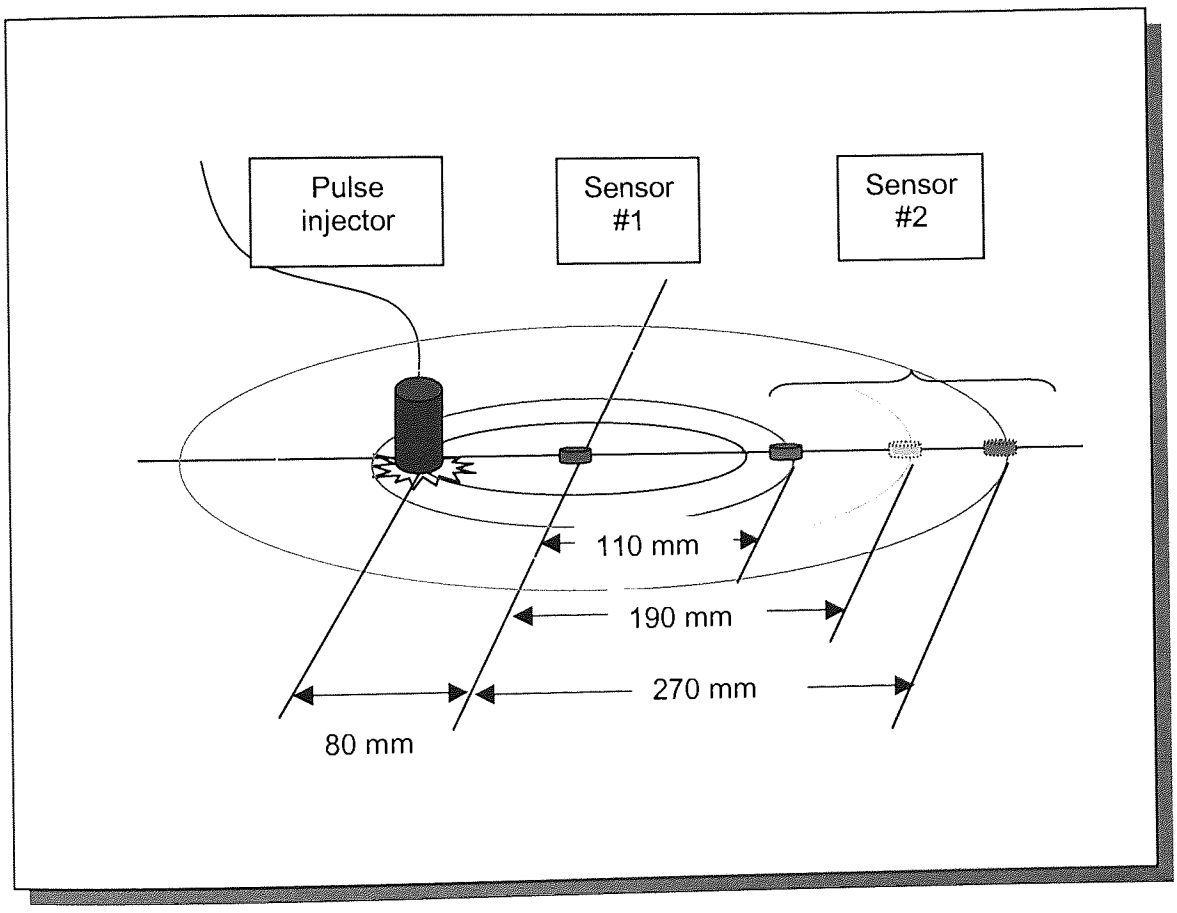

Figure 4-20 Topography of the AE velocity test.

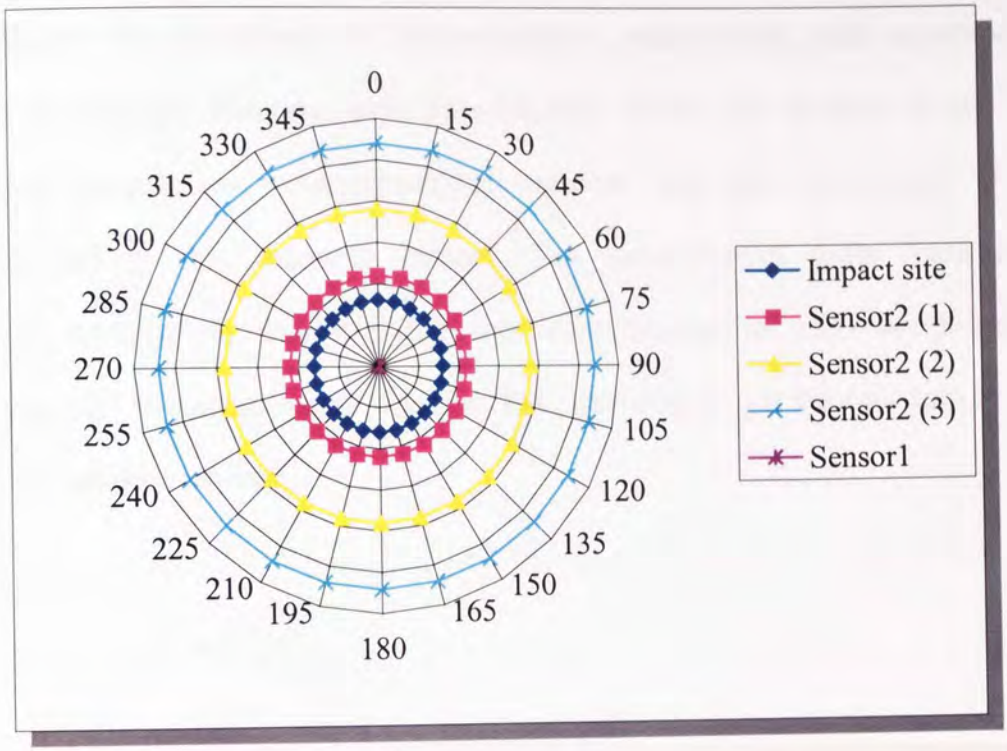

Figure 4-21 Top-view of the AE velocity test.

In Figure 4-21, the impact sites were represented in blue diamonds. What lies in the centre of the circle is Sensor 1, which is a fixed position. Sensor 2 moved its position accordingly along the projecting line which links up the impact site and Sensor 1. Thus, the order of the placements is as: Impact site- Sensor 1(fixed)- Sensor 2 (position1)-move to- Sensor 2 (position2)-move to- Sensor 2 (position3).

4.5 Conclusions

This chapter has described the instrumentation, equipments, and experimental method of both the damage level discrimination study and location study. The measuring parameters were introduced together with the description of the measurement in this research project. The experimental tests have been conducted successfully. Essential data sets were obtained for valid neural training and modelling. The experiments were just the initial step to get the raw data to train the neural network models.

Chapter 5 The study of damage level discrimination

"Nothing is hard in this world if you dare to scale the heights"

(Chinese Proverbs)

5.1 Introduction

This chapter investigated the damage level discrimination using ANNs. The neural training was based upon the least impact energy events of composite panels. Then ANN models acted as damage indicator and corresponded to the different impact events. This section covered a whole range from the mechanism description, the modelling procedures and validation *etc.*

5.2 Background of damage level discrimination

Different levels of damage were produced according to the different impact energy and materials in this study. The topographies of the sample surfaces, being subject to impact load, provided a straightforward expression of impact damage. Photographs of selected samples are shown in the Figure 5-1, Figure 5-2, Figure 5-3, and Figure 5-4. In the low velocity (speed is not in excess of 20 m/s) impact events, the top surfaces generally have delaminated, and consequently buckled, save for a small zone surrounding the impactor, where the transverse compression and small shears have resisted delamination. At the bottom surface, however, delamination resulted in crack formation in the direction of fibre layup. The visibility

of surface damage ranges from barely visible to clearly visible according to the impact energy level.

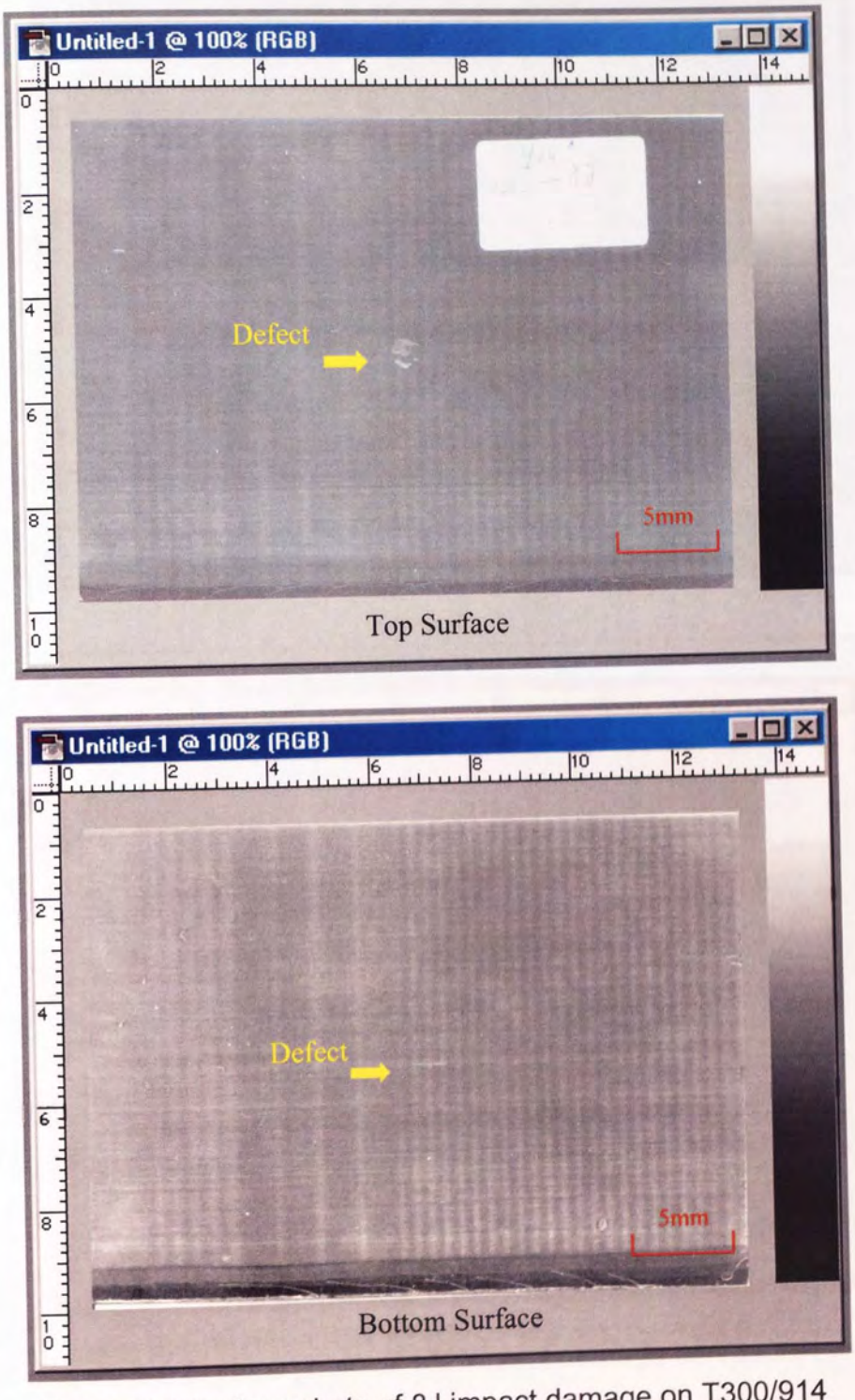

Figure 5-1 Surface photo of 8J impact damage on T300/914

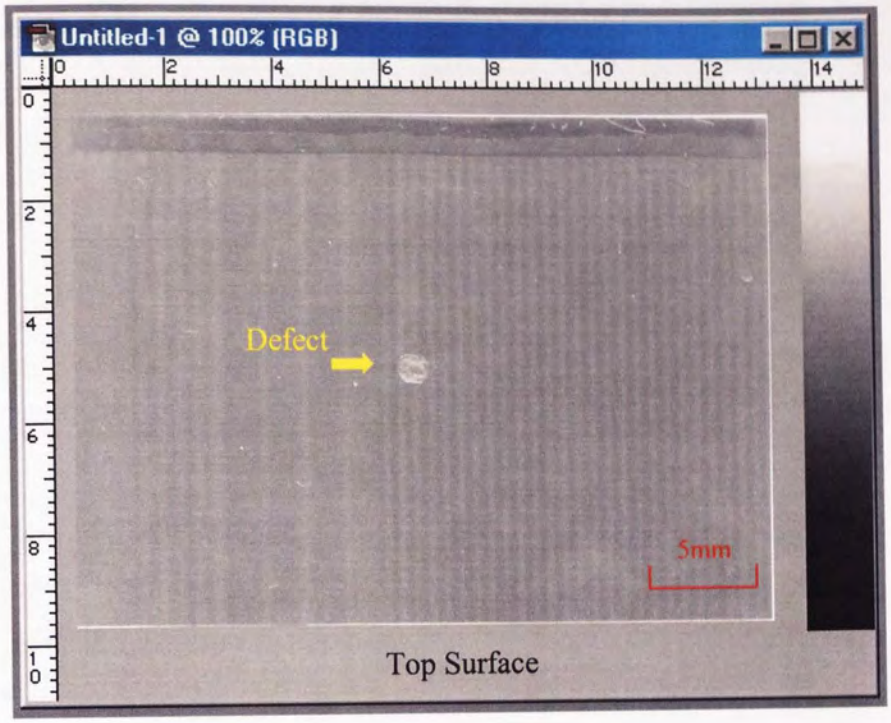

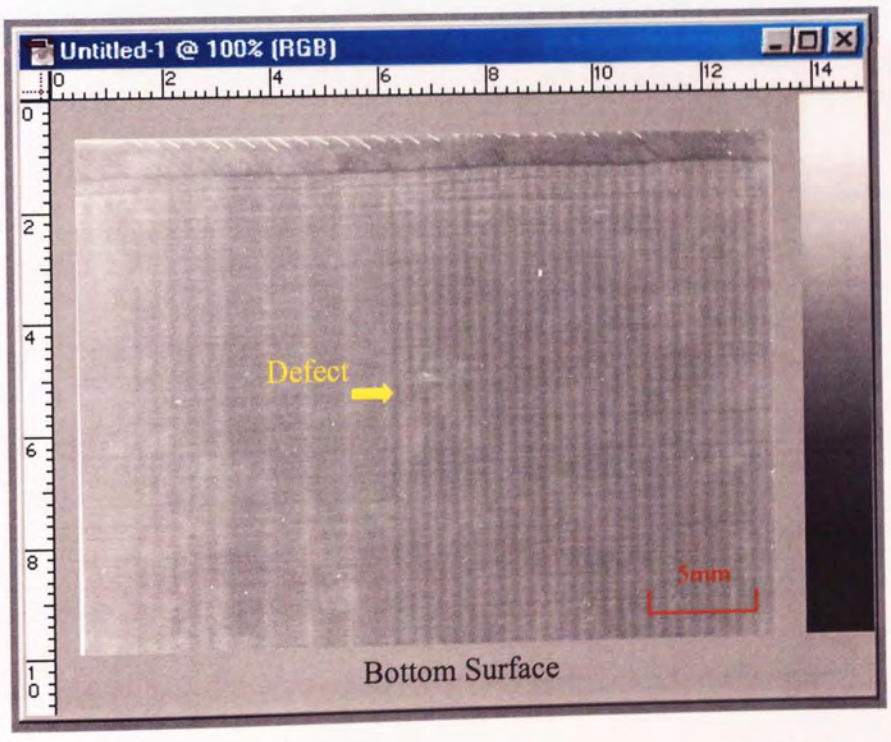

Figure 5-2 Surface photo of 10J impact damage on T300/914

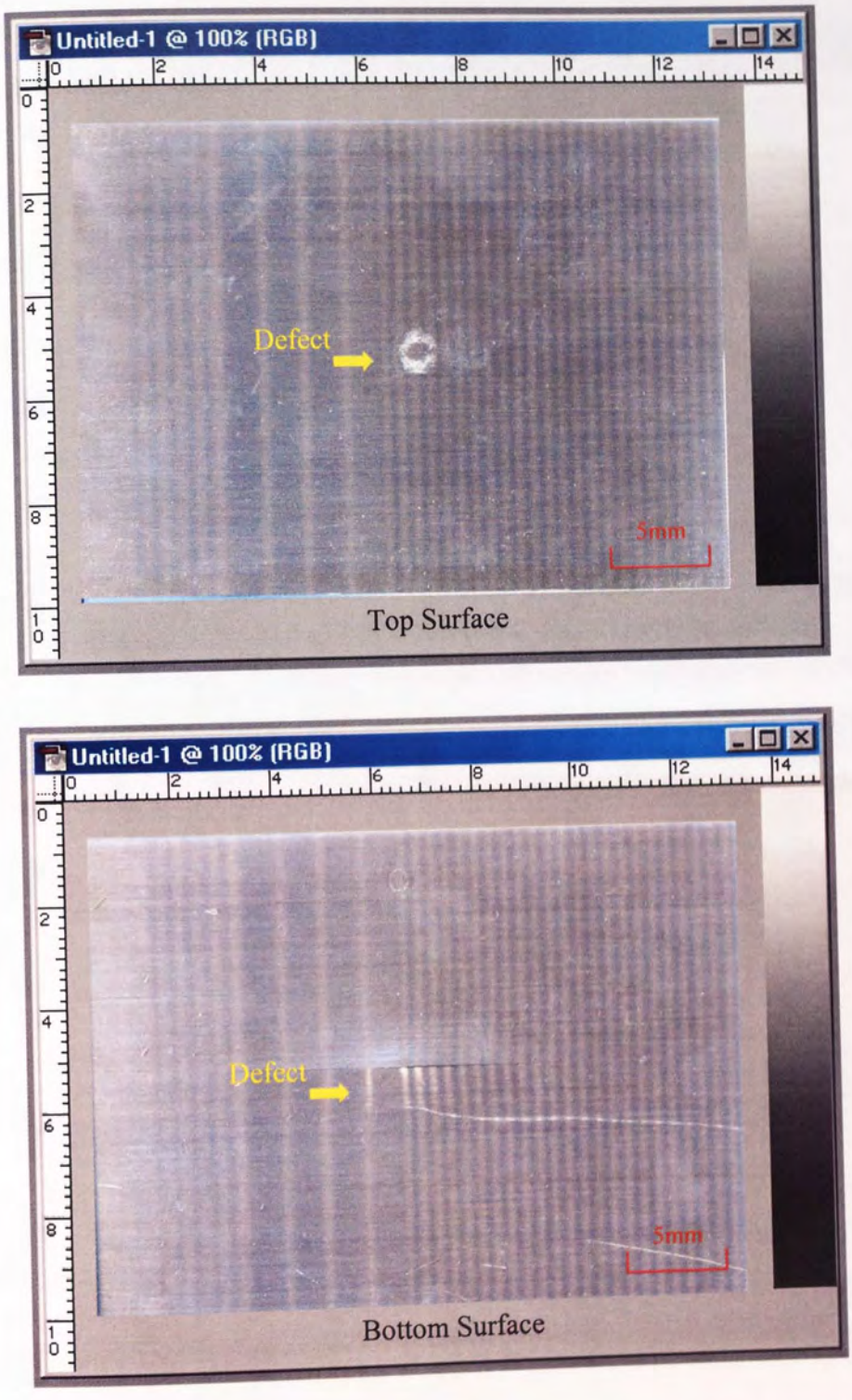

Figure 5-3 Surface photo of 15J impact damage on T300/914

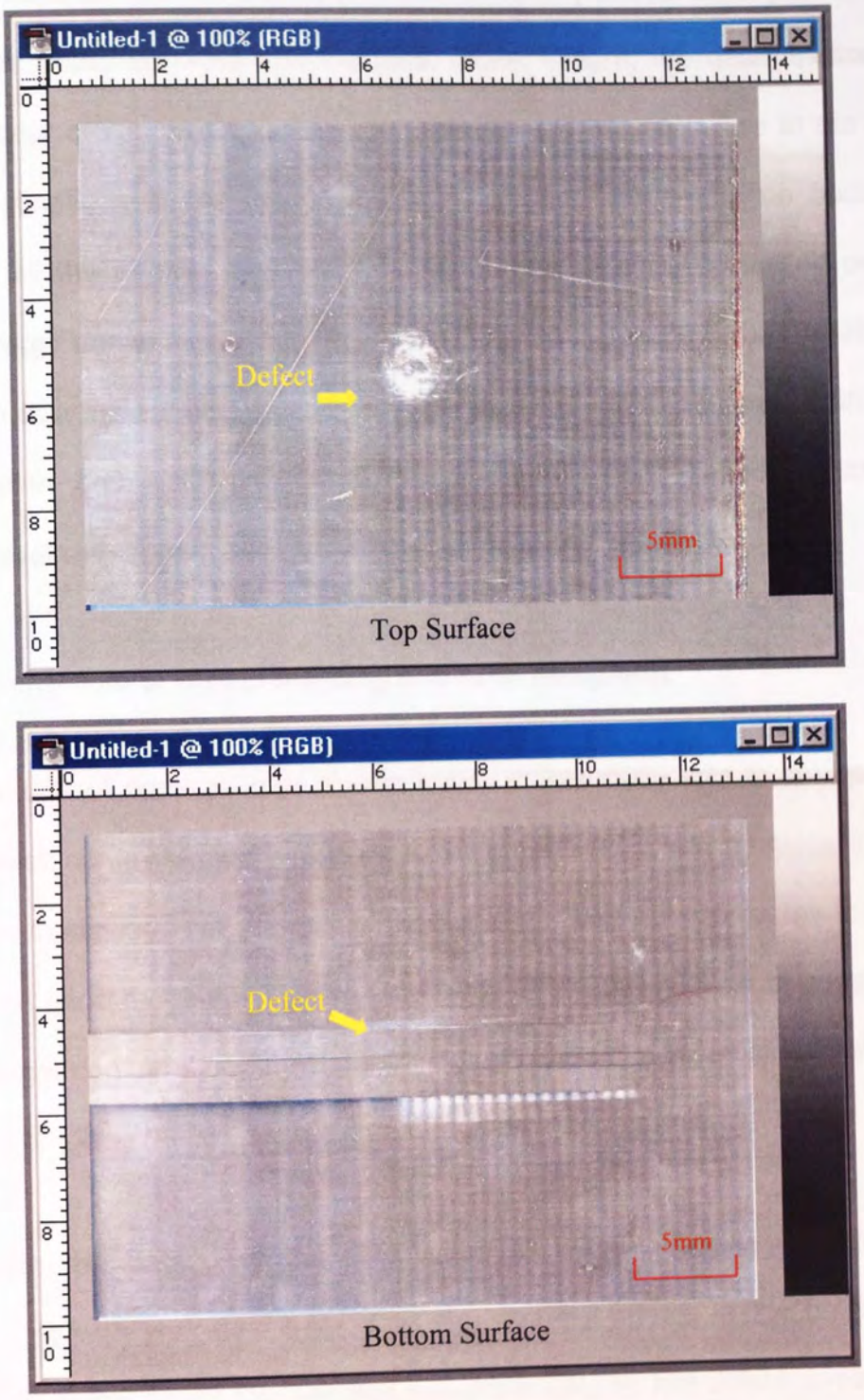

Figure 5-4 Surface photo of 20J impact damage on T300/914

Previous research (Davis, 1994) revealed that locally inertia force yields a stress field on the upper surfaces and the back faces. In turn, the delamination is the direct product of compression failure on the top and tensile failure at the bottom. Those descriptions fit the impacted sample panels very well. The buckles are visible on all the panels. Significant cracking could only be witnessed on higher impact energy cases as in 15J (Figure 5-3) and 20 J (Figure 5-4). Therefore, it is evidenced that impact energy can be correlated with damage level. In this study, determination and discrimination of the damage level is based on correlating damage level with impact energy by implementing an ANN model.

5.2.1 Mechanism of model building and ANN designing

The main idea of damage level discrimination in this study was to set up an ANN model, which can dynamically respond to the impact energy. It is basically an issue of system modelling. Yet, there are no standards and secure routes in terms of guaranteed good models in system modelling. Given the number of possibilities, it is easy to get confused about what to do, what model structures to test, and so on. According to Ljung (2000), practical procedures consist of 4 steps.

1) Observe the data: Plot the data. Look at them carefully. Try to see the dynamics with your own eyes. Can you see the effects in the outputs of the changes in the input? Can you see non-linear effects, like different responses at different levels, or different responses to a step up and a step down? Are there

portions of the data that appear to be "messy" or carry no information? Use this insight to select portions of the data for estimation and validation purposes.

2) Getting a Feel for the Difficulties: Usually plots for spectral, correlation analysis are very helpful to determine the complexity of the problem. Look at the agreement between the:

- Spectral Analysis estimate and the ARX and state-space models' frequency functions.
- Correlation Analysis estimate and the ARX and state-space models' transient responses.

If these agreements are reasonable, the problem is not so difficult, and a relatively simple linear model will do a good job.

3) Examining the Difficulties: There may be several reasons why the comparisons in Step 2 did not look good. The most common cases are that the model is unstable, feedback in data, disturbance model, model order, additional inputs, non-linear effects, *etc*.

4) Fine Tuning Orders and Disturbance Structures: For real data there is no such thing as a "correct model structure." However, different structures can give quite different model quality. The only way to find this out is to try out a number of different structures and compare the properties of the obtained models.

Conceptually, damage level discrimination modelling is similar to the classic system identification method. The starting stage of both methods is to determine the input and output of the plant or neural network model. The difference, however, is that convention system identification method (parametric models) needs to estimate the classification of the issue and specify a certain approximating function accordingly. This more or less relies on the skills and experiences of the modeller. While, the application of ANNs, in general case, is rather like to use a universal approximator. Ideally, ANNs can be used as "plug-in and play" regardless to the classification. It is desirable to map the relationship between relevant or even possibly relevant data and target data. To this degree, this means artificial neural networks is a more user-friendly modelling approach.

When applying a neural network algorithm, a proper analysis is required for data pre-processing, training, and validation as prescribed by Tarassenko (1998). In the study, which is the subject of this thesis, the ANN modelling was conducted in the similar fashion for both damage level discrimination and damage location. In the damage level study, impact energy results and indicates the levels of impact damage. It however can be detected in a form of AE waveform. Thus, a basic model was trained using the AE waveforms feature segments as input and detected AE signals (created by the lowest impact energies) as target. The model was trained to reproduce the input AE signal with as small a mean square error as possible. In T300 CFRP, 2J impact event was used to train the model. The experimental result indicated that the impact damage at 2J was vestigial and was

regarded as non-damaging. Later on, AE waveforms produced by other impact events on this material were fed into the trained model to obtain mean square errors (MSE) between the outputs for AE produced by 2J and those produced by greater impact energies. The process was repeated for the set of AE signals obtained after impact of the T800 material, using the AE from the 5.4 J impact as the training set. The scheme of modelling is shown as in Figure 5-5. In the diagram, neural network training part represents lowest impact energy training. Residual generation part indicates the new impact events input in the ANN.

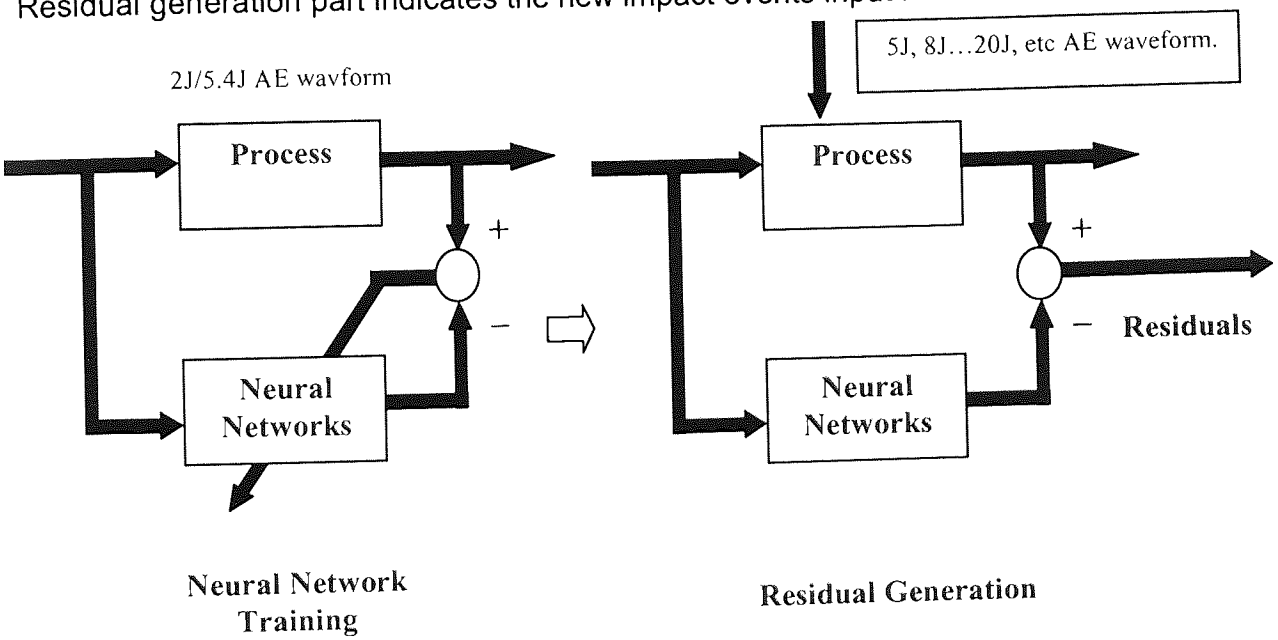

Figure 5-5 Scheme of neural modelling for damage level study

In this study of impact damage discrimination, a Back Propagation (BP) algorithm neural work was used. The BP network model is composed of two layers, a hidden layer and an output layer. In the first layer, 8 neurons calculate the input data and adjust the parameters (biases and weights) of the layer, then transfer the data flow into the next layer where one neuron was set to adjust the biases and weights of

the output layer. Each presentation of the set of training vectors is called an epoch. Since the network performance target was pre-set, the calculation had to be repeated until the pre-set goal was satisfied. In this case, a total of 77 epochs were carried out to achieve the goal. A transfer function was used to map a neuron (or layer) net output "n" to its actual output. The transfer function of the first layer was selected as "hyperbolic tangent (tansig), the algorithm of which is expressed as:

$$O_j^{(1)} = \frac{2}{1+e^{-(2\sum W_{jn}^1 P_n)}} - 1; \qquad j=1\ldots8 \tag{5-1}$$

$O_j^{(1)}$: output of the hidden layer,

$W_{jn}^{(1)}$: weights of the hidden layer

(5-1) provides a function mathematically equivalent to hyperbolic tangent. This approach allows faster modelling than the MATLAB implementation of hyperbolic tangent (Demuth and Beale, 1998). This function is a good approach for neural networks, where speed is important and the exact shape of the transfer function is not critical. The MATLAB verification scripts are given as follows:

% Define the calculation and timing for tansig

x = rand(2048,1); t = clock; tansig(x); Time1= etime(clock,t)

Time1=0.0500

% Define the calculation and timing for hyperbolic tangent

x = rand(2048,1); t = clock; tanh(x); Time2= etime(clock,t)

Time2=5.0200

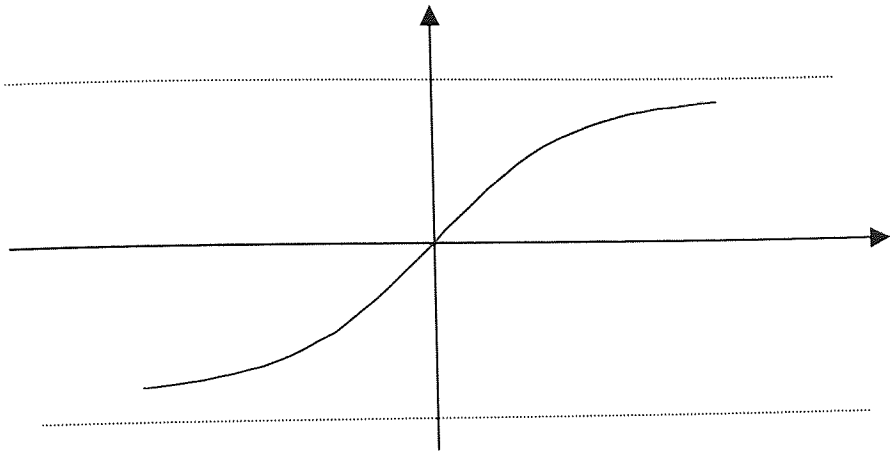

Figure 5-6 Tan-sigmoid transfer function

(Note: During the course of training, the thesis writer noticed another influential factor of the computing speed is the training algorithm. This study used Levenberg-Marquardt algorithm as training algorithm. A speed comparison of different algorithm is given in the further discussion section of this thesis.)

The second layer model is a linear transfer function (purelin), defined by:

$$f_{out} = \sum W_{kj}^{(2)} O_j \; ; k=1, 2 \qquad \textbf{(5-2)}$$

f_{out}: output of the output layer

$W_{kj}^{(2)}$: weights of the output layer

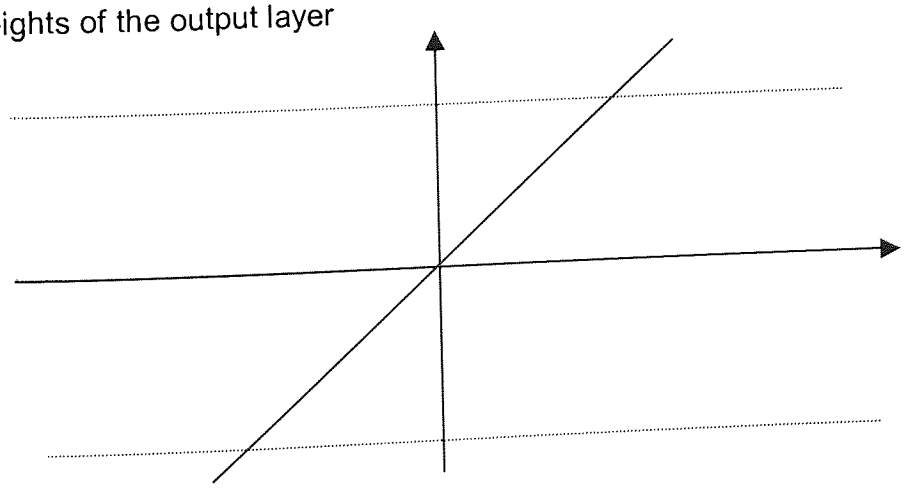

Figure 5-7 Linear transfer function

It has been shown (Cybenko, 1989; Hornik *et al.*, 1989) that a two layer MLP with sigmoid non-linearities can approximate any function with arbitrary accuracy and this therefore reduces the problem of defining the network architecture to one of choosing the number of hidden units. As to the selection of Neurons, there is further discussion in the later chapter. Figure 5-8 shown below gave the description of network structure.

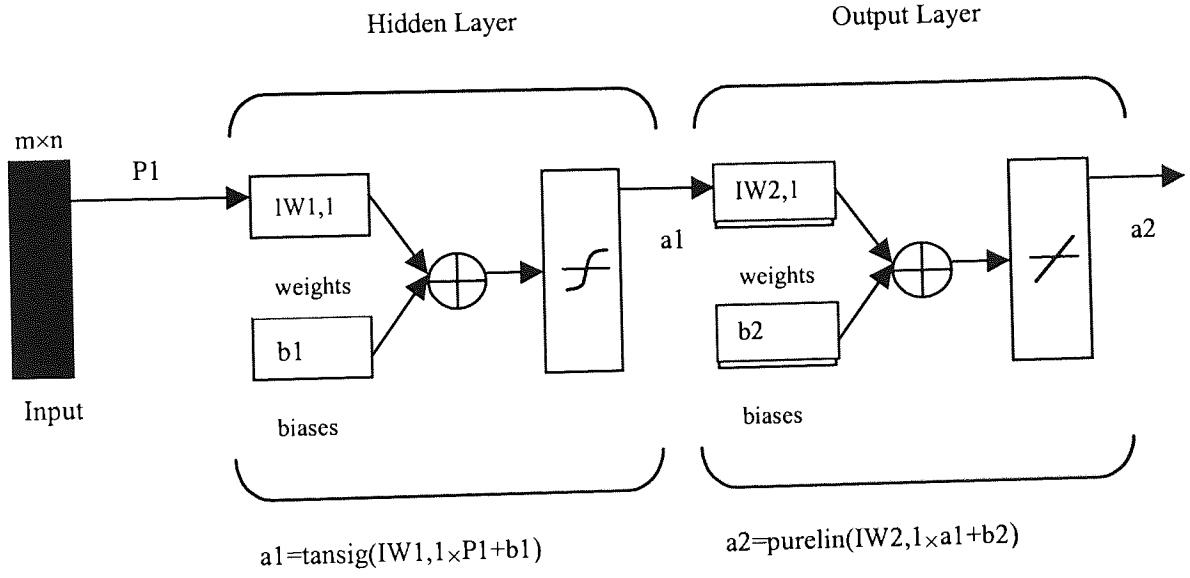

Figure 5-8 Structure of the neural network model (Mathematical)

In the study, the input data used were AE time-domain waveforms. The signal detected from the AE sensors is the combination of a real time AE waveform and its reverberation. It was supposed therefore that the signal consisted of several step delays. Judging from the available data, it was decided to employ an ARX model for the simulation. In practice, an order of 4 gave the best performance. Thus, the input vector to the BP network was in the form of

$[y(t-1) \quad y(t-2) \quad y(t-3) \quad y(t-4)]^T$, as it was shown in Figure 5-9. The parameter $y(t)$ was the target data that was the least damaged AE time-domain waveform (2 J or 5.4 J impacts). In Chapter 7, a further study explains the criterion as how to choose input vectors. AE waveforms detected from other impact energies were then fed into the trained model later to generate the mean square error (MSE).

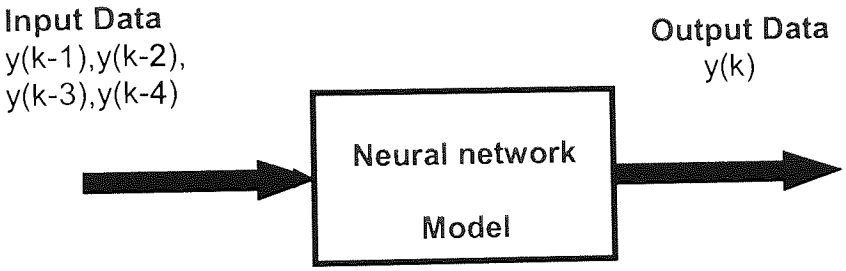

Figure 5-9 Layout of the model

During the network modelling, the MSE was used as the error performance index, given by:

$$MSE = \frac{1}{N}\sum_{t=1}^{N} e(t)^2 = \frac{1}{N}\sum_{t=1}^{N}[y(t) - a_2(t)]^2 \qquad \textbf{(5-3)}$$

where N is the data length and $a_2(t)$ is the NN predicted output. After completion of training, the AE data obtained from the rest of the impacts were used as inputs to the trained model. The MSE values obtained as output then represent the difference between the AE produced by a 2 J impact and the other AE outputs. A set of MSE values was obtained for the detected AE waveform recorded during

each impact test. If a good correlation between the MSE value and impact damage areas is obtained, the MSE of AE waveforms could be used as a damage indicator.

5.2.2 Results and analysis of impact damage level discrimination

After modelling, a set of MSE was generated from the ANN model. To evaluate and interpret the results from ANN models, the AE waveforms and damage areas of the impact events were checked. From the AE waveforms, the number of emission bursts increased remarkably along with the increase in impact energy. AE occurrences created by high-energy impacts have a much greater number of events in the time period. The peak amplitude of the bursts remained constant throughout. This is restricted by the AE recording system, the maximum amplitude of which corresponds to 100 dB (equivalent to 7.8 V). Qualitatively, there appeared to be little difference between the AE waveforms produced by the 7, 10 or 15 J impacts.

A plot of damage area vs. impact energy for the two materials is shown in Figure 5-10. Damage area increases with increasing impact energy in both materials, although at energies greater than 5.5 J. The T800/5245C laminates had 20%-50% less damage area, for a given impact energy, than the T300/914. Polynomial curve fits to the data for each material, using a least squares procedure (the algorithm is illustrated in Appendix A), produced correlation coefficients (R^2) between impact energy and damage area of 0.97 for both materials.

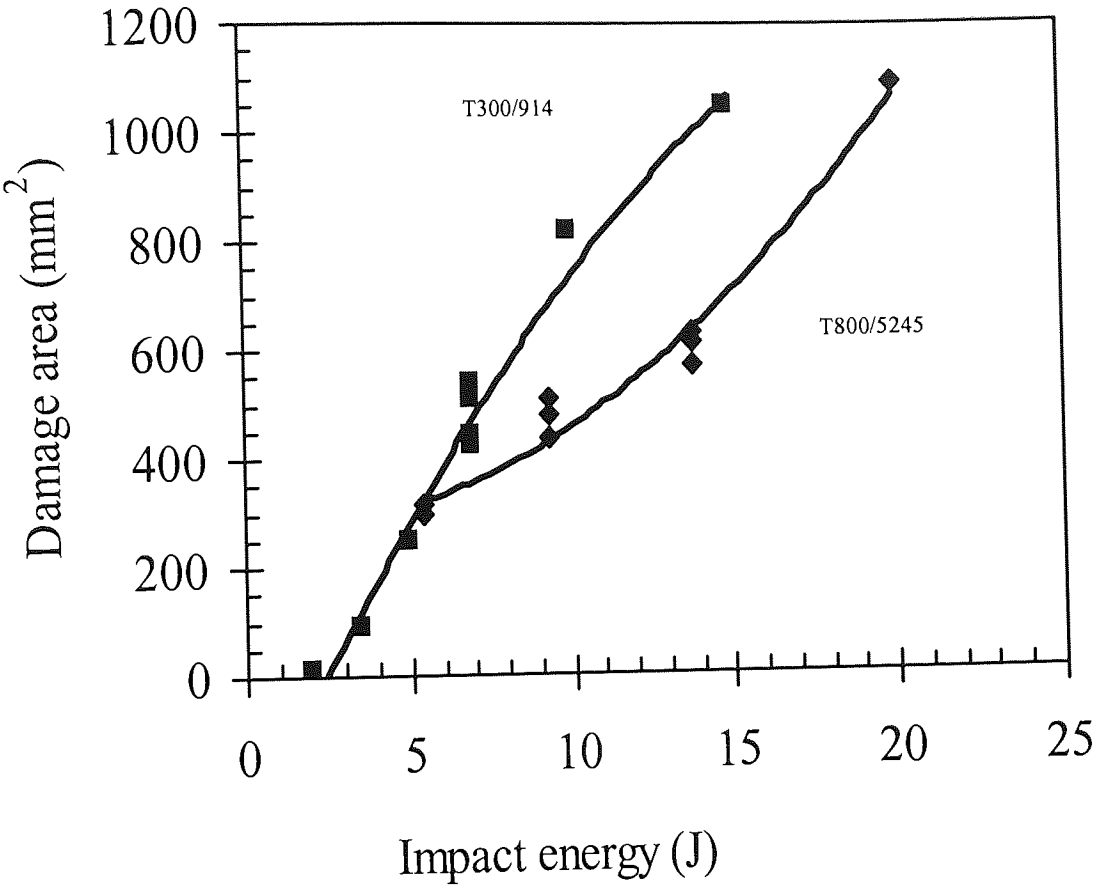

Figure 5-10 Plot of damage area Vs impact energy for the T300/914 and T800/5245 materials

Figure 5-11 shows the MSE values plotted against impact energy for all impacts in the two materials. As the impact energy increases, in most of the tests the MSE values increase. However, a few points had a lower value or remain unchanged with increasing impact energies. A scatter in the MSE values was observed when the materials were subjected to the same impact level. As shown in Figure 5-10, the damage area also varied at the same impact level. This damage variation can be attributed to the inherent scatter properties of composite materials. Further

variation can be induced by factors related to AE detection and signal processing, such as coupling between AE sensor and specimens, and the location of cracks and delaminations. Figure 5-12 showed MSE values and conventional AE parameters for the T300/914 laminates, plotted against damage area produced by the impacts, rather than impact energy itself.

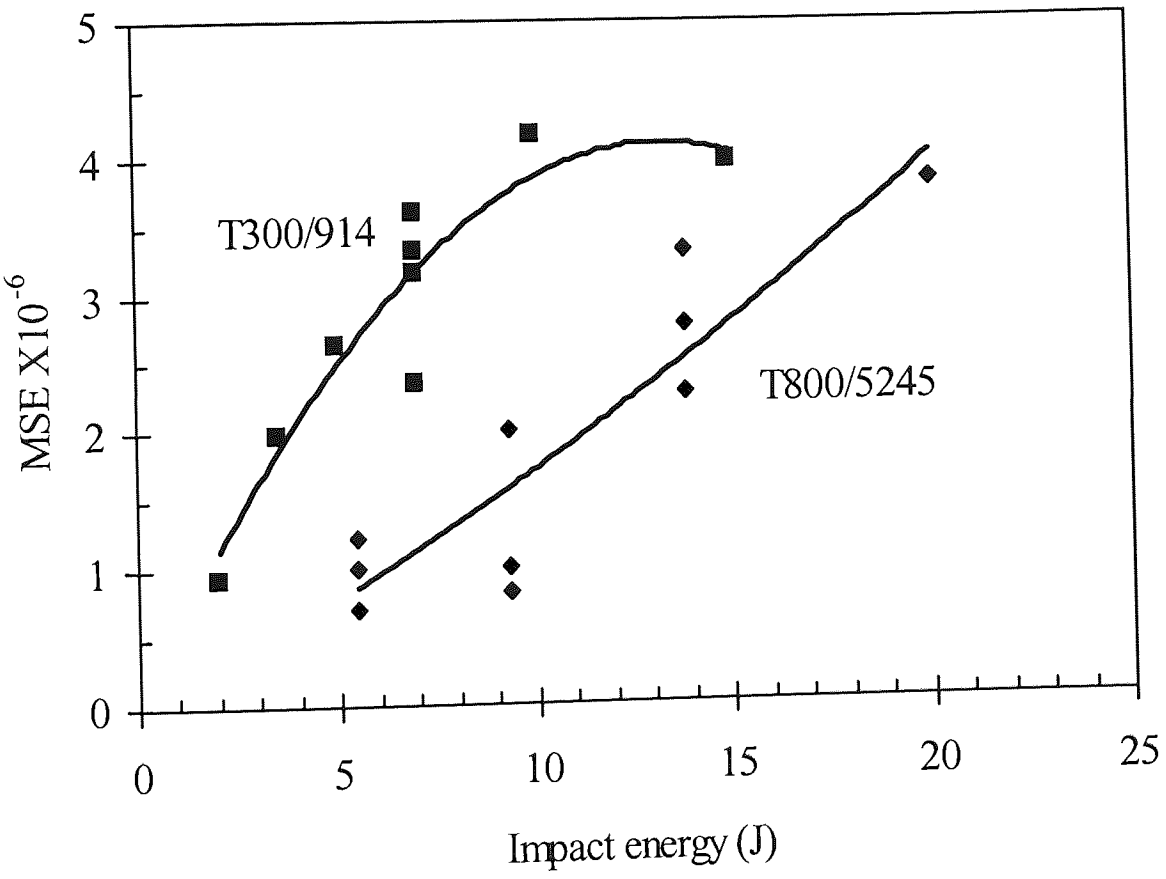

Figure 5-11 MSE value Vs impact energy for the T300/914 and T800/5245

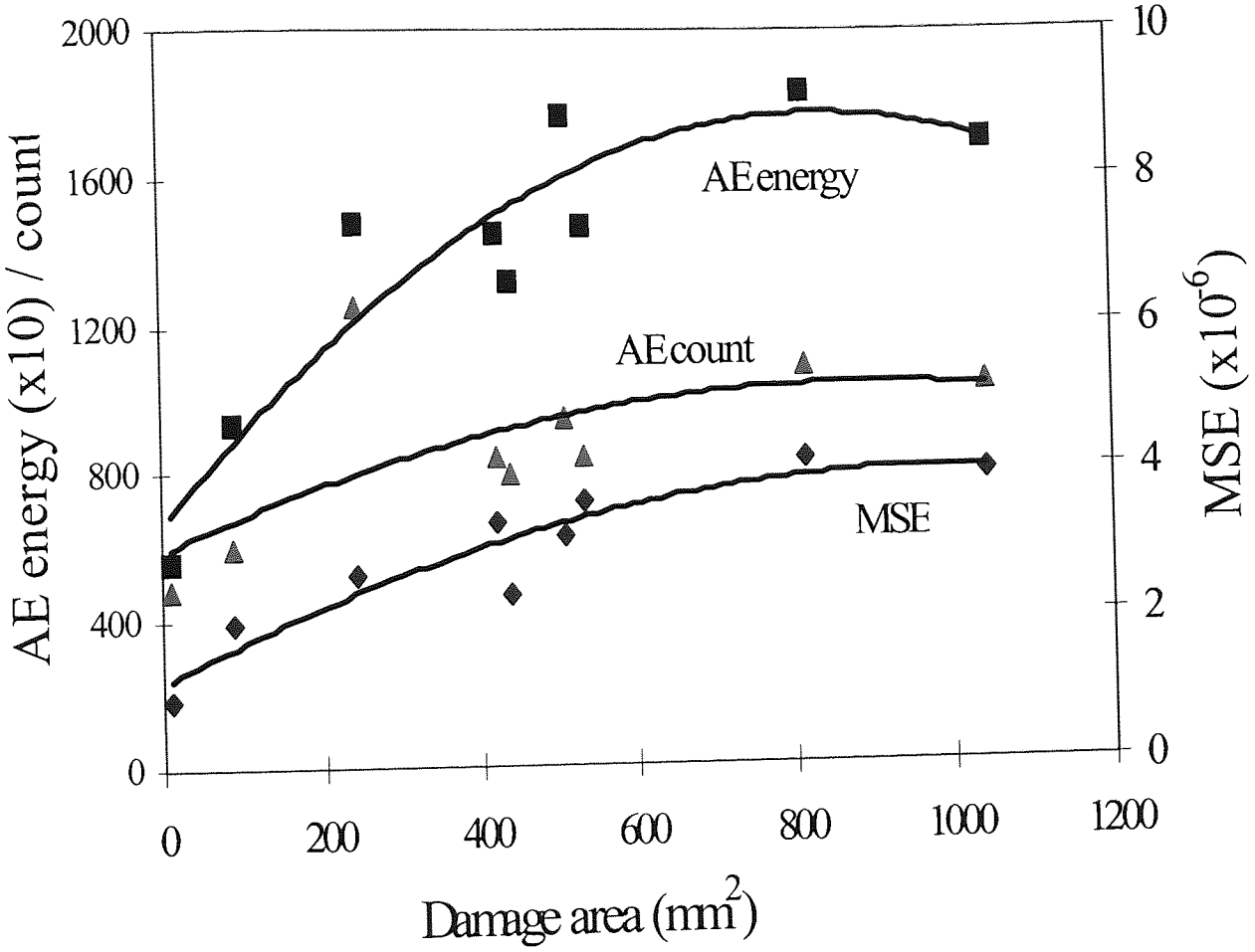

Figure 5-12 MSE value and AE parameters plotted against damage area for the T300/914

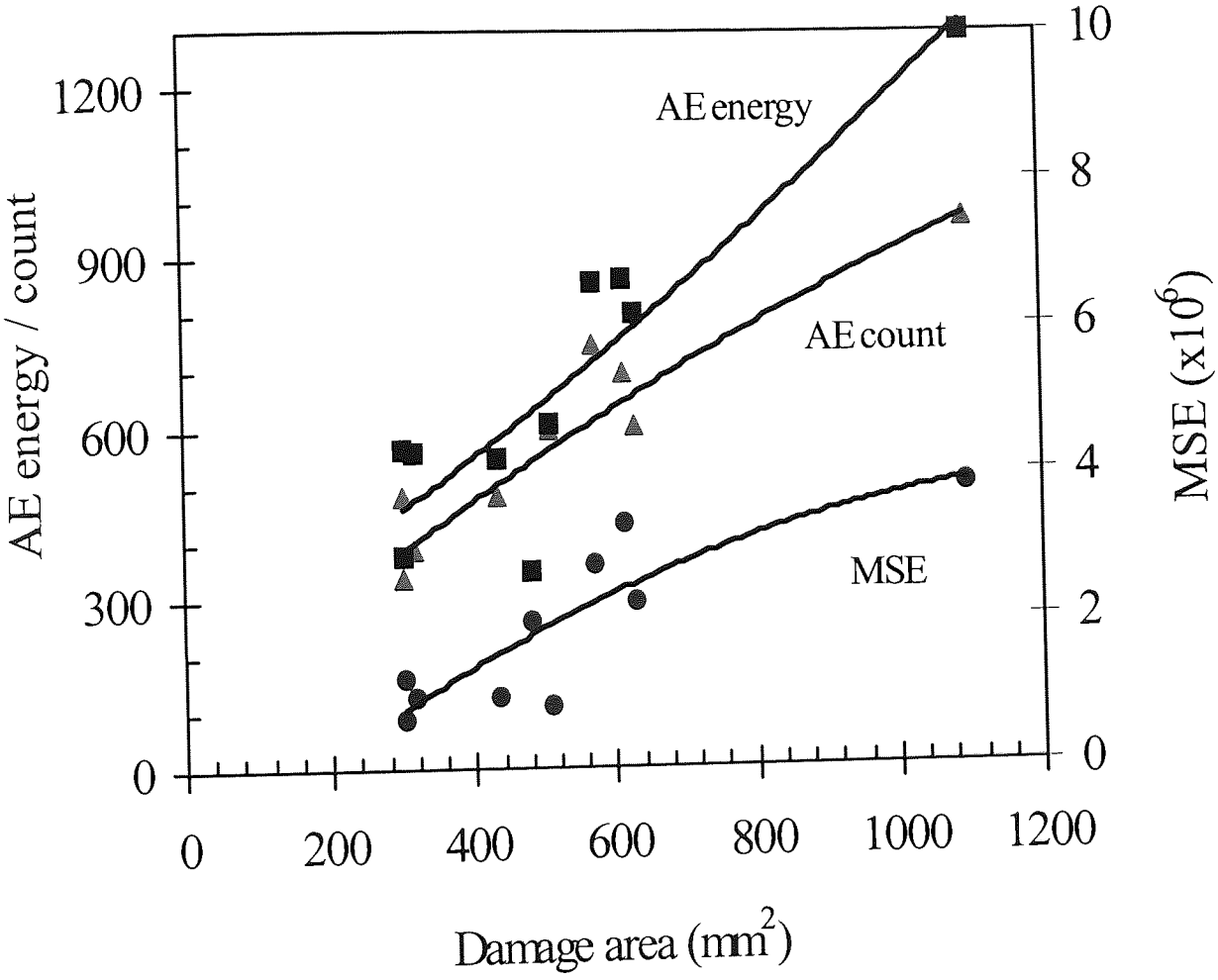

Figure 5-13 MSE value and AE parameters plotted against damage area for the T800/5245 composites

Again it was found that MSE increased along with the increasing damage area. AE energy and AE count were alternative indicators of the damage area produced during the impacts. The MSE values and AE parameters of the T800/5245 material were plotted against damage area in Figure 5-13. AE energy and count rate both increased with increasing damage area. Correlation coefficients obtained from least squares polynomial curve fits to the data in Figures 5-10, 5-11, 5-12 and 5-13 were shown in the table below.

Table 5-1 Correlation coefficients (R^2) for data relations

Parameters correlated	**R^2 for T300/914**	**R^2 for T800/5245**
Impact energy and damage area	0.97	0.97
MSE and damage area	0.88	0.74
AE energy and damage area	0.86	0.81
AE count and damage area	0.41	0.81
MSE and impact energy	0.88	0.86

Table 5-1 shows that the parameter correlated best with damage area is that of impact energy (0.97). Among the correlation between detectable parameters and damage area, the MSE value calculated for data from the T300/914, had a correlation with damage area (0.88) than do the AE energy and count rate (0.86 and 0.41). The MSE correlation with damage area for the T800/5245 material was

not as good (0.74), and was inferior to the correlation with damage area obtained with AE energy and count rate (0.81 for both).

These results demonstrated that of the parameters examined, the best correlator with real damage area is the impact energy itself meanwhile the MSE can give reasonable correlationship as well. Figures below (Figure 5-14, Figure 5-15, Figure 5-16, and Figure 5-17) were obtained from C-Scanner as the evidence schematically. They clearly demonstrate that the damage areas are closely marked by the impact energy as they both increased accordingly. Unfortunately, the impact energy is not available in real application situations. All the monitoring parameters were worse than impact energy in terms of their correlation coefficients. The neural network MSE parameter gave different results for the two materials. For T300/914, the MSE emerged as a better correlation with damage area than AE energy and AE count, while it appears as the worst indicator of impact damage for T800/5245. The BP neural network has successfully assessed damaging levels in T300/914. It was less successful in the T800/5245 material. The errors from AE acquisition may be responsible for the scatter in MSE value in Figure 5-11. It is difficult if not impossible to explain what is responsible for the difference of the results between two materials within the current limited experiments.

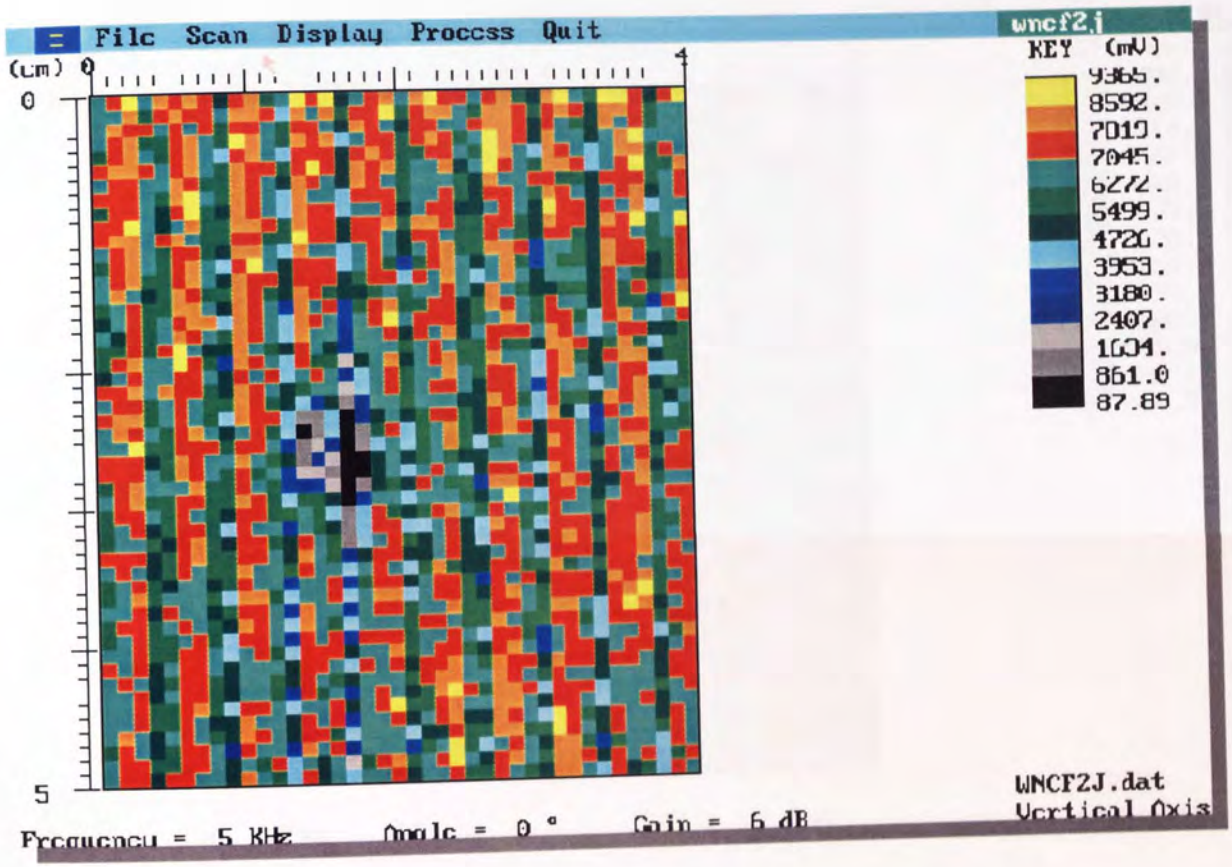

Figure 5-14 C-Scan damage area for 2J Impact

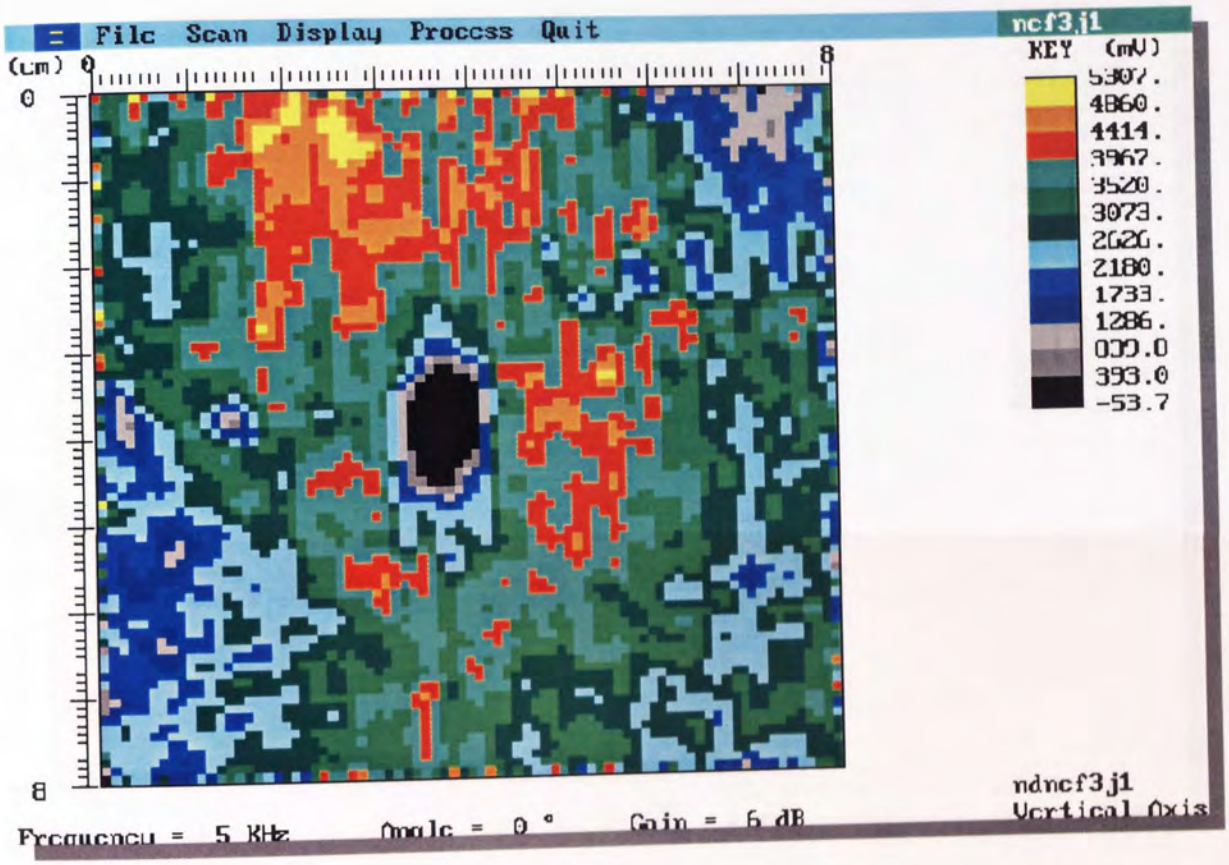

Figure 5-15 C-Scan damage area for 8J Impact

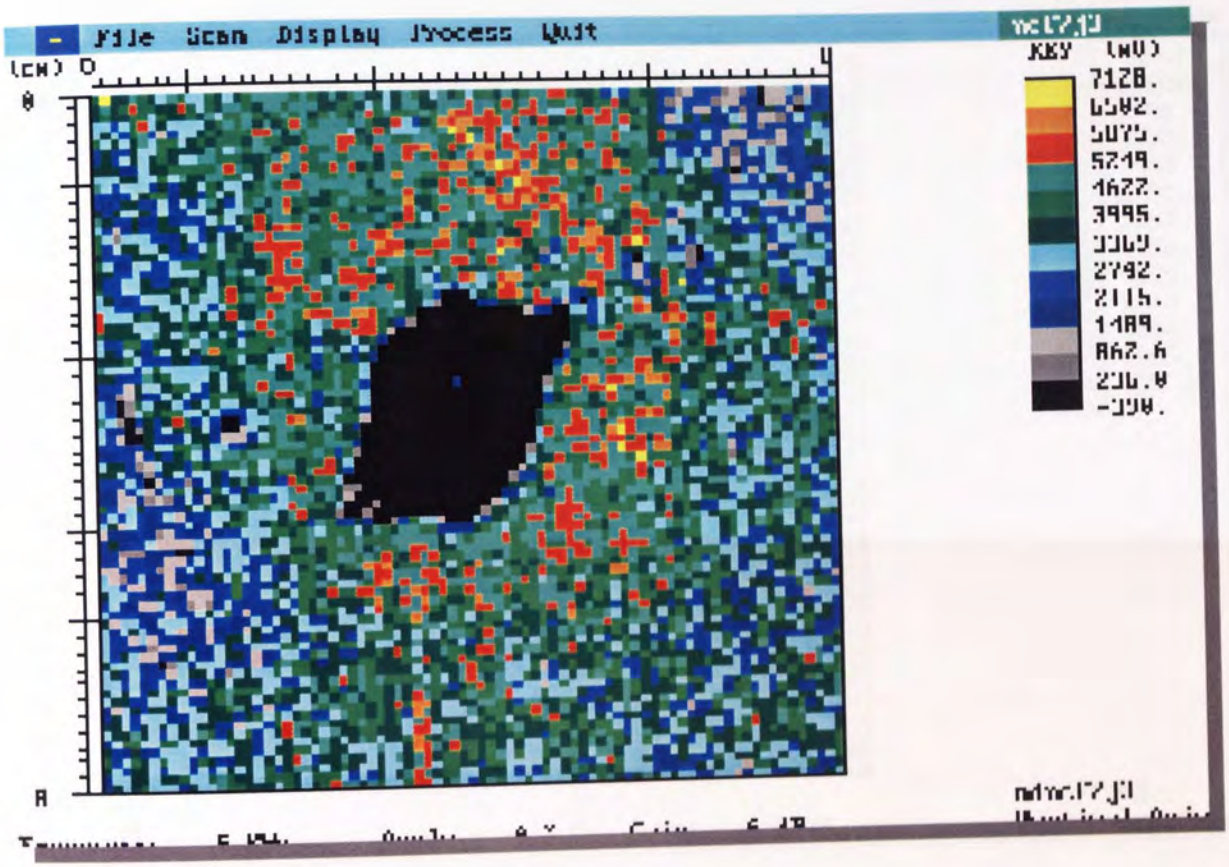

Figure 5-16 C-Scan Area for 10J Impact

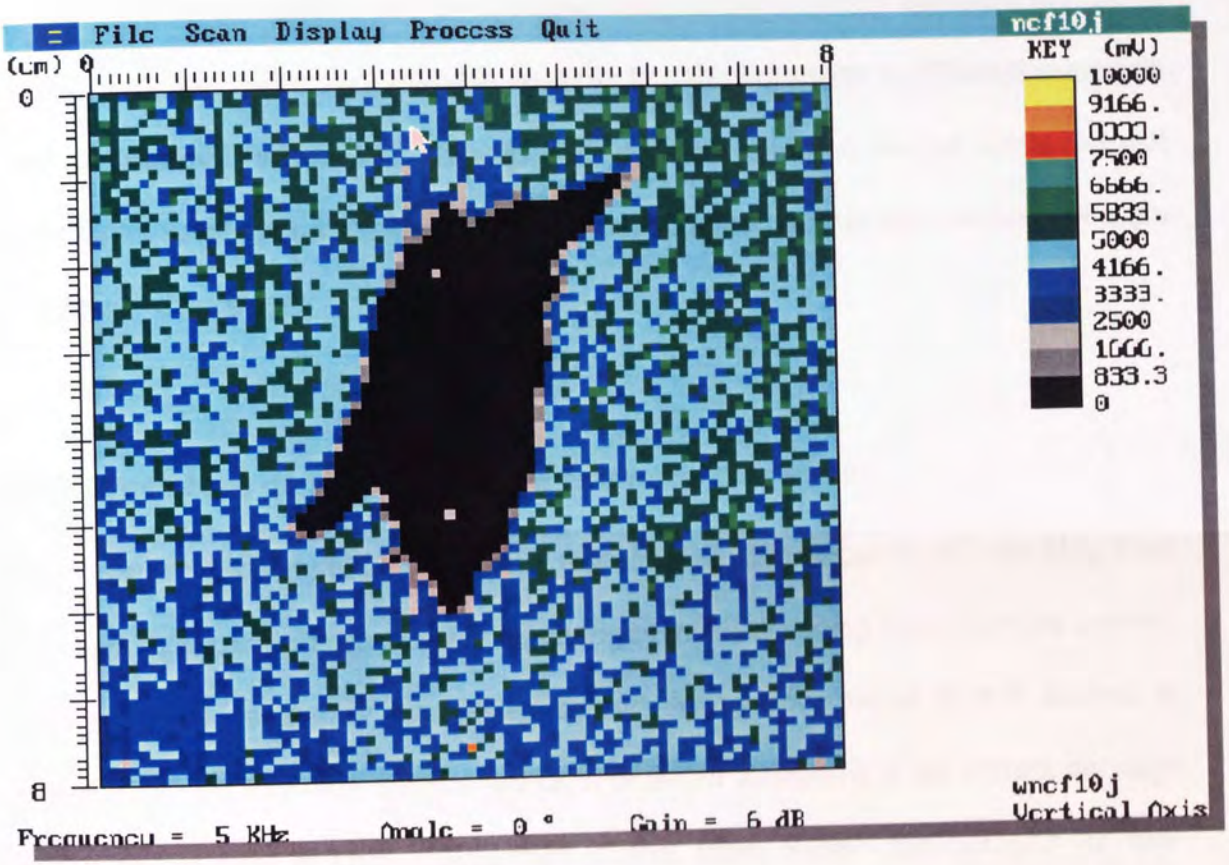

Figure 5-17 C-Scan Area for 20J Impact

However, ANN model can only generated the MSE, which corresponded to the impact energy event. It is not currently possible to decide if the MSE parameter or the AE energies and AE counts are responding to AE emissions caused directly by the impacts, or whether they can detect features in the AE emissions unique to the creation of delaminations or fibre fracture events. Detection of features unique to damage events will ensure that it is possible to detect damage in different materials and geometries, which will respond with different damage to the same impact events. As to this point, further study was investigated by analysis mechanical tests and force -time traces.

5.2.3 The study of mechanical tests and force-time traces

A problem in applying MSE was that it represented differences in AE resulting from changes in impact energy as well as changes in AE resulting from fracture events. ANN may not necessary manifested overwhelming advantages in this aspect. A further analysis however was based on a different viewpoint of an impact damage event, say in light of impact dynamics. In this case, force - time graphs for four impacts in the T300/914 laminates has been measured and studied as shown in Figure 5-18. Judging from the diagrams, it indicated that the peak force achieved in the tests increased with increasing impact energy from just under 2 kN for the 2 J impact to 4 kN for the 15 J impacts. The impact duration was about 8 ms for the 2 J, increasing to 9 ms for the 15 J. Impact events sufficient to cause initiation of delaminations may be identified by a small load drop or discontinuity, at the critical

threshold load, visible on the load- time record of the impact event. Transient load drops, indicting impact damage, first occurred at about 2.4 kN in all impacts except that at 2 J. The maximum force achieved during this impact was less than 2.4 kN. The impact under 2 J energy produces a relatively smooth line, with no evidence of a load drop. As seen in Figure 5-18, under 15 J impact, load drops occurred a few times after the peak of the force history curve. These may correspond to fibre damage occurring in different layers. The load-force traces presented in this paper were used to provide evidence of impact damage. The only drawback is, however, such data are not available in the real situations. (Noted that Force drops within the dotted circles are evidence of impact damage.)

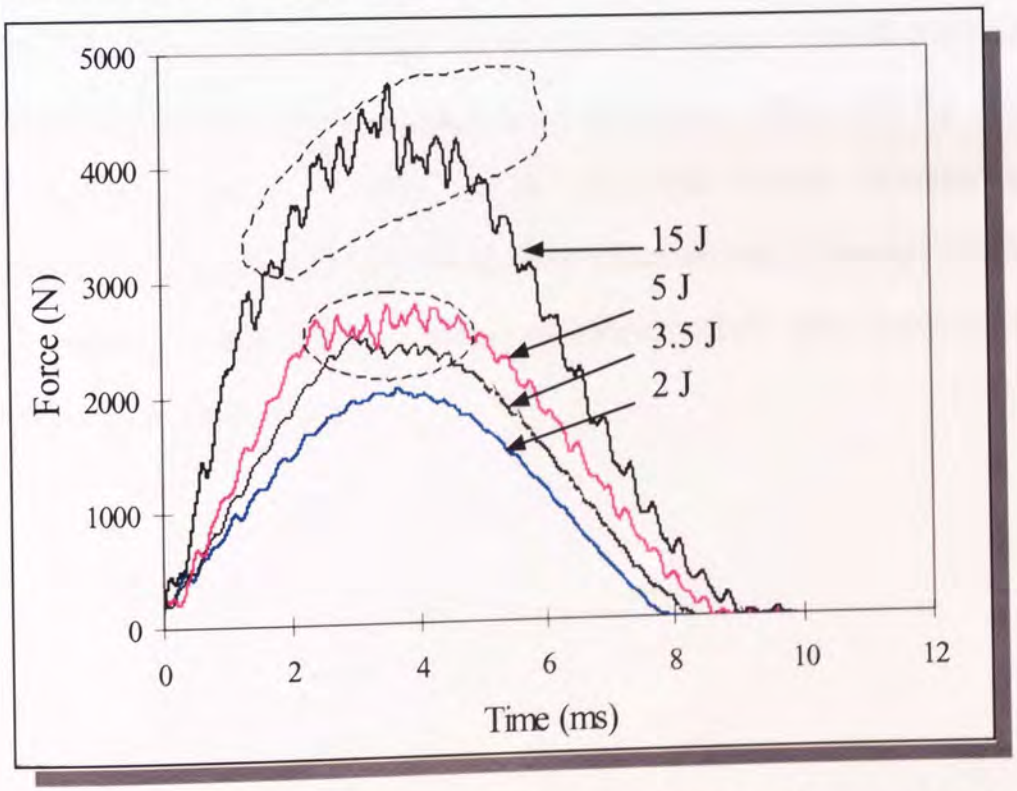

Figure 5-18 Force-time history during impact tests of T300/914 composites for a selection of impact energies

5.3 Conclusions

This chapter introduced the methodologies and background of the damage level detection study. The application of the neural network in damage level discrimination has proved successful to represent AE emissions from non-damaging or minor damaging events, and representing differences from other damaging events as MSE, which provided a general characterising parameter. By implementing neural computation, model of damage indicator was set up based on 2J and 5.4J impact event of two composite panels. ANN models were able to discriminate the damage level according to its impact energy. The results, however, were evaluated and correlated with the impact damage area obtained from ultrasonic C-Scan equipment. Despite its success in damage level discrimination, ANN models could not link its damage level parameter, MSE, with the impact fracture events directly. In other words, the ANN impact damage level discrimination was based upon the energy level discrimination. Although not being the main subject of this study, a further investigation has been conduct upon impact dynamics to fill this gap.

Chapter 6 The study of damage location

"We are locationally challenged"

(John M.Ford, 1957-)

6.1 Introduction

Chapter 6 revealed the mechanism to locate the damage site using ANN models. Conventionally, most of AE detecting systems use single AE wave speed to location an AE source. However, due to the complex structure, assuming single wave speed propagation is impractical in the impact site location of quasi-isotropic and non-isotropic composites. Thus, ANN models were trained to detect the damage sites based on a multi-speed principle.

6.2 Background and the mechanism of damage locating

To illustrate the mechanism, a simplified case is introduced to reveal the mechanism of impact damage locating. In this case, we assume an isotropic panel as shown in Figure 6-1. Therefore, the following equations can be obtained based on the relationship between distance, time, and speed

$$\Delta t_{12} = \left| \frac{\sqrt{(X_1 - X_0)^2 + (Y_1 - Y_0)^2} - \sqrt{(X_2 - X_0)^2 + (Y_2 - Y_0)^2}}{V} \right| \tag{6-1}$$

$$\Delta t_{13} = \left| \frac{\sqrt{(X_1 - X_0)^2 + (Y_1 - Y_0)^2} - \sqrt{(X_3 - X_0)^2 + (Y_3 - Y_0)^2}}{V} \right| \tag{6-2}$$

where

Δt_{12}, Δt_{13}: the time difference between sensor 2 and 1, and between sensor 3 and 1.

V: the velocity of acoustic emission wave

(X_1, Y_1), (X_2, Y_2), (X_3, Y_3), and (X_4, Y_4): the co-ordinates of the sensors

note that (X_4, Y_4) is at 0,0 coordinates

(X_0, Y_0): the co-ordinate of the impact point

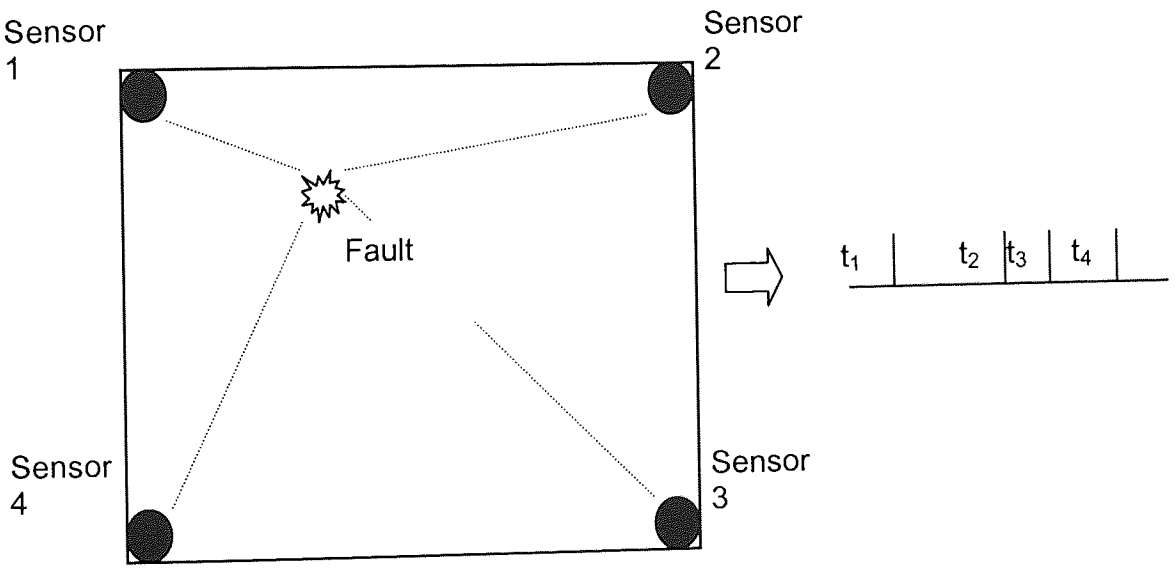

Figure 6-1 Relationship between the time, speed, and coordinates of an isotropic material panel

The co-ordinates of each sensor are known from the experimental set-up. Provided the wave-velocity is known, there are only two unknown variables (X_0, Y_0) with two equations. By solving (6-1) and (6-2), the co-ordinate of the impact point can then be determined.

However, this analysis is an idealised example based on isotropic materials. It assumes the velocity V is the same in all directions at all time and is accurately known. In composite materials and any non-isotropic materials, the velocity of AE propagation won't be a constant value due to the varied structure properties. Thus, velocity V is introduced into (6-1) and (6-2) as another variable and it complicated the issue of location detection. Figure 6-2 shows the speed field obtained from AE velocity measurement from this study.

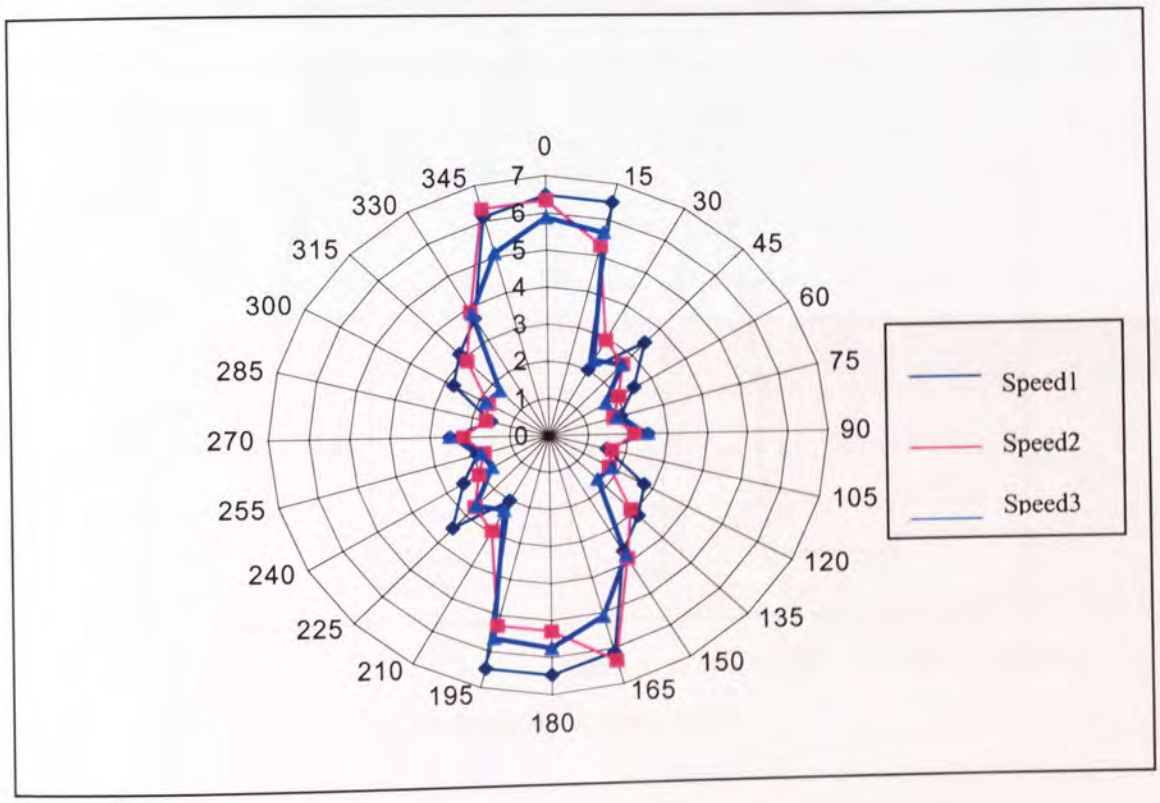

Figure 6-2 Speed contour of an quasi-isotropic panel

As shown in Figure 6-2, each enclosed line, known as speed1-speed3, represents a different wave speed contour. The shape of the equal velocity contour is generally stretched along the vertical direction (0 degree). It coincides with the fact

that the lay-up orientation of the top surface is along the 0 degree and the ribs fixed underneath affected the propagation of AE waveforms as shown in Figure 6-3. The velocity is therefore greater in the fibre's lay-up direction. This geometric feature, however, affects the ANN locating results on x direction (which is normal to 0 degree) as indicated by proceeding study.

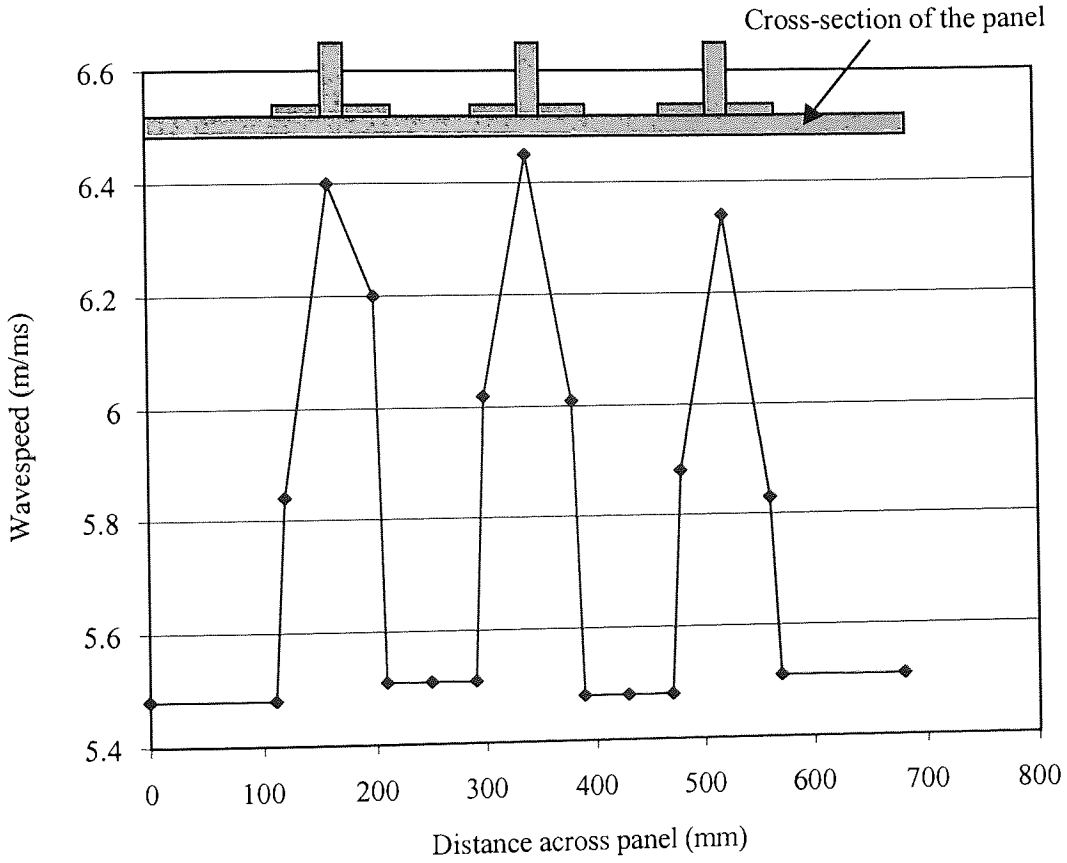

Figure 6-3 Wave speed profile cross the stiffened panel

To locate the impact sites on such panel, a multi-speed model was designed to locate the impact locations by exploiting the generalisation ability of ANNs. In this

circumstance, the impact location could be extended to quasi-isotropic and non-isotropic studies.

In terms of ANNs modelling, physical relationship among time, speed and distance still applied. The inputs and targets of the ANN model are arrival time difference and site coordinates respectively. However, instead of modelling the system using one single speed as that in the isotropic study, ANN modelling basically is based upon multi-speed. To illustrate the mechanism, it is necessary to discuss the speed distribution of a non-isotropic material panel first. Topographically, the speed distribution of a non-isotropic material panel can be approximated by a collection of speed contours as shown in Figure 6-2 and Figure 6-3. Using the single speed principle, only the points geometrically situated on that particular speed contour can be accurately located. As the speed contours ripple out, single speed principle has to keep updating the speed value accordingly in order to remain valid. Hence, if the AE speed can be determined dynamically, the deficiency of single speed principle can thus be compensated. In other words, the single speed principle modelling has to be replaced by the multi-speed principle modelling, which can apply a certain speed according to its speed contour. However, it would be impossible to update the speed manually given a composite material structure. A speed updating tool is expected. Fortunately, the enormous computation can be shifted to ANN models. During the training, ANN model will derive and generalise the information based upon the data collected from experiments. Provided the training is sufficient, the ANN model then can successfully catalogue the points and

interpolate the "missing" point (as an unknown point) after the training. In the real time practice, the AE acquisition equipment can only capture arrival moment from the sensors. It has to be converted into time before it is fed into the neural network model. Time difference Δt of the four arrival moments can generally be converted by subtracting any two of them, as shown below

$$\Delta t=[\Delta t_{12}\ \Delta t_{13}\ \Delta t_{14}\ \Delta t_{23}\ \Delta t_{24}\ \Delta t_{34}] \text{ where } \Delta t_{12}= t_1-t_2\ ;\ \Delta t_{13}= t_1-t_3\ ;\ \ldots \qquad \textbf{(6-3)}$$

By applying the above formula, a set of time difference can be converted from the detected AE signals. Using time difference as input and impact site coordinates as target, the neural networks can then be trained to determine the relationship between input and target. On the other hand, the ANN models are validated directly by comparing the absolute difference between real location and neural network output. Figure 6-4 illustrates the methodology.

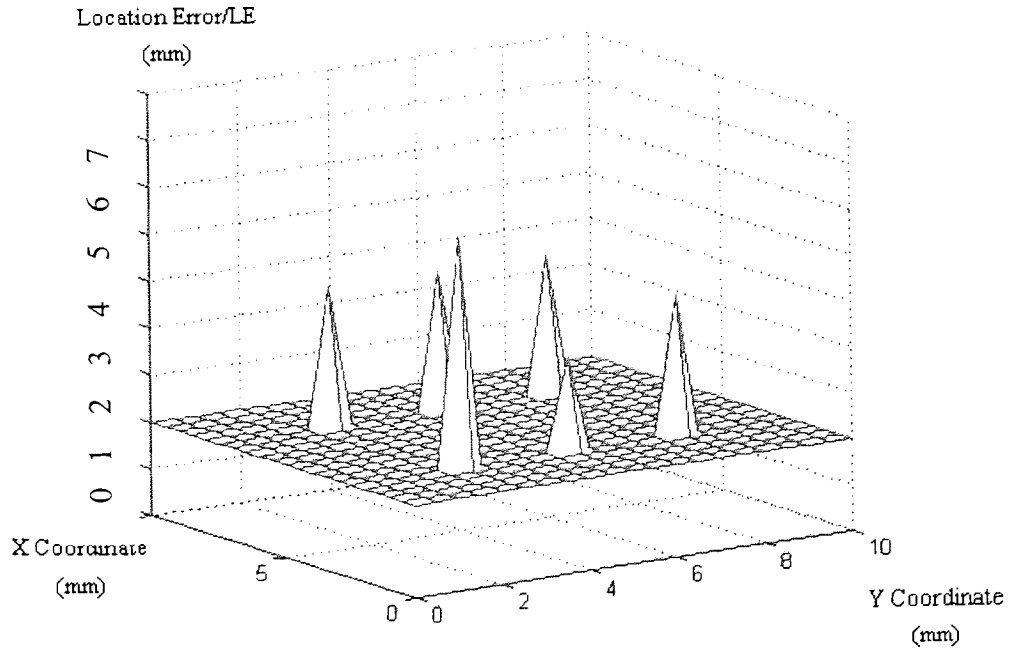

Figure 6-4 Illustration of the source location from the ANN s

As shown in the above study, a series of impact experiments (6 in total) were conducted on the panel (dimension 10×10) to validate the performance of a trained ANN model. The actual impact location corresponds to the location of each peak schematically. The values of the impact location coordinates can be read from the X-axis and Y-axis. The location error (LE), being the peak heights in the diagram, is obtained by calculating the distance deviation against the real sites. Then, the general performance of the ANN model is obtained by taking the arithmetic mean of the location errors.

6.3 Modelling for Damage locating

In the damage locating study, the neural network model was constructed with the similar structure as that used in the damage level detection study. The classic structure and transfer functions were employed again in this study. There were two layers that were constructed from the BP neural network model. The parameters of the neural network were then fixed when the training finished. (In the case of structure of 17 neurons at first layer and 2 neurons at output layer, there are 17×6+17=119 biases and weights in the first layer. There are 2×17+2=36 biases and weights however in the second layer. Overall, there are 155 parameters in the model). Initially there were 42 points measured as training data. After the parameters were adjusted by the training data, the trained ANN were ready to accept new data (24 pairs of new location based on a priori principle) and make

"real" predictions of impact sites. The scheme of training and prediction is however shown in Figure 6-5.

In this study, the influence of the number of neurons in the first layer on prediction accuracy was also investigated. The number of neurons in the first layer was initially set to 8, as shown in Figure 6-6. After the neural network was configured, the six time differences of each known impact site were input to train the ANN. Total 42 sets of data were used in the training. The same process was repeated when the number of neurons in the first layer was changed to 10, 17, and 25. Then the trained ANN was used to predict location of 24 unknown sites, which randomly picked up to manifest the ANN locating performance across the panel.

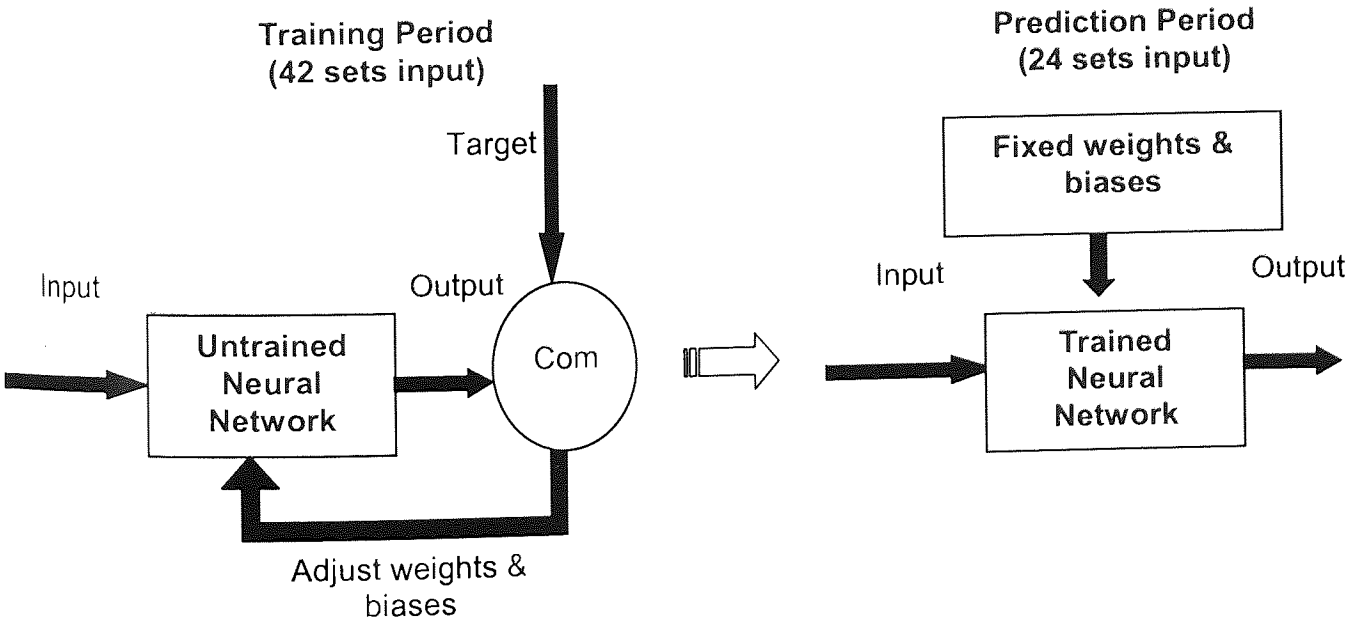

Figure 6-5 Modelling scheme of damage location

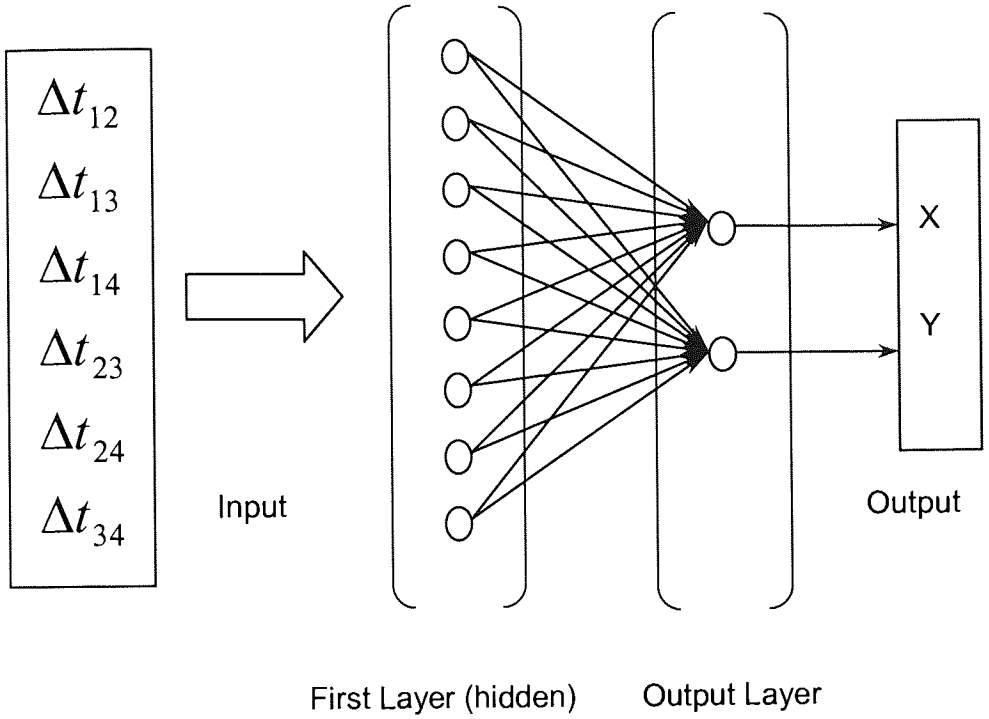

Figure 6-6 Structure of the neural network (Physical)

After training, the mean distance deviations between the ANN results and real locations, also known as average location error (ALE), were used to evaluate the performance of the ANNs modelling. In this study, the distance deviation is composed of two parts: X-axis and Y-axis. They are shown as

$$ALE_x = \frac{1}{N}\sum_{t=1}^{N} | X_{ANN}(t) - X_{Real}(t) | \qquad \textbf{(6-4)}$$

$$ALE_y = \frac{1}{N}\sum_{t=1}^{N} | Y_{ANN}(t) - Y_{Real}(t) | \qquad \textbf{(6-5)}$$

6.3.1 Damage location results

1) PAC MISTRA 2001 prediction (Using single wave speed)

The MISTRAS 2001, described in Section 4.2, can give a location prediction based on single speed mechanism. It yielded reasonable location in the isotropic panel by applying (6-1) and (6-2). The velocity across the panel must be determined by placing two sensors in a line together with the transmitter. The difference in the arrival time at the two sensors defined the velocity of the wave travelling along that line. However in composite panels, it has been shown in Figure 6-2 and Figure 6-3, the wave-speed varied significantly at different sites even in the same direction. The wave travelled faster on the thick section where the ribs were, but slowed down in the skin area. This variation of the wave-speed illustrated the difficulty of applying single speed to the source location.

To verify the location performance, the positions of 24 new validation impacts were calculated by the PAC MISTRAS 2001 system based on (6-1) and (6-2). The input wave speed was 5.5×10^6 m/s (the average speed of AE wave travelling in the skin). The location results of the 24 points were plotted in Figure 6-7. There are considerable errors in all the predictions. The average location error (ALE) was then introduced to evaluate the predication results. Indicated in Table 6-1, the single wave-speed method generated 50 mm ALE in X-ordinate, 133 mm ALE in Y-ordinate. Compared to the results of ANN for the whole panel area, the location yielded an 8.6% increased error in X, and 18.7% in Y.

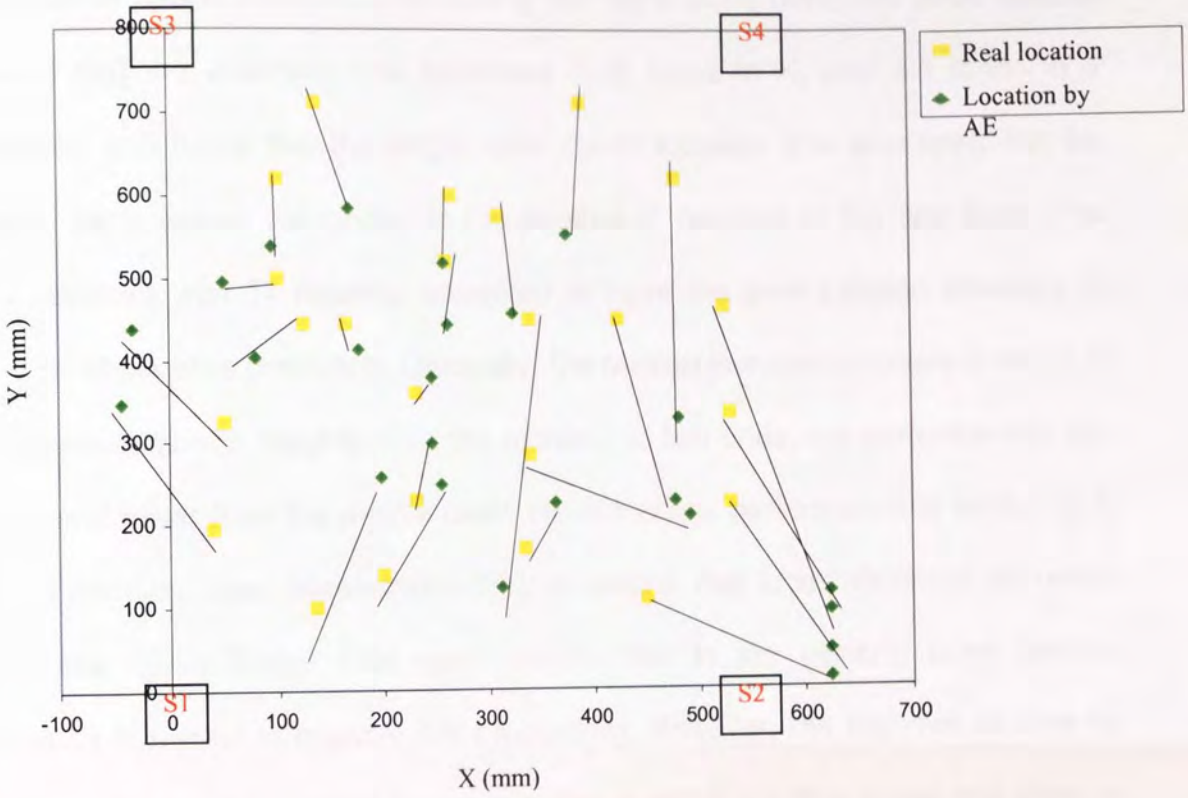

Figure 6-7 Location prediction for 24 randomly generated hits from PAC MISTRAS 2001(single wave-speed method)

2) Neural network results

The results for the same 24 validation impacts, but located using the trained ANN are shown in Figure 6-8 corresponding to 8 neurons structure that was used in the ANN structure. The average location errors were summarised in Table 6-1, showing the influence of the number of neurons on the location accuracy.

In general, the accuracy of all the ANN location is considerably better than the single wave speed method. Even taking the worst ANN data, the ANN location showed that the accuracy was enhanced 1.45 times in X, and 4.4 times in Y compared with better that the single wave speed location. It is also seen that the location performance responded to the number of neurons in the first layer. The ANN structure with 17 neurons appeared to have the best location accuracy in terms of whole area prediction. Generally, the neuron increasing covers a range of 8 to 25 neurons with roughly 17 in the middle. At two ends, the performances are similar and lower than the middle peak. Nevertheless, performance is similar at 8 and 10 neurons case. Mathematically, it is natural that local vibrations do occur during the curve fitting. This won't disturb that in the general case neuron increasing is helpful to improve ANN modelling. However, the theorem as how to determine the most optimised neuron number is still at practice stage and short in literatures currently.

Table 6-1 Average location derivative of the prediction.

ALE	8 neurons		10 neurons		17 neurons		25 neurons		Single speed	
	X	Y	X	Y	X	Y	X	Y	X	Y
Whole Area (W) *	28.91	30.13	34.49	28.94	24.02	28.23	30.19	29.13	50.64	132.8
Shaded area(S)**	54.28	57.17	63.65	54.88	41.34	58.52	48.52	57.62	53.80	155.8
S/W ***	1.88	1.88	1.85	1.88	1.72	2.08	1.61	1.96	1.06	1.17

* Whole Area referred to the location deviations in the whole panel area along X and Y Axis

** Shaded area referred to the patterned area that situated in the middle of the panel.

*** S/W referred to the ALE quotient between that of Whole area and that of shaded area, which illustrated the geographic influence.

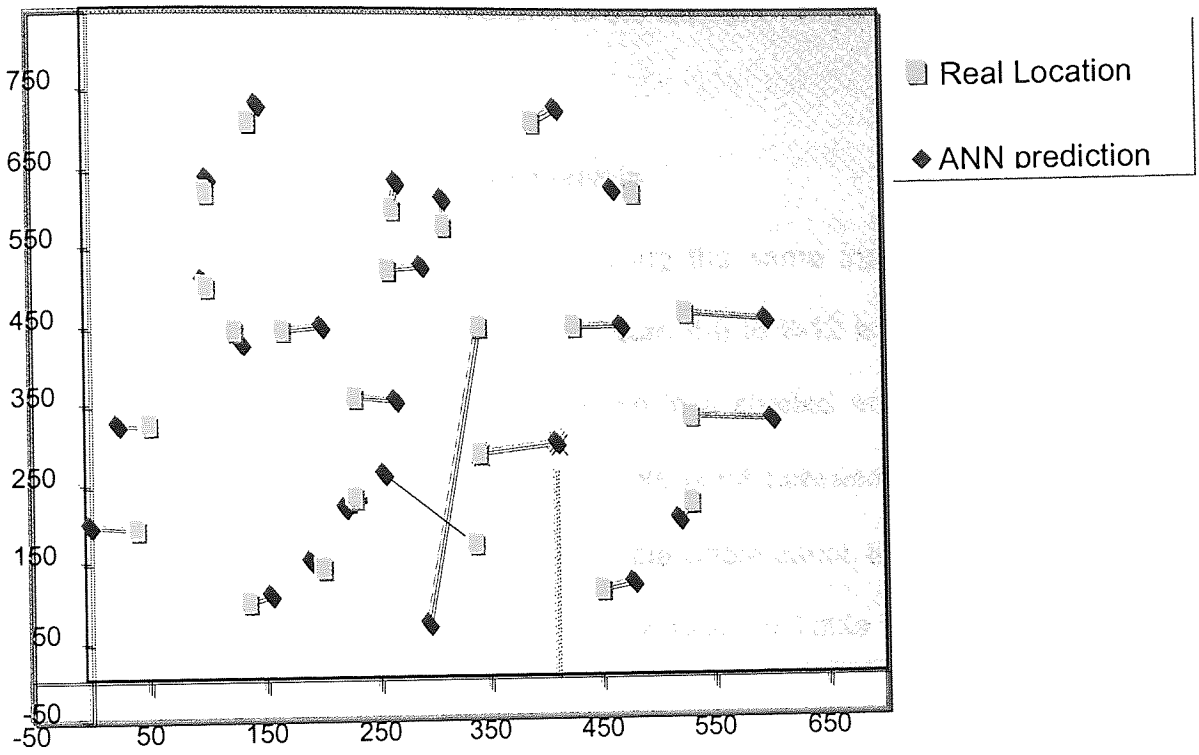

Figure 6-8 Impact location using the ANN with 8 neurons vs. the real location

Another interesting phenomenon is that ANN model rendered a better location prediction in Y direction than in X direction due to the increased AE impedance by the underneath ribs (The reason that ALE of Y direction is bigger than that of X direction is only because of the one biggest LE error at the centre). Figure 6-2 and Figure 6-3 also illustrated that the shape of speed contours twisted and vibrated significantly in X direction, which suggested a more complicated multi-speed cases in X direction than that in Y direction. Conceptually, the demanding of the neurons that are in charge of the prediction of X direction shall be heavier than those of Y

direction. However, current ANN methodology hasn't yet developed an algorithm, which can optimise the neuron contributions to the different variables of the outputs.

6.3.2 Damage location validation and analysis

A set of damage location was obtained by using the same input and different neural structures. A common observation in Figure 6-9 to 6-12 is that those sites with large predication errors by ANNs appeared in a shaded area. The shaded areas are located within ± 100 mm to the middle point between two sensors in either "X" or "Y". To differentiate the errors from the whole panel, the ALE value for the points in the shaded area was calculated and listed in Table 6-1. The ratio of shaded ALE to the whole ALE was indicated as "S/W". In general, the ANN location showed that the average location error in the shaded area was around 1.8 larger than the whole area, while the location errors given by the single speed location were slightly larger in the shaded area, with the "S/W" ratio only around 1.1.

The low accuracy of the predictions in the shaded area by ANN can be explained as follows. The sites located in the middle zone are at similar distances from two sensors. Therefore the signal arrival times will be similar and this results in a small difference from one to another, which may confuse the ANN model. As an simplified, point A ,with arriving moments of [t_1=a t_2=b t_3=a t_4=b], and point B , with [t_1=a+ε t_2=b+ε t_3= a+ε t_4=b+ ε], are located on the middle line of the panel.

They have the similar distance between two sensors like sensor 3 and 2 also sensor 4 and 1. The time difference patterns of these two points hence are [a-b, a-b, 0, 0, a-b, a-b] and [a-b+ έ –ε, a-b+ έ –ε, 0, 0, a-b+ έ –ε, a-b+ έ –ε]. They are in the same pattern. Provided A and B are very close to each other, term έ –ε can be ignored. Thus, the time difference could be identical and make it hard for ANN to distinguish. In other words, the model suffers under-fitting by insufficient pattern information, which leads to poor validation results. A solution is to adjust the neural model structure or increased the training set in such area. Meanwhile, optimised structure and a proper number of processing units will also give improved prediction. The ANN with 17 neurons gives best prediction. The validation results improved from up to 1.5 times by structure tuning compared to the structure using 10 neurons. Another reason to cause the large errors could be introduced by measurement. The measurement of arrival time may contain an error by the possible malcontacting between pulse injector and the sample surface. Such a small error in the arrival time can bring a large deviation in the difference between two sensors, a similar distance away. This is because of the small value (close to zero) in the difference of arrival time. The point in the middle showed a largest error in all the location plots (Figure 6-9 to 6-12). The measurement error was very likely to occur with this point. To overcome the limitation of ANN on the shaded area, a multi-array of sensor net could be used. It means that the shaded area in this sensor array could be the corner or side of other sensor arrays. By applying a multi-array of sensor net, the performance can be improved.

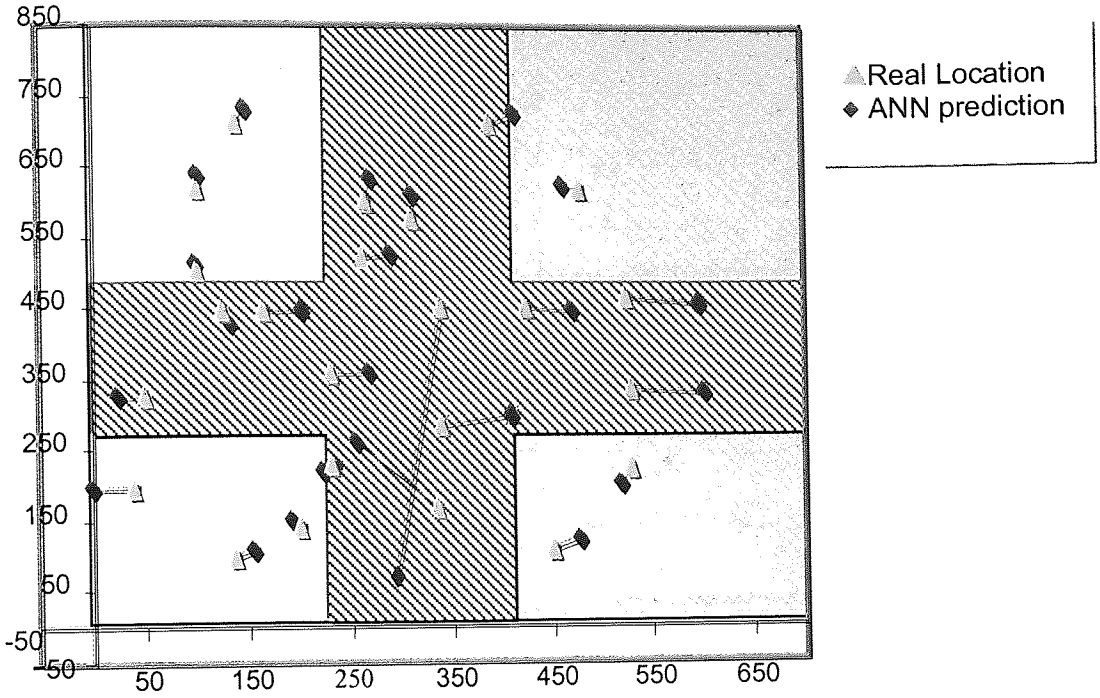

Figure 6-9 ANNs impact location outcome on composite panel (8 neurons)

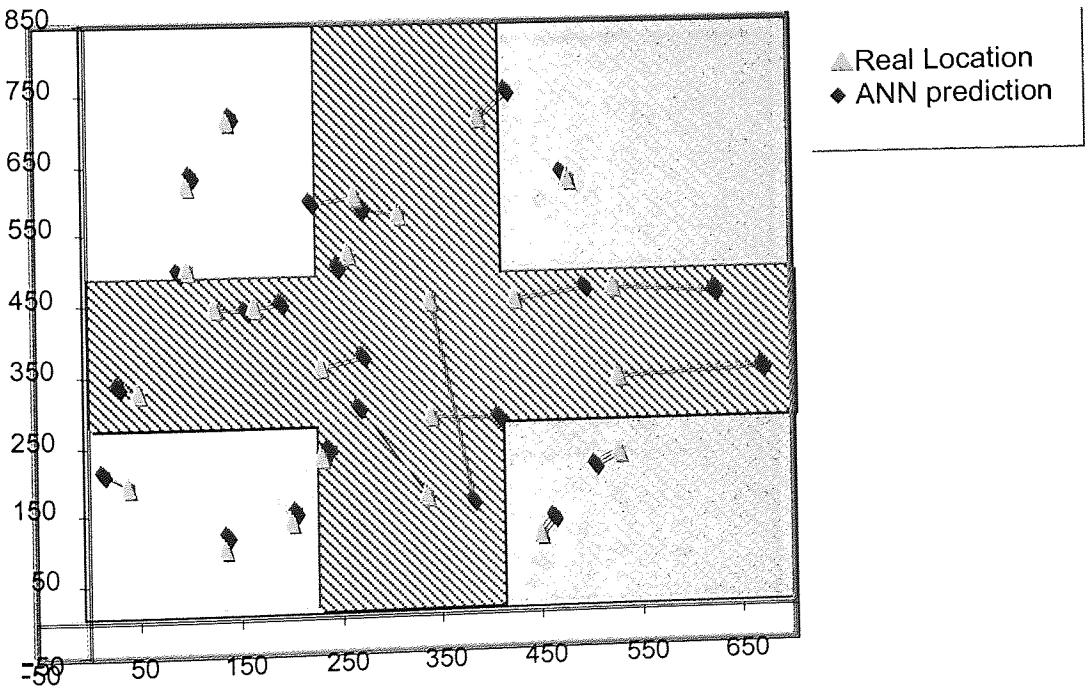

Figure 6-10 ANNs impact location outcome on composite panel (10 neurons)

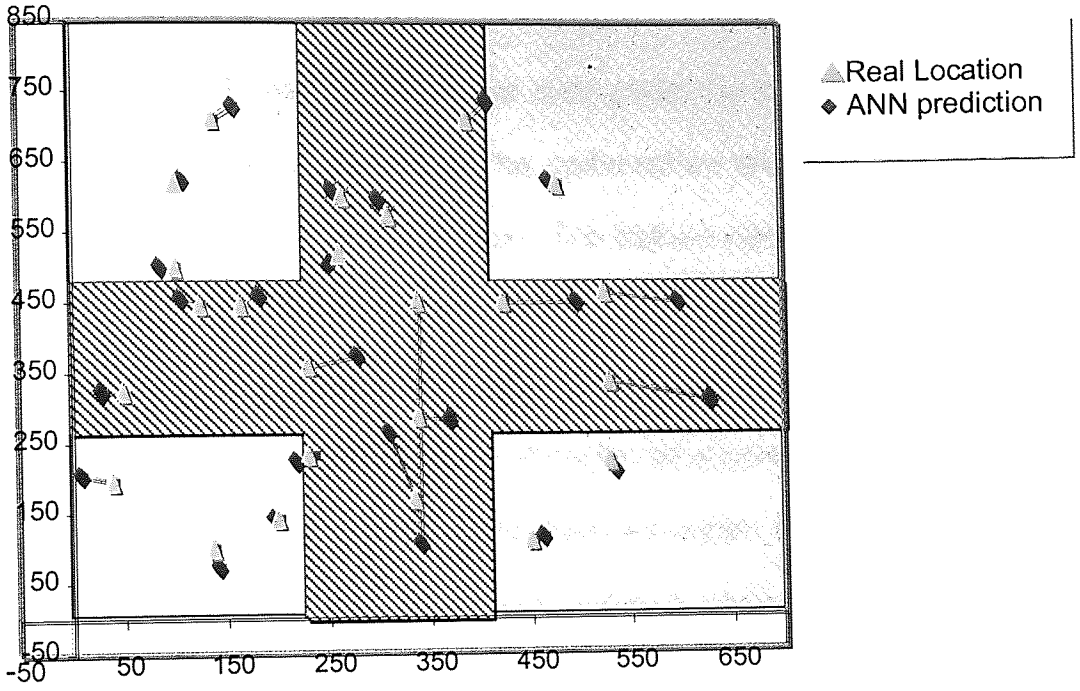

Figure 6-11 ANNs impact location outcome on composite panel (17 neurons)

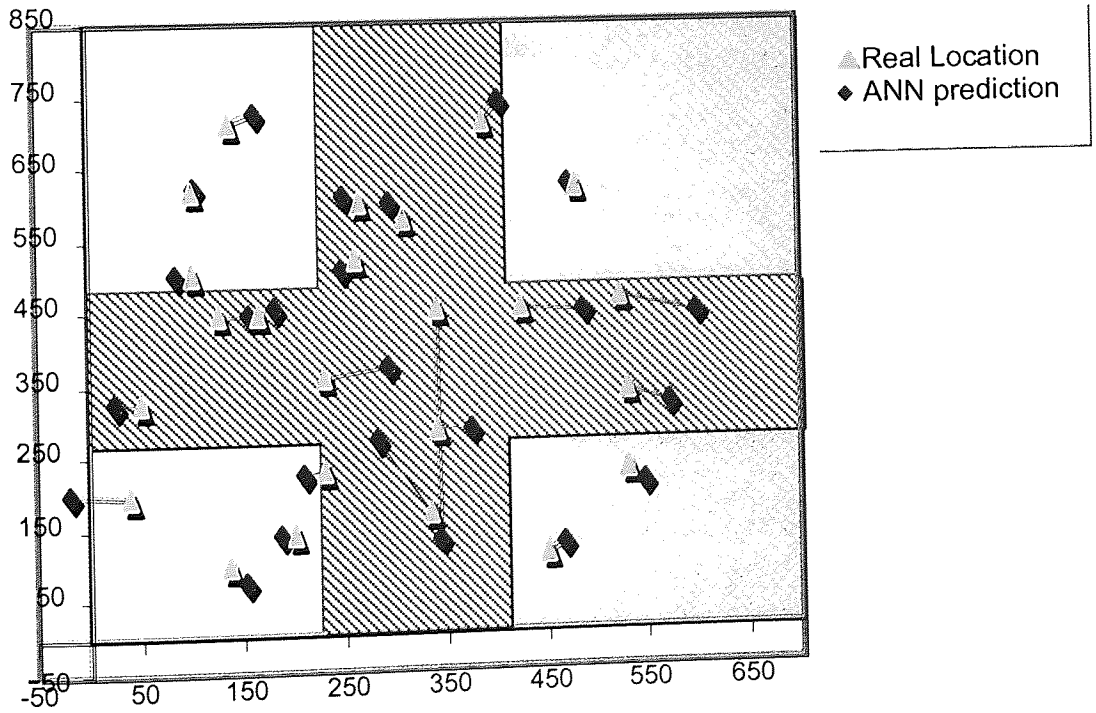

Figure 6-12 ANNs impact location outcome on composite panel (25 neurons).

6.4 Conclusions

In this Chapter, a study has illustrated the mechanism for building-up the ANN models for damage location detection. The performance and outcome of ANN models were also presented in this section. The trained neural network models were able to pinpoint the impact locations using time differences and impact site coordinates as the training variables. Damage location detection was then verified by a new set of 'unknown' data from which ANNs model synthesis out the accurate location. The quality of ANN prediction has been evaluated against that of PAC MISTRAS 2001 System. It was found that different neural network structure (neuron numbers) produced different degrees of locating accuracy. Results from both studies are promising and encouraging. Nevertheless, there are further issues to be addressed in the following chapter about the both impact damage level discrimination and damage location detection.

Chapter 7 Further Discussion

"I envisage a dialogue between two voices, the one imaginative and the other critical"

(Medawar, 1981)

7.1 Intoduction

In the last chapter, BP neural networks were sucessfully trained to produce a damage indicator and evaluate the damage level, which coincides with the impact energy and C-scan results. Neural computation was also introduced to predict the impact damage location based upon the training of time difference and position . However, before the study can be completed, there are some further issues that need to be addressed. The following discussion focuses on some possible factors that can ensure the optimal results from ANNs models.

7.2 The selection of inputs

To identify the controllable and observable (identifiable) part of a dynamic process the input signal has to satisfy certain conditions. Roughly speaking this means that the input signal has to be sufficiently rich to excite all process modes of interest during the experiments (Ljung, 1987). This is also true in the sense of neural modelling. In the damage detection simulation, training is a critical procedure in order to guarantee the performance of ANNs models. During the training, the quality of input as well as target plays an important part. It will lead to a poor

interpretation if there is a poor selection of the input and target. Poor selection could eventually lead to overfitting, underfitting, or even an invalid modelling. In this section, a description is given about the selection of input for both ANN damage level discrimination models and ANN locating models.

7.2.1 Input selection of damage level discrimination

The chosen inputs were based on the physical model of AE waveform. Previous studies revealed that AE wave propagation in structural components, such as plates, is more complex than in large bulk materials. Because of the additional boundary conditions, the AE signals detected by the sensors are actually superimposed by multiple reflections of original signals. So far, only simple modes has been roughly distinguished and discussed in the AE research (Huang, 1998). Figure 7-1 showed an example of an AE signal of a plate. The detected signal is actually a combination of the extensional and flexural modes and their reflections. Thus, the propagation of AE waveforms can be broke into sections and described as of the rippling mode that it goes one section after another. Then, the AE waveforms are mixed up with reflections and interferences as the waves interact with each other. It is just like the ripples undulate through a small pond surface, which is created by a stone impacting on.

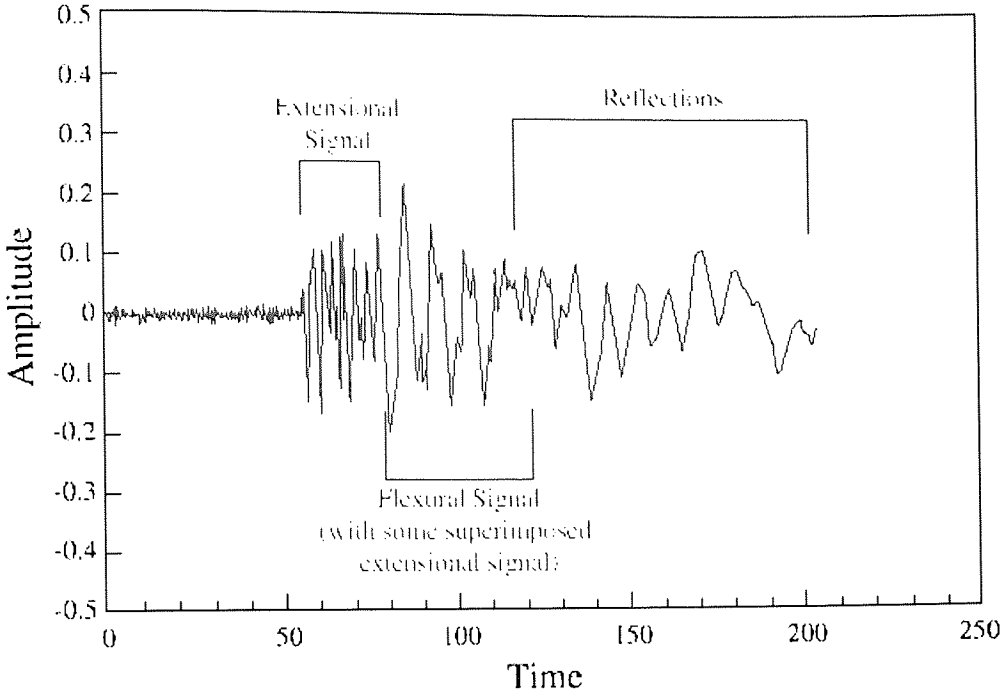

Figure 7-1 A typical AE waveform and its component of a plate

As AE waveform is a time series signal $y(t)$, its reflection can be denoted as the AE signal delay $y(t-n)$. Hence, the AE waveform model is based upon applying its consisting sections as the inputs. The target is detected time series $y(t)$, which contains the impact damage energy. AE It is approximately equivalent to an ARX model in conventional system identification terms. Although the quality of input has been clarified, the quantity the input vector must also be defined. Judging from the outlook, the reflection signals show periodical appearance. As manifested in Figure 7-2, 2J AE waveform (as the energy mode to build ANN model) consisted of 4 sets of reflection signals. The input vector is in the form of 4 reflections combination. Or mathematically, it is written as $[y(t-1) \quad y(t-2) \quad y(t-3) \quad y(t-4)]^T$

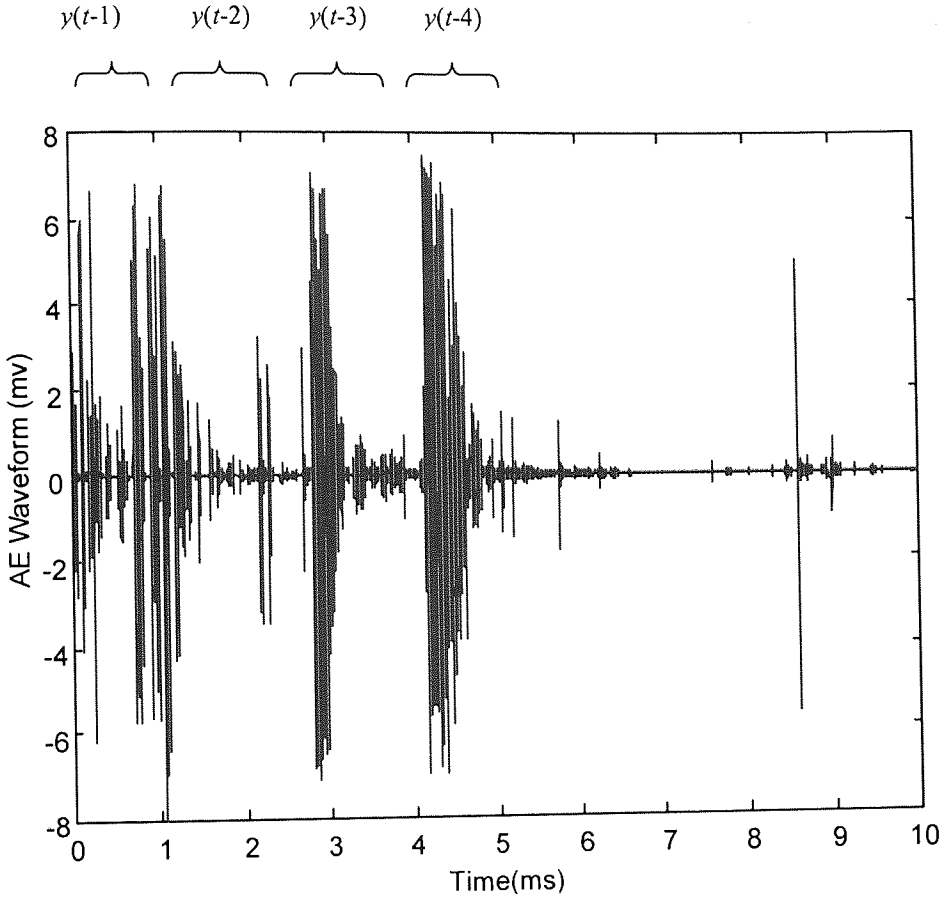

Figure 7-2 AE waveform outlook of 2J impact event on the panel

7.2.2 Input selection of damage location

In the locating study, 6 inputs were used in the neural modelling. They are literally the combination of the time difference among 4 arrival times detected from sensors. Δt=[Δt_{12} Δt_{13} Δt_{14} Δt_{23} Δt_{24} Δt_{34}] where Δt_{12}= $|t_1-t_2|$; Δt_{13}= $|t_1-t_3|$; ... Apparently, there are three time differences, say Δt_{23}, Δt_{24}, Δt_{34}, can be regarded as the derision from the other three time difference Δt_{12} Δt_{13} Δt_{14}. It seems that those three time differences provide no new information in terms of time difference value. However, it was found that the accuracy of the neural network improved when these surplus

inputs were introduced, i.e. when the number of inputs increased from three to six. It was also empirically proved that the neural network model was trained faster when these extras were included. It is believed that this phenomenon is due to the geometric layout of sensor arrays. As a result, it was discovered that the sequence of the time differences as well as their values is the essential factor in determining the location. When there is an occurrence of impact event on the panel, arrival time can be read from the AE sensors. Using value of time differences to locate the impact sites was straightforward as shown in (6-1) and (6-2). Nevertheless, in Figure 7-3 and Figure 7-4, a simple example was studied to illustrate how the sequence can influence the determination of the impact site co-ordinates. In this case, the configuration of three time-differences as inputs proved insufficient. Thus, it is necessary for ANNs to recruit more inputs to make up the deficiency.

In impact event A,

$$\Delta t_{12} = \left| \frac{OO_1 - OO_2}{V} \right| \tag{7-1}$$

$$\Delta t_{13} = \left| \frac{OO_1 - OO_3}{V} \right| \tag{7-2}$$

$$\Delta t_{14} = \left| \frac{OO_1 - OO_4}{V} \right| \tag{7-3}$$

where V is the AE speed.

Impact event A

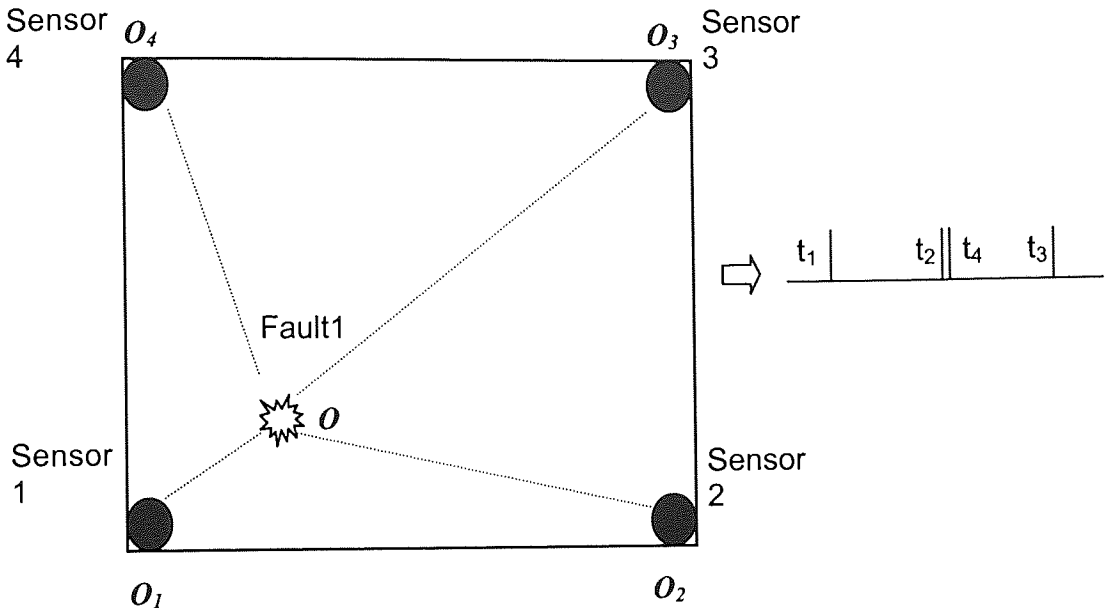

Figure 7-3 Illustration for the sequence effect of time difference on the location detection (A)

In impact event B, however,

$$\Delta t'_{12} = \left| \frac{O'O'_1 - O'O'_2}{V} \right| \quad \textbf{(7-4)}$$

$$\Delta t'_{13} = \left| \frac{O'O'_1 - O'O'_3}{V} \right| \quad \textbf{(7-5)}$$

$$\Delta t'_{14} = \left| \frac{O'O'_1 - O'O'_4}{V} \right| \quad \textbf{(7-6)}$$

Impact event B

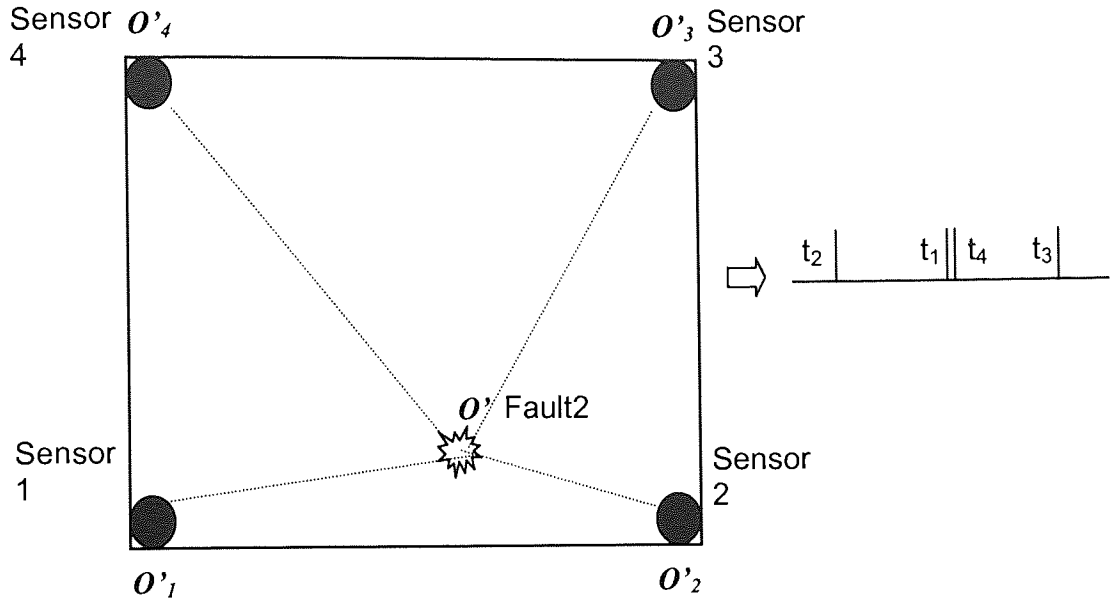

Figure 7-4 Illustration for the sequence effect of time difference on the location detection (B)

For	A	B
	$OO_1=2$,	$O'O'_1=4$,
	$OO_2=5$,	$O'O'_2=1$,
	$OO_3=7$,	$O'O'_3=9$,
	$OO_4=4$,	$O'O'_4=6$,

Accordingly, the values of Δt_{12}, Δt_{13}, Δt_{14} will be identical to those of $\Delta t'_{12}$, $\Delta t'_{13}$, $\Delta t'_{14}$.

A	*B*
$\Delta t_{12}=3$,	$\Delta t'_{12}=3$
$\Delta t_{13}=5$	$\Delta t'_{13}=5$
$\Delta t_{14}=2$	$\Delta t'_{14}=2$
$\Delta t_{23}=2$	$\Delta t'_{23}=8$

$\Delta t_{24}=1$ $\Delta t'_{24}=5$

$\Delta t_{34}=3$ $\Delta t'_{34}=3$

Hence, if only the first three time differences are taken into account, it could confuse the neural network to determine the location. It isn't enough with the combination of 3 time differences for ANN to synthesise the location information. That is to say at least one extra time difference is required, say Δt_{23}, to help identifying the location. It acts as referent time difference. However, there will be another question as 'Which extra arriving time will be helpful?'. A practical solution therefore is to incorporate all the time difference set to build a fixed sequence. Each set of input will then be able to correspond to a unique location on the sample panel. Meanwhile, from the point of neural modelling, this phenomenon can also be interpreted as ANNs is good at intepolation instead of extrapolation. Thus, the sufficient information from input is vital. As a result, higher accurate location prediction using six time differences inputs has verified the researcher's assumption.

7.3 Stopping Criterion

When the neural network is being trained, the weight set is adapted in order to minimise the mean square error over the training set. Ideally, parameter optimisation would be based on the criterion, which we wish to minimise (classification error rate) but there is no principled method for achieving this at the moment (Tarassenko, 1998). A compromise is to continue minimising the training

MSE using the error back-propagation algorithm but to monitor the classification error rate on the validation set in order to decide when to stop training. (In general sense, training continues for longer and minimum obtained on the validation set may be less pronounced. Nevertheless, a poor validation may also be encountered if the training finished too soon.)

Thus the progress of learning is followed by continuously monitoring the classification error on the validation set, e_{val}. This is calculated over all the patterns in the validation set at the end of each training epoch. If e_{val} is plotted as a function of the number of epochs, the behaviour which should be observed (see Figure 7-5) is one in which it decrease quickly at first, in very much the same way as the classification error on the training set, e_{tr}.

Eventually, e_{val} stops decreasing or even starts to rise up whist e_{tr} continuous to decrease. It is at this point that training should be stopped and the network's weights saved. There may be a small amount of oscillation from epoch to epoch but the minimum validation error, $(e_{val})_{min}$ (also known as goal in terms of some neural network software), should be taken to be the first minimum or the 'knee' of the curve, shown in Figure 7-5, and it is the corresponding weight set which should be regarded as the optimal weight set for this network configuration. In the modelling of this study, $(e_{val})_{min}$ was set as 0.0001 of damage level study and 0.01 of location study respectively.

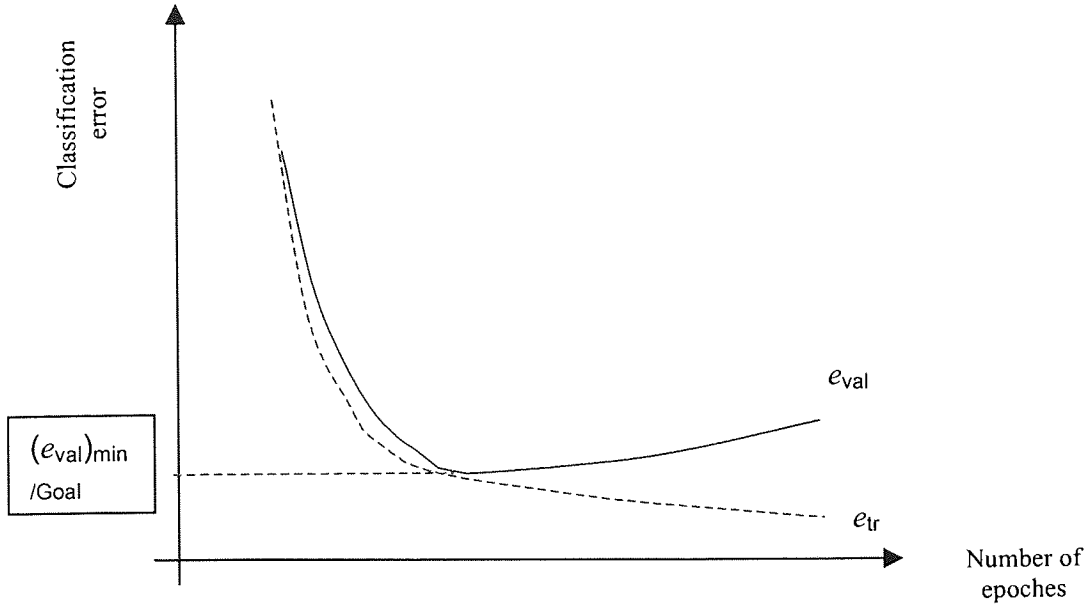

Figure 7-5 Plots of training and validation classification error during training

7.4 Speed and Memory Comparison

As aforementioned, another influential factor on the neural computation speed is the training algorithm. However, it is very difficult to know which training algorithm will be the fastest for a given problem. It will depend on many factors, including the complexity of the problem, the number of data points in the training set, the number of weights and biases in the network, and the error goal. In general, on networks, which contain up to a few hundred weights, the Levenberg-Marquardt (L-M) algorithm will have the fastest convergence. This advantage is especially noticeable if very accurate training is required. The quasi-Newton methods are often the next fastest algorithms on networks of moderate size. The Broyden, Fletcher, Goldfarb, and Shanno (BFGS) algorithm does require storage of the approximate Hessian matrix, and is generally faster than the conjugate gradient

algorithms. The similarity between Levenberg-Marquardt (L-M) algorithm and quasi-Newton methods is that they all adapt approximate Hessian matrix to replace the complex and expensive computation of the Hessian matrix during the weights updating at each iteration of the algorithm. The Hessian matrix can be approximated as

$$H = J^T J \tag{7-7}$$

when the performance function has the form of a sum of squares (as is typical in training feedforward networks). The gradient then can be computed as

$$g = J^T e \tag{7-8}$$

where is the Jacobian matrix that contains first derivatives of the network errors with respect to the weights and biases, and e is a vector of network errors. The Jacobian matrix can be computed through a standard backpropagation technique (Hagan, 1994) that is much less complex than computing the Hessian matrix.

Of the conjugate gradient algorithms, the Powell-Beale procedure requires the most storage, but usually has the fastest convergence. Resilent propagation (Rprop) and the scaled conjugate gradient algorithm do not require a line search and have small storage requirements. They are reasonably fast, and are very useful for large problems. The variable learning rate algorithm is usually much slower than the other methods, and has about the same storage requirements as Rprop, but it can still be useful for some problems. There are certain situations, in which it is better to converge more slowly. For example, when using early stopping,

inconsistent results can be produced if the applied algorithm converges too quickly. A point could be overshot at which the error on the validation set is minimised. The location detection modelling provides a convincing and practical evident case here. In the study, results yielded from L-M algorithm are less accurate than that from Variable Learning Rate algorithm, which is slower than L-M in computation.

In summary, in situations where speed matters, the Levenberg-Marquardt usually is the recommended algorithm first. Whereas memory space is a problem, then the BFGS algorithm is the prior choice. Of course, one of the conjugate gradient methods can also be considered. The Rprop algorithm is also very fast, and has relatively small memory requirements.

The following table gives some example convergence times for the various algorithms on one particular regression problem (Proposed by MathWorks). In this problem a 1-10-1 network was trained on a data set with 41 input/output pairs until a mean square error performance of 0.01 was obtained. Twenty different test runs were made for each training algorithm to obtain the average numbers shown in the table. These numbers should be used with caution, since the performances shown here may not be typical for these algorithms on other types of problems.

Table 7-1 Speed comparison on different algorithm

Technique	Time	Epochs	Mflops
Variable Learning Rate	57.71	980	2.5
Rprop	12.95	185	0.56
Scaled Conj. Grad.	16.06	106	0.7
Fletcher-Powell CG	16.4	81	0.99
Polak-Ribiére CG	19.16	89	0.75
Powell-Beale CG	15.03	74	0.59
One-Step-Secant	18.46	101	0.75
BFGS quasi-Newton	10.86	44	1.02
Levenberg-Marquardt	1.87	6	0.46

(Proposed by Mathwork)

7.5 The correlation of neurons

In the study of neural networks, there is always an interest in finding out how the neurons functioned and how the neurons interacted on each other. In other words, what is the correlation of the neurons? In the training, the neurons will respond differently to the input. The number of the neurons and topology of connection can have a significant impact on its performance in any particular application. The influence from artificial neuron is through its parameters: weights and bias. From these two parameters, the role of each neuron can be review. Usually, a Hinton diagram can provide a qualitative display of the values in a data matrix (normally a weight matrix) after the training. In the Hinton diagram of location study with 8-2 neuron structure, the value of each weight and bias is represented by a square whose size is associated with the magnitude, and whose colour indicates the sign. Therefore from the diagram, the internal specification of a hidden layer can be

seen and the contribution of each neuron discovered. Value of the weights and biases can objectively display the topology of neuron connection. The less the value is, the weaker the connection would be. In the case study of damage location detection, Hinton graph illustrates a weight matrix and a bias vector represented as a grid of squares and is shown in Figure 7-6 and Figure 7-7.

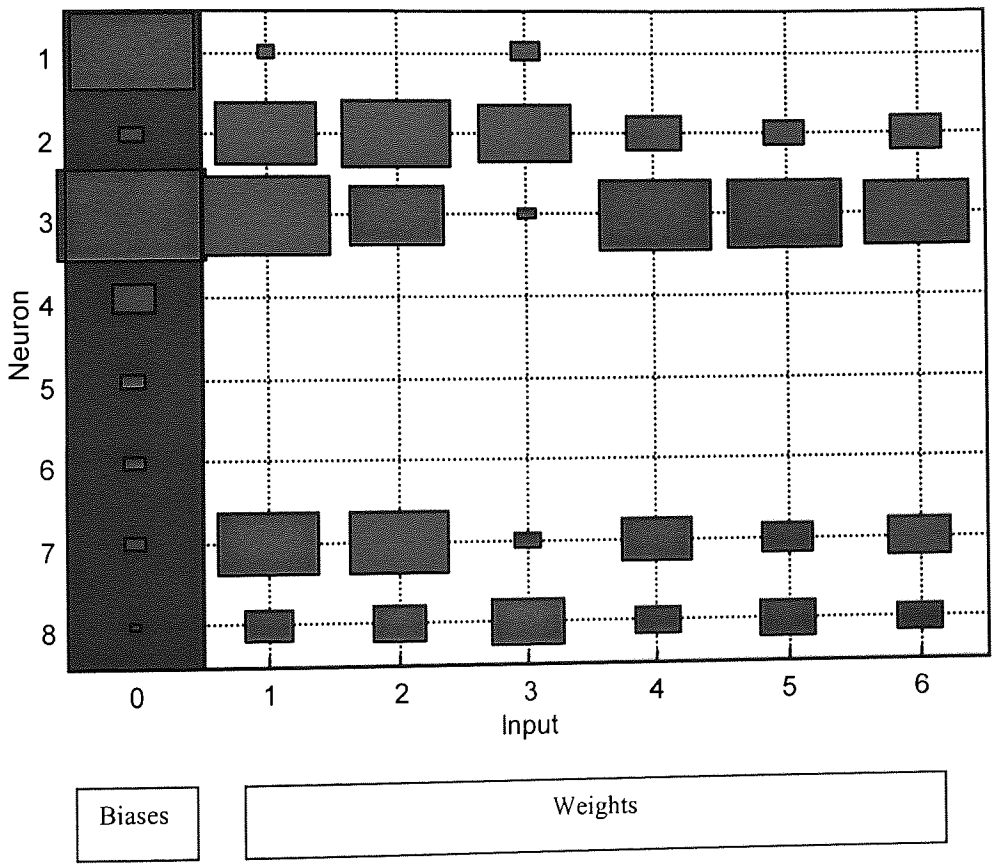

Figure 7-6 Hinton diagram of the 8 neuron location neural model (layer one)

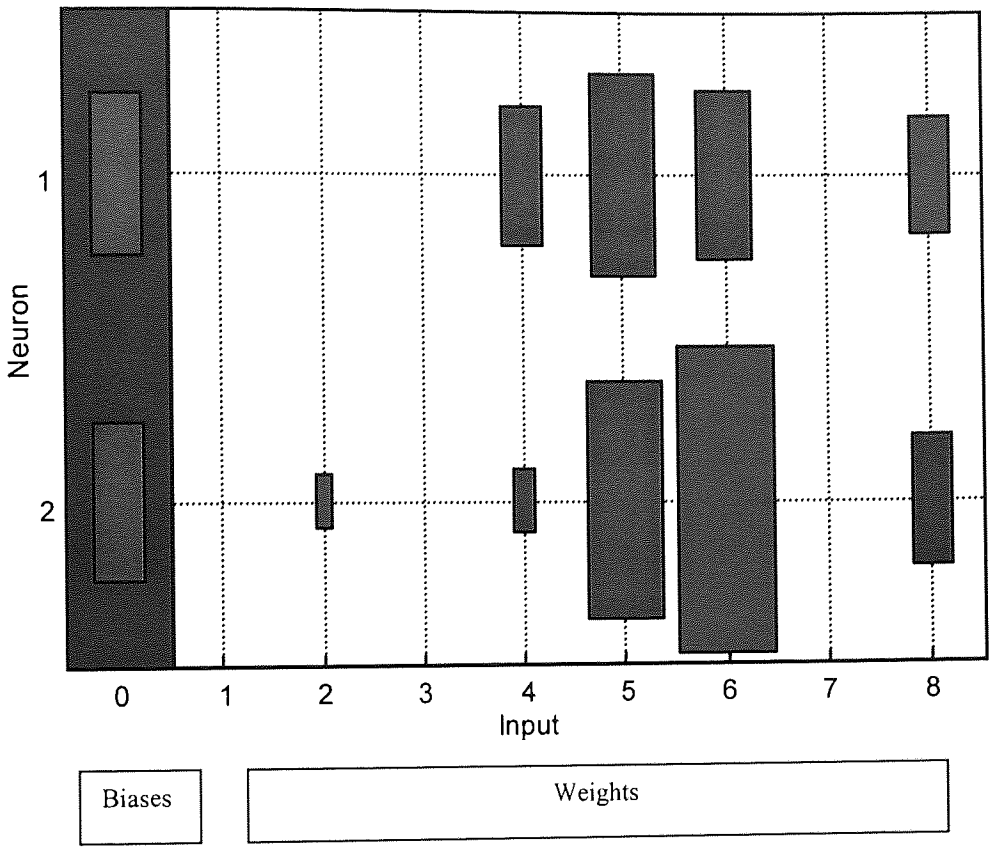

Figure 7-7 Hinton diagram of the 8 neuron location neural model (layer two)

To simplify the problem, only the case study of 8-2 neurons structure is given here. The weights or biases corresponding to the red rectangles are negatives while the green ones are positives. The size of the rectangular corresponds to the value of the weights and bias in the layers. They are all listed in Table 7-2 and Table 7-3. In the first layer, there are 48 weights (6 inputs × 8 neurons) and 8 biases. In Figure 7-6 and Figure 7-7, the weights are all shown in the right hand section, with white background. The left hand sides are the bias in blue background. As shown in

Figure 7-6, 7-7 and Table 7-2 and 7-3, the profile of each neuron is indicated individually. There are relative firmer connections for Neuron 2 and Neuron 3 in the hidden layer while Neuron 4, Neuron 5 and Neuron 6 are far less connected to the input. However, this was compensated in the output layer since there are only strong links among Neuron 4, Neuron 5, Neuron 6 and output neurons.

Table 7-2 Weights and biases of the layer one

	Bias	Weights					
Neuron1	48.3741	-1.4074	-0.2844	-3.2154	0.3726	0.4049	0.1384
Neuron2	-2.3812	-30.7848	-38.1297	-29.5366	-10.4754	-4.8717	-8.5724
Neuron3	70.0747	-51.2662	30.5631	1.4605	44.5771	41.9085	-35.3102
Neuron4	-6.3500	0.0076	-0.0159	0.4274	-0.0129	-0.0291	-0.0249
Neuron5	2.3300	0.0132	-0.1651	0.0141	0.0146	-0.0015	0.0095
Neuron6	2.0332	-0.1091	0.0104	0.0331	0.0078	0.0006	0.0060
Neuron7	-2.0295	32.5539	-33.0654	2.2821	15.7526	8.3686	-12.1570
Neuron8	-1.0436	8.0279	9.7768	19.0362	6.6683	10.1428	7.0139

Table 7-3 Weights and biases for layer two

	Bias	Weights							
Neuron1	-13.3342	-0.0521	-0.4344	0.0694	9.8488	20.8845	14.9439	-0.0206	-7.6082
Neuron2	12.5730	0.2765	-2.0220	0.0926	2.5299	28.5180	-47.332	-0.0889	8.9361

Using a Hinton diagram, it is possible to indicate the contribution of a neuron and its correlation with other neurons. It clearly shows which neuron needed to strengthen the connection with the input, which needs to highlight the ties among neurons in different layers. Naturally, the performance of the neurons raises the

question of optimisation for the neural network structure. A methodology for this is introduced in the following section.

7.6 Neural structure determining and optimisation

The network architecture is an important factor to determine the performance of ANN models. Each application needs to construct its own model architecture that fit the task best. To obtain good generalisation, one has to incorporate into the network as much knowledge about the problem as possible (e.g., the topology of the input space) and limit the number of connections appropriately (to optimise the structure). It is therefore desirable to find algorithms that not only optimise the weights for a given architecture, but also optimise the architecture itself. This means, in particular, optimising the number of layers and the number of units in hidden layers. (Note that the neurons in output layer are fixed by the system.)

Of course there are various different criteria for optimisation, including generalisation ability, learning time, number of units, and so on. In fact, given various hardware restrictions, there may be quite a complicated cost function for the architecture itself. This study focuses mainly on using as accurate computing units (neurons) as possible; this should not only reduce computational costs and perhaps training time, but should also improve the generalisation.

It is possible to mount a search in the space of possible architectures. One can train each kind of architecture separately say, by back-propagation and then evaluate it with an appropriate model that incorporates both performance and number of neurons. Such a study can be carried out by using genetic algorithm so that good building blocks, found in one trial architecture, are likely to survive and be combined with good building blocks from other trials (Harp, 1990; Miller, 1989). Some research has been based on statistical method like generalising Akaike's Information Criterion (Murata *et al*, 1994). The difficulty of determining the number of neurons is because an increase in the number of the parameters lessens the output errors for the training samples, but increases the error for the novel training samples. Such cases can be catalogued as over-fitting. To solve the problem, there are approaches in which one can construct or modify the architecture to suit a particular task, proceeding incrementally. There are two different strategies to approach: the goal- Pruning or Growing

7.6.1 Pruning and weight decay

The network can be trimmed by removing unimportant connections. It is also possible to prune unimportant units (Sietsma and Dow, 1988). Network can remove non-useful connections during training by giving each connection ω_{ij} the inclination to decay to zero. The connections then disappear unless it is reinforced. (Hinton, 1986, Scalettar and Zee, 1988, Kramer and Sangiovanni-Vincentelli, 1989). The simplest way is to use

$$\omega_{ij}^{new} = (1-\varepsilon)\omega_{ij}^{old} \tag{7-9}$$

after each update of ω_{ij}, for some small parameter ε. This is equivalent to adding a penalty term ω_{ij}^2 to the original cost function E_0

$$E = E_0 + \gamma \sum_{(ij)} \varpi_{ij}^2 \tag{7-10}$$

and performing gradient descent $\Delta\omega_{ij} = -\eta \partial E / \partial \omega_{ij}$ on the resulting total E. The ε parameter is then just $\gamma\eta/2$. While (7-10) clearly penalises use of more ω_{ij} than necessary, it overly discourages use of large weights; one large weight costs much more than many small ones. This can be overcome by using a different penalty term, such as

$$E = E_0 + \gamma \sum_{(ij)} \frac{\omega_{ij}^2}{1+\omega_{ij}^2} \tag{7-11}$$

which is equivalent to making ε in (7-9) dependent on ω_{ij}

$$\varepsilon_{ij} = \frac{\gamma\eta/2}{(1+\varpi_{ij}^2)^2} \tag{7-12}$$

so that small ω_{ij} decay more rapidly than large ones.

These decay perform well in removing unnecessary connections, but often we want to remove whole unites. Then we can start with an excess of hidden units and later discard those not needed. It is easy to encourage this by making the weight decay rates lager for units that have small outputs, or that already have small incoming weights (Hanson and Pratt, 1989; Chauvin, 1989). For example we could replace (7-12) by

$$\varepsilon_i = \frac{\gamma\eta/2}{(1+\sum_j \omega_{ij}^2)^2} \qquad \textbf{(7-13)}$$

and use this same ε_i for all connection feeding unit i.

7.6.2 Networks construction growing

The cascade-correlation learning architecture (Fahlman and Lebiere, 1990) is an example of the network growing approach. The procedure begins with a minimal network that has some inputs and one or more output nodes as indicated by input and output requirements. However, there are no hidden nodes employed at the very beginning. The LMS algorithm, for example, may be used to train the network. The hidden neurons are added to the networks one by one, thereby obtaining a multi-layer structure. Each new hidden neuron receives a synaptic connection from each of the input nodes and from each pre-existing hidden neuron. When a new hidden neuron is added, the synaptic weights on the input side of that neuron are frozen; only the synaptic weights on the output side are trained repeatedly. The added hidden neuron then becomes a permanent feature detector in the network. The whole procedure will keep proceeding until the satisfactory performance is achieved.

Yet another network-growing approach developed by Lee *et al* (1990), a third level of computation, termed the structure-level adaptation, is added to the forward pass (function-level adaptation) and backward pass (parameter-level adaptation). In this

third level of computation the structure of the network is adapted by changing the number of neurons and the structural relationship among neurons in the network. The criterion used here is that when the estimation error after convergence is larger than a desired value, a new neuron is added to the network in a position where it supposes to be required. The desirable position for the new neuron is determined by monitoring the learning behaviour of the network. In particular, if after a long period of parameter training, the synaptic weight vector pertaining to the inputs of a neuron continues to fluctuate significantly, it may be inferred that neuron in question does not have enough representation power to learn its proper share of the task. In practice, a neuron is annihilated when it is not a functioning element of the network or it is a redundant element of the network. However, this method may consume intensive CPU power.

7.7 Conclusions

Chapter 7 provides a further discussion in the damage detection study following the evaluation of ANN modelling. There are several crucial subjects that have been examined in this section. They are 1) The selection of input for ANNs models. The input was determined by study the physical nature of AE propagation in the damage level discrimination study. In damage location, it reveals the necessity of choosing six sets of time difference as input instead of three. 2) Computation speed comparison. Different algorithms are used to illustrate the time and memory consuming when applying the computation algorithms. 3) Correlation of neurons

and 4) Neural structure determining and optimisation. The principles and solutions as to how to optimise the neural network structure are illustrated.

This chapter technically gave the thoughts on how to improve the performance and set up criterion to choose the neural structure. It therefore is an indispensable section of the study. There are still some interesting further studies that could be carried out and these are discussed in the recommendation section for future work.

Chapter 8 Conclusions and recommendations

"Life can only be understood backwards, but it must be lived forwards"

(Soren Kierkegaard, 1967)

8.1 Introduction

The research project, which has been described in this thesis, was concerned of two essential aspects of impact damage detection: damage level discrimination and damage location detection. The study was conducted in a qualitative as well as quantitative manner to determine the damage severity and location on composite materials. Artificial Neural Networks, along with the Acoustic Emission techniques, were introduced to perform system identification, model building, signal processing and validation for impact damage detection. In section 8.2, there are the conclusions for the experimental and the modelling work. Conclusions for damage level and damage locating are given in section 8.3 and section 8.4 respectively. Some topics for further research have been identified in section 8.5. These topics are suggested as future recommendation. Closing remarks were finally given in section 8.6

8.2 Conclusions of the experimental and modelling work

The experimental work covered the following areas

1> Test rigs design, sample preparation and test design of data acquisition

2> AE implementation to conduct NDT

3> Experimental measurements for the validation of ANN models

The modelling work covered following areas

1> Input coding and pre-processing

2> ANN model setup and training

3> Validation

4> Neural structure optimisation

In the experimental work, test rigs and test schemes were successfully designed and developed to conduct data acquisition and measurement. Different sample panels were manufactured for the study. In damage severity study, C-scan tests were carried out to calibrate the impact damage areas as verification. While, in damage location, validation data was from the unknown locations measured from a new set of impact location tests. However, there is some inadequacy in the experimental work. For instance, optimising of sensor array layout demands some more thoughts in both damage level study and damage location. Hence, more reliable result can be achieved.

It's evidenced that detected acoustic emission signals, generated by the impact events, accommodate the information of impact damage such as of the damage severity and damage location. Thus, an interpreter has to be invented to decode such information. In the modelling work, artificial neural networks served as the mainstay in this impact damage study and played an essential role in the system

identification and modelling of this project. Taking the advantage of MATLAB neural toolbox, several back propagation (BP) neural network models were built to conduct impact damage severity discrimination and location detection using delayed AE waveform and arriving time differences as input. The performance of the ANN models was encouraging. As the supplements, modelling work also involved further investigations on input pre-processing, validation, and structure optimisation seeking the mechanism to improve the functionality of neural network models. However, Section 8.2 only generates a general summary of the modelling work. More specified conclusions on the damage level discrimination and damage location are given in the following two sections accordingly.

8.3 Conclusions for damage level discrimination

In damage severity study, different levels impact damage energy was used to produce different level of damage in two composite materials (T3000/914 and T800/5245). Neural networks showed great potential for interpretation of large quantities of AE transient waveform data as an impact damage indicator. Using a BP neural network model, MSE were generated providing a novel approach to quantify the severity of impact damage. Under the present training regime, correlation coefficients with damage area were moderate at 0.88 and 0.74 in two types of materials. It was found that the MSE value provided the best indicator for impact damage in the T300/914 material. Simple parameters such as AE energy,

AE counts gave better correlations with damage area in T800/5245. The best correlation (0.97) with damage area was obtained with impact energy in that case.

8.4 Conclusions for damage locating

In damage location study, a new artificial neural network was successfully implemented to perform impact location on a quasi-isotropic material panel. The relationship between arriving time difference of AE signals obtained from transducers located on the panel and the impact site coordinates has been employed to train the ANN models and pinpoint the impact locations. By processing data from acoustic sensors off-line, a BP neural network model was trained to locate the damage impact sites. The accuracy of the prediction from the neural network was verified by the new data time difference obtained from unknown locations, the results were promising and were shown in Table 6-1. The performance of the ANN model, which was evaluated by calculating the distance deviation between model output and real location coordinates, support the application of ANN as an impact damage locator. In the study, the ANN prediction accuracy decreased when approaching the central area of the panel. A further investigation indicated that this is due to the small arrival time difference within such area. A practical solution is proposed by increasing the number of processing unit (neurons), thereby enhancing the generalisation ability of ANN.

8.5 Recommendation for future work

Following aspects are on the recommendation list for future work:

8.5.1 Use of alternative materials

This study is based on composite materials, T300/914 *etc*. The obtained data can therefore reflect the attenuating properties of quasi-isotropic composite materials. Nevertheless, when facing real time applications, there could be a good deal possible choices about materials. A further study is recommended to reveal the different responses from different type of materials such as isotropic and anisotropic materials. Considerable exciting openings are envisaged and indeed may be offered by new materials. On other hand, the new tests could be conducted on more complicated 3D structures rather than the present panel prototypes. It will produce more valuable and practical results based on the potential studies.

8.5.2 Use of alternative sensor system

The AE broadband piezo-electronic sensors provide a trustworthy and practical data acquisition measure in this study. It is economical and reliable according to the outcome of the project. However, there are still some system errors introduced by the layout of PZT transducers. In the location study, four PZT sensors were arranged in rectangle pattern for detection. This may yield some "blind area" which may confuse the ANNs model. In the future project, the sensor array can be designed in different configurations. There are some prompting examples about the layout of sensors array in previous studies such as ACEMAN system from

CEGB (Sinclair, 1977). The sensor array can be modified in numbers as well in layouts. Usually the rectangle, triangle, and star shaped configurations are employed mostly for locating a source on a flat surface; a diamond pattern of sensor array is often adopted on a cylindrical surface (Williams, 1980). These arrays can be randomly placed about a structure as each has its own co-ordinates and monitoring area, totally independent of the others. At the meantime, optical fibre sensors may provide more flexible measuring to replace the existed PZT sensor array if the condition permitted.

8.5.3 Further study of new algorithm of neural structure optimisation

Due to the time restriction, alternative algorithms for neural networks structure optimisation have not been evaluated. A brief touch was given on the neuron growing and pruning, which technically may only be a tip of the iceberg. If the study is continued, priority should be given to the study on neural structure. As stated in the study, a micro view has been focused on determining the numbers of calculation unit using neuron grow algorithm. However, a more efficient and general algorithm is expected to justify the structure determination. Therefore, it can be applied in more diversified cases not only for the impact damage detection but a fundamental supplement to the science of artificial neural network.

8.5.4 Some extra points

There are still some other areas that can be investigated in the future. For instance,

since the form and velocity of AE within the structure is essential to impact damage detection, there could be studies on AE waveform propagation that focus a clear understanding of the damage locating mechanism. Meanwhile, interests of research may also be placed on more specific analysing in frequency domain of impact damage detecting, particularly the possibility to implant the signal filtering in location detection. Recognising the limits of his perceptiveness, the thesis writer numbered only a few recommendations here. However, the writer can perceive the future research in this subject flourishing in dimensions and in depth.

8.6 Final remarks

Projects involving impact damage detection are not new, nor are the applications of artificial neural networks and Acoustic Emission technique. Nevertheless, these techniques and methodologies have been successfully combined together to discriminate the damage severity and to locate the damage sites in this study. Using ANNs, a numerical indicator was developed by extracting the information inside the AE waveform. After the training, the neural model then was able to indicate the damage level according to the different impact energy. Whereas, exploiting the mechanism between time differences and coordinates, ANNs model has also been trained to pinpoint the damage location. There are also studies on impact damage mechanism, experimental designing, structure optimisation and performance improving *etc.* in this project. It is hoped that the work described in

this thesis will make some contributions to the continuous evolution of engineering practice.

References

Abrate, S., 1998, The dynamics of impact on composite structures, *Key Engineering Materials*, Vol. 141-143, pp. 671-694.

Alston, M.D., Chau, P.M., 1990, A decoder for block-coded forward error connecting system, *Proceedings of The International Joint Conference for Neural Networks* (2^{nd}), Vol. 2, pp. 302-305.

Amin, S.M., and Rodin, E.Y., 1997, Application of dynamic neural networks to approximation and control of non-linear system, *Proceeding of the 97 American Control Conference*, Vol. 1, pp. 222-226.

Anderson, R.T. and Delacy, T.J., 1972, *Metal Progress*, pp. 102.

Anthony, D., Hines, E., Barham, J., and Taylor, D., 1990, A comparison of image compression by neural networks and principle component analysis, *Proceedings of the International Joint Conference for Neural Networks* (3^{rd}), Vol. 3, pp. 339-342.

Arteaga-Bravo, F.J., 1990, Multilayer back-propagation network for learning the forward and inverse kinematics equations, *International Joint Conference on Neural Networks*, Vol. 2, pp. 319-324

ASTM, 1975, *Foreign Object Impact Damage in Composites*, ASTM STP **568**, pp. 183.

ASTM, 1995, *Annual Book of ASTM Standards*, Vol. 03.

Backhouse, R., 1998, Multiaxial Non-crimp Fabric Characterisation of Manufacturing Capability for Composite Aircraft Applications, Cranfield University Eng. D. Thesis.

Barai, S.V., and Pandey, P.C., 1997, Time-delay neural networks in damage detection of railway bridges, *Advances in Engineering Software*, Vol. 28, pp. 1-10.

Barto, A, Sutton, R.S., and Anderson, C.W., 1983, Neural-like adaptive elements that vcan solve difficult learning control problems, *IEEE Transactions*, SMC, SMC-13, pp. 834-846.

Bassim, M.N., and Houssny-Emam, M., 1981, Time and frequency analysis of acoustic emission signals, *Material Science Engineering.*, pp. 140-159.

Belajef, W.M., 1924, *Memories on Theory of Structures*, Izdatelstwo Puti, st. Petersburg.

Bleay, S. M., Loader, C. B., Hawyes, V. J., Humberstone, L., and Curtis, P. T., 2001, A smart repair system for polymer matrix composites, *Composites Part A: Applied Science and Manufacturing*, Volume 32, Issue 12, pp. 1767-1776.

Blumenfeld, B., 1990, A connectionist approach to the processing of time dependent medical parameters, *Proceedings of The International Joint Conference For Neural Networks*, Vol. 2, pp. 575-578.

Bullock, D., and Grossberg, S., 1990, FLETE: An opponent neuromuscular design for factorisation of length and tension, *International Joint Conference on Neural Networks*, Vol. 2, pp. 209-212

Carpenter, S. H., and Gorman, M. R., 1997, A waveform investigation of the acoustic emission generated during the deformation and cracking of 7075 aluminium, *International Journal of Fatigue*, Volume 19, Issue 3, pp. 267.

Chauvin, Y., 1989, A back-propagation algorithm with optimal use of hidden units, *Advances in Neural Information Processing System*, Vol. I, pp. 519-526.

Chretien, J.F. and Chretien, N., 1972, A bibliographical survey of acoustic emission, *Non-Destructive Testing*, pp. 220-224.

Clark, G, 1992, Commentary on 'Quantitative acoustic emission source characterisation of microcracking in steel', *Research in Non-destructive Evaluation*, Vol.4, No. 3, pp.183-192.

Claus, R.O, Jackson, B.S., and Bennett, K.D., 1985, Non destructive testing of composite materials by OTDR in imbedded optical fibers, *SPIE International Symposium on Fibre Optics and Laser Sensors III*, V566, pp. 243-248.

Crose, J.G., and Jones, R.M., 1968, The aerospace corporation, TR-0200 (54950)-1.

Cybenko, G., 1989, Approximation by superpositions of a sigmoidal function, *Math Control, Signal & Systems*, Vol. 2., pp.304-314.

Davies, G.A.O., Zhang, X., Zhao, G., and Watson, S., 1994, Numerical modelling of impact damage, *Composites*, Volume 25, pp. 342-347.

Demuth, H. and Beale, M., *Neural Network Toolbox: for Use with Matlab*, 1998, p. 13-220.

Doyle, C and Fernando, G, 1998, Detecting impact damage in a composite material with an optical fibre vibration sensor system, *Smart Materials and Structures*, Volume 7, Issue 4, pp. 543-549.

Dunegan, H.L., Harris, D.O., and Tatro, C.A., 1968, *Engineering Fracture &Mechanics*, 1, pp. 105.

Dvorak, G.L., and Laws, N., 1987, Analysis of progressive matrix cracking in composite laminates II: First ply failure, *Journal of Composite Materials*, Vol. 21, pp. 309-329.

Eckmiller, R., 1989, Neural control of intelligent robots, *New Developments in Neural Computing*, pp. 217-232.

EN 1330-1, Non-destructive testing - Terminology - Part 1: List of general terms.

EN 1330-2, Non-destructive testing - Terminology - Part 2: Terms common to the non destructive testing methods.

EN 1330-9, Non-destructive testing - Terminology - Part 9: Terms used in Acoustic Emission testing.

EN 473, Non-destructive testing – Qualification and certification of NDT personnel - General principles.

EN 13477-2, Non-destructive testing – Acoustic emission – Equipment characterisation – Part 2: Verification of operating characteristic.

EN 13554, Non-destructive testing - Acoustic emission - General principles

FAGAN, M.J., 1992, Finite element analysis: Theory and practice, *Longman Scientific & Technical*, ISBN 0-582-02247-9, England, UK.

Fahlman, S.E., and Lebiere, C., 1990, The cascade-correlation learning architecture, *Advances in Neural Information Processing System* II, pp. 524-532.

Faller, W.E., and Schreck, S.J., 1995, Real time prediction of unsteady aerodynamics application for aircraft control and manoeuvrability enhancement, *IEEE Transaction On Neural Networks*, Vol. 6(6), pp. 1461-1468.

Faller, W.E., Schreck, S.J., and Helin, H.E., 1995, Real time model of 3 dimensional dynamic reattachment using neural networks, *Journal of Aircraft*, Vol. 32(6), pp. 1177-1182.

Flood, I., and Kartam, N., 1994, Neural network in civil engineering I: principles and understanding, *Journal of Computation Civil Engineering*, ASCE, Vol. 8, pp. 131-148.

Flood, I., and Kartam, N., 1994, Neural network in civil engineering I: system and application, *Journal of Computation Civil Engineering*, ASCE, Vol. 8, pp. 148-162.

Ghosh, S., Collins, E.A., and Scofield, C.L., 1988, Prediction of mortgage loan performance with a multiple neural network learning system, *Abstracts of the First Annual INNS Meeting*.

Greenhalgh, E., Bishop, S. M., Bray, D., Hughes, D., Lahiff, S., and Millson, B., 1996, Characterisation of impact damage in skin-stringer composite structures, *Composite Structures*, Volume 36, Issues 3-4, pp. 187-207.

Greszczuk, L.B., 1982, "Damage in composite materials due to low velocity impact", *Impact dynamics*, John Wiley &Sons, New York, USA, pp. 55-93.

Guo, J., and Cherkassky, V., 1989, A solution to the inverse to the kinematic problem in robotics using neural network processing, *International Joint Conference on Neural Networks*, Vol. 2, pp. 299-304.

Ha, C.M., 1995, Neural networks approach to AIAA aircraft control design challenge, *Journal of Guidance, Control and Dynamics*, Vol. 4091), pp. 72-82.

Hagan, M. T., and M. Menhaj, 1994, Training feedforward networks with the Marquardt algorithm, *IEEE Transactions on Neural Networks*, Vol. 5, pp. 989–993, 1994.

Hanson, S.J., and Pratt, 1989, L., A comparison of different biases for minimal network construction with back-propagation. *Advances in Neural Information Processing System* I (Denver 1988), pp. 177-185.

Hardy, C., Baronet, C.N., and Tordion, G.V., The elastoplastic indentation of a half-space by a rigid sphere, *International Journal of Numerical Method Engineering*, Vol. 3, pp. 451-462.

Harp, S.A., Samad, T., and Guha, A., 1990, Layered neural networks with gaussian hidden units as universal approximations. *Neural Computation II*, pp. 210-215.

Hass, D.J., Miland, J., and Fitter, J., 1995, Prediction of helicoptwr component loads using neural networks, *Journal of American Helicopter Society*, Vol. 4091, pp. 72-82.

Haykin, S., 1994, *Neural Networks: A Comprehensive Foundation*, Macmillan College Publishing Company, USA.

Haykin, S., 1999, *Neural Networks: A Comprehensive Foundation* (2nd Edition), Macmillan College Publishing Company, USA.

Hinton, G.E, 1986, Learning distributed representations of concepts, *Proceeding of the Eighth Annual Conference of the Cognitive Science Society*, 1-12.

Hornik, K, Stinchcombe, M., and White, H., (1989), Multilayer feed forward networks are universal approximator, *Neural Networks*, Vol. 2, pp. 359-366.

Hopfield, J.J., 1984, Neurons with graded response have collective computational properties like those of two state neurons, *Proceeding of National Academy Science*, Vol. 81, pp 3088-3092.

Hopfield, J.J., and Tank, D.W., 1990, Computation of decisions in optimisation problems, *Biological Cybernet*, Vol. 52, pp. 141-152.

Huber, M.T., 1956, *Pisma*, Vol. 2, Warsaw.

Huang, M., Jiang, L., Liaw, P.K., Brooks, C.R., Seeley, R., and Klarstrom, D.L., 1998, *Using Acoustic Emission in Fatigue and Fracture Materials Research, The Journal of Minerals, Metals & Materials Society*, Vol. 50, no. 11.

Huchson, W.R., and Stephens, K.R., 1987, The airline marketing tactician (AMT): A commercial application of adaptive networking, *Proceeding of* 1st *IEEE International Conference on Neural Networks*, Vol. 2., pp. 753-756.

Irving,P., Thiagarajan, C., and Kuntz, M., 1997, Damage detection in carbon fibre composite materials by use of electrical potential technique, *Proceeding of DAMAS97*, pp. 313-324.

Isermann, R., 1980, Practical aspects of process identification, *Automatica*, Vol. 16, pp. 575-587.

Jones, R.T., Sirkis, J.S., Friebele E.J. and Kersey, A.D.,1995, Location and magnitude of impact detection in composite plates using neural networks, *SPIE*, Vol2444, pp. 469-479.

Johansson, R., 1993, *System Modelling and Identification*, Prentice Hall, Englewood Cliffs, New Jersey, USA.

Jordan, M., 1989, Generic constraints on underspecified target trajectories, *IJCNN Proceedings*, New York, IEEE.

Jorgensen, C.C., and Schley, A., 1990, A neural network baseline problem for control of aircraft flare and touch down, *Neural Networks for Control*, London, MIT press.

Josin, G., 1988, Integrating neural networks with robots, *AI Expert*, pp. 50-58.

Journal of Neural Network, 1995-, The Official Journal of the International Neural Network Society, Vol. 8-Vol. 14

Kaiser, J., 1950, *Undersuchungen uber das auftreten Gerauschen beim Zugversuch*, Ph.D. thesis, Technische Hochschule, Munich.

Kramer, A.H., and Sangiovanni-Vincentelli, A., 1989, Efficient parallel learning algorithm for neural networks, *Advances in Neural Information Processing System* I, pp. 40-48.

Kubo, J.T. and Nelson, R.B., 1975, Analysing of impact stresses in composite plates, *Foreign Object Impact Damage to Composites*, ASTM STP568, American Society for Testing and Materials, pp 228-244.

Kuperstein, M., 1988, An adaptive neural model for mapping invariant target position, *Behaviour of Neuroscience*, Vol. 102., pp. 148-162.

Kwon, Y.W., and Bang, H., 1996, *The Finite Element Method Using MATLAB*, CRC Press, ISBN 0-8493-9653-0, New York, USA.

Lafrarie-Frenot, M.C., and Henaff-Gardin, C., 1991, Formation and growth 90^0 ply fatigue cracks in carbon/epoxy laminates, *Composite Science Technology*, Vol. 40, pp. 307-324.

Lansing, Matthew D. Walker, James L., and Russell, Samuel S., 1999, Residual strength prediction of impact-damaged composite structures by optical and acoustical computer sensing with neural network techniques, ASTM Special Technical Publication, pp. 285-297.

Lee, T.C., Peterson, A.M., and Tsai, J.C., 1990, A multilayer feed forward neural network with dynamically adjustable structures, *IEEE International Conference on Systems*, pp. 367-369.

Li, L.Y., Thornton, C., and Wu, C.Y., Impact behaviour of elastoplastic spheres with a rigid wall, *Proceeding of Institute of Mechanical Engineering*, pp. 1107-1114.

Lippman, R.P., 1987, An introduction to computing with neural nets, *IEEE ASSP Magazine*, Vol. 4(2), pp. 4-22.

Liptai, R.G., Harris, D.O., Tatro, C.A., 1972, An introduction to acoustic emission, *Acoustic Emission*, ASTM STP 505, pp. 3-10.

Little, J.N., and Shure, L., 1993, *Signal Processing Toolbox: for use with MATLAB*, The MathWorks, Inc.

Liu, N., Zhu, Q.M., Wei, C.Y., Dykes, N.D., and Irving, P.E., 1999, Impact damage detection in carbon fibre composites using neural networks and acoustic emission, *Key Engineering Materials*, Volume 167, pp. 43-54.

Liu, N., Zhu, Q.M., Wei, C.Y., Dykes, N.D., and Irving, P.E., 2000, Acoustic emission signal processing to detect impact damage location using neural networks, *Proceedings of PREP2000*.

Liu, N., Penny, J.E.T., Wei, C.Y., Irving, P.E., Dykes, N., and Zhu, Q.M., 2001,Impact Location on Stiffened Composite Structures Using Neural Networks, *Key Engineering Materials*, Volume 204, pp. 395-408.

Ljung, L., 1987, *System Identification: Theory for the User*, Prentice Hall, Englewood Cliffs, New Jersay, USA.

Ljung, L. and Glad, T., 1994, *Modelling of Dynamic Systems*, Prentice Hall, Englewood Cliffs, New Jersay, USA.

Ljung, L, 2000, System identification toolbox: For use with Matlab, The MathWorks, Inc.

Lord Rayleigh, 1906, Phil. Mag., Vol. 11, pp. 283.

Love, A.E.H., 1929, Phil. *Transactions of Royal Society*. London. A, pp. 228.

Lowe, D., 1995, On the use of nonlocal and nonpositive definite basis functions in radial basis function network, *Proceedings of 4th IEE International Conference on Arifitial Neural Networks*, Cambridge, pp. 206-211.

McCulloch, W.S., and Pitts, W., 1943, 'A logical calculus of the ideas immanent in nervous activity ', *Bulletin of Mathematical Biology*, Vol. 5, pp. 115-133.

Mill, W.T, 1987, Sensor based control of robotic munipulator using a general learning algorithm, *IEEE Journal: Robotics Automat.*, RA-3, pp.

Miller, W.T., Sutton, R.S., and Werbos, R.S., 1989, *Neural Networks for Robotics and Control*, Cambridge, MIT Press.

Miller, G.F., Todd, P.M., and Hegde, S.U., 1989, Designing neural networks using genetic algorithms. *Proceedings of the 3rd International Conference on Genetic Algorithms*, pp. 379-384.

Morse, P.M., and Ingard, K.U., 1968, *Theoretical Acoustics*, McGraw-Hill, New York, USA.

Morton, W.B., and Close, L.J., 1922, Phil. Mag., S.G., Vol. 43, pp. 254-320.

Murata, N., Yoshizawa, S. and Amari, S.I., 1994, Network information criterion-Determining the number of hidden units for an artificial neural network model, *IEEE Transactions on Neural Networks*, Vol. 6, pp. 865-872.

NDT Abstracts, 1992-, *Abstracts of NDT&E International*, Vol25-.

Nichols, R.W., 1976, *Acoustic Emission*, Barking, Essex: Applied Science, UK.

Norton, J.P., 1986, *An Introduction to Identification*, London, Academic press, pp. 59-84.

Owston C.W., 1972, Non-destructive testing and inspection Applied to composite material and structures, *Proceedings of 32nd AGARD Structures and Material Panel Meeting*, London.

Pandey, P.C., and Barai, S.V., 1995, Multilayer perceptron in damage detection of bridge structures, *Computers & Structures*, Vol. 54, No. 4, pp. 597-608.

Patrick, K.S., 1990, Neural networks for sonar signal processing, *Handbook of Neural Computing Application*, pp. 319-333.

Penny, J., and Lindfield, G., 1995, *Numerical Methods Using MATLAB*, MEE Dept, Aston University.

Philippidis, T.P., Nikolaidis, V.N., and Anastassopoulos, A.A., 1998, *NDT&E International*, Vol.31 No 5., pp. 329-340.

Pierce, A.D., 1981, *Acoustics: An Introduction to Its Physical Principles and Applications*, McGraw-Hill, New York, USA.

Pollock, A.A., 1989, *Acoustic Emission Inspection*, Physical Acoustic Corporation.

Powell, M.J.D., 1987, Radial basis function for multivariable interpolation: A Review. In J.C.Mason and M.G.Cox, *Algorithms for Approximation*, pp143-167. Oxford: Clarendon Press.

Proceedings of DAMAS, 1995-, Proceedings of structural damage assessment using advanced signal processing procedures, Vol.1-Vol.4.

Rosenblatt, M., 1956, Remarks on some nonparametric estimates of a density function, *Annal of Mathematical Statictis*, Vol. 27, 832-837.

Rosenblatt, F., 1962, *Principles of Neurodynamics: Perceptron and the Theory of Brain Mechanisms*, Washington DC: Spartan.

Rumelhart, D.E., Hinton, G.E., and Willams, R.J., 1986, Learning internal representations by error propagation, *Parallel Distributed Processing: Explorations in the Microstructures of Cognition*, Vol. 1, pp. 318-362.

Sagoo, H.S., 1987, *Reduction of Noise levels in vacuum cleaners*, PhD Thesis, Aston University, UK.

Seo, D.C., and Lee, J.J, 1999, Damage detection of CFRP laminates using electrical resistance measurement and neural network, *Composite Structures*, Vol. 47, pp. 525-530.

Scalettar, R., and Zee, A., 1988, Emergence of grandmother memory in feed forward networks: learning with noise and forgetfulness, *Connectionist Models and Their Implications/ Readings from Cognitive Science*, pp. 309-332.

Schofield, B.H, Bareiss, R.A., and Kyrala, A.A., 1958, *Acoustic Emission under Applied Stress*, ASTIA Document AD 155674, WADC Technical Report.

Shaw, J.K., Schindler, P.M., May, R.G., and Clus, R.O., Location of impacts on composite panels by embedded fiber optic sensors and neural network processing, *SPIE*, Vol. 2444. pp. 481-489.

Sietsma, J., and Dow, R.J.F., 1988, Neural net pruning- why and how, *IEEE International Conference on Neural Networks*, vol. I, pp. 325-333.

Simmon, J.A., and Clough, R.B., 1980, Theory of Acoustic emission, *Dislocation Modelling of Physical Systems* (Proceedings of the international conference), Florida, pp. 464-497.

Sinclair, A.C.E., 1977, CEGB Berkelay Nuclear Laboratory Report RD/B/N/4066.

Sneddon, I., 1951, *Fourier Transforms*, McGraw-Hill, New York, USA.

Staszewski, W.J., Side, S., Wardle, R., and Worden, K., 1997, Fail-safe sensor distributions for damage detection, *Proceedings of DAMAS97*, pp.135-146.

Staszewski, W.J., Worden, K., and Tomlinson, G.R., 1996, Optimal sensor placement for neural network fault diagnosis, *Proceedings of Adaptive Computing in Engineering Design and Control'96*, pp. 92-99.

Staszewski, W.J., and Holford, K.M., 2001, Wavelet signal processing of acoustic emission data, *Proceeding of DAMAS2001*, pp. 351-359.

Stebut, J.V., Lapostolle, F., Bucsa, M., and Vallen, H., 1999, Acoustic emission monitoring of single cracking events and associated damage mechanism analysis in indentation and scratch testing, *Surface and Coatings Technology*, Volumes 116-119, pp. 160-171.

Sung, D.U, Oh, J.H, Kim, C.G, and Hong, C.S., 2000, Impact monitoring of smart composite laminates using neural network and wavelet analysis, *Journal of Intelligent Material Systems and Structures*, Volume 11, Issue 3, pp. 180-190.

Susic, E., and Grabec, I., 1995, Application of a neural network to the estimation of surface roughness from AE signals generated by friction process, *Journal of Machine Tools Manufacturing*, Vol. 35, No. 8, pp. 1077-1086.

Swingler, K., 1996, *Applying Neural Networks- A Practical Guide*, Academic Press, London.

Szewczyk, Z.P., and Hajela, P., 1994, Damage detection in structure based on feature-senstive neural networks, *Journal of Computational Civil Engineering*, ASCE, Vol. 8, pp. 163-178.

Tatro, C.A., 1959, Sonic techniques in the detection of crystal slip in metals, Status report, Michigan State University, USA.

Tarassenko, L., 1998, *A Guide to Neural Computing Applications*, Arnold, London, UK.

Thapa, B.K., 2001, *Neural Network Enhanced Self-Tuning Adaptive Control Application for Non-Linear Control of Dynamic Systems*, PhD Thesis, Aston University, UK.

Thomas, M. D., and Flockton, A.J., 1994, 2nd European Conf on Smart structures & materials, *Proceedings of SPIE*, Vol. 2361, pp. 55-58.

Thornton, C., 1997, Coefficient of restitution for collinear collisions of elastic-perfectly plastic spheres, Transactions of ASME, *Journal of Applied Mechanics*, Vol. 64, pp. 383-386.

Timoshenko, S., 1934, *Theory of Elastcity*, McGraw-Hill, New York, USA.

Vu-Quoc, L., Zhang, X., and Lesburg, L., 2001, Normal and tangential force-displacement relations for frictional elasto-plastic contact of spheres, *International Journal of Solids and Structures*, Vol. 38, pp. 4-17.

Werbos, P, 1991, Stochastic modelling and representations of reality: a linear starting point, *Journal of Neural Networks*.

Wevers, M., 1997, Listening to the sound of materials: acoustic emission for the analysis of material behaviour, *NDT&E International*, Vol. 30, No. 2, pp.99-106.

Whittemore, H.L., and Petrenko, S.N., 1921, *U.S. Bur. Standards Tech*, paper201.

Widrow, B., and Smith, F.M., 1963, Pattern recognising control system, *Proceeding of Computer and Information Science*.

Williams, R.V., 1980, *Accoustic Emission*, Adam Hilger Ltd. Bristol, UK.

Worden, K., Manson, G., and Allman, D.J., 2001, An experimental appraisal of the strain energy damage location method, *Proceedings of International Conference for DAMAS2001*, pp. 35-46.

Wu, X., Ghaboussi, J., and Garrett, J.H., 1992, Use of neural networks in detection of structure damage, *Computing Structures*, Vol. 42, pp. 649-659.

Bibliography

Following internet resources are maintained in this section for general information quoted in this study.

http://www.mathworks.com

http://www.sciencedirect.com

http://www.inns.org

ftp://ftp.sa.com/pub/neural/ and Usenet: comp.ai.neural-nets.

Appendix A Utilisation of Least square method

As the matter of fact, least square method is the powerful tool to estimate the parameter of the linear equation. When one try to find the values of the coefficients in a given model, which minimise the sum of the squared errors between the model output and observations output, least squares can estimates the coefficients [Norton, (1986)]. Supposing the model has the unknown coefficient θ per explanatory variable. If the U's was input and the θ's are collected into p-vectors. That is

$$U_t = \left[u_{1t}\, u_{2t} \quad \cdots \quad u_{pt}\right]^T, \qquad \theta_t = \left[\theta_1\, \theta_2 \quad \cdots \quad \theta_p\right]^T \tag{1}$$

then the model turns out to be

$$y_t = f(u_t, \theta) + e_t, \quad t = 1,\ 2,\ 3 \ldots N \tag{2}$$

where e_t accounts for observation error (measurement noise) and modelling error. To purchase a more perfect model, We aimed to find the value of θ, which minimises

For the practically useful case where $f(.\ ,.)$ is linear in the unknown coefficients making up θ. That is ,

$$S \equiv \sum_{t=1}^{N} e_t^2 = \sum_{t=1}^{N} (y_t - f(u_t, \theta))^2 \tag{3}$$

$$y_t = u_t^T \theta + e_t, \quad t = 1,\ 2,\ 3 \ldots N \tag{4}$$

To make the algebra tidy, collect all the samples y_1 to y_N into an N-vector, all the u_t vectors into an $N \times p$ matrix U and e_1 to e_N into e, giving

$$y = U\theta + e \tag{5}$$

Therefore

$$S = e^T e = (y^T - \theta^T U^T)(y - U\theta) \tag{6}$$

The value, which minimises S, makes the gradient of S with respect to θ zero:

$$T = \frac{\partial S}{\partial \theta} = \left[\frac{\partial S}{\partial \theta_1} \frac{\partial S}{\partial \theta_2} \ldots \frac{\partial S}{\partial \theta_p} \right]^T = 0 \tag{7}$$

To evaluate T we need two standard results for derivatives of vector-matrix expressions, namely

$$\frac{\partial(a^T\theta)}{\partial\theta} = \left(vector\ with\ element\ i\ \frac{\partial}{\partial\theta_i}\sum_{j=1}^{p} a_j\theta j \right) = a \tag{8}$$

And

$$\begin{aligned}\frac{\partial(\theta^T A\theta)}{\partial\theta} &= \left(vector\ with\ element\ i\ \frac{\partial}{\partial\theta_i}\sum_{k=1}^{p}\sum_{j=1}^{p} a_{jk}\theta_j\theta_k \right) \\ &= \left(vector\ with\ element\ i \sum_{k=1}^{p} a_{jk}\theta_k + \sum_{j=1}^{p} a_{ji}\theta_j \right) \\ &= (A + A^T)\theta\end{aligned} \tag{9}$$

After we multiply out the expression for S in (6), we got the express as following

$$\begin{aligned}S &= (y^T - \theta^T U^T)(y - U\theta) \\ &= y^T y - \theta^T U^T y - U\theta y^T + \theta^T U^T U\theta\end{aligned} \tag{10}$$

Note that $\theta\ U^T y$ is [1×p]×[p×N]×[N×1], which turn out to be a scalar, and therefore is identical to $y^T\ U\ \theta$. Now putting $U^T y$ for a and $U^T\ U$ for A in (8) and (9) and obtain

$$S = y^T y - \theta^T U^T y - U\theta y^T + \theta^T U^T U\theta$$
$$= -2\theta^T U^T y + \theta^T U^T U\theta \quad (11)$$

$$0 = \frac{\partial S}{\partial \theta} = -2U^T y + 2U^T U\theta \quad (12)$$

The θ that makes the gradient of S zero is therefore

$$\theta = [U^T U]^{-1} U^T y \quad (13)$$

And this is so call Least Squares Method; We therefore could estimate the parameters of the given model (2).

Case study for Least Square Method

Following is the case study for least square method. Assuming that a given system is about to be identified, which turns out to be

$$y(k) = 0.5 * y(k-1) + 0.7 * u(k) + e(k) \quad (14)$$

Noted that *u(k)* is input, *e(k)* is white noise and *y(k)* is output of the system, while *y(k-1)* is one step delay of the output. The task is that, under the condition, *y(k)* and *u(k)* are pre-known variant shown in Figure (1), then how to find the parameter of the system, in other word, how to determine the model.

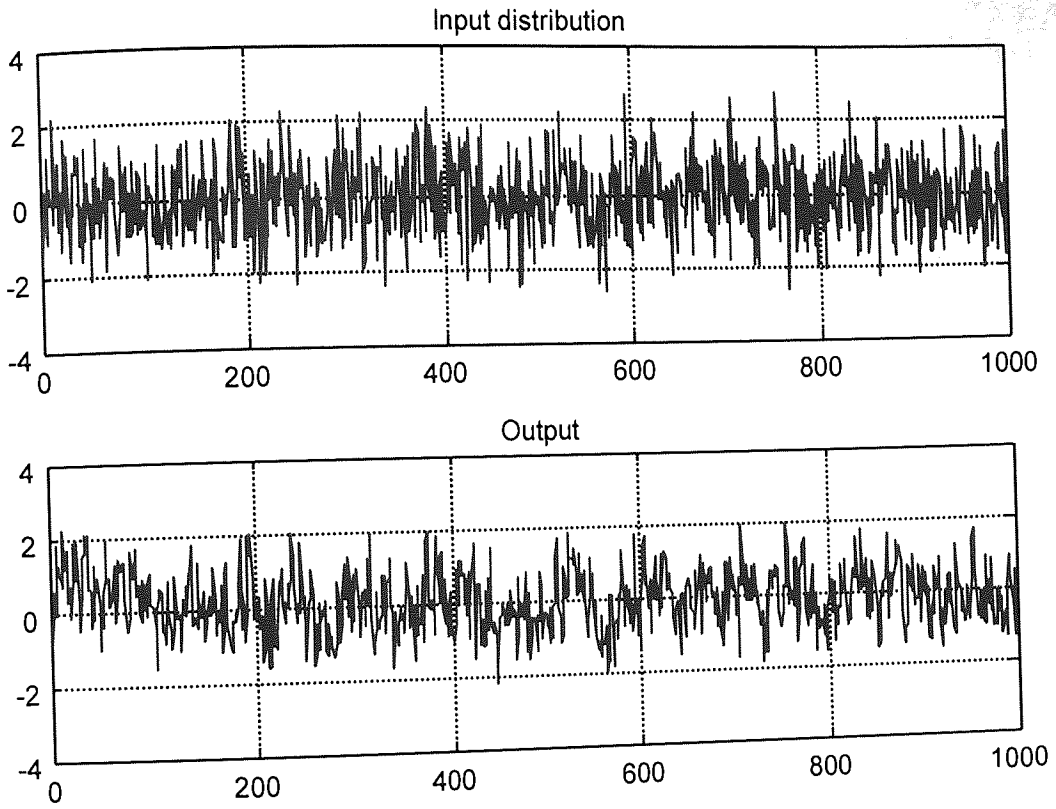

Figure (1) The output and input of the system

In practice, applying least square method, it can find out the parameters of the model easily. The codes in the form of MATLAB m-file and result are shown in the attachment. Due to white noise, there is a small deviation of the parameter after the identification

Appendix B Utilisation of Fast Fourier Transform

Introduction of FFT

The FFT algorithm for computing the discrete Fourier transform of a sequence is the important measure for digital signal processing. Its uses range from filtering, convolution, computation of frequency response and group delay, to applications in power spectrum estimation. [Little, (1993)]

Actually, Fourier analysis provides a set of mathematical tools, which enable people to break down data into various frequency components. The two functions implement the transform and inverse transform are given by (15) and (16):

$$X(k+1) = \sum_{n=0}^{N-1} x(k+1)e^{-i(2kn\pi/N)} \tag{15}$$

$$x(k+1) = 1/N \sum_{n=0}^{N-1} X(k+1)e^{i(2kn\pi/N)} \tag{16}$$

Note N here is the length of the data x. And Fourier Transform is called.

Meanwhile, using the fact that $e^{i(2kn\pi/N)} = cos(2kn\pi/N) + i\,sin(2kn\pi/N)$ (17), it then will find that the periodic signals could actually be divided into a finite set of sine and cosine function.

During the analysing, there are several factors, which play an important role in FFT. First, it is the frequency increment Δf, which is equal to the reciprocal of the time

period T. Second, it is the sampling rate, which is the quotient of time period T and data length n. Third, the maximum frequency, $f_{max}=n/2T$, known as Nyquist frequency and Nyquist sampling rate are another two important subjects to FFT. A very interesting phenomenon should also be mentioned here, which is so called "aliasing". Due to the periodic nature of the discrete Fourier transform (DFT), there will appear a symmetrical appearance of frequency component per cycle, when it goes higher than the Nyquist frequency. [Penny and Lindfield, (1995)] The illustration is shown in Figure (2)

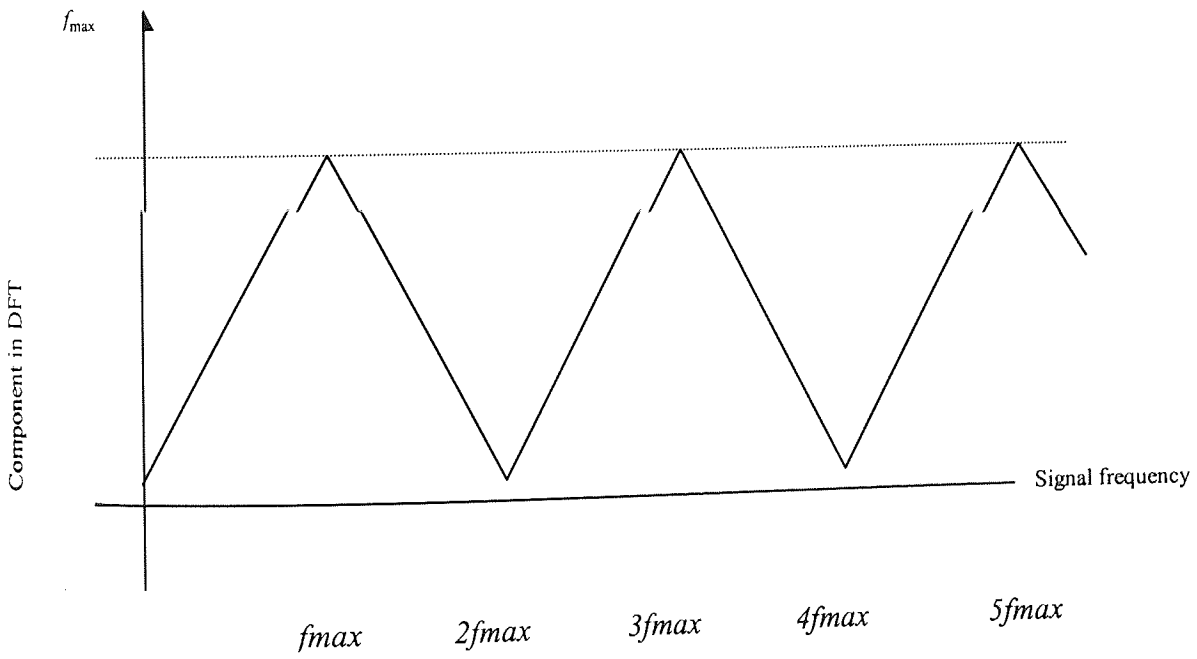

Figure (2) Aliasing in signal frequency

When the sequence length is a power of two, a high-speed radix-2 fast Fourier transform algorithm is employed. The radix-2 FFT routine is optimised to perform a real FFT if the input sequence is purely real, otherwise it computes the complex

FFT. This causes a real power-of-two FFT to be about 40% faster than a complex FFT of the same length.

While, when the sequence length is not an exact power of two, an alternate algorithm finds the prime factors of the sequence length and computes the mixed-radix discrete Fourier transforms of the shorter sequences.

The time it takes to compute an FFT varies greatly depending upon the sequence length. The FFT of sequences whose lengths have many prime factors is computed quickly; the FFT of those that have few is not. Sequences whose lengths are prime numbers are reduced to the raw (and slow) discrete Fourier transform (DFT) algorithm. For this reason it is generally better to stay with power-of-two FFTs unless other circumstances dictate that this cannot be done. For example, on one machine a 4096-point real FFT takes 2.1 seconds and a complex FFT of the same length takes 2.7 seconds. The FFTs of neighbouring sequences of length 4095 and 4097, however, take 7 seconds and 58 seconds, respectively.

Case study for FFT

An example is shown as following. Considering that we determine the spectrum of a sequence of 512 data points sampled over 2 seconds from the function

$$y = 0.2\cos(2\pi f_1 t) + 0.35\sin(2\pi f_2 t) + 0.3\sin(\pi f_3 t) + random \quad noise \tag{18}$$

,where f_1=20 Hz, f_2=50 Hz, f_3=70 Hz. The random noise is normally distributed with a standard deviation of 0.5 and a mean of zero. The following scrip plots the time series and the DFT scaled by the factor 256. Using MATLAB function FFT, we could obtain the Figure (3) shown as following.

Note that the lower plot of Figure (3)shows that random noise in the signal does not prevent the frequency components 20 50 and 70 Hz from revealing themselves in the spectrum. From above example, it shows that Fourier Transform could be the powerful measure to interpret signals, when the frequency of data may give the insight into the mechanism that it generated it. The code of the program is *available in appendix at end* of the report

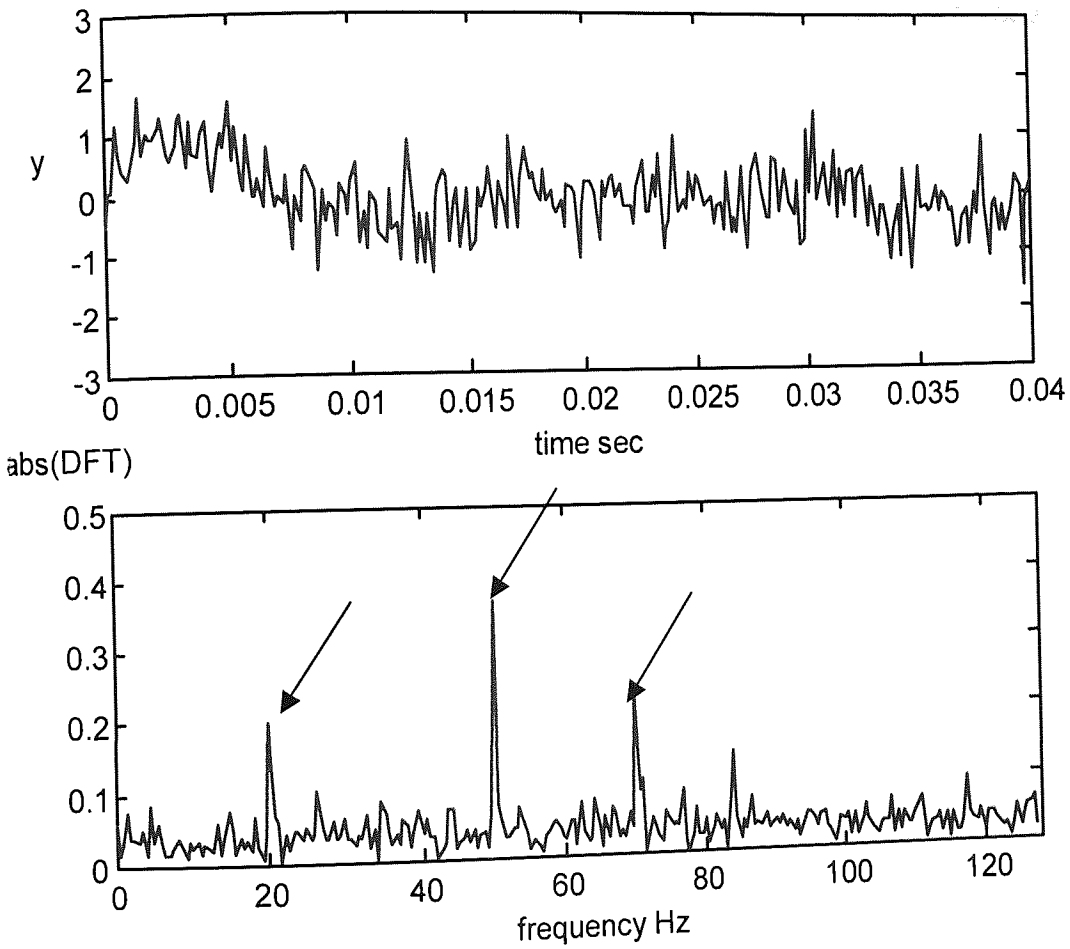

Figure (3) Signal and frequency spectrum

show frequency components at 20, 50, 70 Hz

Appendix C Back propagation algorithm

For pattern p, the Equation (3-7) in Section 3.3.2 can be rewritten as follows:

$$E = \tfrac{1}{2}(y_k - t_k)^2 = \tfrac{1}{2}\sum_k (g(\sum_j \omega_{jk} y_j) - t_k)^2 \qquad (19)$$

For a ω_{jk} weight, the minimisation of E by gradient descent can be expressed as

$$\Delta \varpi_{jk} = -\eta \frac{\partial E}{\partial \varpi_{jk}} \qquad (20)$$

Using the chain rule, the right hand item on the right hand part of the equation can be expanded:

$$\frac{\partial E}{\partial \varpi_{jk}} = \frac{\partial E}{\partial a_k}\frac{\partial a_k}{\partial \varpi_{jk}} \qquad \text{where } a_k = \sum_j \varpi_{jk} y_j \qquad (21)$$

The first two items on the right-hand side is expanded as follows

$$\frac{\partial E}{\partial a_k} = \frac{\partial E}{\partial y_k}\frac{dy_k}{da_k} \qquad (22)$$

Now, it can be worked out in turn

$$\frac{\partial E}{\partial y_k} = y_k - t_k \quad \text{from Equation (19)}$$

$$\frac{dy_k}{da_k} = \frac{dg}{da_k} = \frac{d}{da_k}\left(\frac{1}{1+e^{-a_k}}\right) = \frac{e^{-a_k}}{(1+e^{-a_k})^2} = y_k(1-y_k)$$

and combine these results with the fact that $\frac{\partial a_k}{\partial \varpi_{jk}} = y_j$, we can now substitute all of this into Equation (20) to give

$$\Delta \varpi_{jk} = -\eta \frac{\partial E}{\partial \varpi_{jk}} = -\eta \delta_k y_j \tag{23}$$

$$\text{where } \delta_k = \frac{\partial E}{\partial a_k} = (y_k - t_k) y_k (1 - y_k) \tag{24}$$

The extension of the above to the ω_{ij} weights from the input to the hidden units only requires the further application of the chain rule since the output error is a continuous differentiable function of these weights also, as shown in (3-8) in Section 3.3.2.

$$\text{Thus } \Delta \varpi_{ij} = -\eta \frac{\partial E}{\partial \varpi_{ij}} \tag{25}$$

$$\text{with } \frac{\partial E}{\partial \omega_{ij}} = \frac{\partial E}{\partial a_j} \frac{\partial a_j}{\partial \omega_{ij}} \quad \text{where } a_j = \sum_i \omega_{ij} y_i \tag{26}$$

Note that, for consistency of notation, y_j represents the ith input feature here. Expanding $\partial E / \partial a_j$ as before, it obtains

$$\frac{\partial E}{\partial a_j} = \frac{\partial E}{\partial y_j} \frac{dy_j}{da_j} = \frac{\partial E}{\partial y_j} y_j (1 - y_j) \tag{27}$$

Then it is necessary to find a means of evaluating $\partial E / \partial y_j$ because it is not possible to work it out directly. We, however, can use the fact that we have just computed $\delta_k = \partial E / \partial a_k$ in order to obtain $\Delta \omega_{jk}$.

$$\text{Thus}\frac{\partial E}{\partial y_j} = \frac{\partial E}{\partial a_k}\frac{\partial a_k}{\partial y_j} = \sum \delta_k \omega_{jk} \tag{28}$$

Summing over k since each of the j hidden units is connected to all of the k output units. The update equation for the input to hidden weights therefore is

$$\Delta \varpi_{ij} = -\eta \frac{\partial E}{\partial \varpi_{ij}} = -\eta \delta_j y_i \tag{29}$$

where

$$\delta_j = \frac{\partial E}{\partial a_j} = \sum_k \delta_k \varpi_{jk} y_j (1 - y_j) \tag{30}$$

Appendix D Published papers

Paper1

Liu, N., Zhu, Q.M., Wei, C.Y., Dykes, N.D., and Irving, P.E., 1999, Impact damage detection in carbon fibre composites using neural networks and acoustic emission, *Key Engineering Materials*, Volume 167, pp. 43-54.

Paper2

Liu, N., Zhu, Q.M., Wei, C.Y., Dykes, N.D., and Irving, P.E., 2000, Acoustic emission signal processing to detect impact damage location using neural networks, *Proceedings of PREP2000*.

Paper3

Liu, N., Penny, J.E.T., Wei, C.Y., Irving, P.E., Dykes, N., and Zhu, Q.M., 2001, Impact Location on Stiffened Composite Structures Using Neural Networks, *Key Engineering Materials*, Volume 204, pp. 395-408.

Appendix E ASTM Standard

Appendix F Experimental Data Sheet

Impact damage level detection
1)AE signals detection

Sample1:

Material: T300 carbon fibres and Hexcel 914 resin
Size: 100 mm × 150mm × 3.8mm

Impact experiments was conducted in follow order: 2J impact event, 3.5 J impact event, 5 J impact event, 7 J impact event(repeated 4 times), 10 J impact event, and 15 J impact event

Equipments:
Rosand Impact testor;
PAC MISTRAS 2001.

Measured data:
AE waveforms at different impact levels.

Sample2:

Material: BASF 5245C resin with T800 carbon fibre
Size: 100 mm × 150mm × 2mm

Impact experiments was conducted in follow order: 5.4J impact event(repeated 3 times), 9.3 J impact event (repeated 3 times), 13.8 J impact event (repeated 3 times), 20J impact event.

Equipments:
Rosand Impact testor;
PAC MISTRAS 2001.

Measured data:
AE waveforms at different impact levels.

2) Impact damage area measuring

Sample1 and Sample2

C-Scan were conducted on each impact damaged panel

Equipment:
HFUS 2000 C-Scanner

Measured data:
Impact damage area

Impact damage location
1) AE time difference acquisition

Sample
T300 carbon fibres and Hexcel 914 resin composite panel with rib underneath.
Sampling zone: 760mm x 580 mm x 3.3 mm rectangle area

Experiments was conducted for training (42 data set evenly distributed) and validation (24 data set randomly generated)

Equipment:
PAC MISTRAS2001

Measured data:
AE arrival moments.

2) AE propagation speed
Sample: same as above.

Experiments was conducted detect the AE speed contours within a circular area with a radius 270mm

Equipment:
PAC MISTRAS2001

Measured data:
AE speed field.